PhD-FSTC-2017-44
The Faculty of Sciences, Technology and Communication

DISSERTATION

Presented on 15/09/2017 in Luxembourg

to obtain the degree of

DOCTEUR DE L'UNIVERSITÉ DU LUXEMBOURG

EN BIOLOGIE

by

Sarah Louise NICKELS
Born on 09 December 1988 in Esch-sur-Alzette (Luxembourg)

NEURAL STEM CELLS FOR MODELING PARKINSON'S DISEASE

LSRU | LIFE SCIENCES RESEARCH UNIT

NEURAL STEM CELLS FOR MODELING PARKINSON'S DISEASE

A dissertation by

Sarah Louise Nickels

In partial fulfilment of the requirements for the degree of

DOCTOR of PHILOSOPHY

University of Luxembourg

Luxembourg Centre for Systems Biomedicine
Developmental and Cellular Biology
&
Life Science Research Unit
Systems Biology

Luxembourg 2017

To my family

Affidavit

I hereby confirm that the PhD thesis entitled “Neural stem cells for modeling Parkinson’s disease” has been written independently and without any other sources than cited.

Luxembourg, _____ _____

Sarah Louise Nickels

"If the human brain were so simple that we could understand it,

We would be so simple that we couldn't."

(Emerson M. Pugh)

ACKNOWLEDGMENTS

ACKNOWLEDGMENTS

This work is the result of many people's hard work and collaborations and would not have been possible without their help and support. My thanks go to:

- Jens Christian Schwamborn

Most of all I would like to express my sincere appreciation and gratitude to Jens Christian Schwamborn, my supervisor. You have been a great mentor. Thank you for your patient guidance, confidence, and time during these four years. Your support and optimistic enthusiasm motivated and inspired me a great deal. I had the wonderful opportunity of working on an extraordinary project and I have benefited and learned a lot from your knowledge, experience, and scientific excellence. Thank you for establishing a culture of fruitful collaboration and a positive atmosphere in the lab. Your guidance helped me to leave my comfort zone, push myself to excel, and become a better scientist.

- Thomas Sauter and Lasse Sinkkonen

Besides my main supervisor, I would like to thank Thomas Sauter and Lasse Sinkkonen, who kindly hosted me in their laboratory and advised me during my PhD project. It gave me the opportunity to gain an insight into a computational systems biology lab as well as work together with an epigenetics team, which enlarged my scientific horizon. I would like to thank you for your encouragement, insightful comments, and critical inquiries about my research, which helped me to broaden my perspectives. Special thanks go to Lasse who always had an open ear and gave me valuable advice whenever needed. Thank you for your excellent guidance and support.

- My defense committee

I would like to give special acknowledgment to all my thesis committee members Prof. Jens Christian Schwamborn, Prof. Thomas Sauter, and Dr. Maria Adele Rüger for their helpful suggestions and critical feedback during the comité d'encadrement de thèse (CET) meetings. Moreover, I would like to thank Dr. Lasse Sinkkonen and Dr. Demetrios K. Vassilatis for agreeing to evaluate my thesis and being part of my defense jury. Thank you all for reviewing my thesis, for your helpful suggestions and for the valuable assessment of my work.

- Both my groups.

By doing a joint PhD project between two laboratories I had the luck of being a part of two great research teams. I would like to thank my fellow labmates and former members:

- From the systems biology group: *Aurélien Ginolhac, Déborah Gerard, Elisabeth John, Julia Becker, Jochen Ohnmacht, Lasse Sinkkonen, Maria Pacheco, Marco Albrecht, Maria Livrand, Mafalda Sofia*

Galhardo, Panuwat Trairatphisan, Philippe Lucarelli, Susann Mudrich, Sébastien Delandtsheer, Tamara Jean Rita Bintener, Thomas Pfau, Thanh-Phuong Nguyen, and Yujuan Gui.

- From the developmental and cellular biology group: *Anna-Lena Hillje, Anna Monzel, Annegraet Daujeumont, Antoine Treff, Emanuel Berger, Gabriela Novak, Gemma Gomez, Inga Werthschulte, Jonas Walter, Javier Jarazo, Johann Tisserand, Jonathan Arias, Kathrin Hemmer, Lisa Smits, Laura González Cano, Lamia Bahnassawy, Maria Pavlou, Maria Bermudez, Marie Fossépré, Matthieu Sainlez, Marlen Weber, Nicole le Grand, Nirupama Ramanathan, Silvia Bolognin, Sarah Nicklas, Stephanie Smith-Eckhardt, Thea van Wüllen* and *Xiaobing Qing.*

Thank you for the warm welcome, your hospitality, the stimulating discussions, as well as all the fun we had together over the last four years. Without you and the great environment you created, this work would not have been possible. I would like to offer my special thanks to you for your help in the lab and your scientific rigor, which improved my own skills, confidence, and knowledge. My thanks go to Kathrin, Inga, and Anna H. for their introduction to the cell culture and for their great patience with me. A big thank you goes to Laura, Anna H., and Sarah for helping me perfecting my love-hate for Western blotting. My thanks go to Maria and Deborah for helping me and showing me ChiP. I would also like to extend Thea a million thanks for a million answers on a million questions, mostly starting with "where is" ☺. Also, I would like to thank Emu, Anna H. Lasse, and Silvia for their great advice and scientific wisdom. Special thanks go to Jonas for having backup cells to save my xx every time I messed up, and for the long and useful discussions of our projects. Four years of shared blood, sweat and tears were great fun ☺. My thanks go to the Dexia people who sweetened the "hard" time we had in that building. Furthermore, my gratitude goes to Lisa, Silvia, Kathrin, Anna M., Jonas, and Emu for their constant encouragements and emotional support. Finally, special thanks go to everyone who considers me a friend, which, in a great group with great people, is hard not to become. Thanks for all the amazing time we spent outside the lab. Thanks for four years of great well-done-beers, dinners, brunches, badminton games, parties, birthdays, New Year's Eve celebrations, and thanksgivings.

- My friends and family

I would like to thank Erin for the perfect job she did, and for the time she invested in correcting the English of this thesis. Then I would like to express my deepest gratitude to my parents, my sister, my parents in law and my best friends for being so supportive during this time. Thank you for your understanding, help, and advice in every situation. Finally, and most importantly I would like to thank Fab my best friend and almost husband. Thank you for your support, patience, confidence, encouraging words, and love. Thanks for being there for me, although I was not always easy to deal with ☺.

CONTENTS

CONTENTS

1 TABLE OF CONTENTS

CONTENTS

CONTENTS

2 LIST OF FIGURES

3 LIST OF TABLES

4 LIST OF ABBREVIATIONS

Abbreviations

AA	**A**scorbic **A**cid
ALS	**A**myotrophic **L**ateral **S**clerosis
ATP	**A**denosine **T**ri**p**hosphate
cAMP	**c**yclic **A**denosine **M**ono**p**hosphate
BWA	**B**urrows **W**heeler **A**ligner
Cas9	**C**RISPR **A**ssociated **P**rotein nuclease **9**
CC3	**C**leaved **C**aspase **3**
ChIP-seq	**Ch**romatin **I**mmuno**p**recipitation- **seq**uencing
CNS	**C**entral **N**ervous **S**ystem
COR	**C**arboxyl Terminal **O**f **R**oc
CRC	**C**ore **R**egulatory **C**ircuit
CRISPR-Cas9	**C**lustered **R**egularly **I**nterspaced **S**hort **P**alindromic **R**epeats-**C**RISPR **as**sociated gene
crRNA	**CR**ISPR **RNA**
DEG	**D**ifferentially **E**xpressed **G**ene
DG	**D**entite **G**yrus
DMSO	**Dim**ethyl**s**ulf**o**xid
DN	**D**opaminergic **N**euron
DNA	**D**eoxyribo**n**ucleic **A**cid
L-DOPA	L-3,4-**D**ihydr**o**xy**p**henyl**a**lanin
ESC	**E**mbryonic **S**tem **C**ell
EDTA	**E**thylene**d**iamine **T**etraacetic **A**cid
EGTA	**E**thylene **g**lycol-bis(β-amino-ethyl ether)-N,N,N’,N’-**t**etraacetic **a**cid
FACS	**F**luorescence-**a**ctivated **C**ell **S**orting
FCS	**F**etal **C**alf **S**erum
FP	**F**loor **P**late

GC/MS	Gas Chromatography/Mass Spectrometry
GP	Globus Pallidus
GTP	Guanosine-5'-triphosphate
GWAS	Genome Wide Association Studies
G2019S	Glycine to serine substitution at amino acid position 2019
H	Healthy
h	human
HEK 293	Human Embryonic Kidney cells
HGNC	Hugo Gene Nomenclature Committee
H3K27ac	Histone 3 lysine 27 acetylation
indel	insertions or deletions
iPSC	induced Pluripotent Stem Cell
KO	Knock Out
LB	Lewy Body
lt-hESNSC	long term human Embryonic Stem Cell derived Neural Stem Cell
MHB	Midbrain-hindbrain Border (or Boundery)
MID	Mass Isotopomer Distribution
miRNA	microRNA
mRNA	messenger RNA
MLDC	Multilineage Differentiation Culture
MPTP	1-Methyl- 4-phenyl-1,2,3,4-tetrahydropyridine
m/ms	mouse
MTT	3-(4,5-dimethylthiazol-2-yl)-2,5-diphenyltetrazolium
NEP	Neural Epithelial Progenitor
NESC	Neuroepithelial Stem Cell
NHEJ	Non Homologous End Joining
NOD/SCID	Non-Obese Diabetic/Severe Combined Immunodeficiency
NPBSC	Neural Plate Border Stem Cell
NP-40	4-Nonylphenyl-polyethylene glycol
NSC	Neural Stem Cell
NT	Non-transgenic
OB	Olfactory Bulb
o/n	over night
O4	Oligodendrocyte specific myelin lipid antigen

P	Patient
PAM	Protospacer-associated Motif
PBS	Phosphate-buffered Saline
PCR	Polymerase Chain Reaction
PD	Parkinson's Disease
PFA	Paraformaldehyde
PH3	Phospho-histone 3
PIC	Protease Inhibitor Cocktail
PMA	Purmorphamine
PNS	Peripheral Nervous System
pNSC	primitive Neural Stem Cell
rb	rabbit
Rab	Ras related in brain
Ras	Rat sarcoma (oncogene, small GTPase)
RGC	Radial Glial Cell
RNA	Ribonucleic acid
R-NSC	Rosette like Neural Stem Cell
ROC	Ras Of Complex
SE	Super-enhancer
SSEA4	Cell Surface Glycosphingolipid Antigen
sgRNA	single guide RNA
SNP	Single Nucleotide Polymorphism
SNpc	*Substatia Nigra pars compacta*
SNpr	*Substantia Nigra pars reticularis*
smNPC	small molecule induced Neural Progenitor Cell
SVZ	Subventricular Zone
TALENS	Transcription-activator Like Effector Nucleases
TCA	Tricarboxylic Acid
TLK	Tousled-like Kinase
tracrRNA	trans-activating CRISPR RNA
TMEM	Transmembrane Protein
VZ	Ventricular Zone
WT	Wild Type

Genes and proteins

HGNC	Gene symbol	Protein	Name
DDC	-	AADC	Dopa Decarboxylase
AKT1	*AKT1*	AKT1	Serine/Threonine Kinase 1
AQP4	-	AQP4	Aquaporin 4
ARL17a/b	*ARL17a/b*	ARL17a/b	ADP Ribosylation Factor Like GTPase 17a and b
ATP13A2	*ATP13A2*	ATP12A2	ATPase 13A2
BDNF	-	BDNF	Brain-derived Neurotrophic Factor
FABP7	-	BLBP	Brain Lipid Binding Protein
BMP family	-	BMP	Bone Morphogenetic Protein
CDC25a	*CDC25A*	CDC25A	Cell Division Cycle 25A
CASP3	-	C3	Caspase 3
CER1	-	CERBERUS	Cerberus
CHCHD2	*CHCHD2*	CHCHD2	Coiled-coil-helix-coiled-coil-helix domain containing 2
CHRD	-	CHORDIN	Chordin
CSNK1A1	-	CK1	Casein Kinase 1
COMT	-	COMT	Catechol-*o*-methyltransferase
CNTD	-	CNTF	Ciliary Neurotrophic Factor
MYC	-	c-MYC	MYC proto-oncogene, bHLH transcription factor
SLC6A3	-	DAT	Dopamine Transporter
DACH1	-	DACH1	Dachshund Homolog 1
DCX	*DCX*	DCX	Doublecortin
PARK7	*DJ-1*	DJ1	Protein Deglycase DJ-1
DMRT3	-	DMRT3	Doublesex and Mab-3 Related Transcription Factor 3
DNAJC6	*DNAJC6*	DNAJC6	DnaJ Heat Shock Protein Family (Hsp40) Member C6
DNAJC15	*DNAJC615*	DNAJC15	DnaJ Hsp Family (Hsp40) Member C15
DNM3	*DNM3*	DNM3	Dynamin 3
EIF4EBP1	-	4E-BP	Eukaryotic Initiation Factor 4E Binding Protein
EIF4E	-	EIF4E	Eukaryotic Translation Initiation Factor 4E
SLC1A2	-	EAAT2	Excitotoxic Amino Acid Transporter 2
EGF	-	EGF	Epithelial Growth Factor
EN1	-	EN1	Engrailed1
EN2	-	EN2	Engrailed2
EMX1	-	EMX1	Empty Spiracles Homeobox 1
MAPK	-	ERK	Extracellular-signal regulated kinases
FASLG	-	FAS-L	Fas ligand
FADD	-	FADD	Fas-associated Protein with Death Domain
FOXA2	*FOXA2*	FOXA2	Forkhead Boxa2
FST	-	FOLLISTATIN	Follistatin
FGF	-	FGF	Fibroblast Growth Factor
SLC6A11	-	GABA	Neurotransmitter Transporter, GABA
GAK	-	GAK	Cyclin G Associated Kinase
GAPDH	*GAPDH*	GAPDH	Glyceraldehyde-3-Phosphate Dehydrogenase
GBA	*GBA*	GBA	Glucosylceramidase Beta
GBX2	*GBX2*	GBX2	Gastrulation Brain Homeobox 2
GDNF	-	GDNF	Glial Derived Neurotrophic Factor
GFAP	*GFAP*	GFAP	Glial Fibrillary Acidic Protein
SLC1A3	-	GLAST	Glutamate Aspartate Transporter
GSC	-	GOOSECOID	Goosecoid Homeobox
GPX7	*GPX7*	GPX7	Glutathione Peroxidase 7

GRIN family	-	NMDAR	*N*-methyl-D-aspartate Receptor
GSK3A/B	-	GSK3	Glycogen Synthase Kinase
HES3	*HES3*	HES3	Family BHLH Transcription Factor 3
HES5	*HES5*	HES5	Family BHLH Transcription Factor 5
HESX1	-	HESX1	Homeobox, ES Cell Expressed 1
HSP70 family	-	HSP70	Heat Shock Protein Family 70 kDa
HSP90 family	-	HSP90	Heat Shock Protein Family 90 kDa
HIST3H3	-	H3	Histone 3
IKBK subunits	-	IKKs	IkappaB Kinases
KLF4	-	KLF4	Kruppel Like Factor 4
LEFTY1/2	-	LEFTY	Left-Right Determination Factor
-	*Let-7a*	-	miRNA let-7a
LHX1	*LHX1*	LHX1	LIM Homeobox 1
LIF	-	LIF	Leukemia Inhibitory Factor
LMX1A	*LMX1A*	LMX1A	LIM Homeobox Transcription Factor 1
LMO3	-	LMO3	LIM Domain only 3
LRRK1	*LRRK1*	LRRK1	Leucine Rich Repeat Kinase 1
LRRK2	*LRRK2*	LRRK2	Leucine Rich Repeat Kinase 2
MAPK family	-	MAPK	Mitogen-activated Protein Kinases
MAPT	*MAPT*	TAU	Microtubule Associated Protein Tau
MAP2	*MAP2*	MAP2	Microtubule Associated Protein 2
MKI67	-	Ki67	Marker of Proliferation Ki-67
MSX1	*MSX1*	MSX1	Msh Homeobox1
NANOG	*NANOG*	NANOG	Nanog Homeobox
NES	-	NESTIN	Nestin
NEUROG1	*NGN1*	NGN1	Neurogenin1
NEUROG2	*NGN2*	NGN2	Neurogenin2
NEUROG3	*NGN13*	NGN3	Neurogenin3
NODAL	-	NODAL	Nodal Growth Differentiation Factor
NOG	-	NOGGIN	Noggin
NOTCH1/2	*NOTCH*	NOTCH	Notch
NR2F1	*NR2F1*	NR2F1	Nuclear Receptor Subfamily 2 Group Member 1
NR2F2	*NR2F2*	NR2F2	Nuclear Receptor Subfamily 2 Group Member 2
NTS	*NTS*	NTS	Neurotensin
NR4A2	*NURR1*	NURR1	Nuclear Receptor Subfamily 4 Group A Member 2
PAX2	*PAX2*	PAX2	Paired Box2
PAX5	*PAX5*	PAX5	Paired Box5
PAX6	*PAX6*	PAX6	Paired Box6
PC	-	PC	Pyruvate Carboxylase
PRKAC subunits	-	PKA	Protein Kinase 1 cAMP-activated
PITX3	*PITX3*	PITX3	Paired-like Homeodomain Transcription Factor 3
PARK2	*PARK2*	PARKIN	Parkin E3 Ubiquitin Ligase
PINK1	*PINK1*	PINK1	Pten Induced Putative Kinase 2
PPP1R subunits	-	PP1	Protein Phosphatase 1
POU6F	*POU6F2*	POU6F2	POU Class 6 Homeobox 2 also RPF-1
POU5F1	*OCT4*	OCT4	Octamer-binding Transcription Factor 4
POU3F2	*OCT7*	OCT7	Octamer-binding Transcription Factor 7
POU3F4	*OCT9*	OCT9	Octamer-binding Transcription Factor 9
DLG4	-	PSD95	Postsynaptic Density Protein 95
OTX1	*OTX1*	OTX1	Orthodenticle Homolog 1
OTX2	*OTX2*	OTX2	Orthodenticle Homolog 2

RAB29	*RAB7L1*	RAB7L1	Member RAS Oncogene Family 7L1
RAB32	*RAB32*	RAB32	Member RAS Oncogene Family 32
RPS15	-	RPS15	40S Ribosomal Protein S15
SHH	-	SHH	Sonic Hedgehog
SOX1	*SOX1*	SOX1	RY (sex determining region Y)-box 1
SOX2	*SOX2*	SOX2	RY (sex determining region Y)-box 2
SOX3	*SOX3*	SOX3	RY (sex determining region Y)-box 3
SOX11	*SOX11*	SOX11	RY (sex determining region Y)-box 11
SMAD family	-	SMAD	Mother against DPP Homolog
SNCA	*SNCA*	α-SYN	α-Synuclein
SNARE family	-	SNARE	Soluble NSF Attachment Protein Receptor
SRR	*SRR*	SRR	Serine Racemase
S100B	*S100β*	S100β	S100 Calcium Binding Protein B
TGFB family	-	TGF-β	Transforming Growth Factor β
TH	*TH*	TH	Tyrosine Hydroxylase
TNF	-	TNF-a	Tumor Necrosis Factor alpha
PODXL	-	TRA-1-81/60	Podocalyxin
TUBB3	-	TUJ1	Neuron-specific Class III beta-tubulin
VPS35	-	VPS35	Vacuolar Protein Sorting-associated Protein 35
SLC17A7	*vGLUT1*	vGLUT1	Vesicular Glutamate Transporter 1
SLC18A2	-	VMAT2	Vesicle Monoamine Transporter Type 2
WNT family	-	WNT	Wingless-type MMTV integration site
YWHA family	-	14-3-3	Tyrosine 3-monooxygenase/tryptophan

SUMMARY

RESUMÉ OP LËTZEBUERGESCH (vereinfacht)

An dëser Aarbecht get beschriwen, wei een neuronal Stammzelle ka benotze fir d'Parkinson Krankheet ze erfuerschen. Säit der Entdeckung vun induzéierte pluripotente Stammzellen, huet d'Feld vun der Erfuerschung vun neurodegenerative Krankheete gréisser Fortschrëtter gemaach. Well ass et méiglech aus Hautzelle vu Patienten, Gehirzellen hierzestellen déi da kënne benotzt gi fir zum Beispill eng bestëmmte Mutatioun ze erfuerschen. An dëser Aarbecht si mir un der LRRK2-G2019S Mutatioun interesséiert déi d'Parkinson Krankheet ausléise kann. Och erfuersche mir des Mutatioun net an erwuessene Gehirzelle mä an neuronale Stammzelle wei déi, déi een am Embryo fënnt. Parkinson ass bekannt fir d'ofstierwe vun dopaminergeschen Neuronen an der schwaarzer Substanz vum mëttel Gehir wat och déi typesch motor Symptomer déi mat der Krankheet erhier ginn ausléist. Do freet een sech vläicht firwat mir Stammzellen erfuerschen. Parkinson ass eng ganz komplizéiert Krankheet, wou vill verschiddene Faktoren eng Roll spillen. Vill verschidde genetesch Mutatiounen a Risk Faktore goufe schon identifizéiert, déi kënnen zu der Krankheet bäidroen. Et ass awer nach net gewosst, wisou d'Neuronen iwwerhaapt stierwen a wei ee Grond et huet dass grad déi Neuronen aus der groer Substanz stierwen. An dëser Thees gëtt d'Hypothees opgestallt dass der Predispositioun eng entwécklungsbiologesch Stéierung ënnerläit. Zum Beispill ass gewosst, dass LRRK2 schon während der Entwécklung expriméiert gëtt an dass d'LRRK2-G2019S Mutatioun Dereguléierunge vun erwuessenen neuronale Stammzellen erbäiféiert. Eng zweet Hypothees op där des Aarbecht berout, an déi mat der éischter erhier geet, ass dass Parkinson eng multifaktoriell Krankheet ass an dass verschidde vun deenen uewe genannte Faktoren zesummespillen an nëmme gemeinsam Parkinson ausléisen. Esou gesi wär deen Entwécklungs-neurologeschen Defizit just als eng vu villen Ursaachen unzegesinn, déi da mei spéit am Liewen zur Entwécklung vun der Krankheet bäidroen kéint. LRRK2-G2019S ausgeléiste Parkinson spillt an der Hisiicht eng ganz interessant Roll, vu dass Mutatiounen am LRRK2 Gen net nëmmen d'Ursaach vu familiär ierflechem Parkinson si mä och a sporadesche Fäll eng wichteg Roll spillen. En plus kritt net jiddwereen deen des Mutatioun a sech dréit automatesch Parkinson, wat weist dass aner Faktore eng Roll an der Krankheet spillen. Fir den Ënnerscheed tëscht der Roll vun LRRK2-G2019S an de sougenannten anere Faktoren ze maachen, déi eng Roll spille kéinten, benotze mir Kontrollzellen an deene mir entweder d'Mutatioun agefüügt hun (am Fall vun deene gesonden Zellen) oder korrigéiert hun (am Fall vun de Patienten Zellen). Mir konnten hei weisen dass LRRK2-G2019S neuronal stam Zellen dereguléiert, andeems et an den Zellen wou mir d'Mutatioun agefüügt hunn den Zelldout ausléist an d'Zelldeelung reduzéiert. En Ënnerscheed an der Zelldeelung an dem Zelldout a Stammzellen déi en Entwécklungsstadium representéieren, kéint während der embryonaler Entwécklung schwéier Folgen hun. An eiser Studie konnte mir awer och feststellen, dass net nëmme LRRK2-G2019S eng Roll am Zelldout an an der Proliferatioun spillt me och de geneteschen Hannergrond

vum Patient ganz wichteg ass. Mir waren zum Beispill net an der Lag, déi Ënnerscheeder, déi mir gesinn hun, ze retten andeems mir d'Mutatioun corrigéieren, wat weist, dass aner Faktoren eng Roll spille mussen. Mir hunn dunn ënnersicht wei eng Faktoren dat kéinte sinn andeems mir eng genomesch Expressiounsanalyze gemaach hun. Ënnert de Kandidatgenen, déi ënnerscheedlech reguléiert waren, zwëschen de Patientelinnen an deene gesonde Linnen, war Serine Racemase, en Enzym dat L-Serine an D-Serine convertéiert. De Serine Metabolismus and D-Serine spillen eng wichteg Roll a verschidden neurodegenerative Krankheeten, an et as och gewisen dass Serine Parkinson Symptomer reduzéiere kann, an dass et eng wichteg Roll an der neuronaler Entwécklung spillt. Esou gesinn, ass D-Serine den ideale Kandidat vir d'Ënnerscheeder déi mir gesinn hun ze retten, andeems mir D-Serine op d'Zelle ginn. Den Traitement mat D-Serine konnt den Zelldout an d'Zelldeelung erëm op normal Levelen ajustéieren. Interessanterweis, konnte mir och gesinn dass am Blutt vu LRRK2-G2019S Patienten Serine Levele mei héich ware wei bei gesonde Leit an dëst war net de Fall a Patienten ouni déi Mutatioun. Dëst weist, dass et wahrscheinlech eng Verbindung tëschent LRRK2-G2019S an dem Serine Metabolismus gëtt. SRR Dereguléierungen kéinten eng Ursaach sinn, firwat verschidde Leit mei eng grouss Sensibilitéit fir Parkinson hunn ewéi anerer. Dës Entdeckung kéint potential wichteg si fir nei Traitementstrategien a fir d'Fréierkennung vun der Krankheet. Esou konnte mir am groussen a ganze beweisen dass Zelle vu Parkinson Patienten an engem entwécklungsbiologesche Stadium schonn Dereguléierungen opweisen, an dass déi Dereguléierungen deels un d'Mutatioun an awer och deels un de geneteschen Hannergrond vum Patient gebonne sinn. Dëst weist, dass Parkinson eng nach mei komplex Krankheet ass ewéi schon geduecht an dass et wichteg as d'Krankheet ze studéiere laang ier d'Motorsymptomer optauchen, fir erauszefanne wisou d'Nervenzellen am Gehir stierwen.

SUMMARY

Due to ethical implications and the limited availability of human neural tissue specimens, the discovery of induced pluripotent stem cells has drastically improved the generation of *in vitro* disease models. In this thesis, neural stem cells (NSCs) derived from induced pluripotent stem cells were used as *in vitro* models for studying neurodegenerative diseases like Parkinson's disease (PD). NSCs are physiologically relevant, lineage-committed and can give rise to neurons and glial cells, including dopaminergic neurons as well as astrocytes. *In vitro* disease modeling permits the unravelling of the complex mechanisms underlying the disease's manifestations. PD is an age-related progressive neurodegenerative disease that has been extensively studied *in vitro* using neurons and in particular dopaminergic neurons, while other cells from the CNS have been neglected. The death of dopaminergic neurons, most commonly within the adult brain, is – besides the aggregation of α-synuclein (*SNCA*) – the main characteristic of PD, and the loss of 70% of dopaminergic denervation at the late stages of the disease is typically responsible for its motor symptoms. The underlying causes of midbrain dopaminergic neuron cell death within the *substantia nigra pars compacta*, however, are poorly understood and the disease seems to start long before that. It is hypothesized that PD is a progressive neurodevelopmental disease, where diverse cumulative impacts at different stages of life trigger neurodegeneration and cause clinical Parkinsonism only in the late phases of the disease, in line with the so-called multiple hit hypothesis. Dopaminergic neurons seem to have a higher sensitivity towards the triggers causing PD compared to other neuronal populations. This leads to the hypothesis that the susceptibility is caused by a "first hit" resulting in a developmental deficiency during neurogenesis that predisposes for PD later in life. In line with this hypothesis, the focus is put on studying NSCs as models of embryonic neurogenesis to address the developmental defects underlying PD. The multifactorial hypothesis and the neurodevelopmental component might be especially relevant for the variant of PD that is induced by the glycine to serine substitution at the amino acid position 2019 (G2019S), a mutation in the leucine-rich repeat kinase 2 (*LRRK2)* gene. First, mutations in LRRK2 are of special interest as they represent not only the most common genetic cause of familial PD, but are also associated with non-familial sporadic cases of LRRK2-G2019S induced PD, and a single nucleotide polymorphism associated with LRRK2 makes it a common risk modifier. Secondly, the penetrance and age of onset in LRRK2-related PD is highly variable, includes asymptomatic carriers, and strongly depends on the individual genetic background, such as polymorphisms and ethnicity. Furthermore, the phenotypes associated with LRRK2 are highly diverse. LRRK2 was shown to be at the crossroad of different molecular pathways involved in PD. Regarding the neurodevelopmental manifestations, LRRK2 is already expressed in the developing CNS, and mutations in LRRK2 induce NSC deregulations. The different ages of onset and variable penetrance, together with the highly diverse phenotypes of

LRRK2-G2019S, suggest that there are genetic modifiers in the genetic background of patients that predispose them for developing PD. Given the role of LRRK2-G2019S in NSCs and its expression in development, this predisposition might already arise at the NSC level and impair proper neural development. The first aim of this thesis was to generate a novel induced pluripotent stem cell-derived NSC model that represents radial glial-like progenitors and is able to differentiate into mature astrocytes. The study of non-dopaminergic neuron models is of high importance for PD, as the triggers causing cell death at the late stage of the disease are still elusive. Astrocytes play an important role in dopaminergic neuron differentiation and in brain maintenance and integrity, and as such, could increase dopaminergic neuron susceptibility in PD. Hence, creating a model that recapitulates astrocytic development and is able to robustly generate functional, active, and mature astrocytes is of major importance in understanding PD. The second aim was to generate isogenic controls. As PD is a multifactorial disorder with multiple genetic contributions and LRRK2-G2019S was shown to be involved in a panoply of phenotypes, gene-edited isogenic control NSCs were used to distinguish between the LRRK2-G2019S-specific and background-related mechanisms underlying the disease. A new CRISPR-Cas9-based method that allows fast and deterministic genome editing was established and used as proof of principle for integrating a PD-causing mutation into *SNCA*. We were able to show that mutations in *SNCA* cause mitochondrial deficits in NSCs from a developmental stage, highlighting the role of PD-associated proteins in development. Our third and major objective was to study LRRK2-G2019S induced PD in NSCs. We observed major deregulations in patient NSC death and proliferation, providing further support for the role of PD causing factors in neurodevelopment. Interestingly, within NSCs, LRRK2-G2019S is sufficient but not necessary for inducing PD-associated phenotypes, meaning that the patient genetic background contributes to the phenotypes. In contrast, in the differentiated neurons, the phenotypes were mainly LRRK2-G2019S dependent, demonstrating that by studying dopaminergic neurons, the susceptibilities that might affect NSC maintenance and differentiation are potentially missed. To study the LRRK2-G2019S- and PD background specific genes underlying the NSC phenotypes, we performed a transcriptomic analysis. Interestingly, we discovered in both cases that genes involved in neurodevelopment are enriched. We further identified several differentially expressed genes that might underlie the genetic background related phenotypes that were not rescuable by gene-correcting LRRK2-G2019S. From these alterations, serine racemase (SRR) reduction qualified best as a genetic modifier, as it converts L-serine to D-serine, and serine metabolism plays a role in several neurodegenerative diseases. D-serine, for instance, has a CNS-specific function in neurotransmission and neuronal development. We hypothesized that a deficiency in D-serine is the driving force behind the phenotypes and eventually D-serine treatment rescued LRRK2-G2019S and genetic background dependent cell death and proliferation. Moreover, LRRK2-G2019S carrying patients

showed increased blood serine levels compared to healthy controls and idiopathic PD cases, suggesting an interplay between serine metabolism and LRRK2-G2019S in PD. Thus, the discovery of a novel susceptibility factor within LRRK2-G2019S carrying NSCs might open up new strategies for prevention, early diagnosis, stratification, and treatment of PD.

INTRODUCTION

INTRODUCTION

1 PARKINSON'S DISEASE

1.1 CHARACTERIZATION OF THE DISEASE

1.1.1 History

Parkinson's disease (PD) has been known to mankind since ancient times. Partial descriptions of PD can already be found in the ancient Indian medical system of Ayurveda and in Egyptian texts. In Western literature it was Galen, a Greek physician, who first referred to PD (García Ruiz, 2004). The first clear medical description, however, was only written 200 years ago by James Parkinson in An Essay on the Shaking Palsy, where he described the disease as follows in his definition of shaking palsy (*paralysis agitans*):

"Involuntary tremulous motion, with lessened muscular power, in parts not in action and even when supported; with a propensity to bend the trunk forward, and to pass from a walking to a running pace: the senses and intellects being uninjured." (Parkinson 1817)

A century later, in 1912, Friedrich Lewy discovered the central neuropathological feature of the disease, which was later named after him, the Lewy body (LB) (Lewy, 1912; Tretiakoff, 1919). The discovery of α-synuclein (α-SYN), the main component of the protein aggregations associated with Lewy bodies, represented another milestone in the exploration of PD (Spillantini *et al*., 1997). Nevertheless, the origin and the underlying mechanisms of the disease remain elusive until this day. Only recently, with the advances of the 21st century in genetics and neurobiology, did it become possible to elucidate the genetic causes of PD and thereby uncover the dimensions of its complexity.

1.1.2 Epidemiology, classification and aetiology

PD is currently the second most common neurodegenerative disease after Alzheimer's disease. It is a complex age-associated progressive disorder of the central nervous system (CNS) that affects 0.3% of the entire population. The prevalence of PD increases with age up to 1% in people over 60 (De Lau and Breteler, 2006). Other epidemiologic differences as variations between ethnic groups or between males and females are still controversially discussed, but it seems, that Caucasian males have a higher susceptibility compared to Asian females (Van Den Eeden, 2003; Pringsheim *et al*., 2014). PD is a highly variable disease with different ages of onset, progression, and mortality rates and has been classified as having two main forms (Hoehn and Yahr, 1967). 85% of those affected suffer from a sporadic, late-onset form of PD, whereas 15% are affected by familial heritable early onset PD (Klein and

Schlossmacher, 2006). Most sporadic cases remain idiopathic and only rarely correlate with one or more PD-associated risk factors, whereas most familial cases can be directly linked to one of the known monogenetic causes. Moreover, some diseases are classified under the umbrella term of "parkinsonian syndrome", including symptomatic secondary or acquired Parkinson syndrome and Parkinson plus syndromes that strongly resemble PD and share PD features, such as, multiple system atrophy, progressive supranuclear palsy and dementia with Lewy bodies (Massano and Bhatia, 2012).

The triggers causing PD are not well understood. As mentioned above, most of the cases are sporadic and idiopathic, and familial cases are relatively rare, which makes the aetiology complicated to assess. PD can have multiple origins and seems likely not to be a single disease, but rather an "interplay of phenotypically similar illnesses" (Dick *et al.*, 2007). Environmental and external risk factors, genetic predispositions, aging, as well as unknown factors can contribute to the onset and progression of PD (Wirdefeldt *et al.*, 2011). Most possibly, a combination of these various effects are causative of PD (Reeve *et al.*, 2014). So far, 34 gene loci have been identified and linked to familial PD (Brás *et al.*, 2015) (Table 1.). These include 11 Mendelian inherited genes causing autosomal dominant or recessive PD, and several very common genetic variants that represent low-risk loci, associated with PD through genome wide association studies (GWAS) (see section 1.2.1). Besides genetic predispositions, several environmental risk factors like the exposure to pesticides, insecticides, heavy metals, and rural life styles may contribute to the onset of PD (Dick *et al.*, 2007). Moreover, viral infections, head injuries, and intoxications can cause acquired Parkinsonism. In contrast, a diet rich in antioxidants and serine, coffee intake, increased circulating levels of uric acid, nicotine and exercise may have neuroprotective roles decreasing the incidence or the symptoms of PD (Cox *et al.*, 2016; Gelfin *et al.*, 2011; Guebila and Thiele, 2016; Nagashima *et al.*, 2016; Wirdefeldt *et al.*, 2011).

1.1.3 Symptoms and pathophysiology

Clinically, PD is characterized by motor and non-motor symptoms. The latter usually precede the motor disabilities by several decades (Chaudhuri and Schapira, 2009). The cardinal motor symptoms resume in Parkinsonism, a syndrome which typically includes resting tremor, bradykinesia, rigidity, postural instability and the loss of reflexes (Hoehn and Yahr, 1967). The disruption of the motor circuit is accompanied by a multitude of neuropsychiatric and sensory symptoms as well as sleep disorders. These non-motor symptoms include dementia, depression, apathy, anosmia, behavioral disorders, pain, anxiety, hallucinations, constipation, and restless leg syndrome to name a few (Chaudhuri and Schapira, 2009).

In terms of pathophysiology, PD is considered a synucleinopathy characterized and identified by the degeneration of dopaminergic neurons (DNs) in the *Substantia Nigra pars compacta* (*SNpc*) and the

accumulation of LBs and Lewy neurites (Hasseler, 1938; Ehringer and Hornykiewicz, 1960; Spillantin, 1997). However, it should be noted that not all PD patients suffer from LB pathology and that inclusions are found in asymptomatic carriers as well as in other PD-related syndromes (Braak *et al.*, 2003; Gaig *et al.*, 2007). Anatomically, besides the formation of inclusion bodies, the pathology can be identified by a reduction of neuromelanin pigmentation within the *SNpc* – a characteristic of DNs within that area. Physiologically, the degeneration of the DNs projecting from the *SNpc* into the putamen and the caudate nucleus of the striatum lead to a decrease of dopamine release (Lanciego *et al.*, 2012). The loss of almost 70% of dopamine signalling at the late stage of the disease results in severe deficiencies within the nigrostriatal motor pathway of the basal ganglia, which is responsible for learning and the execution of motor functions (Cheng *et al.*, 2010; Lanciego *et al.*, 2012) (Figure 1). Consequently, the dopamine depletion of the motor circuits directly leads to the above-described motor symptom occurrences and progression.

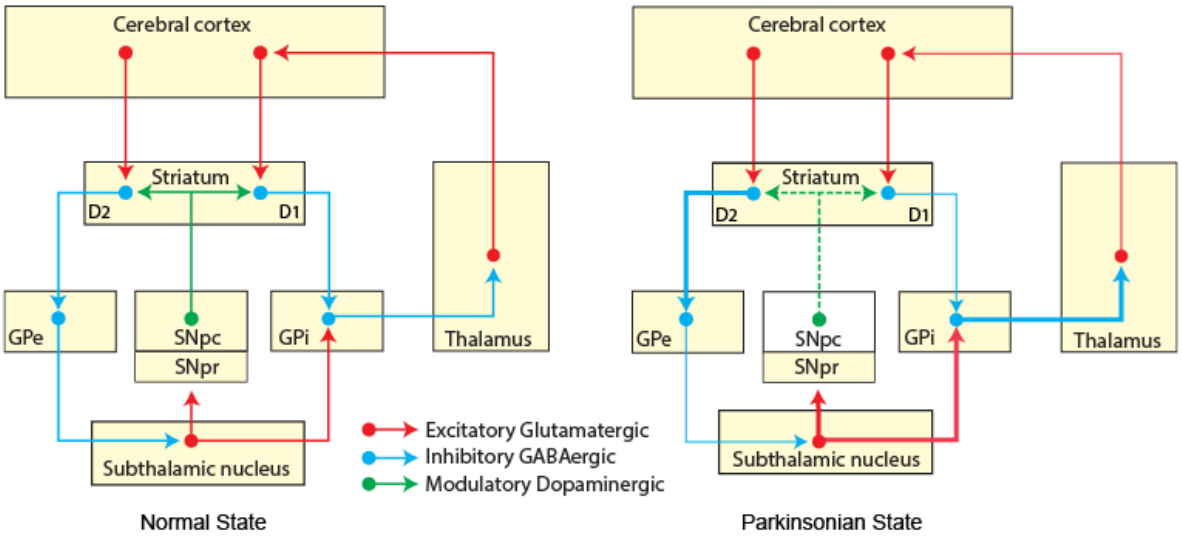

Figure 1. Schematic representation of the motor circuit of the basal ganglia during normal and parkinsonian states. Modified from Lanciego *et al.*, 2012. The system is composed of a cortico-striatal projection and two major pathways leading from the striatum to the internal and external globus pallidus (GPi and GPe), with one being direct (D1: promoting movement) and the other indirect (D2: inhibiting movement). The third projection closing the loop leads from the GP to the thalamus and back to the cortex. Please note that the thickness of the arrows indicates hyper- or hypoactivity. For PD, the loss of dopaminergic signalling from the *SNpc* to the striatum leads to a hypoactivity towards the cortex and reduced kinesia. Please also note that a glutamatergic hyperactivity within subthalamic nucleus towards the *Substantia Nigra pars reticularis* (*SNpr*) worsens PD symptoms, as will be elaborated in chapter C of the discussion.

In 2003, Braak and colleagues classified the disease into six different stages with three pre-symptomatic and three symptomatic stages, based on the anatomical examination of PD patient brains. The autopsies led them to the hypothesis that the disease follows a well-defined pattern depending on the brain regions involved, especially regarding LB pathology (Braak *et al.*, 2003). According to Braak, the disease starts in the olfactory bulb, the enteric and peripheral autosomal nervous system, and the lower brain stem to only proceed to the *SNpc* at stage 3-4, where the first motor symptoms occur. While, it

is difficult for laboratories to routinely assess all brain regions included in the staging and individual variabilities may occur, the system correlates well with the progress of the disease. The first motor symptoms that are direct signs of neurodegeneration, for instance, only occur after the reduction of 50% of dopaminergic innervation and degeneration increases independently of the age of onset and linearly to the last stage of the disease (Scherman *et al*., 1989; Riederer and Wuketich, 1976). Furthermore, the oft neglected non-motor symptoms, which include constipation, hyposmia and sleep disorders, often occur decades before the motor symptoms and correlate with Braak's defined areas of origin (Goedert *et al*., 2013).

1.1.4 Molecular mechanisms of PD

On a cellular level, the loss of up to 70% of DNs may be the result of an interplay between different factors (Cheng *et al*., 2010). The accumulation, aggregation, spreading and ubiquitination of α-SYN may be toxic for the cells and directly lead to neurodegeneration. Furthermore, other mechanisms leading to neuronal cell death may be impaired. For instance, hallmarks of PD are mitochondrial dysfunction, the accumulation of reactive oxygen species, proteasomal and lysosomal dysfunctions, calcium dyshomeostasis, synaptic deficiencies and neuro-inflammation which all play an important role in neurodegeneration (Figure 2).

α-Synuclein aggregation

As mentioned above, α-SYN (*SNCA*) is the main component of LBs and has been associated with different neurodegenerative diseases characterized as synucleinopathies. In PD, mutations in *SNCA* as well as duplications and triplications of the wild type (WT) allele are found in dominantly inherited cases (see section 1.2.1.) (Krüger *et al*., 1998; Polymeropoulos *et al*., 1997; reviewed in Bendor *et al*., 2013). Furthermore, common variants of α-SYN are associated with an increased risk for developing sporadic PD (Cookson, 2009; Mueller *et al*., 2005). The physiological role of α-SYN is associated with synaptic transmission and membrane trafficking, such as vesicle transport, synaptic plasticity and dopamine release, although its precise function is still unknown (Bendor *et al*. 2013). In PD, however, its main pathologic feature is the formation of insoluble inclusions. Under physiological conditions, α-SYN occurs as a monomer or tetramer and only forms (proto-) fibrils and oligomers upon pathogenic aggregation (Bartels *et al*., 2011; Vekrellis *et al*., 2004). The accumulation can be explained by either an overproduction, as seen in duplication and triplication phenotypes, or by a deficiency in protein clearance (Bendor *et al*., 2013). Different pathways that are affected or can be disrupted in PD regulate proper synuclein degradation. Protein clearance is linked to improper ubiquitination and proteasomal degradation or depends on macro- and chaperone-mediated-autophagy (Bendor *et al*., 2013). Besides protein levels and improper clearance, misfolding of α-SYN, for instance upon a mutation, plays a crucial

part in its accumulation and aggregation process. Synuclein misfolding may self-propagate and the misfolded protein is thought to spread throughout the brain, as well as from host to graft tissue, making synucleinopathies resembling prion-like diseases (Recasens and Dehay, 2014). Hence, α-SYN misfolding and aggregation can be both the cause and consequence of pathways deregulated in PD. Interestingly, it is still subject to some controversy whether aggregated and misfolded α-SYN is toxic for the cell. The most widely held opinion is that it induces neurodegeneration by blocking the transport between the endoplasmic reticulum and the Golgi, by decreasing synaptic vesicle release and impairing energy production and protein degradation (Cookson, 2009). As mentioned above, the misfolded and aggregated protein is stored in LBs within the cells. The physiological role of the inclusions and their contribution to neuronal cell loss, however, still remain elusive. Although it is known that *SNCA* is a causative gene for PD and that LB pathology is a common feature among most PD cases, it is not clear if the inclusions are causative or consequential of the disease (Cookson, 2009). Two hypotheses exist regarding synuclein aggregation and LB toxicity. The question remains whether the inclusions cause cell death or whether they have a protective function. Interestingly, in PD α-SYN is not the only component of LBs. Besides α-SYN inclusions, Parkinsonism is often accompanied by the aggregation of microtubule-associated protein TAU (tautopathy) and mutations in its gene are commonly associated with an increased risk of developing PD (see section 1.2.2.) (Dickson, 2012; Spillantini and Goedert, 1998). Note that TAU is the main component of neurofibrillary tangles in Alzheimer's disease, and in PD it interacts with α-SYN to form filaments within LBs (Clinton *et al*., 2010; Ishizawa *et al*., 2003; Pollanen *et al*., 1992). Hence, the aggregation and inclusion of α-SYN into insoluble LBs is not synuclein and PD specific and may have a cytoprotective function in order to reduce the exposure to the toxic protein (Tanaka *et al*., 2004). Accordingly, neurons of the *SNpc* with LBs showed, for instance, the same amount of apoptotic cells as neurons without inclusions (Tompkins and Hill, 1997). Moreover, other types of neurons are similarly affected by LBs, showing that LBs may be an epiphenomenon of the disease (Goedert *et al*., 2013). In addition, the cells with LBs generally survive until autopsy in the case of a PD diagnosis. Furthermore, LB pathology has also been reported in a number of healthy individuals (Markesbery and Jicha, 2009). In contrast to the neuroprotective role, it has been widely found *in vitro* that in particular LB-bearing cells die and that α-SYN is toxic for DNs in a dose-dependent manner (Cookson, 2009; Xu *et al*., 2002). Moreover, injections of synthetic α-SYN fibrils into mouse models, or mutant human α-SYN into the *SNpc* of marmosets, causes toxic accumulations and leads to neurodegeneration of inclusion bearing cells (Kirik *et al*., 2003; Luk *et al*., 2012; Osterberg *et al*., 2015). In addition, in human brain tissue, inclusion formation and the resulting LBs were shown to be cytotoxic leading to microtubule regression and mitochondrial and nuclear degradation (Power *et al*., 2015). Altogether, it seems that

aggregated misfolded α-SYN is able to induce cytotoxicity in different contexts and models, but its exact role within the human brain and especially within LBs remains elusive.

Mitochondrial dysfunctions

Mitochondria (*mitos* "thread" and *chodrion* "granule") are double-membraned organelles of eukaryotic cells, which have evolved through endosymbiosis with independent genomes and represent the major energy source of the cell by generating ATP through oxidative phosphorylation. Furthermore, they harbor the tricarboxylic acid (TCA)/KREBS cycle, are involved in lipid and amino acid metabolism, calcium homeostasis, the production and scavenging of free radicals and controlling programmed cell death. Owing to their vital functions in cellular integrity, mitochondrial dynamics need to be tightly regulated. Under general physiological conditions mitochondria undergo constant movement, as well as fission and fusion events to repair damaged components, and regulate mitochondrial homeostasis. Furthermore, mitochondrial quality is controlled by their own proteolytic system, interactions with the proteasome and damaged mitochondria are removed via mitophagy (autophagy of mitochondria see Protein trafficking and degradation), mitochondrial derived vesicles and mitochondrial spheroids (Ni *et al*., 2015).

Mitochondrial dysfunctions in PD are linked to increased cellular respiration, membrane depolarisation events, reactive oxygen species accumulation, and deficiencies in mitochondrial degradation. The relation between PD and mitochondria was for instance discovered through the coincidence that a designer drug, containing 1-methyl- 4-phenyl-1,2,3,4-tetrahydropyridine (MPTP), caused Parkinsonism in drug abusers by inhibiting oxidative phosphorylation (Betarbet *et al*., 2000). Rotenone, another toxin, inhibiting the complex I of the electron transport chain is also able to reproduce PD-associated phenotypes (Langston *et al*., 2010). Moreover, damage caused by reactive oxygen species, such as protein oxidation and nitration, DNA breaks and lipid oxidation, are cellular hallmarks within PD patients (Keane *et al*., 2011). Interestingly, proteins involved in reactive oxygen scavenging, mitophagy and proteasomal degradation, as well as the damaged and misfolded proteins resulting from mitochondrial stress, genetically link or cause PD (further elaborated in section 1.2.1.). The relationship between protein accumulation, mitochondrial stress, and reactive oxygen species has been clearly established in α-SYN transgenic mice, where *SNCA* overexpression impairs mitochondria, increases oxidative stress, and enhances the toxic effects induced by MPTP (Song *et al*., 2004). Moreover, mutated α-SYN (see section 1.2.1) induced mitochondrial degeneration in another mouse model and mitochondria were stained positive for human transgenic *SNCA*, elucidating a potential direct link between synuclein and mitochondrial damage (Martin, 2006). Finally, damaged mitochondrial DNA, impaired mitochondrial dynamics, calcium dis-homeostasis, dopamine oxidation, and mitochondrial induced cell death through

the loss of membrane potential are mitochondrial-related pathways that contribute to the PD pathogenesis (Abou-Sleiman *et al.*, 2006; Keane *et al.*, 2011).

Protein trafficking and degradation

As already described for α-SYN improper protein degradation and accumulation is one the major hallmarks of PD. The major fraction of α-SYN is degraded by chaperone-mediated autophagy within the lysosome (Cuervo, 2004). Besides synuclein, other proteins involved in the protein clearing and trafficking pathway have been shown to be deregulated or mutated in PD (Roosen and Cookson, 2016) (Table 1). Protein trafficking and degradation is characterized by three major pathways, namely endo/exocytosis, autophagy and proteasomal degradation. During endocytosis, extracellular particles are engulfed by the plasma membrane to form endosomes. The engulfed- and membrane proteins are either recycled through early endosomes and recycling endosome formation, brought back to the Golgi by the retromer complex or degraded by late endosomal fusion with a lysosome (Galvez *et al.*, 2012). Exocytosis represents the opposite pathway, the transport from the *trans*-Golgi to the plasma membrane and the cell exterior. Besides protein trafficking, proper protein degradation is essential. Autophagy is defined as the process of degrading intra- or extracellular compartments by the fusion of autophagosomes with lysosomes. Three different kinds of autophagy exist: macro-, micro- and chaperone-mediated autophagy. Mitochondrial autophagy (mitophagy), for instance can be mediated by all three processes and its malfunction may result, as described above, in severe cellular defects. Whereas the endosomal and autophagic pathway directly interplay on the lysosomal level, a second independent protein degrading mechanism further guarantees proper protein turnover and homeostasis. The ubiquitin proteasome pathway specifically degrades damaged and misfolded proteins within the cytoplasm.

Dysfunction in vesicular trafficking and protein degradation have been shown to be one of the mechanism underlying PD. Proper vesicular trafficking and degradation are especially important for neurons to maintain synaptic function. In DNs, endocytosis is needed to recycle synaptic vesicles and receptors, and exocytosis releases neurotransmitters (Buckley *et al.*, 2000). Mutations in proteins regulating one of these major pathways might be sufficient to dramatically increase the risk of developing PD. The main molecules regulating the endosomal-lysosomal pathways, for instance, are the Rab (Ras related in brain) family of small GTPases, where several of the members have been linked to PD (MacLeod *et al.*, 2006; Steger *et al.*, 2016). Moreover, other vacuolar sorting proteins such as VPS proteins (vacuolar protein sorting), SNARE proteins (soluble NSF attachment protein receptor), clathrin mediated trafficking proteins, transmembrane (TMEM) proteins, synaptogamins and α-SYN itself are involved in vesicular trafficking and were shown to be deregulated in PD (Roosen and Cookson, 2016).

In addition, proteins involved in proper ubiquitination and de-ubiquitination, which is essential for proteasomal protein degradation, have been shown to cause familial PD (Table 1). In contrast to improper protein degradation, in the case of PD, different disease-associated genes are regulated and regulate or limit protein production by microRNA (miRNA) interference (Sonntag, 2010). Furthermore, the endosomal protein trafficking pathway gives rise to melanosomes, strongly resembling the neuromelanin pigment granules within DNs (Fedorow *et al.*, 2005). Although the exact pathway of neuromelanin production and function remains unknown, it might be involved in both neuroprotective and neurotoxic mechanisms (Fedorow *et al.*, 2005).

Neuro-inflammation and the contribution of microglia and astrocytes to PD

The brain is not, as was believed during the last century, an immune privileged site. Rather, it participates actively in the inflammatory and immune response, and was recently discovered to be in direct contact with meningeal lymphatic vessels (Louveau *et al.*, 2015; Ransohoff and Engelhardt, 2012). Neuro-inflammation is a complex phenomenon that can have both beneficial and detrimental effects on brain function and represents a common feature of all the neurodegenerative diseases. During brain inflammation, both pro- and anti-inflammatory cytokines are released that can either lead to neuronal dystrophy or regeneration and tissue repair. The main players in the inflammatory response of the brain are microglial cells and astrocytes. Whereas microglia represent the resident macrophages of the brain, the main characteristic of astrocytes in the immune response, besides cytokine release, similar to microglial cells, is reactive astrogliosis (scar tissue formation). The physiological role of astrocytes will be further described in section 2.1.3. At this day, the occurance of astrogliosis in PD is still controversally discussed, but most authors report minimal or no astrogliosis in PD post-mortem brains (Mirza et al., 1999; Song et al., 2009). Nevertheless, microglia, astrocytes, and the immune system are involved in the inflammatory reactions during neurodegeneration. One hypothesis is that inflammation is not consequential of neurodegeneration, but rather causative and that midbrain DNs are selectively vulnerable to the immune response (Deleidi and Gasser, 2013). In the *SNpc* of post mortem brain tissue from patients, activated microglia and an elevated level of cytokines have been detected together with mild astrogliosis (Deleidi and Gasser, 2013). The cytokines excreted - during the inflammatory response for instance - are able to impair synaptic transmission and axonal transport, which increases neuronal susceptibility (Deleidi and Gasser, 2013). Furthermore, blocking inflammation using anti-inflammatory drugs attenuated DN degeneration in mouse models (Deleidi and Gasser, 2013). Also, several proteins involved in PD have been directly linked to impairments of the immune system (Table 1), were shown to activate microglia and astrocytes, and are highly expressed within those cell types (Deleidi and Gasser, 2013). Additionally, α-SYN is not only highly expressed within astrocytes, but inclusions have been observed within these cells, which may result from endocytosis of

misfolded α-SYN excreted by neurons (Braak et al., 2007). Interestingly, compared to other neurodegenerative diseases, the attenuated reactivity of astrocytes in PD, might be linked to their accumulation of α-SYN (Song et al., 2009; Tong et al., 2015). All in all, the study of both microglial cells and astrocytes in PD is of major importance in order to understand the disease in its entirety.

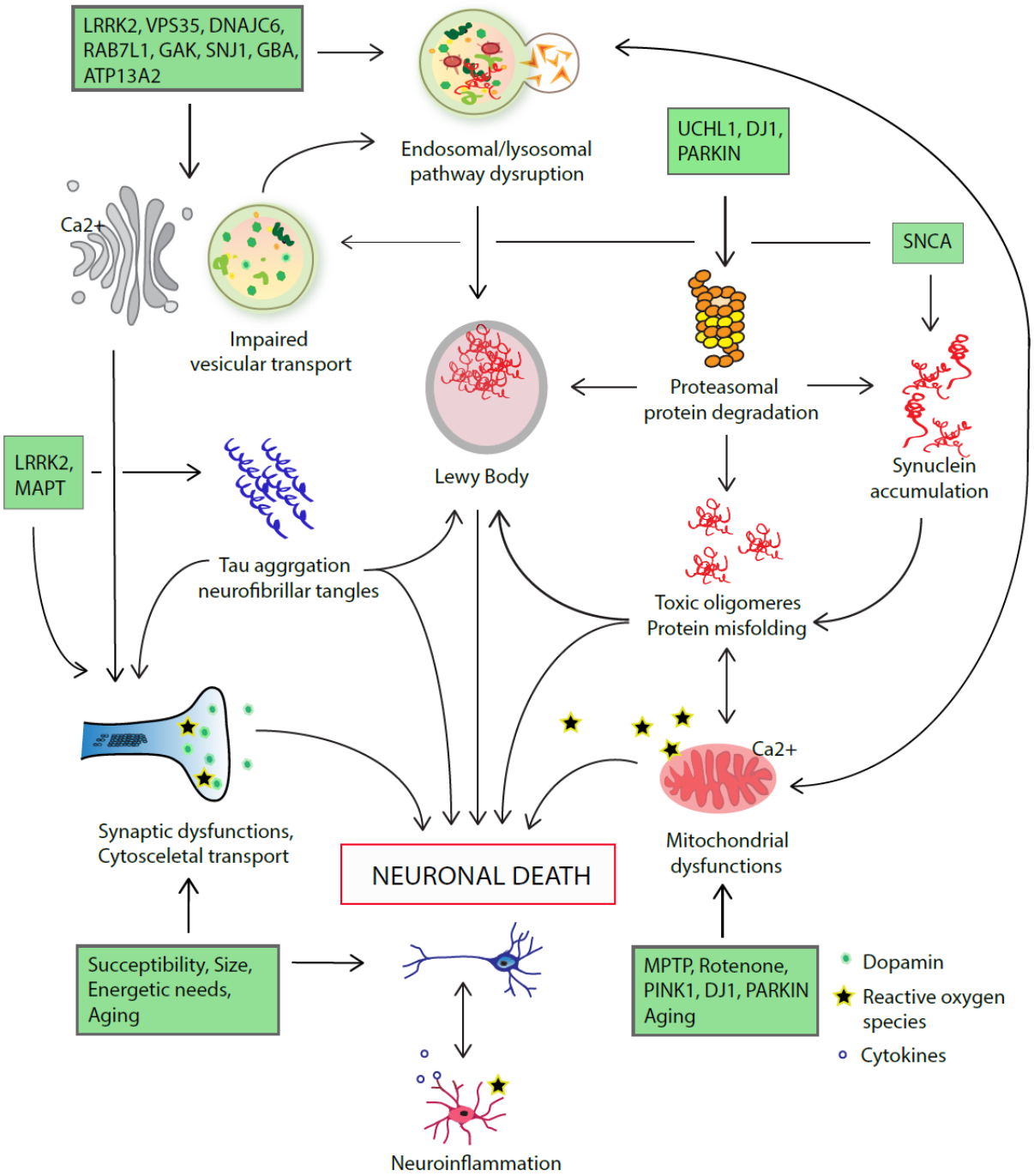

Figure 2. Molecular hallmarks and mechanisms underlying PD. Inspired from Farrer, 2006. LB formation, accumulation of α-SYN and TAU, protein degradation and vesicular trafficking pathways as well as mitochondrial, synaptic and cytoskeletal dysfunctions and neuroinflammation are major hallmarks of the disease. Inflammation is characterized by microglia or reactive astrocyte activation. The contribution of the mutations to the disease will be described in section 1.2. For gene abbreviations see Table 1.

1.1.5 DN cell death and susceptibility

The selective vulnerability of DNs may play an important role in understanding the disease. The precise loss of DNs within the *SNpc* might be linked to their increased vulnerability to the molecular mechanisms of PD. Increased vulnerability could be partially explained by their morphology. Compared to other neurons, midbrain DNs are very big, have a very long, complex axon arborisation with a massive number of synapses, and are often poorly myelinated (Braak *et al.*, 2003; Pacelli *et al.*, 2015; Sulzer, 2007). With an average axonal length of 466,800 µm, an estimated number of 4438-24,998 branching points and 100,000-250,000 synapses, DNs are much bigger than, for instance, human adult pyramidal neurons (length=10,000-30,000 µm, branching points=56, synapses=30,000) (Mohan *et al.*, 2015; Pissadaki and Bolam, 2013). These physiological aspects make axonal transport, such as mitochondrial-, vesicular-, and autophagic vacuole trafficking as well as membrane maintenance, more difficult (Sulzer, 2007). Additionally, DNs have very high energetic needs, and operate close to their maximal energy production capacity (Pacelli *et al.*, 2015). To propagate and recover the action potential through a DN with a total length of 4 m (axons plus dendrites and 17 levels of branching points), costs $9.36x10^{10}$ ATP molecules (Pissadaki and Bolam, 2013). This energetic cost is an order of magnitude greater than what a rat DN needs and might explain why PD is a human specific disease (Pissadaki and Bolam, 2013). Together, these characteristics make them more prone to all kinds of physiological stress, such as reactive oxygen species, mitochondrial dysfunctions and aging (Pacelli *et al.*, 2015). Any situation that perturbs the energetic balance can easily "tip them over the edge" and lead to neuronal cell death (Pissadaki and Bolam, 2013). Furthermore, DNs have several unique characteristics. Ca2+ dependent pace-making to maintain dopamine levels, and dopamine handling itself are, for instance, two mechanisms that come at a high metabolic cost and can lead to endoplasmic reticulum induced stress, protein unfolding and the production of reactive oxygen species (González-Hernández, 2010). Nevertheless, midbrain DNs other than those from the *SNpc* are not – or not so strongly – affected in PD. Compared to the A9 DNs from the nigrostriatal pathway, the neighboring A10 DNs in the ventral tegmental area from the mesolimbic and mesocortical pathways, responsible for reward-related cognition and executive functions, are relatively spared (Hirsch *et al.*, 1988). Furthermore, non-DNs (such as serotonergic, noradrenergic, and cholinergic neurons) and a multitude of other brain regions (such as the brain stem, olfactory bulb, and neurogenic niches) are affected in PD (Cookson, 2009; Langston, 2006). In the end, the loss of DNs in the *SNpc* must only be considered as the tip of the iceberg and investigating what lies beneath should be of major importance in achieving a better understanding of PD (Langston, 2006).

1.1.6 Diagnosis and treatment

Due to the complexity of the disease, as described in the paragraphs above, the triggers and molecular mechanisms leading to the onset and progression of PD, and ultimately to irreversible DN degeneration and cell death, are still not fully understood. As such, to this day, PD pathogenesis remains largely elusive with no effective cure. Diagnosis of PD is very difficult because of the lack of biomarkers and is often exclusively based on clinical features such as the motor symptoms (Wirdefeld *et al*., 2011). However, the associated movement disorders only occur after at least 50% of the nigral neurons have been lost, which dramatically reduces the chances of an effective treatment. For future therapies and prevention strategies, the discovery of early diagnostics and markers is necessary. The target of choice would be a biomarker linked, for instance, to the appearance of the early non-motor symptoms, or even better: a biomarker that assesses the individual's condition before the appearance of any symptoms. As previously mentioned, PD remains until today a disease with no effective cure. The most common and promising disease-modifying treatment is based on levodopa paired with dopa-decarboxylase (AADC) activators (dopamine production) or catechol-*o*-methyltransferase (COMT) inhibitors (dopamine degradation) and dopamine agonists, which are able to reduce the symptoms but not the outcome of the disease (Calne *et al*., 1969; Bonifácio *et al*., 2007) (for further details on dopamine metabolism, see also section 2.1.2 and discussion chapter A). Experimental strategies that have not yet received Food and Drug Administration approval are based on inhibiting the mutated proteins underlying familial PD. In addition, deep brain stimulation is a surgical option for severe cases and levodopa-resistant patients. Other possibilities being explored are stimulating endogenous neurogenesis and personalized autologous cell replacement therapies. Due to the existence of induced pluripotent stem cells (iPSCs) (see section 2.4.1), it is now possible to produce patient-specific stem cells and neurons that could potentially be used for regenerative therapeutic purposes, and clinical trials have already showed promising results in the treatment of PD (Fu *et al*., 2015).

1.2 GENETICS OF PD

1.2.1 Genetic contributions

Gene official symbol	Gene name	Location	Possible pathways / pathological biological processes
MENDELIAN GENES			
SNCA	Synuclein, alpha	4q21	Synaptic function; mitochondrial function; autophagy/lysosomal degradation
PARK2	Parkin RBR E3 ubiquitin protein ligase	6q25.2-q27	Mitochondrial function/mitophagy; ubiquitination; synaptic function
PINK1	PTEN -induced putative kinase 1	1p36	Mitochondrial function/mitophagy
PARK7/DJ-1	Parkinson protein 7	1p36.23	Inflammation/immune system; mitochondrial function
LRRK2	Leucine-rich repeat kinase 2	12q12	Synaptic function; inflammation/immune system; autophagy/lysosomal degradation
PLA2G6	Phospholipase A2, group VI	22q13.1	Mitochondrial function
FBXO7	F-box protein 7	22q12.3	Ubiquitination; mitochondrial function/mitophagy
VPS35	Vacuolar protein sorting 35 homolog (*S. cerevisiae*)	16q12	Autophagy/lysosomal degradation; endocytosis
ATP13A2	ATPase type 13A2	1p36	Mitochondrial function; autophagy/lysosomal degradation
DNAJC6	DnaJ (Hsp40) homolog, subfamily C, member 6	1p31.3	Synaptic function; endocytosis
SYNJ1	Synaptojanin 1	21q22.2	Synaptic function; endocytosis
RISK GENES			
GBA	Glucosidase, beta, acid	1q21	Inflammation/immune system; autophagy/lysosomal degradation; metabolic pathways
RISK LOCI			
MAPT	Microtubule-associated protein tau	17q21.1	Microtubule stabilization and axonal transport
RAB7L1	RAB7, member RAS oncogene family-like 1	1q32	Autophagy/lysosomal degradation
BST1	Bone marrow stromal cell antigen 1	4p15	Immune system
HLA-DRB5	Major histocompatibility complex, class II, DR beta 5	6p21.3	Inflammation/immune system
GAK/	Cyclin-G-associated kinase	4p16	Autophagy/lysosomal degradation; synaptic function; endocytosis
ACMSD	Aminocarboxymuconate semialdehyde decarboxylase	2q21.3	Tryptophan metabolism; metal ion binding; metabolic pathways
STK39	Serine threonine kinase 39	2q24.3	Inflammation/immune system; protein kinase binding; cellular stress response
SYT11	Synaptotagmin XI	1q21.2	Synaptic function; transporter activity; metal ion binding; substrate for PARK2
FGF20	Fibroblast growth factor 20	8p22	Growth factor activity; FGF receptor binding
STX1B	Syntaxin 1B	16p11.2	Synaptic function; SNAP receptor activity; protein domain-specific binding
GPNMB	Glycoprotein (transmembrane) nmb	7p15	Integrin binding; heparin binding; cancer pathways
SIPA1L2	Signal-induced proliferation-associated 1 like 2	1q42.2	GTPase activator activity
INPP5F	Inositol polyphosphate-5-phosphatase F	10q26.11	Phosphoric ester hydrolase activity
MIR4697HG	MIR4697 host gene (non-protein coding)	11q25	
GCH1	GTP cyclohydrolase 1	14q22.1-q22.2	GTP binding; calcium ion binding; BH4 metab; metabolic pathways
VPS13C	Vacuolar protein sorting 13 homolog C (*S. cerevisiae*)	15q22.2	Endocytosis
DDRGK1	DDRGK domain containing 1	20p13	Protein binding
MCCC1	Methylcrotonoyl-CoA carboxylase 1 (alpha)	3q27	Biotin carboxylase activity; methylcrotonoyl-CoA carboxylase activity; metabolic pathways
SCARB2	Scavenger receptor class B, member 2	4q21.1	Autophagy/lysosomal degradation; receptor activity (lysosomal receptor for GBA targeting); enzyme binding
CCDC62	Coiled-coil domain containing 62	12q24.31	Nuclear receptor coactivator; cancer pathways
RIT2	Ras-like without CAAX 2	18q12.3	Synaptic function; calmodulin binding; GTP binding
SREBF1	Sterol regulatory element binding transcription factor 1	17p11.2	Chromatin binding; cholesterol and steroid metabolic processes

Table 1. Genetics of PD (Brás *et al.*, 2015). 11 Mendelian inherited genes, one non-inherited gene with high risk and 22 common risk modifiers are linked to PD. Genes are involved in mitochondrial function, inflammation, synaptic dysfunctions, and endo-, phago-, lysosomal pathways.

As previously described, PD is a multifaceted and multifactorial disease with major genetic contributions. However, only 5-15% of patients suffer from familial PD, caused by one of the above-mentioned multiple monogenetic genes, with classical Mendelian inheritance (Table 1). The five major familial PD related genes that conclusively cause dominant or recessive PD are *SNCA*, E3 ubiquitin ligase (*PINK1),* pten induced putative kinase 2 *(PARK2)*, protein deglycase daisuke-junko 1 (*DJ-1)* and leucine rich repeat kinase 2 (*LRRK2)* (Brás *et al.*, 2015; Kalinderi *et al.*, 2016; Lesage and Brice, 2009). The scientific community has mainly concentrated on studying the mutation-related cases in order to elucidate the underlying molecular mechanisms of PD pathogenesis as described in Figure 2 of section 1.1.4. Most of these genes are closely associated to α-SYN aggregation, the phagosomal/lysosomal protein clearing pathway, synaptic and mitochondrial dysfunctions, and the immune response (Table 1 and Figure 2 in section 1.1.4.) (Shin *et al.*, 2009). The different mutations in *SNCA*, E46K, A53T, and A30P cause dominantly inherited PD (see also section 1.1.4.) (Krüger *et al.*, 1998; Polymeropoulos *et al.*, 1997;

Zarranz *et al*., 2004; reviewed in Bendor *et al*., 2013). All three mutations were shown to enhance α-SYN aggregation and fibril formation (Bertoncini *et al*., 2005; Narhi *et al*., 1999). Furthermore, duplications and triplications of the WT allele are found to cause a dose-dependent aggregation of α-SYN resulting in PD (Chartier-Harlin *et al*., 2004; Fuchs *et al*., 2007; Singleton *et al*., 2013). The major PD-causing genes involved in mitochondrial stress are *DJ-1*, *PINK1,* and *PARKIN*. *DJ-1* encodes an enzyme that functions as a peroxidase in scavenging reactive oxygen species and has been linked to autosomal dominant PD (Bonifati *et al*., 2003). Mutations in *PINK1*, an important protein regulating mitochondrial dynamics, such as fission and fusion events as well as quality control through mitophagy causes autosomal recessive PD (Valente *et al*., 2004). PARKIN*,* another protein involved in mitochondrial degradation, is a ligase involved in mitochondrial protein ubiquitination and consequently, its mutation leads to improper mitophagy and causes mitochondrial stress-related recessive PD (Greene *et al*., 2003; Kitada *et al*., 1998). Besides mitochondrial deficiencies many proteins underlying PD are involved in the protein trafficking and clearing pathway. These include, LRRK2, the dnaJ6 heat shock protein family (HSP40) member c6 (DNAJC6), the vacuolar protein sorting-associated protein 35 (VPS35), α-SYN, and the risk modifiers glucosylceramidase beta (GBA) and the Ras oncogene family member 7L1 (RAB7L1), to name a few (Roosen and Cookson, 2016). The role of *LRRK2* – the most common genetic cause of PD – will be extensively elaborated on in section 1.2.2. Interestingly, all the different mutations mentioned above lead to a similar phenotypic outcome that clinically results in PD. However, while the final outcome of the inherited cases is similar, the symptoms and progression of the disease is highly individual. The penetrance of the different mutations, for instance, is often incomplete and the age of onset of the disease is highly variable, including early onset and juvenile cases such as seen in cases carrying mutations in *DNAJC6* and *PARKIN* (Kitada *et al*., 1998; Köroğlu *et al*., 2013; Sánchez-Danés *et al*., 2012). Whereas some mutations cause mutation-specific symptoms and progression, others like LRRK2-G2019S strongly resemble idiopathic cases (Cheon *et al*., 2012; Lesage *et al*., 2006). Moreover, variable expressivity of a mutation within the same family, and phenocopy phenomena, in which a patient shows similar symptoms as their relatives but without carrying the disease causing mutation, play an important role in the disease (Klein and Schlossmacher, 2006; Klein and Westenberger, 2012).

Besides the rare Mendelian inherited genes, many common risk factors exist that might underlie and enhance the risk of developing sporadic PD. In sporadic forms, the age of onset is often later, indicating that aging and environmental factors might play major roles. The most strongly associated risk locus is found within the *GBA* gene that was discovered because of a correlation between Gaucher's disease and Parkinson's disease within the same families (Lwin *et al*., 2004; Sidransky and Lopez, 2014). Mutations in GBA are leading to an increased risk of PD, but without Mendelian inheritance (Table 1). Another locus correlating with an increased risk of developing PD is, as previously mentioned in section

1.1.4, the microtubule associated protein TAU *(MAPT)*. *MAPT* was shown to be a common genetic variant correlating with sporadic PD cases (Charlesworth *et al*., 2012; Simón-Sánchez *et al*., 2009). For most of the sporadic cases, however, only vague correlations between risk loci and the origin of PD can be drawn and they remain idiopathic with no known underlying genetic cause. Nevertheless, evidence suggests that in idiopathic cases, there might also be a genetic component (Sánchez-Danés *et al*. 2012). In fact, PD-associated phenotypes like DN degeneration could be reproduced in iPSC-derived DNs from patients having idiopathic PD, showing that the reason for neurodegeneration must be encoded in their genome (Sánchez-Danés *et al*., 2012). Most probably a combination of age, environmental factors and risk modifiers or unknown genetic susceptibility factors cause sporadic, idiopathic PD (Kitada *et al*., 1998).

One hypothesis for the origin of PD is the "multiple hit hypothesis", where different factors and different mutations are additive and interact to ultimately converge and form the PD syndrome (Sulzer, 2007). This hypothesis is given credence by the fact that some Mendelian inherited mutation carriers also remain asymptomatic (see section 1.2.2) (Hillje and Schwamborn, 2016). In addition, the different susceptibility factors, genes, risk loci, and polymorphisms associated with PD interplay to increase susceptibility, severity, and age of onset of the disease, as will be further elucidated for LRRK2 in section 1.2.2 (Davis *et al*., 2016). Moreover, two different hypotheses exist to explain the contribution of age to the disease. While the first one propounds an increase in susceptibility of DNs over a life time in which aging is the major cause for developing PD, the other follows the multiple hit hypothesis, assuming that PD arises from an accumulation of different insults (Bourdenx *et al*., 2015; Hillje and Schwamborn, 2016). These insults occur independently of aging, and aging represents, only an aggravating factor, if any (Bourdenx *et al*., 2015; Hillje and Schwamborn, 2016). Overall, the high number of different mutations leading to the same disease, their partly incomplete penetrance and the fact that idiopathic cases might also have a genetic contribution suggests that in patients suffering from all sorts of PD, modifiers and susceptibility factors in the genetic background should have major contributions to the disease's manifestations.

1.2.2 LRRK2 and LRRK2-G2019S

Epidemiology and expression

LRRK2 is also called Dardarin. Its name is derived from the Basque word “dardara”, which means “to tremble”. With an abundance of around 10%, mutations within LRRK2 are the most frequent genetic cause of dominant familial Parkinson’s disease and are found in 2% of PD patients suffering from a sporadic form without familial history (Clark *et al.*, 2006; Gilks *et al.*, 2005; Healy *et al.*, 2008; Klein and Schlossmacher, 2006). Additionally, protein coding variants, and a single nucleotide polymorphism (SNP) in the non-coding region of the *LRRK2* gene have been linked to an increased risk of developing PD, which makes LRRK2 both a rare causative gene and a common risk modifier (Figure 3) (Di Fonzo *et al.*, 2006; Nalls *et al.*, 2014). Moreover, the familial cases, including G2019S, symptomatically resemble idiopathic cases, typically having a mid to late onset and following a slow progression (Gatto *et al.*, 2013; Klein and Schlossmacher, 2006; Lesage *et al.*, 2006).

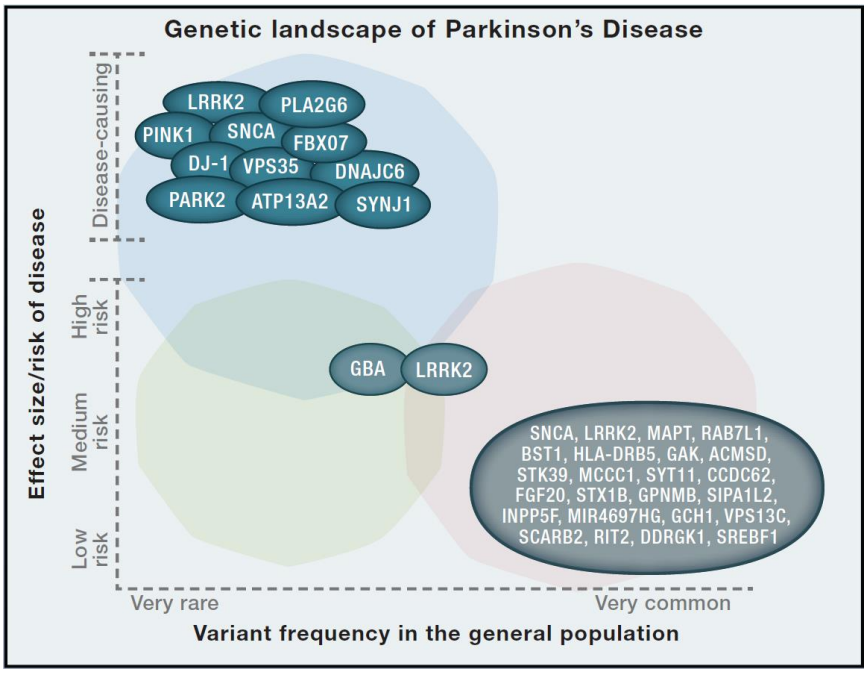

Figure 3. Genetic landscape of PD: LRRK2 is of special interest as it is found in familial and sporadic PD (Brás *et al.*, 2015). Very rare disease-causing genes in comparison to very common low risk modifiers. LRRK2 is not only shown to be the cause of familial monogenetic PD, but also a common risk modifier with a high but incomplete risk for developing PD.

The link between PD and LRRK2 had first been established in 2002 by Funamaya *et al*. They discovered that a novel autosomal dominant genetic risk locus on chromosome 12 caused PD within a Japanese cohort (Funayama *et al.*, 2002). Later in 2004, mutations in the LRRK2 gene were associated with the previously observed locus and linked to familial PD (Paisán-Ruíz *et al.*, 2004; Zimprich *et al.*, 2004). So far, 6 mutations within the LRRK2 gene have been linked to autosomal dominant PD: G2019S, R1441C, R1441G, R1441H, I2020T, and Y1699C, and others were shown to segregate with the disease but in a

non-Mendelian fashion (Cookson, 2010; Zimprich *et al*., 2004) (Figure 2). Here, the focus is on the glycine to serine substitution at position 2019 (G2019S), which was linked to 1% of sporadic and 4% of autosomal dominant forms of PD (Healy *et al*., 2008). Being responsible for 5% of all PD cases, LRRK2-G2019S is not only the most abundant mutation within LRRK2 but also the most common single cause of PD, and has a penetrance of 30% (Healy *et al*., 2008; Ozelius *et al*., 2006; Pankratz and Foroud, 2007). Its abundance and penetrance, however, strongly depend on age, gender and ethnicity (Cilia *et al*., 2014; Hentati *et al*., 2014; Ozelius *et al*., 2006). Although the relative risk of developing PD is generally higher in males, an Italian population study showed that mutations in LRRK2 have a higher prevalence in females (Cilia *et al*., 2014). Moreover, compared to Norwegian patients, the penetrance and onset of LRRK2-G2019S was, for instance, significantly increased in patients from Tunisia (Hentati *et al*., 2014). Furthermore, the age of onset is highly variable between individual carriers. This variability might be explained by genetic variants within the patient's specific genetic background. Different polymorphisms that contribute to PD are, for instance, directly linked to the age of onset of LRRK2-G2019S-induced pathogenesis (Botta-Orfila *et al*., 2012; Golub *et al*., 2009; Reinhardt *et al*., 2013a; Trinh and Farrer, 2013; Trinh *et al*., 2016). The factors increasing the susceptibility of LRRK2-G2019S carriers to develop PD at an early age are *SNCA*, dynamin 3 (*DNM3*) and ATPase 13A2 (*ATP13A2*) variants (Botta-Orfila *et al*., 2012; Trinh *et al*., 2016; Lubbe *et al*., 2016 and John Hardy ADPD conference 2017). In contrast, in the case of LRRK2-G2019S, *MAPT* polymorphisms were shown to reduce the risk (Davis *et al*., 2016). LRRK2-G2019S neuropathology is typically characterized by the formation of LBs and neurites, however, cases with filamentous TAU inclusions and without any deposits also exist (Goedert *et al*., 2013).

LRRK2 is expressed in various tissues and cell types. In humans, it is mainly found in the kidney, liver, pancreas, lung, heart, colon, cells of the immune system, and brain tissue (The Human Protein Atlas). In other tissues than the brain, mutations in LRRK2 lead to an increased risk of cancer formation and LRRK2-G2019S is associated with Crohn's disease (Saunders-Pullman *et al*., 2010; Liu and Lenardo, 2012). Within the adult brain, LRRK2 is expressed in microglia, oligodendrocytes, astrocytes, and neurons and is strongly associated with pathologic inclusions in neurodegenerative diseases (Miklossy *et al*., 2006). In mice, similar mRNA patterns throughout the whole brain were observed with especially high expression levels in regions affected by PD (Simón-Sánchez *et al*., 2006). LRRK2 is, however, more strongly expressed within dopamine receptive areas such as the striatum, cortex, and olfactory tubercle compared to dopamine synthetizing neurons and the *SNpc* (Melrose *et al*., 2006). Additionally, it has been shown that LRRK2 is already expressed during embryonic development throughout the neuroepithelium and later in the neocortex, where it is concentrated at the ventricular and sub-ventricular zones, reinforcing the hypothesis that PD may have developmental components (Zechel *et al*., 2010) (see section 2.3).

Structure, function and regulation

LRRK2 is a large multi-domain protein of 2,527 amino acids and 280 kDa encoded by the *PARK8* (*LRRK2*) gene localized on chromosome 12q12. LRRK2 is localized in multimeres within the cytoplasm and dimerizes upon activation and translocation to the mitochondrial inner- and vesicular membranes. It is made up of different protein-protein interaction regions such as the WD40, LRRK/HEAT/ankryn repeats, and leucine-rich repeats, which surround a catalytic core (Figure 4). The high number of protein-protein interacting domains indicate that LRRK2 might function as a scaffold protein for larger complexes (Mata *et al*., 2006). The core of the protein is formed out of a Ras of complex (ROC) and a carboxyl terminal of Roc (COR) domain possessing a GTPase- as well as a kinase function (Cookson, 2010).

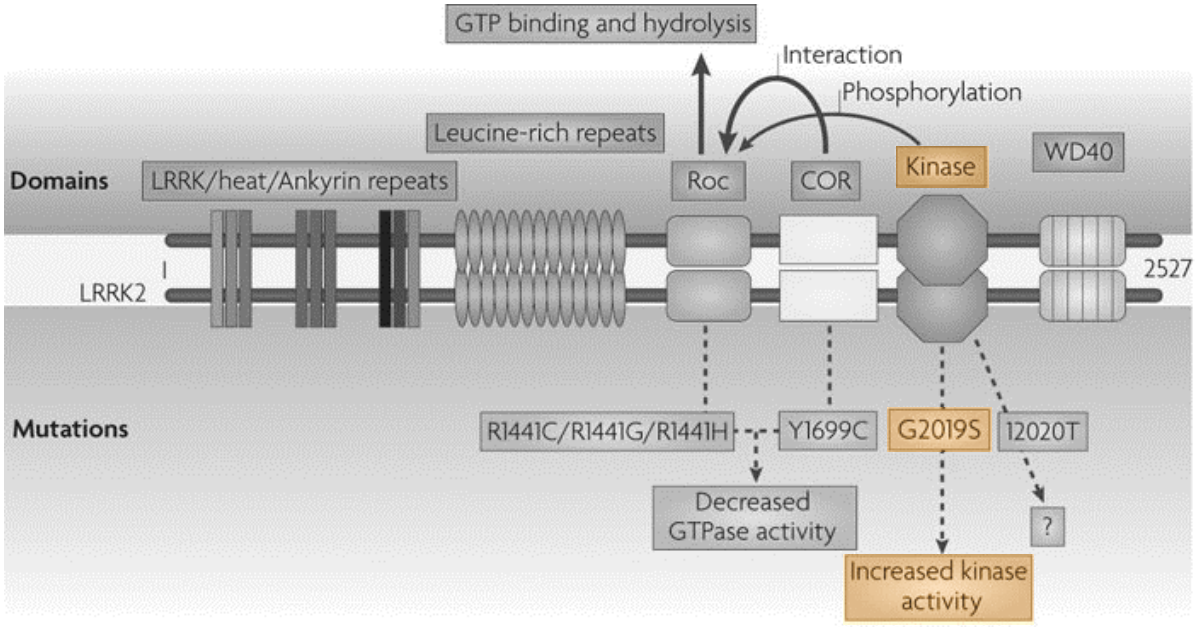

Figure 4. Structure of LRRK2 protein domains and mutations. Modified from Cookson, 2010. Schematic representation of the LRRK2 dimer with different protein interacting domains, GTPase-, and kinase function, as well as the major PD associated mutations. The G2019S mutation in the kinase domain leads to increased kinase activity as is highlighted in orange.

The determination of the exact role of LRRK2 is very complex, as its function differs in a context-specific manner. For instance, its role may change within cell types, tissues, species, and developmental stages and probably during aging. Furthermore, while the pathological role has been extensively studied, the physiological role has been neglected. Contradictory literature, a lack of reproducibility and *in vitro* kinase assays, which only partly reflect physiological conditions, represent further hurdles. The search for LRRK2 kinase substrates has been the objective of pharmaceutical companies for years, with mixed success. A computational study of the LRRK2 interactome showed that potential physiological functions of LRRK2 are predominantly vesicular transport, and cellular and cytoskeleton organization. Moreover, lower gene ontology enrichment scores, based on the interacting proteins, were associated with

development, mitochondria, metabolic regulations, immune response and cell death (Manzoni *et al.*, 2015).

LRRK2 belongs to the tousled-like kinase (TLK) family and one of its main functions is its kinase activity. Kinases are enzymes that catalyze the transfer of phosphate groups from high energy molecules like ATP to specific low energy molecules, the substrates. Upon phosphorylation, the substrate is activated. Reliable LRRK2 substrates identified so far include serine/threonine kinase 1 (AKT1), cell division cycle 25A (CDC25A), LRRK2, LRRK1, mitogen-activated protein kinase (MAPK) and RAB GTPases (Lobbestael *et al.*, 2012; Steger *et al.*, 2016). LRRK2 mainly induces the MAPK/ERK (extracellular-signal regulated kinases) (Chen *et al.*, 2012; Verma *et al.*, 2014; Reinhardt *et al.*, 2013a; Plowey *et al.*, 2008) and AKT (Chuang *et al.*, 2014; Ohta *et al.*, 2011) signalling pathways. Upstream signal transduction pathways are the wingless-type MMTV integration site (WNT) and tumor necrosis factor alpha (TNF-a)/fas ligand (FAS-L) (Berwick and Harvey, 2011). LRRK2 kinase activity is regulated by proteins such as protein kinase 1 (PKA), casein kinase 1 (CK1), IkappaB kinases (IKKs) and protein phosphatase 1 (PP1), which can phosphorylate and dephosphorylate different serine and threonine residues within LRRK2 and regulate its activity (Cookson, 2015; Muda *et al.*, 2014; Parisiadou *et al.*, 2014). Furthermore, LRRK2 kinase can auto-phosphorylate itself to regulate its activity. The G2019S mutation is found within the kinase domain of the protein (Figure 4). The mutation is not directly located in the catalytic cleft but in the activation segment, which upon phosphorylation changes conformation and enables substrate binding. More precisely, the glycine at position 2019 belongs to the well-conserved DF/YG amino acid sequence within kinase domains, and plays an important role in $Mg2^{+}$ positioning, which is necessary for ATP binding (Mata *et al.*, 2006). The mutation was shown to increase LRRK2 kinase activity (West *et al.*, 2005). Moreover, the kinase domain is regulated by the GTPase domain, which was shown to activate the kinase through GTP binding and consequently regulate protein stability and dimerization (Biosa *et al.*, 2013). The GTPase domain itself is also relevant for PD and belongs to the ROCO (ROC and COR domain) subfamily, which is the closest family to the RAB GTPase and, similarly to the RAB proteins, is involved in vesicular trafficking. Furthermore, the COR domain of LRRK2 can interact with E3 protein ligases and as such plays an important role in proteasomal degradation (Mata *et al.*, 2006).

The major roles of LRRK2 are defined through its pathogenic function. As previously mentioned, the focus is set on the LRRK2-G2019S mutation. The G2019S mutation is a gain of function mutation, which leads to an increase in kinase activity and to a stabilization of the protein (Jaleel *et al.*, 2007; West *et al.*, 2005). In particular, the G2019S mutation was linked to rearrangements of actin cytoskeleton and microtubules through the phosphorylation of moesin/radixin and tubulin (Parisiadou and Cai, 2010; Parisiadou *et al.*, 2010). These deregulations are potentially responsible for synaptic dysfunctions (Parisiadou *et al.*, 2014; Sweet *et al.*, 2015) and reduced neuritogenesis, which have been abundantly

shown to be impaired by the LRRK2-G2019S mutation (Chan *et al.*, 2011; Winner *et al.*, 2011; Lin *et al.*, 2010; MacLeod *et al.*, 2006; Plowey *et al.*, 2008). Furthermore, due to its association with vesicles, it plays a role in membrane and protein trafficking and mutant LRRK2 has been shown to be responsible for deregulations in RAB GTPase function (Steger *et al.*, 2016; Waschbüsch *et al.*, 2014). Additionally, pathogenic LRRK2 has been linked to autophagy, mitochondrial dynamics, mitophagy and proteasomal degradation (Sanders *et al.*, 2014; Lichtenberg *et al.*, 2011; Plowey *et al.*, 2008; Su and Qi, 2013; Liu *et al.*, 2012b) and consequently to protein degradation, accumulation or misfolding and energy metabolism. Moreover, LRRK2-G2019S has been associated with neurodegeneration and shown to increase DN cell death (Reinhardt *et al.*, 2013a; Sánchez-Danés *et al.*, 2012; Nguyen *et al.*, 2011; Ramsden *et al.*, 2011; Chen *et al.*, 2012). Various direct interactions between LRRK2 and neuronal cell death – in particular apoptosis – have been established e.g. through its interaction with the fas-associated protein with death domain (FADD) or through mitochondria (Ho *et al.*, 2009; Iaccarino *et al.*, 2007). Other LRRK2 interaction partners which play an important role in PD are α-SYN, 14-3-3 protein, RAB7L1, cyclin G associated kinase (GAK), TAU and heat shock protein family (HSP) 70 and 90 (Cookson, 2015). These proteins can either be linked to vesicle and membrane trafficking (RAB7L1, GAK) through endosomes and autophagosomes (Beilina *et al.*, 2014; MacLeod *et al.*, 2013) or underline its function in cytoskeleton and microtubule association (TAU, HSP70) (Kawakami and Ichikawa, 2015). Furthermore, HSP90 and HSP70 play a role in LRRK2 mediated proteasomal degradation and protein accumulation (Wang *et al.*, 2008; Lichtenberg *et al.*, 2011). Although some papers show an association of LRRK2 with α-SYN within LBs, a direct interaction of both proteins or a phosphorylation of α-SYN by LRRK2 could not yet be established (Guerreiro *et al.*, 2013; Liu *et al.*, 2012a). However, both proteins may coexist in the same complex with 14-3-3 (Berg *et al.*, 2003). Furthermore, both proteins are involved in the same PD-associated pathways. For instance, they both interact with microtubules, protein trafficking, mitochondria, and are associated with malfunctions within the ubiquitin-proteosome system and autophagy (Tong and Shen, 2009). Other functions of LRRK2 are its role in mRNA translation through its interaction with 40S ribosomal protein, ribosomal protein S15 (RPS15) (Martin *et al.*, 2014) and translational initiation factor, eukaryotic initiation factor 4E binding protein (4E-BP) (Imai *et al.*, 2008). In addition, LRRK2 interacts with several miRNAs, such as *let-7a* and associates with argonaute proteins (Gehrke *et al.*, 2010; Gonzalez-cano *et al.*, 2017) that supports its role in mRNA regulation. Moreover, LRRK2 is tightly associated with the immune response. LRRK2 is, for instance, highly expressed in microglial cells and was shown to be upregulated in immune cells from PD patients (Cook et al., 2017; Lee et al., 2017). Finally, LRRK2 and pathogenic LRRK2 were shown to play a role in neural stem cells (NSCs) and neurogenesis, as will be discussed in section 2.3. It is worth

noting that the phenotypes underlying the LRRK2-G2019S mutation are highly diverse and that LRRK2 is at the crossroads of all the highlighted molecular mechanisms of PD (Figure 5).

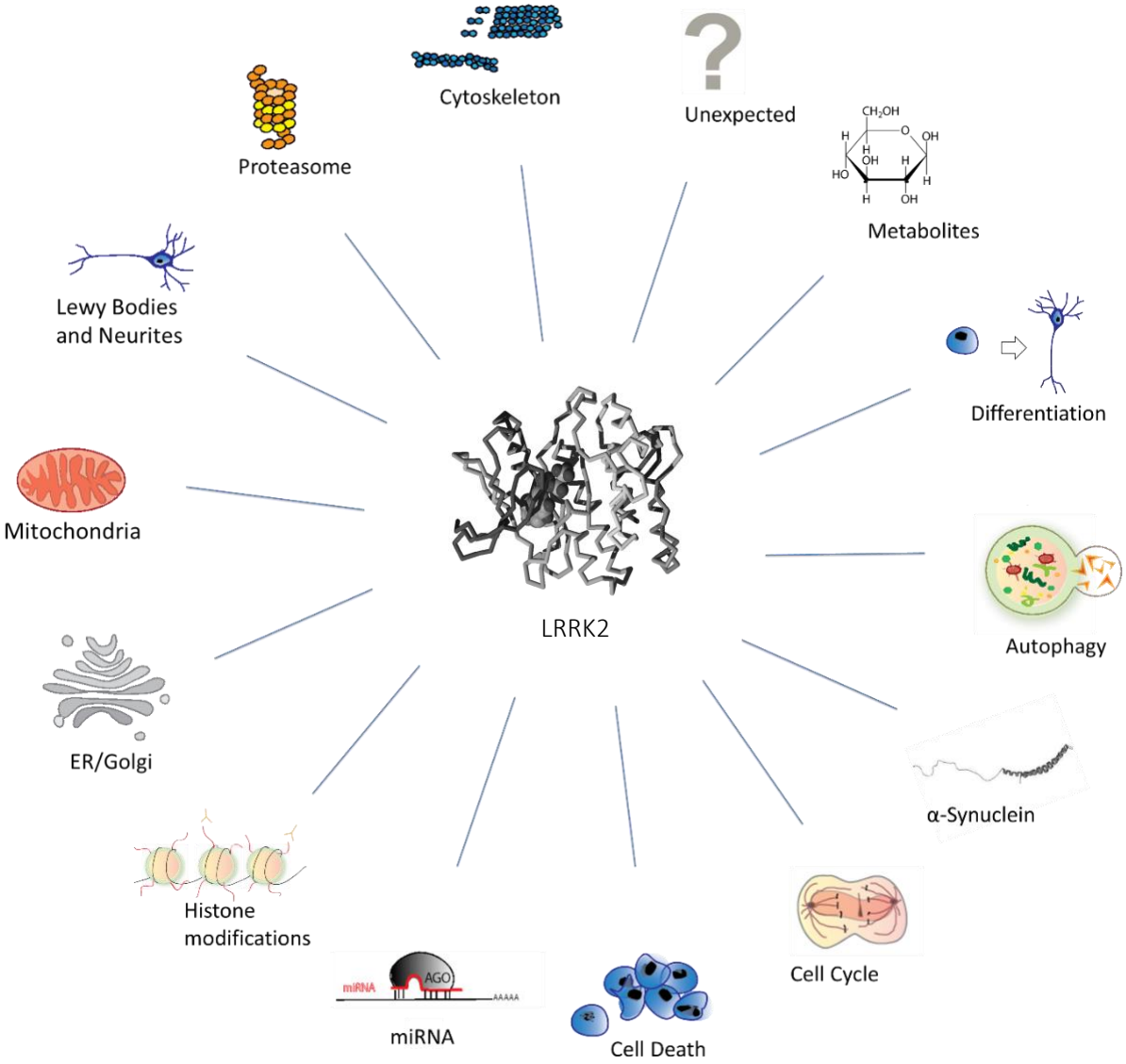

Figure 5. Overview of potential functions and interactions of LRRK2. LRRK2 has been linked to a variety of disease-associated mechanisms, although its pathogenic mechanism remains largely elusive. Here its pathogenic role on neuronal differentiation, cell death and proliferation, proteasomal and mitochondrial stress, protein degradation and it's interaction with α-SYN and LBs is shown. Furthermore, its association with the retrograde transport, the cytoskeleton, and miRNA regulations are depicted. In addition its potential influence on chromatin remodeling, metabolite expression and unexpected functions are depicted.

2 NEURAL STEM CELLS FOR MODELING PD

2.1 MIDBRAIN DEVELOPMENT

2.1.1 Neural induction

Neural induction is similar to the whole embryogenic process, a well-defined spatio-temporal patterning event regulated by a fine balance of different morphogen gradients and signalling molecules that lead to neuronal specification and regionalization (Figure 6). During embryogenesis, the CNS is derived from the neurectoderm that induces the formation of the neural plate. The neurectoderm arises from the ectoderm, one of the three germ layers that are formed during gastrulation. The ectoderm is similar to the mesoderm and endoderm derived from the epiblast, one of the two layers formed out of the inner stem cell mass of the blastocyst. In humans, the epiblast and hypoblast layers form the embryonic disk. The hypoblast gives rise to extraembryonic tissue, whereas the epiblasts produces the embryo (Figure 6).

Upon development, the ectoderm subdivides into the neurectoderm, the non-neuronal ectoderm, and the plate border. The neurectoderm together with the plate border form the neural plate (Figure 7). The process of neural induction, from the initiation of gastrulation, to ectoderm and neural plate formation, is tightly regulated by different organizing structures, transcription factors, and morphogen gradients that counteract each other. The neural default model postulates that neural induction results from the inhibition of non-neuronal stimulating factors such as the bone morphogenic protein (BMP), transforming growth factor beta (TGF-ß), WNT, and nodal growth differentiation factor (NODAL). Furthermore, a second classical model from Nieukoop states that the anterior neuronal tissue is activated and induced first and might subsequently be posteriorized. While the dorsal parts of the epiblast secrete BMP, WNT and NODAL, different organizers and extraembryonic tissues counteract these signals by secreting factors such as CHORDIN, NOGGIN, Left-Right Determination Factor (LEFTY) and CERBERUS (Figure 6).

In human development, prerequisites for neural induction include firstly cranial regionalization and secondly – during gastrulation – the development of the primitive streak and the formation of the node organizer. In humans, gastrulation takes place around day 17. The cells that do not migrate through the primitive streak during gastrulation will become the ectoderm. The first commitment of the epiblast to later become neuronal ectoderm results from the suppression of the induction of the anterior epiblast to become non-neuronal tissue. The anterior posterior axis is determined by the anterior visceral

endoderm (head organizer) at the cranial end of the hypoblast, which expresses the genes orthodenticle homolog 2 (*OTX2),* LIM homeobox 1 (*LHX1),* and HESX homeobox 1 *(HESX1)* and secretes the morphogens such as CERBERUS and LEFTY. CERBERUS and LEFTY inhibit NODAL to establish the cranial end of the embryo. The expression of NODAL continues at the posterior part of the embryo and establishes and maintains the formation of the primitive streak that extends towards the anterior region of the embryonic disk. BMP, the main ventralizing factor, is expressed throughout the embryonic disc and inhibited by the node organizer located at the anterior part of the primitive streak. The node organizer secretes CHORDIN, NOGGIN and FOLLISTATIN, which are induced by the transcription factor GOOSECOID. The suppression of BMP leads to the dorsalization of the embryo. Later, the notochord maintains the expression of CHORDIN, NOGGIN and FOLLISTATIN to induce the neural ectoderm within the cranial region. The inhibition of BMP signalling together with the upregulation of fibroblast growth factor (FGF) induces the neural plate formation that becomes visible on the medial dorsal surface of the developing embryo by an increase in the height of the cells. Whereas CHORDIN, NOGGIN and FOLLISTATIN signalling are responsible for fore- and midbrain formation, the hindbrain and caudal neural plate are induced by FGF together with WNT3a and retinoic acid. Similar to NODAL, forkhead box A2 (FOXA2) is expressed by the organizer and plays an important role in the specification of the anterior fore- and midbrain structures alongside CHORDIN, NOGGIN and FOLLISTATIN.

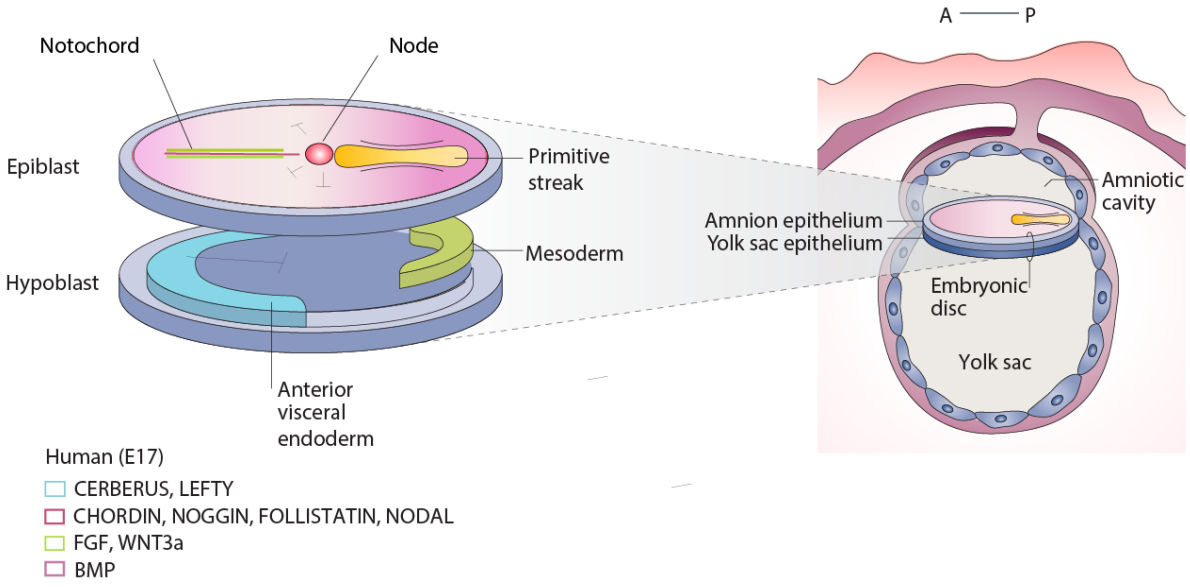

Figure 6. Signalling centers and neural induction in the human embryo. Modified from Tang *et al.*, 2016. Schematic representation of a human E17 gastrula with some of the embryonic regional identities as well as signalling centers. After gastrulation, the different morphogen gradients lead to the default formation of anterior neural ectoderm.

Around the 3rd week of development, the neural plate is formed. First, the neural plate lengthens and thereby extends anteriorly and posteriorly. After the formation of the neural plate, neurulation gives rise to the neural tube (Figure 7). The neural plate border gives rise to cells from the neural crest and

neural tube, as well as epidermal cells. The non-neuronal ectoderm generates the epidermis. During neurulation, the neural plate forms a groove and the neural folds rise and fold together. Fusion starts in the cervical region and proceeds to the anterior and posterior. Neurulation is induced by sonic hedgehog (SHH) signals from the notochord and WNT signals from the non-neuronal ectoderm that induce the elevation of the neuronal folds and lead to groove formation. Once the neural tube is closed, the future roof plate cells start expressing BMP/TGF-ß, which counteracts the SHH signals from the floor plate leading to dorso-ventral patterning gradients within the neural tube (Liu and Niswander, 2005) (Figure 8). In humans, a less prominent secondary neurulation event of mesenchymal cells in the posterior part of the embryo produces a secondary neural tube that fuses with the primary one. The prepatterned anterior part of the neural tube gives rise to three primary cerebral vesicles: the forebrain (prosencephalon), midbrain (mesencephalon) and hindbrain (rhombencephalon) (Figure 8). The posterior part of the neural tube gives rise to the spinal cord. The specification of the neural cells within the neural tube depends on their position along both axes (see also 2.1.2 and 2.2.2) (Casarosa *et al.*, 2013). (Medical Embryology 13th edition Langman, Sadler; Larsen and Sherman, 2002; Levine and Brivanlou, 2007; Developmental Biology 6th edition, Gilbert)

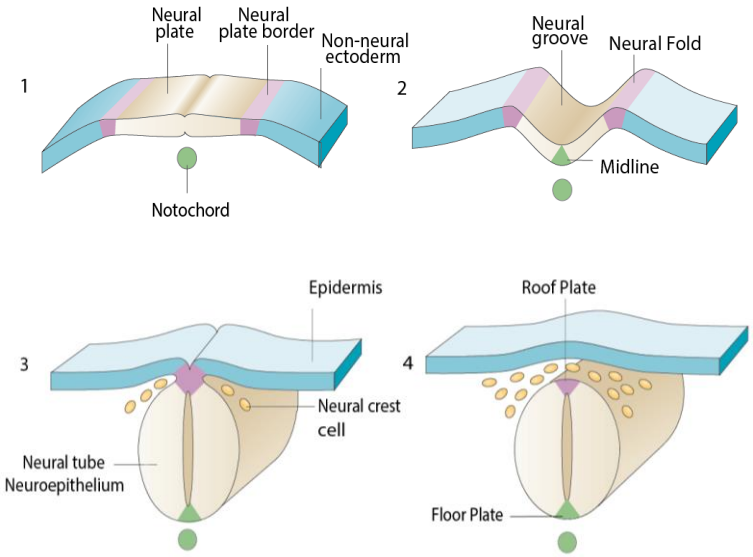

Figure 7. Neurulation. Modified from Liu and Niswander, 2005. The neural folds (2) of the neural plate (1) rise and fold together in order to form the neural tube (3-4). This process (1-4) is called neurulation. Neurulation leads to the formation of the neural tube, neural crest cells, and the epidermis (3) from the neural plate, neural plate border, and non-neuronal ectoderm (1). The neural tube has a dorso-ventral pattern characterized by the roof and floor plate (4).

2.1.2 The genesis of midbrain DNs

Midbrain DNs of the *SNpc* are essential for controlling voluntary movements (see 1.1.3). As PD is characterized by motor symptoms resulting from the loss of DNs in the *SNpc* of the midbrain and as NSCs are used in this thesis for disease modeling, it is important to understand the process of midbrain development. Mid and forebrain initiation mainly depend on two genes that are already expressed

during gastrulation, namely LHX1 and OTX2 (Langman 13th edition). The transition from the first neural plate cells to final DNs within the mature midbrain can be divided into three major developmental stages: the regionalization of the neural plate, the determination of the fate of the midbrain and the final differentiation of the neurons (Gale and Li, 2008). The first step in midbrain development consists in the subdivision of the neural plate into the different regions of the fore-, mid- and hindbrain and the spinal cord before and during neurulation as described above. The regional identity of the mid- and forebrain is further specified by homeobox genes including OTX1, empty spiracles homeobox 1 and 2 (EMX1 and 2) (Langman 13th edition). One of the main neuroepithelial organizers patterning the midbrain cell fate is the isthmus, known as the midbrain hindbrain boundary (MHB). In contrast, the forebrain fate underlies signals from a different organizing center, the anterior neuronal ridge (Langman 13th edition). The MHB and its positioning is defined by the co-repressive interaction of gastrulation brain homeobox 2 (GBX2) from the posterior and OTX2 from the anterior neural plate or -tube cells (Figure 8) (Rhinn and Brand, 2001). Upon MHB formation, signalling genes such as paired box 2 (PAX2), FGF8, WNT1 and engrailed 1/2 (EN1/2) are expressed and maintain the regionalization of the midbrain territory (Rhinn and Brand, 2001).

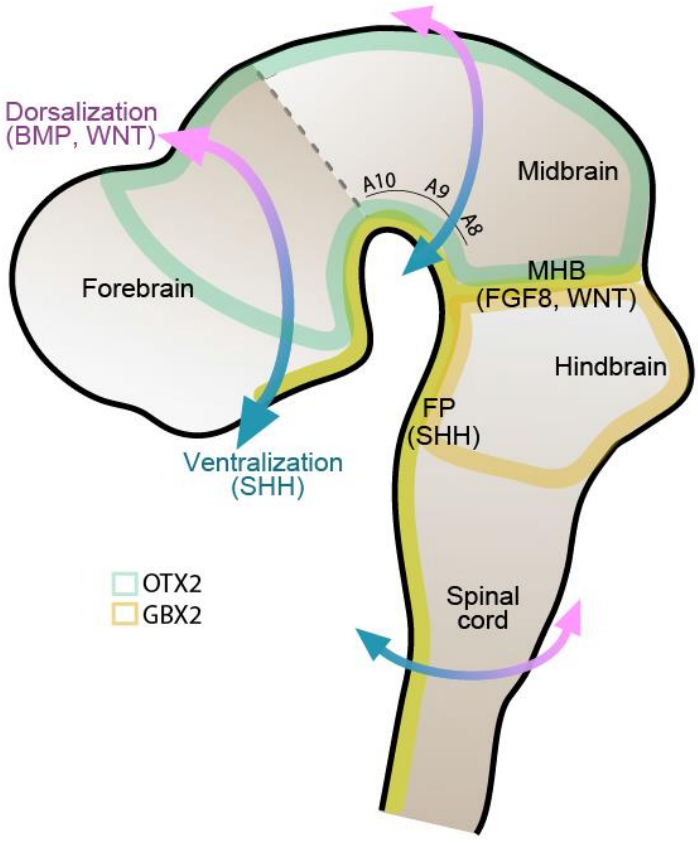

Figure 8. Midbrain development and patterning. Modified from Suzuki and Vanderhaeghen, 2015. During brain development midbrain patterning depends on the SHH signals from the floor plate (FP) and the signals establishing the MHB. Furthermore a dorso-ventral axis is established and the different midbrain DN regions A10, A9, and A8 are generated.

Midbrain DNs originate from the midline of the neural plate, which subsequently forms the ventral floor plate of the resulting neural tube. The regionalization is determined by signals from the underlying notochord (the mesoderm (SHH)) and from the primitive neuroepithelium (the neuroectoderm itself). Once the midbrain territory is defined, the ventral floor plate cells start expressing SHH themselves. Together with the surrounding signals, a progenitor pool is formed and maintained, the midbrain floorplate radial glia (Aguila *et al*., 2012; Bonilla *et al*., 2008; Gale and Li, 2008). SHH induces the formation of DN progenitors expressing precursor marker LIM homeobox transcription factor 1 alpha (LMX1A) and floorplate marker FOXA2. Once expressed, both FOXA2 and LMX1A take over and guarantee neurogenesis by activating the genes Msh homeobox 1 (*MSX1*) and neurogenin 2 (*NGN2*) (Gale and Li, 2008). Furthermore, they induce paired-like homeodomain 3 (PITX3) and nuclear receptor subfamily 4 group A member 2 (NR4A2/NURR1), two midbrain DN precursor markers (Gale and Li, 2008). External signals at this stage are morphogens and growth factors such as several members of the WNT pathway, retinoic acid, TGF-ß, BMP, glial cell line-derived factor (GDNF) and brain-derived neurotrophic factor (BDNF) (Aguila *et al*., 2012). PITX3 and NURR1 are both able to induce tyrosine hydroxylase (TH) expression, the rate limiting enzyme for dopamine production (Abeliovich and Hammond, 2007). TH catalyzes the reaction from tyrosine to L-3,4-dihydroxyphenylalanine (L-DOPA/Levodopa), the precursor amino acid of dopamine. AADC then converts L-DOPA to dopamine, which is used as a neurotransmitter in DNs (Daubner *et al*., 2012). Based on their localization and target region, three different kinds of midbrain DNs exist, the A8, A9, and A10 DNs (Figure 8). The A9 midbrain DNs are located within the *SNpc* and form the nigrostriatal pathway. They extend to the dorsolateral striatum (putamen and caudate nucleus), and are essential for controlling voluntary movements as well as being selectively vulnerable in PD (as described in section 1.1.4 and 1.1.5). The neighboring DNs within the ventral tegmental area (A10) as well as those from the retrorubral field (A8), form the cortical mesolimbic system and control emotional behavior, novelty, reward mechanisms and addiction (Abeliovich and Hammond, 2007).

2.1.3 Astrogliogenesis and the role of astrocytes in DN development

Astrocytes represent by far the most abundant cells of the CNS and play a role in PD pathogenesis, as described in section 1.1.4. During development, gliogenesis directly follows neurogenesis. Astrocytes are generated from RGCs or basal progenitors (Figure 9). During the late stages of brain development, most RGCs detach from the basal ventricular zone, migrate to the cortical plate and transform into astrocytes (see section 2.2.2) (Kriegstein and Alvarez-buylla, 2011). Astrocytes are very heterogeneous and display a very high degree of plasticity (Zhang and Barres, 2010). They play major roles in brain development, function, and integrity (Barres, 2008). The main function of astrocytes is to support the neurons. They are involved in blood-brain barrier regulation, synapse formation and plasticity, glio- and

neurotransmission, as well as ion homeostasis and glucose storage. Astrocytes provide neurons with neurotrophic factors and metabolic substrates and protect them through the uptake of neurotoxic agents (Rappold and Tieu, 2010). Furthermore, they play an important role in glial scar formation and the inflammatory reaction in response to injury, infection, and disease (as described in section 1.1.4) (Barres, 2008). Moreover, astrocytes are able to de- or trans-differentiate and are involved in neuronal fate determination (Song *et al*., 2002; Zhang and Barres, 2010). For instance, astrocytes were shown to promote NSC differentiation (Song *et al*., 2002) and different studies have demonstrated that they play a role in midbrain DN development (Wagner *et al*., 1999; Wang *et al*., 2009; Yang *et al*., 2014). GDNF – a well-known neurotrophic factor secreted by astrocytes – induces, for instance, DN differentiation *in vitro* (Lin *et al*., 1993). Moreover, by excreting factors, such as basic fibroblast growth factor (bFGF) and TGF-ß, astrocytes can induce dopaminergic neurogenesis (Wang *et al*., 2009; Yang *et al*., 2014). Additionally, midbrain specific astrocytes can potentiate A9 biased DN differentiation *in vitro*, highlighting the importance of the physiological environment (Roy *et al*., 2006). Furthermore, DNs generated under astrocytic influences were shown to promote brain repair and restore motor functions upon transplantation in PD mouse models (Roy *et al*., 2006; Yang *et al*., 2014). As highlighted, the importance of astrocytes in midbrain development, integrity, and PD should not be underestimated.

2.2 NEURAL STEM CELLS

2.2.1 Definition

stem cell

noun \'stem-\

: an unspecialized cell that gives rise to differentiated cells <*hematopoietic stem cells in bone marrow*>

First Known Use of stem cell

1896

Merriam-Webster

A stem cell is a cell, which has the ability to self-renew and to differentiate into diverse other cell types. Its differentiation potential is restricted by its potency (toti-, pleni/omni-, pluri- and multipotency). The only existing totipotent cell is the zygote (plus one or two more cell divisions). A totipotent cell is by definition a cell able to develop and organize a complete organism (Condic, 2014). The next stage of potency, here called plenipotency, is defined as the capacity to generate extraembryonic and

embryonic tissue. These cells are either found within the late morula and are able to give rise to the trophoblast and to the inner stem cell mass, or within the inner stem cell mass, which generates the epiblast as well as the hypoblast (Condic, 2014). A general confusion is that totipotency is often defined as the capacity of generating extraembryonic tissue, however, cells from the late morula and early blastocyst, if isolated, cannot give rise to a complete organism. Pluripotent stem cells are typically found within the epiblast and are able to differentiate into all three germ layers. Embryonic stem cells (ESCs) are pluripotent and can give rise to every cell type of the human body. Within the tissues, stem cells are called multipotent as they are still able to generate different lineage committed progenitors, but are, unlike pluripotent stem cells, more restricted in their differentiation potential. NSCs are multipotent and committed to the neural lineage. Thus, they are able to differentiate into all the cell types of the CNS and PNS. The differentiation is called neurogenesis when cells turn into neurons and gliogenesis when cells develop into glial cells, such as astrocytes and oligodendrocytes (Gage, 2000). NSCs is a loose term used for different nevous system-specific multipotent stem cell types. Three of these are present during development: neuroepithelial stem cells (NESCs), radial glial cells (RGCs) and basal progenitors. One type, the adult NSCs, are only found in the stem cell niches of the adult brain.

2.2.2 NSCs during development

NESCs are derived from the neural plate and persist in the developing neural tube. As the NESCs of the neural plate give rise to the neural tube, the only difference between the cells consists in different morphogen exposures. As mentioned in section 2.1.1, anterior-posterior, as well as dorso-ventral patterning signals define NESC fates. Within the same section of the developing neural tube, the NESCs from the ventral midline differ from those at the neural plate border. The NESCs of the plate border as seen in Figure 7 are also called neural plate border stem cells (NPBSCs) (Milet and Monsoro-Burq, 2012). While the NPBSCs receive WNT signals from the non-neuronal ectoderm as well as SHH signals from the notochord that induce their proliferation, the cells within the center of the neural plate, as described in section 2.1.2 are only exposed to SHH signals that induce their ventral floorplate fate. As a result of this morphogen exposure, the NESCs at the border of the neural plate (dorsolateral hinge points) proliferate and form the neural folds which rise and fold together to form the neural tube. In contrast, the cells from the midline (median hinge point) only slowly proliferate allowing the bending and formation of the neural groove (McShane *et al.*, 2015). The NPBSCs do not only give rise to the neural tube, but also to neural crest cells directly after neurulation. This pre-patterned type of NESCs, is located at the roof plate upon closure of the developing neural tube and undergoes epithelium to mesenchymal transition to migrate and to form most of the peripheral nervous system (PNS), as well as melanocytes and mesenchymal structures within the head (Lefcort and George, 2007; Theveneau and Mayor, 2012).

After neurulation, the developing neural tube consists of a single unique cell layer: the germinal neuroepithelium. As the name suggests, the neuroepithelium is made up of a second type of NESCs, the so called rosette-type NCSs, giving rise to the CNS (Mertens *et al*., 2016). They are, as all epithelial cells, radially elongated and have an apical basal polarity. The NESCs from the developing neural tube are in contact with both the apical and basal surface of the germinal neuroepithelium. First, they divide symmetrically to increase the neural stem cell pool, then they divide asymmetrically to induce the first wave of neurogenesis. Upon nervous system development, NESCs give rise to basal progenitors and RGCs. The RGCs replace the NESCs and line the lumen of the neural tube called the ventricular zone (VZ) (Kennea and Mehmet, 2002). Like NESCs, RGCs have an apical basal polarity. During brain development and cortex extension (MA in Figure 9), the RGCs extend themselves: the lumen of the neural tube turns into the ventricles and their extensions to the basal surface establish contact with the meninges, basal lamina, and blood vessels. RGCs are particular in that they go through interkinetic nuclear migration upon cell division, meaning the cell body undergoes periodic movement in phase with the cell cycle, such that cellular division happens within the VZ (Kriegstein and Alvarez-buylla, 2011). Once again, their symmetric division enlarges the NSC population, while their asymmetric division leads to progenitor cells that migrate and differentiate to develop into the CNS (Götz and Huttner, 2005). Newly generated neurons use the RGCs as scaffolds to migrate into the most distal cortex layer. During early embryogenesis, the asymmetric division of RGCs gives rise to a second neurogenic wave and new basal progenitor cells. During late embryogenesis, astrocytes, oligodendrocytes, and ependymal cells are formed. RGC identity is heterogeneous and strongly depends on their spatio-temporal location within the developing embryo. The basal progenitors are found in the subventricular zone (SVZ). Produced by NESCs and RGCs, their main role is to increase, through one or two divisions, the production of neurons. Thus, they can be seen as transit amplifying cells. In the postnatal brain, RGCs are converted into astrocyte-like type B NSCs, which give rise to adult progenitors. (Conti and Cattaneo, 2010; Kriegstein and Alvarez-buylla, 2011). For further details on different kinds of *in vitro* NSCs within the neural plate and neural tube, see section 2.4.2.

2.2.3 Adult neural stem cells

Compared to other tissues, the human nervous system possesses, only very restricted regeneration potential, as neurons are mostly exclusively generated during development and adult neurogenesis is limited to specific areas within the human brain (Horner and Gage, 2000). In the adult brain, NSCs are found in two neurogenic niches, the SVZ of the lateral ventricle and the subgranular zone of the dentate gyrus (DG) of the hippocampus (Doetsch, 2003). Both zones maintain neurogenesis and gliogenesis throughout life. Whereas neurogenesis is restricted to these two areas, gliogenesis is more prevalent and occurs not only in the neurogenic niches but throughout the brain. In the case of astrocytes, for

instance, gliogenesis is spread throughout the entire brain as they retain their mitotic potential. Similarly, for oligodendrocytes, genesis happens predominantly in the parenchyma (Rusznák *et al.*, 2016). The first evidence of postnatal hippocampal neurogenesis in rats was established by Altman in 1965 (Altman and Das, 1965). It was, however, only 34 years later that adult neurogenesis was first reported within the human brain (Eriksson *et al.*, 1998). While new dentate granule cells are produced in the DG, the SVZ gives rise to new neurons which migrate through the rostral migratory stream to the olfactory bulb (Gage, 2000). Interestingly, it has recently been shown that subventricular neurogenesis of interneurons within the striatum (the brain region that DNs project their axons to) persists during adulthood (Ernst *et al.*, 2014). Although the exact function of adult neurogenesis is still under discussion, common belief holds that newly generated neurons contribute to learning, memory, brain function and integrity (Spalding *et al.*, 2013). The neurogenic potential is variable and can increase through exercise and pregnancy (Ming and Song, 2011). In contrast, stress and aging, as well as injury and disease, have negative effects on adult neurogenesis, as will be further discussed in the next section (Curtis *et al.*, 2007a; Ming and Song, 2011).

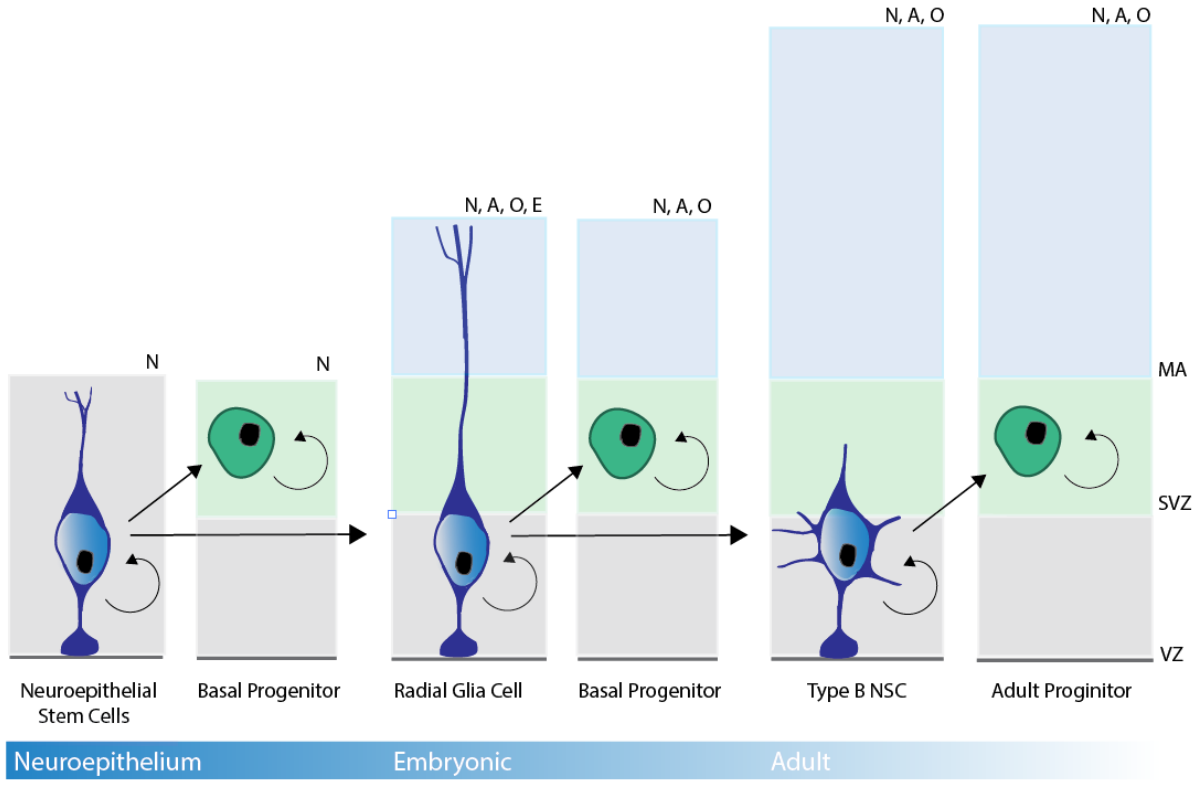

Figure 9. Neural stem cells in development and in the adult brain. Inspired from Kriegstein and Alvarez-buylla, 2011. The primitive neuroepithelium is formed out of NESCs, which can self-renew, give rise to basal progenitors and neurons. NESCs are replaced in the developing brain by RGCs that produce more basal progenitors, generate more neurons, and act as a scaffold for neuronal migration. Furthermore, after the second neurogenic wave, they first give rise to astrocytes and ependymal cells, and then to oligodendrocytes. In the adult brain, two types of NSCs persist: type B NSCs, and adult progenitor cells that are located in the SVZ and subgranular zone. VZ=Ventricular Zone, SVZ=Subventricular Zone, MA=Mantel, N=Neurons, A=Astrocytes, O=Oligodendrocytes, E=Ependymal cells.

2.3 NSCs IN PD WITH FOCUS ON LRRK2

2.3.1 NSCs in neurological diseases, such as PD

Neural stem cell deregulations are prevalent in several neurological diseases. The most common diseases are stress, clinical depression, and stroke. Furthermore, NSCs are directly involved in cancer and brain tumor formation and several neuropsychiatric diseases such as schizophrenia and autism spectrum disorders, as well as cognitive disorders are caused by reduced neurogenesis. Similarly the cognitive declines linked to several neurodegenerative diseases such as Huntington's, PD and Alzheimer's have been linked to NSC deregulations (Apple *et al.*, 2016; Winner *et al.*, 2011b). In addition, neuro-inflammation plays a role in all major diseases of the CNS and has been shown to decrease the neurogenic potential (Carpentier and Palmer, 2009). This chapter is focused on the role of stem cells in PD (see section 1.1.3).

The development, maintenance, and plasticity of the brain is guaranteed by the fine balance between cell generation and cell death. While increased neuronal cell death is the key component of neurodegenerative diseases, most of the diseases also present alterations within neurogenic niches as highlighted above (Winner *et al.*, 2011). In PD, the appearance of the less-studied non-motor symptoms, which often precede the motor symptoms by decades, correlates with neural stem cell deregulations (Braak et al., 2003; Le Grand et al., 2014; Marxreiter et al., 2013; Regensburger et al., 2014). The very early loss of smell (hyposmia), for instance, might be linked to reduced neurogenesis within the olfactory bulb (Curtis *et al.*, 2007b). Furthermore, depression – which is another cardinal non-motor symptom – has been linked to a decreased number of progenitor cells within the hippocampus (Boldrini *et al.*, 2009; Lucassen *et al.*, 2010). In addition, analogies and genetic comorbidities between PD and other neuropsychiatric diseases, such as schizophrenia, represent an indication for impaired adult neurogenesis in PD (Apple *et al.*, 2016; Nalls *et al.*, 2014). In the adult brain suffering from PD, dopamine depletion has been shown to decrease neural precursor cell proliferation (Höglinger *et al.*, 2004). Additionally, post mortem brains of PD patients have fewer precursor cells in the subgranular zone and olfactory bulb compared to healthy individuals (Höglinger *et al.*, 2004). Reduced neurogenesis in brains of PD patients, however, is still the root of some controversy and has been contradicted by another study showing no difference in the number of NSCs post mortem (Figure 10) (Van Den Berge *et al.*, 2011).

The effect of LRRK2 on neurogenesis and NSCs has been extensively studied in mouse models (Figure 10). The LRRK2-G2019S mutation was shown to reduce proliferation in the SVZ and neurite outgrowth

in the DG of LRRK2-G2019S transgenic mice (Winner *et al*., 2011). LRRK2 and LRRK2-G2019S seem not only to regulate – and in the case of the mutation, reduce – neuron progenitor cell proliferation, but also perturb proper neuronal differentiation leading to the well-established phenotype of reduced neuritogenesis of DNs as described in section 1.2.2. Mouse ESC neuronal differentiation, induced by retionic acid, for instance, was increased in LRRK2 knock out (KO) cells (Schulz *et al*., 2011). Similarly, LRRK2 KO mice, in contrast to LRRK2-G2019S transgenic mice, showed enhanced dentrito- and axogenesis of neuroblasts (Paus *et al*., 2013). Furthermore, the LRRK2-R1441G mutation similarly to the LRRK2-G2019S muation, inhibits neuronal differentiation of mouse NSCs *in vitro* (Bahnassawy *et al*., 2013). Additionaly, not only NSC deregulations and impaired neurogenesis were linked to LRRK2 induced pathogenesis, but also behavioral traits were shown to underly LRRK2-G2019S induced PD. LRRK2-G2019S carrying mice, for instance, showed increased anxiety compared to WT mice (Melrose *et al*., 2010).

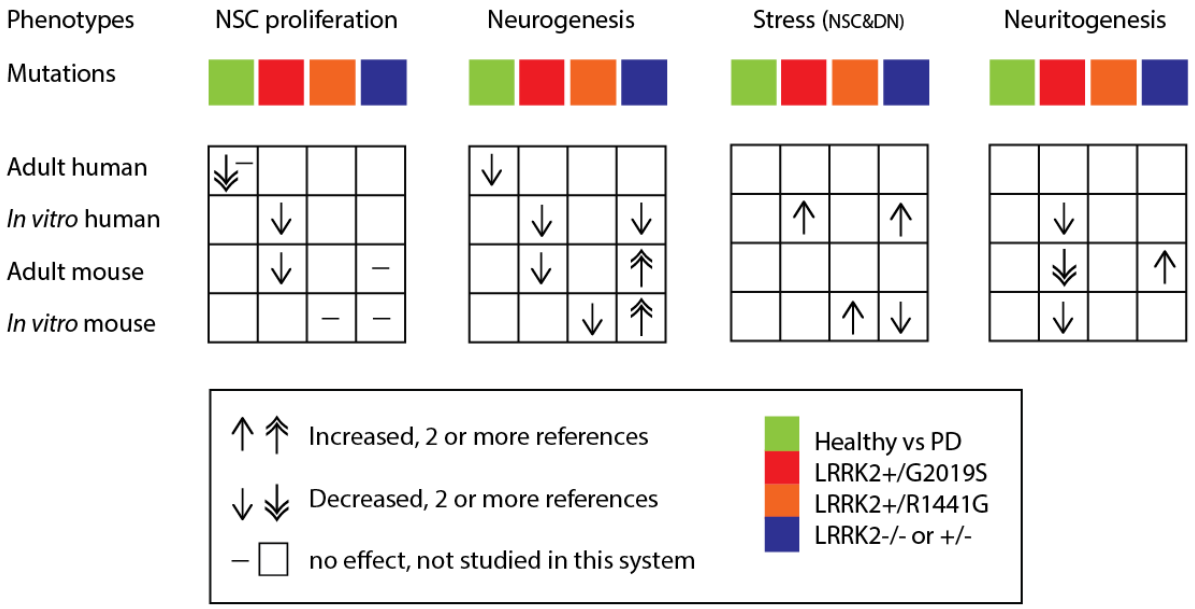

Figure 10. The role of LRRK2 in NSC maintenance and differentiation as well as comparisons between the healthy and diseased adult human brain (I). Summary of literature showing NSC deregulations upon LRRK2 or in PD patient brains. LRRK2 reduces NSC proliferation and impairs neural development and neuritogenesis. Furthermore, NSCs and DNs with LRRK2 deregulations show increased susceptibility to stress. (Bahnassawy *et al*., 2013; Van Den Berge *et al*., 2011; Curtis *et al*., 2007a; Höglinger *et al*., 2004; Liu *et al*., 2012b; MacLeod *et al*., 2006; Milosevic *et al*., 2009; Paus *et al*., 2013; Plowey *et al*., 2008; Schulz *et al*., 2011; Winner *et al*., 2011a)

As mouse models do not fully recapitulate the loss of DNs (see section 2.4.1), studies of human NSCs and neurogenesis are necessary (Figure 10). *In vitro* models using fetal midbrain-derived human NSCs reported that, in contrast to mouse LRRK2 KO cells, LRRK2-deficient cells show reduced neurogenesis by decreasing DN survival (Milosevic *et al*., 2009). However, in accordance with the observations in mouse models, LRRK2 knock down DN progenitor cells show a reactivation of the cell cycle (Milosevic *et al*., 2009). With the discovery of iPSCs, which will be further elaborated in section 2.4.1, it became

possible to study human patient-specific stem cells. iPSC-derived NSC models showed that the G2019S mutation impairs nuclear envelop organization and leads to proteasomal stress. It was possible to rescue the phenotypes through targeted gene correction and reproduce them in ESCs by knock-in of the mutation. Additionally, in the same study, NSC degeneration by pathogenic LRRK2 could be reproduced in brain tissue of PD patients (Liu *et al*. 2012b). This observation correlates with the reports of Hoeglinger *et al*., although the underlying reason for the degeneration is different.

2.3.2 The developmental contribution to PD

The functions and dysfunctions in NSCs highlighted in Figure 10 provide evidence that LRRK2 plays a role in neuronal differentiation and stem cell maintenance. Most of the studies on NSCs so far, however, have been based on the concept of adult neurogenesis. As LRRK2 is important for keeping the balance between cell generation and degeneration, it might play a role during neuronal development and preservation. Hence, LRRK2 malfunction may lead to deficiencies during the development of the CNS. Increasingly, evidence suggests that several of the PD-associated genes are expressed and directly involved in embryonic development, and also impair neurogenesis and deregulate NSCs (Le Grand *et al*., 2014). As an example, *SNCA* KO mice show a reduced number of DNs in the *SNpc* during embryonic development (Garcia-Reitboeck *et al*., 2013). Moreover, mutations in NURR1, a gene necessary for DN development (see midbrain development), has been linked to PD, and PD patients show lower NURR1 expression within the *SNpc* (reviewed in Jankovic *et al*., 2005). Furthermore, as highlighted in section 1.2.1, idiopathic cases might also involve a genetic contribution. Once expressed, the genes underlying PD cause uncompensable deficits sooner or later. In cases, where the mutated genes are already expressed during development, these deficiencies might appear as soon as embryogenesis. LRRK2, for instance, is strongly expressed in the developing brain (see section 1.2.2), and co-localizes in neural progenitor cells with the NSC marker nestin (Milosevic *et al*., 2009; Zechel *et al*., 2010). Two studies in ESCs from mice and from humans showed in both cases that processes involved in stem cell maintenance depend on proper LRRK2 expression (Liu *et al*., 2012b; Schulz *et al*., 2011). Furthermore, LRRK2 has been shown to be regulated by the WNT signaling pathway, which plays a major role in embryonic neuronal development, as seen in section 2.1.1 and 2.1.2 (Berwick and Harvey, 2013). The role of LRRK2 in NSCs suggests that developmental deficiencies might underly DN vulnerability and patient susceptibility to develop PD.

2.4 *IN VITRO* DISEASE MODELING: iPSC DERIVED NSCs FOR PD

2.4.1 Induced pluripotent stem cells

Induced pluripotent stem cell (iPSC) technology opened up the possibility of recapitulating patient-specific changes in physiologically relevant cellular models called *in vitro* disease modeling. *In vitro* disease modeling aims to understand the underlying mechanisms of a disease and to develop strategies and personalized therapeutics for treatment and prevention (Hillje and Schwamborn, 2016).

Potency is defined as the spectrum of different cellular potential states, ranging from a pluripotent naive state, with unbiased developmental capacity to a unique lineage-specified state with a well-defined unique differentiation capacity (Hackett and Surani, 2014). As highlighted in section 2.2.1, ESCs are by definition pluripotent and can give rise to every cell of the human body. The generation of iPSCs from somatic cells that regained pluripotency, and as such, are able to differentiate into all three germ layers just like ESCs, revolutionized the study of human development and diseases. iPSCs opened the door to a new area of regenerative medicine and now represent a cutting edge technology in studying neurodegenerative diseases such as PD. In 2012, Yamanaka *et al.* were awarded the Nobel Prize for the discovery of iPSCs. The technique for producing pluripotent stem cells out of terminally differentiated cells is called reprogramming. Reprogramming was originally done by overexpressing a cocktail of the four transcription factors POU class 5 homeobox 1 (POU5F1/OCT4), MYC proto-oncogene (c-MYC), SRY-box 2 (SOX2) and kruppel like factor 4 (KLF4), using retroviral transfection (Takahashi and Yamanaka, 2006). Nowadays, advances are being made using non-integrative reprogramming techniques such as episomal RNA methods and the Sendai virus in order to reduce the mutagenic potential (Schlaeger *et al.*, 2015). Fibroblasts, or blood cells, are the cells of choice for reprogramming as they can be easily accessed. Nevertheless, in theory it is possible to reprogram every somatic cell of the human body.

Previously, the sources of human stem cells and in particular neural cells were limited. As the postnatal human brain has very limited regeneration capacity and the two existing NSC niches are inaccessible to sampling, the access to primary adult human neural cells was limited to adult post mortem human brain tissue at first. The discovery that human neural cells could be obtained through derivation from ESCs or from fetal NSCs accelerated stem cell research, however, serious ethical implications rose (Evans and Kaufman, 1981; Reubinoff *et al.*, 2000). Until the discovery of iPSCs, the limitations to human cells with neuronal lineage commitment were highly restricted and ethically controversial, thus often compensated by the use of animal models. *In vivo* studies using animal models, such as mice, however, often do not recapitulate the complexity of human neurodegenerative diseases. PD, for instance, is a human-specific disease and LRRK2-G2019S carrying mice do not show signs of neurodegeneration (Li

et al., 2010). Also, mouse models differ significantly in development, physiology, and genetics and do not recapitulate the genetic background associated with complex diseases (Avior *et al*., 2016). The use of iPSCs makes it possible to study human neural cells *in vitro* without ethical implications in a disease-relevant context such as the genetic background. Besides deciphering the mechanisms of a disease, *in vitro* disease models can also be used for personalized applications, such as patient- or disease-specific drug screening. Moreover, due to the restricted adult neurogenesis and neuro-regeneration potential of the CNS, iPSC-derived neural cells represent a promising tool for autologous transplantation strategies in neurodegenerative diseases (Daley and Scadden, 2008; Fu *et al*., 2015).

Limitations to consider when working with iPSCs are mainly linked to the reprogramming process. In order to avoid mutations caused by viral integration, non-integrative reprogramming techniques, are becoming the state of the art. Furthermore, so far, it is not known to which extent epigenetic modifications contribute to neurodegenerative diseases. The loss of age-related epigenetic signatures and the retention of an epigenetic memory that persists during reprogramming might influence PD disease models. On the one hand, iPSCs should have a highly accessible chromatin state with very similar miRNA, DNA methylation patterns, and histone modifications to ESCs (Buganim and Faddah, 2013). Therefore, they are considered to be their perfect counterpart and are, as such, in this state not appropriate for epigenetic disease modeling. Ideally, after the differentiation process, iPSCs should take the epigenetic signature characteristic of the cell type they have been differentiated into, which then makes them suitable for studying epigenetics (Fernández-santiago *et al*., 2015). On the other hand, however, it is not clear to which extend epigenetic changes are retained during reprogramming. An epigenetic memory from the somatic cell of origin can persist in iPSCs, which might influence the disease model or the differentiation potential (Hargus *et al*., 2014; Kim *et al*., 2010). In these models, the reprogrammed cells cluster more closely to their parental cell of origin than to ESCs. Moreover, different imprinting disorders have been modelled using iPSCs, showing that epigenetic signatures might be retained (Chamberlain *et al*., 2010). Additionally, aberrant DNA methylation patterns have been observed in iPSCs derived from twins demonstrating that these changes come from the reprogramming itself and are independent of the genetic background (Panopoulos *et al*., 2017). When working with iPSCs, further hurdles to overcome, include costs, correct handling techniques and the dependence on reliable differentiation protocols. For PD modeling, the derivation of homogenous NSC cultures as well as DNs are necessary. Although iPSCs are the ideal tool to model complex genetic disorders with multiple involved loci, other factors such as somatic mosaicisms, clonal variability, and non-genetic factors, including environmental influences and age, might play a role (Hillje and Schwamborn, 2016). Firstly, environmental influences such as life style, diet, exercise, and exposure to toxins are insufficiently recapitulated – if at all – in *in vitro* disease models based on patient cells.

Treatment of iPSCs with PD-associated chemicals such as rotenone, MPTP or 6-hydroxydopamine can simulate external stress factors in cellular models (Reinhardt *et al*., 2013a), but simultaneously creates a rather artificial environment. A second difficult factor to mimic in iPSCs is age. The reprogramming into iPSCs can be seen as a rejuvenation process, where the aging factor is lost (Hillje and Schwamborn, 2016). Although some age-related factors might be retained, such as damaged or mutated DNA, most of them (such as short telomeres, dysfunctional mitochondria, and changes in the transcriptome and epigenome) are lost (Frobel *et al*., 2014; Mahmoudi and Brunet, 2012). Several methods have been established to mimic aging in a dish. For instance, iPSC treatment with progerin, a truncated form of laminin which causes progeria (a premature aging disease), showed promising effects in modeling late onset disorders (Miller *et al*., 2013). Moreover, direct trans-differentiation protocols from fibroblasts to neurons with intact age signals have been generated (Tang *et al*., 2013, and follow up ADPD conference unpublished data). Furthermore, another important factor to consider, in paricular when studying PD, is the right control for individual genetic variabilities, as will be discussed in section 2.4.3.

2.4.2 *In vitro* NSC models

In vitro human NSC models are either derived from ESCs and iPSCs or from primary fetal or post-mortem brain tissue. Due to ethical reasons and tissue availability as described above, before the discovery of iPSCs, most neural studies were performed on rat or mouse models. As for every *in vitro* model, the production of NSCs by any strategy that perfectly recapitulates the *in vivo* situation is challenging. Primary NSC cultures that are directly extracted from *in vivo* seem to represent the physiologically most relevant cultures, but their availability is limited. Moreover, here too, their extraction from the natural environment and the culture under artificial 2D conditions, can lead to differences in gene expression, providing them with no advantages over iPSC- or ESC-derived lines (Conti and Cattaneo, 2010). Besides the usage of ESCs and iPSCs, recently, different direct conversion strategies from one somatic cell to another have been established (Xu *et al*., 2015). Nevertheless, significant work is still needed to optimize the protocols that often generate low numbers and impure functionally immature populations (Xu *et al*., 2015). To obtain patient-specific NSCs, the reprogramming through a pluripotent stem cell state still seems to represent the best option. As the use of ESCs for disease modeling was discovered long before iPSCs, most of the protocols in generating NSCs are based on mouse ESCs. As iPSCs are thought to have the same potential for generating NSCs *in vitro* as ESCs, similar derivation strategies can be used (Conti and Cattaneo, 2010). Different pluripotent stem cell derived *in vitro* NSC models recapitulating various developmental stages have been described over the last two decades (Figure 11). Four of the described NSC types, model neural plate identity and can adopt CNS and PNS fates. Two others represent cells from the developing neural tube, with restricted differentiation potential towards the CNS and two more can be associated with the fetal and adult brain. Upon neuronal

induction *in vitro*, the first neuroepithelial markers expressed in human pluripotent cells are PAX6 followed by SOX1 (Casarosa *et al.*, 2013). Other markers for NESCs are the stem cell marker SOX2, which cooperates with PAX6 and persists during neuroectodermal induction, and NESTIN, an intermediate filament protein that was first discovered in NESCs (Wegner and Stolt, 2005; Thakurela *et al.*, 2016; Lendahl *et al.*, 1990).

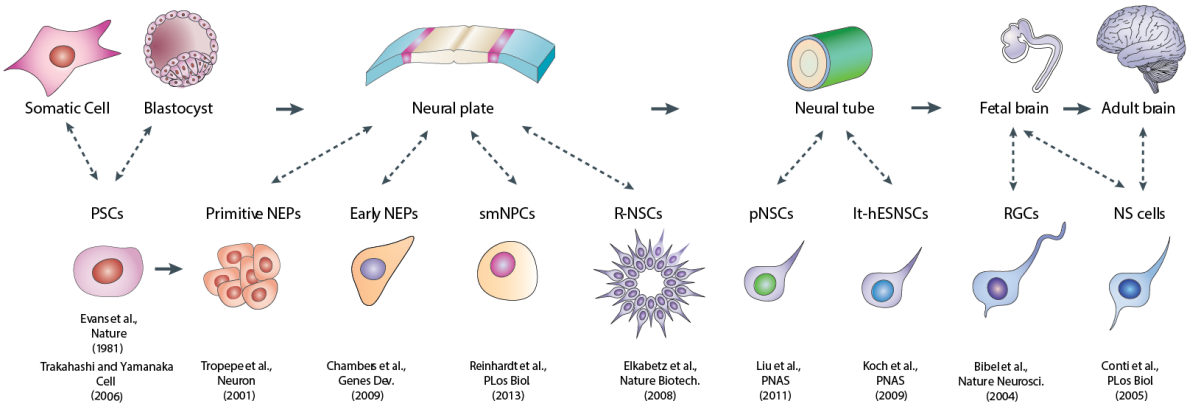

Figure 11. NSC populations that can be generated *in vitro* and their *in vivo* counterpart (I). Modified from Conti and Cattaneo, 2010. Pluripotent stem cells can give rise to different NESCs from the developing neural plate: primitive and early NEPs, smNPCs, and R-NSCs. NSCs with neural tube identity are pNSCs and lt-hSNSCs. Furthermore, RGCs and adult NSCs can be generated or cultivated *in vitro*. The papers giving their first description are cited below.

The most primitive NSC model represents neural eepithelial progenitors derived from mESCs that form neurospheres in presence of leukaemia inhibitor factor (LIF), a colony stimulating factor, in the absence of any other signals, demonstrating that neural induction can be induced through a default program (see section 2.1.1) (Tropepe *et al.*, 2001). Furthermore, similarly to during *in vivo* neural induction, TGF-ß inhibition enhances the transition into primitive neural epithelial progenitors (NEPs) (Tropepe *et al.*, 2001). These cells typically express NESC markers, but also exhibit ESC-like features, such as the expression of OCT4, and spontaneously differentiate into a more mature NSC stage, partly losing their differentiation potential (Conti and Cattaneo, 2010; Elkabetz *et al.*, 2008). Chambers *et al.* (2009) were the first to describe the formation of early NEPs by using small molecules in order to induce NSC fate from hESCs and iPSCs (Chambers *et al.*, 2009). The use of small molecules to induce stem cell fates permits cost-efficient, highly defined patterning (Reinhardt *et al.*, 2013b). Neural fate was induced by dual SMAD inhibition (SMAD=intracellular mediator of BMP/TGF-ß pathway inhibited by dorsomorphin/SB-431542) and SHH activation (Chambers *et al.*, 2009). These cells can differentiate into TH positive neurons, but also constitute a transient pre-rosette population that cannot be stably maintained (Conti and Cattaneo, 2010). Rosette-NCSs (R-NSCs) derived from hESCs by SHH and NOTCH signals were the first NESCs that stably retained their differentiation ability into region-specific neuronal fates, including dopaminergic neurons, of the CNS and PNS for several passages (Elkabetz *et al.*, 2008). R-NSCs typically arrange themselves in rosette-like structures similar to the developing neural tube and

start interkinetic nuclear migration as seen in RGCs (Elkabetz *et al.*, 2008). It should be noted that during *in vivo* development, the mature neural tube loses the ability to produce cells from the PNS. Another model that combines the advantages of stable maintenance, early neural plate differentiation potential and defined patterning by small molecules are the small molecule induced neural progenitor cells (smNPC) (Reinhardt *et al.*, 2013b). The smNPCs represent one of the cellular models used in this thesis, which are called here NESCs (paper III and discussion). The smNPCs are patterned from iPSCs, similar to the early NEPs, by dual SMAD inhibition. Furthermore, they can be maintained for long term in an immature state using CHIR, a glycogen synthase kinase (GSK3) inhibitor that induces WNT signalling, and purmorphamine (PMA), a molecule that induces the SHH pathway. The patterning gives them a NPBSC-like identity. Furthermore, they were shown to be able to differentiate into DNs (Reinhardt *et al.*, 2013b). Similar to smNPCs, primitive NSCs (pNSCs) are also induced by small molecules. In this study, the authors simultaneously inhibited the NOTCH, WNT, and TGF-ß pathways (Li *et al.*, 2011). They describe the production of a stable, LIF-dependent line able to differentiate into neurons from the CNS including mid and hindbrain neuronal subtypes, but not PNS. Thus, they represent cells from the early neural tube. Another neural tube-like NSC model is the rosette like long term human ESC derived NSC (lt-hESNSC), which still expresses the same traditional NESC markers (Conti and Cattaneo, 2010). Nevertheless, their rosette-like morphology, as well as a restricted differentiation potential towards the CNS, provides them – similar to the pNSCs – with a neural tube identity. The cells have long-term self-renewing capacities, can give rise to DNs, and are patterned by the mitogens' epidermal growth factor (EGF) and FGF-2 (Koch *et al.*, 2009). During *in vivo* development, the transition from the neural tube to the fetal brain is a continuum, making the positioning of *in vitro* NSCs from this stage difficult. Cultivation in the presence of EGF and FGF-2, which are normally used to cultivate RGCs, shows that the lt-hESNSC correspond to a later neural tube stage. Lt-hESNSC, however, are not mature RGCs, as the latter generally lose SOX1 expression in contrast to lt-hESNSC (Conti and Cattaneo, 2010). RGCs and adult NSCs can be isolated from fetal and adult mouse brains or derived from ESCs and iPSCs (Bibel *et al.*, 2004; Conti *et al.*, 2005). RGCs express similar to mature NSCs the proteins, SOX2, NESTIN and PAX6. Moreover RGCs express glial marker glutamate aspartate transporter (GLAST) and brain lipid binding protein (BLBP) (Conti and Cattaneo, 2010). The patterning of cells with EGF and FGF-2 highly affects their transcriptome and might influence cellular identities or create artificial ones. Interestingly, *in vitro* RGC- and adult NSC models are biased towards GABAergic neuron differentiation and their neuronal differentiation potential decreases in favor of gliogenesis over cellular passages (Conti and Cattaneo, 2010). In general, *in vitro* models cannot recapitulate the complete complexity of *in vivo* processes. *In vitro* NSCs, for instance, might lose their positional identity and their differentiation potential to generate neuronal subtypes, and long-term expansion often leads to an RG-like identity (Conti and

Cattaneo, 2010). Furthermore, sometimes only partial functional maturations are achieved (Conti and Cattaneo, 2010). Nevertheless, several NSC models are able to generate TH positive DNs *in vitro* with good efficiencies and their different differentiation potentials are reminiscent of chronological neurodevelopmental stages (Figure 11).

2.4.3 Isogenic controls for modeling PD

The study of PD, as already mentioned in section 1.2.1, often focuses on the rarer mutation-induced PD cases to understand the underlying cellular processes, rather than on the more prevalent complex disorder. However, even in those cases with an underlying monogenetic cause, the high degree of variability between patients requires the use of matched control lines that only differ in the mutation itself. Including gene-edited isogenic controls is necessary for iPSC-based *in vitro* disease modeling in order to recapitulate disease-relevant genetic alterations (Liu *et al.*, 2012b; Reinhardt *et al.*, 2013a; Soldner *et al.*, 2011). PD is, as elaborated in section 1.2.1, a multifactorial disease caused by a combination of different factors (environmental and/or genetic hits), and PD-associated phenotypes are susceptible to genetic background variations, such as polymorphisms. In addition the late onset of most PD cases, and the slow progression of the disease *in vivo* makes it difficult to recapitulate robust and rapid cellular phenotypes *in vitro* when compared to healthy donors (Soldner *et al.*, 2011). To discriminate between these subtle mutation-related phenotypes and genetic background induced differences, isogenic controls are necessary (Soldner *et al.*, 2011). Two kinds of isogenic controls can be defined to exclude the influence from the genetic background on the observed phenotypes. Gene-correcting a mutation in the diseased background can be used to investigate if the mutation is necessary to induce a phenotype, whereas the introduction of the mutation into the healthy background can be used to investigate if the mutation is sufficient to induce a phenotype. Different genome-editing techniques based on double stranded breaks followed by homologous recombination and repair have been used to generate iso-genetically matched controls. First, zinc-finger nucleases were used, followed by TALENS (transcription-activator like effector nucleases) and currently the CRISPR-Cas9 (clustered regularly interspaced short palindromic repeats-CRISPR associated genes) system is the most promising tool in order to introduce a synthetic donor DNA carrying a gene correction or a point mutation into the genome of a cell (Kim and Kim, 2014).

CRISPR-Cas9 genome editing

The CRISPR-Cas system acts as a prokaryotic “immune system” and protects bacteria and archaea from viruses and plasmids by integrating new spaces derived from genomic sequences of the intruder into their own DNA (Boyaval *et al.*, 2007). The integration of foreign DNA into the genome provides the bacteria with an “adaptive immunity” against the pathogen. The tool used for genetic editing is derived

from the type II CRISPR-Cas9 (protein 9 nuclease) from *Streptococcus pyrogens*. In this system, the intruding DNA is cut into small pieces of 20 nucleotides prior to integration, which are then incorporated into the host genome (Figure 12). These genomic spaces in the bacterial genome serve as templates to generate small RNA's, the so-called CRISPR RNA's (crRNA) that are used to guide a bacterial endonuclease. The endonuclease Cas9 then targets and cuts the intruding DNA of the invasive species based on sequence complementarity. As the newly transcribed variable crRNA encodes not only a single but multiple pre-crRNA's upon immune system activation, a second non-variable, stable trans-activating RNA (tracrRNA) needs to be generated. This tracrRNA is complementary to one part of the mature crRNA and, as it represents the non-variable fraction of the interfering RNA, it is recognized by the Cas9 protein. Besides cutting foreign DNA, the Cas9 protein also helps in the crRNA maturation. Once the mature crRNA:tracrRNA is produced and recognized by Cas9, it guides the endonuclease to the target sequence that needs to be destroyed (Figure 12). The destruction of double-stranded foreign DNA is based on the generation of double-stranded breaks that are performed by two domains of the protein, the HNH and Ruv-C motifs. In order to cleave the foreign DNA, the Cas9 protein needs not only to recognize the tracrRNA, but also a conserved sequence of two to five nucleotides, known as the protospacer-associated motif (PAM) that immediately follows the 3´- end of the produced crRNA. (Nishimasu *et al*., 2014; Deltcheva *et al*., 2011; Sapranauskas *et al*., 2011).

Within cells, double-strand nicks, such as produced by Cas9, are either repaired by non-homologous end joining (NHEJ) or homologous recombination if a homology arm is present. In order to use the mechanism to introduce a mutation into a cell, a donor template displaying shared homology with the targeted locus needs to be supplied. This sequence is called the donor DNA and needs to be inserted by homology-directed recombination into a specific target sequence. The first step completed in order to use this mechanism for targeted gene editing was to provide the system *in vitro* with a synthetic single guide RNA (sgRNA) that replaced the crRNA and tracrRNA and directs the Cas9 protein to a targeted sequence-specific DNA cleavage (Jinek *et al*., 2012). Other hurdles to overcome in order to exploit the system's potential for targeted gene editing are the repair through NHEJ leading to insertions or deletions (indel), as well as random integration (Cho *et al*., 2013). To prevent indel forming NHEJ, the system was optimized through the usage of paired nickases that only produce a single-strand break and increase the system's specificity (Cong *et al*., 2013; Ran *et al*., 2013). This improvement in specificity, however, often reduces efficiency. In addition to the challenges linked to NHEJ, off-target mutations present a real problem. Random integration results from the fact that, in human cells, Cas9 is able to tolerate up to five mismatches in the protospacer region or one mismatch in the PAM sequence (Fu *et al*., 2014a). To counteract this miss-pairing, different techniques have been established. Using truncated sgRNAs, adding two extra guanine nucleotides into the 5'- end and once

again, using paired nickases can address the problem and minimize the off-target integrations (Fu *et al.*, 2014b; Ran *et al.*, 2013; Ren *et al.*, 2014). In general, the efficiency of the CRISPR-Cas9 system is, with 2-4% in iPSCs and even higher percentages in other eukaryotic cells, better than most other systems (Yang *et al.*, 2013). Furthermore, to increase efficiency, multiple guide sequences can be introduced simultaneously to edit multiple sites at once (Cong *et al.*, 2013). All in all, CRISPR-Cas9 gene editing technology is an important tool for disease modeling and beyond this, can have broad applications in biotechnology and medicine.

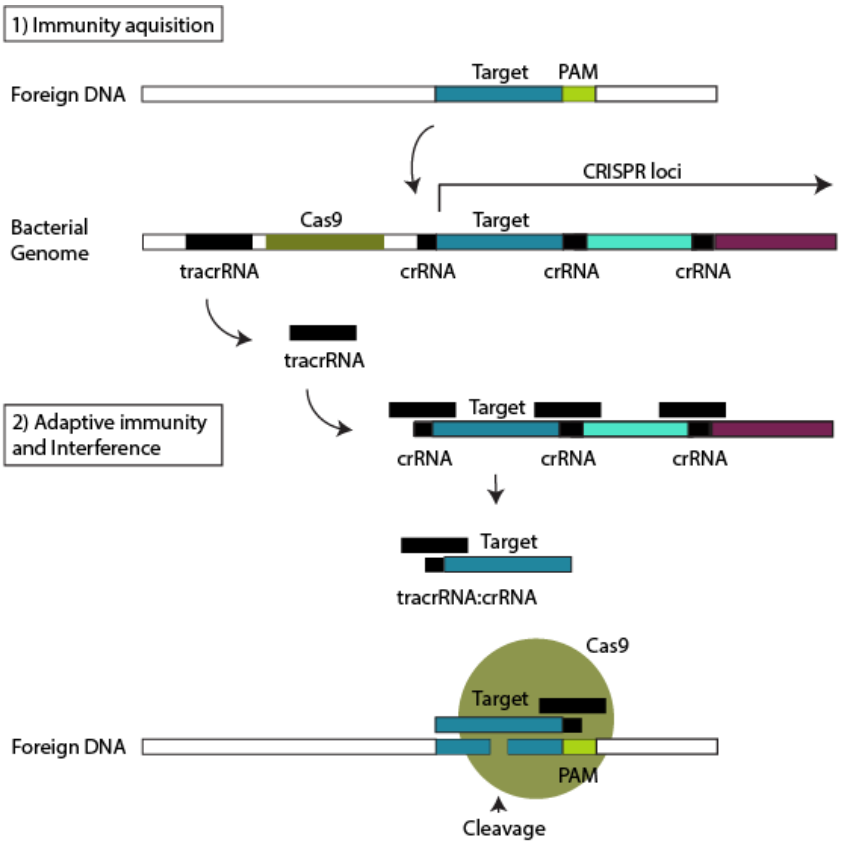

Figure 12 CRISPR-Cas9 adaptive immune system. Inspired from New England biolabs. In the acquisition phase, foreign DNA is incorporated into the bacterial genome. During interference, the target sequence is used in order to generate a complementary sequence that binds and guides Cas9 to cleave the foreign DNA.

AIMS AND HYPOTHESIS

AIMS AND HYPOTHESIS

iPSC derived *in vitro* disease models aim to compare healthy individuals to diseased ones on a cellular level to gain new insights into the disease-causing mechanisms. The aim of this thesis is to use neural stem cells as a model for neurodegenerative diseases, notably PD, and thereby unmask the conditions underlying the disease (Figure 13). Patient-specific NSCs have the inherent potential to self-renew and give rise to all three neural cell lineages and, as such, represent the ideal basis for *in vitro* disease models of the CNS. By using traditional cellular and molecular biology as well as high throughput omics techniques, a top-down systems biological-like approach was adopted to characterize the different cell lines and unravel the potential causes underlying the disease phenotypes. Top-down, meaning that knowledge from the entire biological system (the NESC phenotypes) and system-wide data of different omic levels was used in order to identify the underlying molecular pathways (Shahzad and Loor, 2012). Furthermore, the disease models were enhanced by the generation and usage of isogenic control lines in order to investigate the different genetic contributions to disease manifestation.

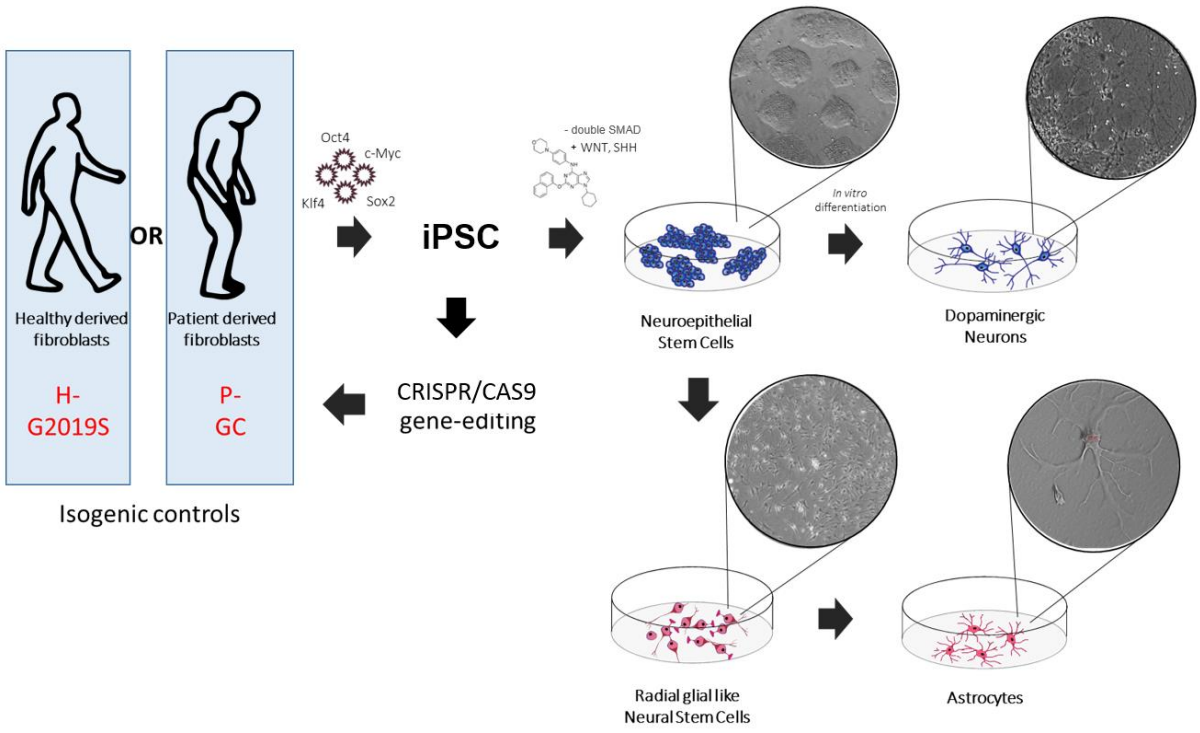

Figure 13. Disease models. Human fibroblasts are sampled from PD patients and healthy donors and reprogrammed into iPSCs using a cocktail of at least the four transcription factors KLF4, OCT4, c-MYC and SOX2. iPSCs are further patterned into NESCs using small molecules. NESCs (paper III) can be differentiated into DNs (paper III) or further derived into radial glia, such as NSCs (paper I), that can generate astrocytes (paper I). CRISPR-Cas9 gene editing technology, on the iPSC level, allows the production of isogenic control lines, by insertion or gene-correction of the mutation into the healthy or patient genetic background respectively (paper II).

AIMS AND HYPOTHESIS

The main focus of the thesis is on the role of neural stem cells (paper **I**, **II** and **III**) as a physiologically relevant *in vitro* model for PD. Our first aim was to derive and characterize different cell lines for studying PD. Two different neural stem cell lines (NSCs and NESCs) were used and astrocytes (paper **I**) and DNs (paper **III**) were generated. The proper cell type specific characterisation is of major importance in creating a homogenous cell population that reflects the desired properties of the model. As PD is a multifactorial disease, our second aim was to produce isogenic control lines to take into consideration individual genetic variabilities during PD modeling. A new method was established in order to ameliorate the derivation process of matched control lines and phenotypes were established as proof of principle (paper **II**). The third and main objective was to use the models in order to study PD with a focus on the LRRK2-G2019S mutation (paper **III**). Highlighting differences between healthy and patient-derived cells, as well as between isogenic controls, provides new insights into the genetic background of the patient and the function of the LRRK2-G2019S mutation in PD. Firstly, LRRK2-G2019S or genetic background dependent phenotypes were established. Secondly, transcriptomics were used to analyze the genetic causes underlying these phenotypes. This approach allowed to identify the potential mechanism of LRRK2-G2019S functionality and discover new susceptibility factors for PD within the patient genetic background. Lastly, rescue strategies for reversing the observed phenotypes were implemented to validate the model and the integrity of the results.

The aim to study PD-associated phenotypes in neural stem cells was based on the hypothesis that PD has a strong neuro-developmental component (Figure 14). The predisposition to suffer from PD in later stages of life may already be determined during embryogenesis. Various evidence shows that stem cell proliferation, differentiation and cell death are affected by several PD relevant mutations including LRRK2-G2019S (elaborated in section 2.3). Consequently, an imbalance in the tight regulation of NSC homeostasis may lead to impairments of the CNS development. Some of the major pathways in neuronal development have been shown to be deregulated by PD-associated mutations and these disease-causing genes were shown to be expressed or play a role in neural development. Moreover, it was shown that idiopathic and sporadic PD cases might also have a genetic contribution (see section 1.1). The very diverse development and outcome of the disease, and the highly variable age of onset, compared to other age-associated neurodegenerative diseases, strengthens the possibility of a genetic origin of PD and a neurodevelopmental component. As PD is a multifactorial disease, a further hypothesize is that genetic modifiers within the PD patient's genetic background act as susceptibility factors for developing PD. LRRK2-G2019S carriers, for instance, have an incomplete penetrance where familial, sporadic, and asymptomatic cases have been reported. In addition, polymorphisms contribute to the LRRK2-G2019S associated phenotypes and are linked to the age of onset of the disease. Hence, LRRK2-G2019S induced PD represents a suitable model for discovering new genetic modifiers within

the patient genetic background and to address the neural developmental hypothesis in PD pathogenesis.

Interestingly, different mutations lead to a phenotypically similar disease where the symptoms share a common overall characteristic, a complex genotype-phenotype relationship with altered metabolism and cellular activity. The fact that different factors and genetic mutations lead to the same outcome might imply a common origin. An early occurring event leading to developmental deficiencies could explain why a panoply of different factors are able to induce the same disease. Midbrain DN susceptibility could result from NSC impairments that deregulate the DN differentiation process and make DNs more vulnerable. In this thesis, PD is considered in terms of a multi-hit hypothesis, implying genes, age, and environment together with a predisposed developmental anlagen lead to the disruption of the system's compensation strategy, such as metabolic adaptation, and tips it "over the edge". Together with modifiers in the genetic background, the developmental deficiencies in PD might explain why most of the mutations have an incomplete penetrance, and why some people have a higher susceptibility to develop PD than others. Susceptibility factors in neural stem cells might contribute to a neurodevelopmental predisposition for PD.

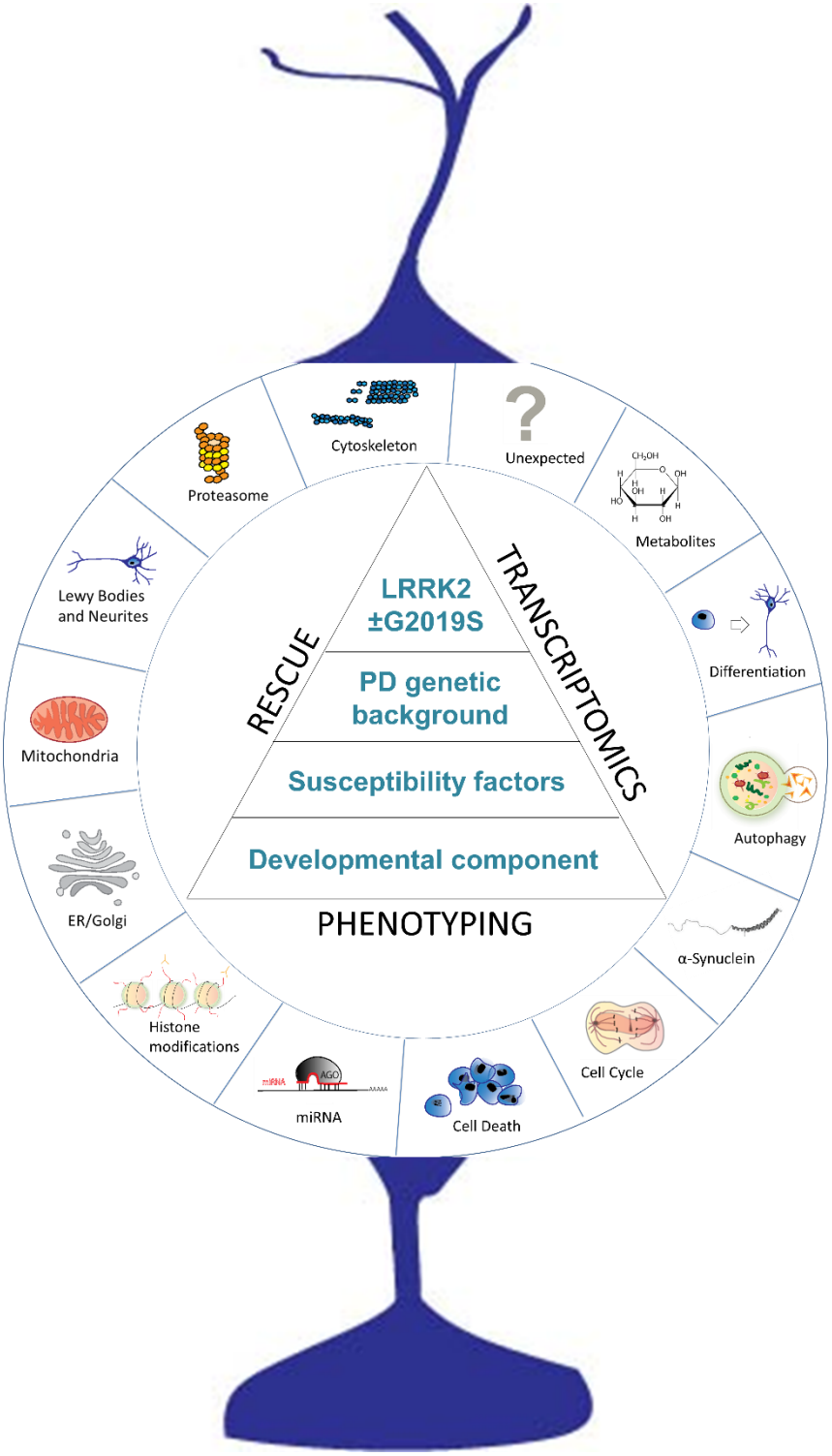

Figure 14. Aims and hypothesis. We studied LRRK2-G2019S in hNESCs in order to identify LRRK2-G2019S dependent phenotypes linked to any of the cellular processes LRRK2 is involved in. We further tried to unravel the contribution of the genetic background to the observed phenotypes by using isogenic controls. We carried out transcriptomic analysis aiming to identify the genes underlying the phenotypes and discover new susceptibility factors. These genetic modifiers might be implicated in any of the PD-associated processes and could potentially be used to discover new rescue strategies. Most importantly, we wanted to demonstrate that cells from a developmental stage already show impairments in PD.

MATERIAL AND METHODS

MATERIAL AND METHODS

Detailed information about the material and methods used can be found in the publications listed (see Results). In the following section a concise summary of all the experimental procedures I participated in will be described, and if not stated otherwise, I performed them myself.

Cell culture: Two NSC types were used in the following publications, hNSCs (publication **I**) and hNESCs (publication **II** and **III**). hNSC lines were maintained and differentiated 6 weeks into astrocytes or multi-lineage differentiation cultures for metabolomic profiling (my contribution to publication **I**). hNESCs were maintained and differentiated into DNs as described in publication **III**.

Immunocytochemistry: All stainings of hNESCs in publication **III** were performed by myself as described in the corresponding material and methods.

Microscopy: Confocal and high-throughput microscopy using OPERA was performed by myself. Analysis of confocal images of NESCs was done by hand counting or Image J, see paper **III**. Analysis of high throughput images by a computational script was done by coauthors of paper **III** and see **appendix 1.5**. Biological interpretation was done by myself.

MTT essay: MTT essay was performed as described in publication **III**.

Metabolomics: Intracellular polar phase metabolite extractions were performed in publication **I** and publication **III**. Additionally stable isotope glucose labelling was done within publication **I**. Blood sample metabolite extractions for publication **III** were performed by a coauthor.

GC/MS and metabolic analysis: Metabolomics were conducted by a facility (LCSB or LACDR), biological interpretation was performed by myself for publication **III**, but not **I**.

Western blotting: Protein extraction and Western blots were performed as described in paper **III**.

Transcriptomics: RNA was extracted and sent out for microarray analysis (Genomics Core Facility EMBL). RNA quality controls were performed by myself (paper **III** and **II**). Array generation was the contribution to paper **II** that was performed by myself.

Transcriptomic analysis: Computational analysis of microarray data was performed by collaborators, biological interpretation, and Ingenuity pathway analysis was performed by myself (paper **III** and **II**). A second, stricter statistical analyzing strategy using the limma package from Bioconductor and the eBayes method was performed by a collaborator (**appendix 1.4** related to paper **III**).

qPCR: qPCR was performed as indicated in paper **III**.

Statistical analysis: Was performed using Graphpad prism as described in the corresponding figures in paper III.

ChIP-seq: Chromatin was extracted by myself. Immuno-precipitation, analysis and modeling was performed by a collaborator. Interpretation was done by myself see **appendix 1.3**, related to paper III.

Disease network modeling: Was performed by a collaborator, see **appendix 1.2**, related to paper **III.** Interpretation was done by myself.

Writing and editing: Paper III was written by myself, paper II was edited, paper I was read.

All other methods used in the papers not described here above were performed and interpreted by the authors of paper I and II.

A description of the methods, where the results are shown in **appendix 1**, and which are not described in the material and methods of the papers I, II and III, will follow:

ChIP-seq for H3K27ac and core regulator network formation; related to paper III (In collaboration with Déborah Gérard and Aurélien Ginolhac):

For chromatin immunoprecipitation-sequencing (ChIP-seq) cells were seeded in 10 cm dishes and chromatin was extracted after 6 days in culture. DNA and proteins were crosslinked using 1% formaldehyde (Sigma-Aldrich, F8775-25ML) for 8 min. 5 min quenching was done by 125 mM glycine (1 M) (Carl Roth, 3908.3). Cells were washed 2x with PBS, 1x protease inhibitor cocktail (PIC) (Roche, 11846145001) and scraped in 1.5 ml lysis buffer [5 mM 1,4-Piperazinediethanesulfonic acid, pH 8.0 (Carl Roth, 9156.3); 85 mM potassium chloride (KCl) (PanReac AppliChem, A2939); 0.5% 4-Nonylphenyl-polyethylene glycol (NP-40) (Fluka Biochemika, 74385)]. After a 30 min incubation phase on ice, cells were re-suspended in 1.5 ml shearing buffer [50 mM Tris Base, pH 8.1 (Carl Roth, 4855.2); 10 mM Ethylenediamine tetraacetic acid (EDTA) (Carl Roth, CN06.3); 0.1% Sodium Dodecylsulfate (SDS) (PanReac Applichem, A7249); 0.5% Sodium deoxycholate (Fluka Biochemika, 30970)] and sonicated for 25 cycles (30s ON, 30s OFF). For the immunoprecipitation 30 µg of sheared chromatin and 3 µg as input were used. The chromatin was diluted 1:10 with modified RIPA buffer [140 mM sodium chloride (NaCl) (Carl Roth, 3957.2); 10 mM Tris, pH 7.5; 1 mM EDTA; 0.5 mM ethylene glycol-bis(β-amino-ethyl ether)-N,N,N',N'-tetraacetic acid (EGTA) (Carl Roth, 3054.3); 1% Triton X-100 (Carl Roth, 3051.2); 0.01% SDS; 0.1% sodium deoxycholate; 1xPIC]. The sample was incubated with 5 µg of an antibody against acetylated histone 3 lysine 27 (H3K27ac) (Abcam, ab4729). The antibodies were captured using 25 µL of PureProteome™ Protein A Magnetic Beads System (Millipore, LSKMAGA10) for 2 hours at 4°C on a rotating wheel. After, the beads were captured using a DynaMag™-2 magnetic stand (Life Technologies, 12321D), the supernatant was discarded and the beads were washed twice with 800 µL of

immunoprecipitation wash buffer 1 [20 mM Tris, pH 8.1; 50 mM NaCl; 2 mM EDTA; 1% Triton X-100; 0.1% SDS], once with 800 µL of immunoprecipitation wash buffer 2 [10 mM Tris, pH 8.1; 150 mM NaCl; 1 mM EDTA ; 1% NP-40; 1% sodium deoxycholate; 250 mM of lithium chloride (Carl Roth, 3739.1)], and twice with 800 µL of Tris-EDTA buffer [10 mM Tris, pH 8.1; 1 mM EDTA, pH 8.0]. Finally, the beads and the inputs were incubated with 100 µL of ChIP elution buffer [0.1 M sodium bicarbonate ($Na_2CO_{3)}$ (Sigma-Aldrich, S5761); 1% SDS]. The cross-linking was reversed by adding 10 µg of RNase A (ThermoFisher, EN0531) and 20 µg of proteinase K (ThermoFisher, EO0491) at 65°C overnight. Then, the eluted chromatin was purified using a MinElute Reaction Cleanup Kit (Qiagen, 28206) according to the manufacturer's instructions. The DNA concentration was measured using the Qubit® dsDNA HS Assay Kit (ThermoFisher, Q32851) and the Qubit 1.0 fluorometer (Invitrogen, Q32857) according to the manufacturer's protocol. The sequencing of the ChIP samples was done at the Genomics Core Facility in the EMBL Heidelberg, Germany. For sequencing, single-end and unstranded reads were used and the samples were processed in an Illumina CBot and sequenced in an Illumina HiSeq 2000 machine. The mapping of the reads was done using Burrows Wheeler Aligner (BWA) [v0.7.10, (Li and Durbin, 2009)]. The ChIP-Seq peaks were called with HOMER for H1 H3K27ac, using input from H1. The quality of reads from FASTQ files was assessed using *fastqc* [v0.11, Andrews, 2010; see www.bioinformatics.babraham.ac.uk/projects/fastqc]. A short fraction of reads showed adapter sequences at the 3'- end. The trimming of those sequences was performed by AdapterRemoval [v1.5, Lindgreen 2012] requiring a minimum length of 25 bp. Bases with a poor Phred score (0-2) were also trimmed out. The PALEOMIX pipeline [v1.0.1 (Schubert *et al.*, 2014)] was used for trimming and mapping. Trimmed reads were then mapped using BWA with the backtrack algorithm adapted to short sequences. The human reference was the human genome GRCh38.p1 (accession number: GCA_000001405.16) downloaded from NCBI. In order to keep reads mapped to a unique location in the genome, reads with a mapping quality below 30 were filtered out.

Disease network modeling; related to paper **III** (by Muhammad Ali)

Disease network modeling, using the transcriptomic data of differentially expressed genes (DEGs) between healthy and patient lines was performed by a collaborator. It is based on a compilation of gene–gene interaction maps from literature resources. A reconstruction of phenotype-specific gene regulatory networks was performed and candidate genes for network perturbation were selected. This approach permits the identification of drugs and multitarget combinations for reversing the disease phenotype. The method is described in Zickenrott *et al.* (2016), and none of the steps were performed by myself.

Microarray limma analysis; related to paper **III** (by Aurélien Ginholac)

The *limma* R package enabled contrast comparison using linear models and moderated *t*-tests. Briefly put, this method (Ritchie *et al*., 2015) computed several summary statistics via the *eBayes()* function for each gene and each contrast. The M-value is the log2-fold change for that gene. The moderated *t*-statistic is the ratio of the M-value to its standard error. Compared to the ordinary *t*-statistics, the standard errors are moderated across all genes, thus shrunk to a common value using a Bayesian model. This approach helps in borrowing data from the ensemble of genes to infer information about each individual gene. From moderated *t*-statistics, *p*-values are deduced as for ordinary t-statistics, but degrees of freedom are increased, reflecting the greater reliability associated with the smoothed standard errors (Smyth, 2004).

Quantification of TH compared to TUJ1 positive neurons; related to paper **III** (by Silvia Bolognin and Paul Anthony)

Neurons were seeded and differentiated by myself for 14 days, and TH and TUJ1 were stained according to the protocol described in paper **III**. Images were acquired by myself using the Opera High Content Screening Microscope (Perkin Elmer). Images were analyzed using a Matlab script generated in-house based on the following steps. For the segmentation of TUJ1+ neurons, a strategy combining global and local thresholding was implemented. For global thresholding, image preprocessing was done via low pass filtering. The raw TUJ1 channel was convolved with a Gaussian filter of size 10 and standard deviation 3, and the resulting global neuronal mask was defined by threshold 150. For local thresholding, a difference of Gaussians was applied in the preprocessing step. In particular, the background defined via convolution with a Gaussian filter of size 20 and standard deviation 6 was subtracted from the foreground defined via convolution with a Gaussian filter of size 10 and standard deviation 3. The local neuronal mask was then defined by those pixels with values larger than 3. The concepts of global and local thresholding were combined by retaining those pixels in the neuronal mask, which were detected by at least one of these methods. For further refining the neuronal mask, connected components with less than 200 pixels were removed. To analyze TH+ neurons, the raw channel was convolved with a Gaussian filter of size 10 and standard deviation 1. The resulting mask was defined by threshold 100. For further refining the TH mask, connected components with less than 10 pixels were removed. TH mask was normalized to TUJ1 for each cell line.

RESULTS

RESULTS

1 Publication I

Rapid and robust generation of long-term self-renewing human neural stem cells with the ability to generate mature astroglia

Thomas Palm[1,*], Silvia Bolognin[2,*], Johannes Meiser[2], Sarah Nickels[2], Claudia Träger[1], Ralf-Leslie Meilenbrock[1], Johannes Brockhaus[3], Miriam Schreitmüller[3], Markus Missler[3,4] & Jens Christian Schwamborn[1, 2]

*These authors contributed equally to this work.

[1] Stem Cell Biology and Regeneration Group, Institute of Cell Biology (ZMBE), Westfälische Wilhelms-Universität Münster, 48149 Münster, Germany

[2] Luxembourg Centre for Systems Biomedicine (LCSB), University of Luxembourg, Esch-Belval, Luxembourg

[3] Institute of Anatomy and Molecular Neurobiology, Westfälische-Wilhelms University, Münster, Germany

[4] Cluster of Excellence EXC 1003, Cells in Motion, CiM, Münster, Germany

Nature Scientific Reports. 2015; 5:16321

1.1 Preface

Astrocytes represent the most abundant cells of the CNS and outnumber neurons fivefold. They exert many essential and complex functions within the CNS and respond to all forms of insults (Sofroniew and Vinters, 2010). Here we show how to use iPSC derived NSCs to generate mature astrocytes that can be used as a model to study neurodegenerative diseases. Astrocytes, for instance, play important roles in the development of DNs and are affected in PD (see sections 1.1.4 and 2.1.3). The use of iPSCs in order to model neurodegenerative diseases represents, as previously discussed in section 2.4.1, the state of the art in the field. However, some hurdles still must be overcome. It still remains challenging and time consuming to efficiently differentiate iPSCs to the desired cell type. Here we describe a robust and rapid method in order to generate NSCs with radial glial-like features that can be maintained under self-renewing conditions. Another difficulty to address is the developmental stage, maturity, and functional activity of the generated cell lines. The NSCs were derived through the intermediate state of NESCs and therefore represent cells from the developing neural tube. Their radial glial-like features make them a perfect precursor cell type for generating astrocytes (see section 2.2.2). Most importantly, the differentiated astrocytes showed a mature and functional phenotype. Hence, the NSCs and astrocytes both represent worthy models to address the contribution of development and the role of astrocytes in PD.

My contribution to this study was the culturing and differentiation of NSCs into mature astrocytes and multilineage differentiation cultures (MLDCs) for 6 weeks followed by metabolite extraction. Material and methods are described in the “cell culture” and “extraction of intracellular metabolites” sections respectively. Results are depicted in Figures 5 and 6. Interpretation of the results was not done by myself.

SCIENTIFIC REPORTS

OPEN

Received: 27 May 2015
Accepted: 12 October 2015
Published: 06 November 2015

Rapid and robust generation of long-term self-renewing human neural stem cells with the ability to generate mature astroglia

Thomas Palm[1,*], Silvia Bolognin[2,*], Johannes Meiser[2], Sarah Nickels[2], Claudia Träger[1], Ralf-Leslie Meilenbrock[1], Johannes Brockhaus[3], Miriam Schreitmüller[3], Markus Missler[3,4] & Jens Christian Schwamborn[1,2]

Induced pluripotent stem cell bear the potential to differentiate into any desired cell type and hold large promise for disease-in-a-dish cell-modeling approaches. With the latest advances in the field of reprogramming technology, the generation of patient-specific cells has become a standard technology. However, directed and homogenous differentiation of human pluripotent stem cells into desired specific cell types remains an experimental challenge. Here, we report the development of a novel hiPSCs-based protocol enabling the generation of expandable homogenous human neural stem cells (hNSCs) that can be maintained under self-renewing conditions over high passage numbers. Our newly generated hNSCs retained differentiation potential as evidenced by the reliable generation of mature astrocytes that display typical properties as glutamate up-take and expression of aquaporin-4. The hNSC-derived astrocytes showed high activity of pyruvate carboxylase as assessed by stable isotope assisted metabolic profiling. Moreover, using a cell transplantation approach, we showed that grafted hNSCs were not only able to survive but also to differentiate into astroglial *in vivo*. Engraftments of pluripotent stem cells derived from somatic cells carry an inherent tumor formation potential. Our results demonstrate that hNSCs with self-renewing and differentiation potential may provide a safer alternative strategy, with promising applications especially for neurodegenerative disorders.

Recent advances in the field of somatic cell reprogramming have enormously furthered the use and optimization of pluripotent stem cells (iPSCs) since the seminal studies by Yamanaka and coworkers[1,2]. Despite enormous progresses have been made in the methods for efficiently generating hiPSCs, their directed differentiation into a specific cell type remains technically challenging. This limited ability to generate pure specific cell populations renders the clinical use of pluripotent-derived cells still an obstacle.

The utilization of somatic fate restricted stem cells may be an alternative to achieve faster and more homogenous differentiation into the desired terminally differentiated cell types. It has been shown in mice that primary neural stem cells (NSCs) bear the advantage of being expandable while maintaining their neurogenic and gliogenic differentiation potential[3,4]. Therefore, the use of hiPSC derived hNSCs as a source for glia cells and neurons represents a promising strategy[5]. Stable cultures of hNSC may avoid

[1]Stem Cell Biology and Regeneration Group, Institute of Cell Biology (ZMBE), Westfälische Wilhelms-Universität Münster, 48149 Münster, Germany. [2]Luxembourg Centre for Systems Biomedicine (LCSB), University of Luxembourg, Esch-Belval, Luxembourg. [3]Institute of Anatomy and Molecular Neurobiology, Westfälische-Wilhelms University, Münster, Germany. [4]Cluster of Excellence EXC 1003, Cells in Motion, CiM, Münster, Germany. *These authors contributed equally to this work. Correspondence and requests for materials should be addressed to J.C.S. (email: jens.schwamborn@uni.lu)

time and cost consuming maintenance of pluripotent stem cells as well as potential immune rejection and teratoma formation[6].

Particularly interesting is the possibility of generating human astrocytic cultures starting from the same precursor cells used to generate neurons. Traditionally, astrocytes were solely described as supporting elements for neurons. Now, astrocytes are recognized as essential players involved in brain information processing[7–10]. Alteration of their functions has emerged as a clear factor in disease pathogenesis, especially for neurodegenerative diseases. Additionally, increasing data support the critical role of astroglia in disease progression. As an example, it has been shown that glia cells have a direct, non-cell autonomous effect on motor neuron survival in a mouse model of amyptrophic lateral sclerosis[11]. Despite this growing evidence, astrocytes are less investigated compared to neurons. The lack of an acknowledged and well-characterized set of human astroglial markers and the difficulty to obtain cultures of human astrocytes under defined conditions is partly accounting for that.

Optimizing robust and reproducible protocols for the derivation of multiple cell types is clearly necessary to fully explore the enormous potential offered by iPSC technology. Several human iPSC lines derived from patients suffering from different diseases have been generated, including Parkinson´s disease[12] (PD), Alzheimer´s disease[13] and schizophrenia[14,15]. Gene-editing approaches have been used to correct genetic mutations on PD patient derived-iPSC, resulting in the successful reversal of pathological phenotypes[12]. As iPSCs are derivable in a patient-specific manner, they are suitable for autologous engraftments[16] and for personalized disease modeling[17]. iPSCs might also offer a powerful tool in preclinical research to test both toxicity and efficacy of new drug candidates. Basing preclinical tests directly on the target human cells rather than on surrogate cell models, often from other rodents, hold the promise of leading to more efficient drug screening[18]. Notably, in the field of neurodegenerative diseases, hundreds of compounds have been successfully used in animal models to ameliorate induced-neuropathology or cognitive deficits. Yet this has not translated into effective disease-modifying therapies for humans. Obviously, differences between rodent and human physiology impede translation of rodent results to humans[19]. Thus, the possibility of testing drug candidates on patient-specific cells is of fundamental importance for diseases such as neurodegenerative disorders, which only affect humans.

A second application of iPSC is replacement therapies[20,21]. The use of iPSCs overcomes the legal/ethical concerns as well as the risks of immune rejection of human embryonic stem cells (hESCs). Despite these advantages, iPSCs, as well as hESCs, have the inherent potential for teratoma formation[6].

In this study, we describe the robust and rapid generation of hNSCs from hiPSCs. Furthermore, their maintenance and directed differentiation is described. In contrast to most other NSC studies we focus on a detailed characterization of human astroglial differentiation. We put a specific emphasis on the generation of long-term expandable human astrocyte cultures, which can be of use for modeling of disease-specific pathological traits.

Materials and Methods

Cell culture. iPSC from 3 individuals were cultured in feeder-free maintenance media (mTeSR, StemCell Technologies) and detached from plates using dispase (1 mg/mL) for 30min at 37°C with the help of a scraper in case of big colonies. Colonies were collected by sedimentation and resuspended in "EB Medium": Knockout™ DMEM (Gibco), 20% Knockout™ SR (Gibco), NEAA (Gibco), penicillin/streptomycin (Invitrogen) and ß-mercaptoethanol (Gibco) supplemented with 10 µM SB-431542 (Ascent Scientific), 1 µM dorsomorphin (Tocris), 3 µM CHIR 99021 (Axon Medchem) and 0.5 µM PMA (Alexis). 48 hours later, the medium was replaced by N2B27 medium (DMEM-F12 (Gibco)/Neurobasal (Gibco) 50:50 supplemented with 1:200 N2 supplement (Invitrogen), 1:100 B27 supplement lacking vitamin A (Invitrogen), penicillin/streptomycin and glutamine (Invitrogen) supplemented with 10 µM SB-431542, 1 µM dorsomorphin, 3 µM CHIR 99021 and 0.5 µM PMA. After additional 48 hours, the medium was replaced by N2B27 medium supplemented with 3 µM CHIR 99021, 0.5 µM PMA and 150 µM ascorbic acid (Sigma Aldrich). Two days later, neural tube like structures were disintegrated by pipetting and small pieces were plated on Matrigel (BD Biosciences) coated 12-well plates in N2B27 medium supplemented with 3 µM CHIR 99021, 0.5 µM PMA and 150 µM ascorbic acid. At day 8, the medium was exchanged by N2B27 medium supplemented with 3 µM CHIR 99021, 0.5 µM PMA, 150 µM ascorbic acid and 20 ng/ml basic (b) FGF (Peprotech). At day 12, cells were detached using dispase and cultivated in hNSC Maintenance Medium on Matrigel coated 10cm dishes. "Human NSC Maintenance Medium" was composed by DMEM HAM's F12 medium (Gibco) supplemented with 40ng/ml EGF (Peprotech), 40 ng/ml bFGF, N2 supplement, B27 supplement (with vitamin A), glutamine, Penicillin/Streptomycin and hLIF (1.5 ng/ml). Human NSCs were splitted (1:2 ratio) at a confluence of 70–80% by using dispase.

At a confluence of 70–80% the hNSC Maintenance Medium was switched to "Neuron differentiation medium" which was composed by N2B27 Medium supplemented with 10 ng/mL BDNF (Peprotech), 10 ng/mL GDNF (Peprotech), 1 ng/mL TGF-β3 (Peprotech), 200 µM ascorbic acid and 500 µM dbcAMP (Sigma Aldrich). Cultures were tested/harvested after 4 weeks of neuronal differentiation. Astrocytic differentiation was induced by switching the hNSC Maintenance Medium to the basic medium (DMEM HAM's F12 medium, glutamine, Penicillin/Streptomycin) supplemented with 1% FCS (Gibco)[3,4]. Finally, multilinear differentiation was achieved by replacing the maintenance medium by the basic medium containing 10% of FCS.

Immunocytochemistry. For immunohistochemical analysis, cells were fixed with 4% paraformaldehyde (PFA) in 120mM phosphate buffer (PBS), pH 7.4, permeabilized with 0.05% Triton X-100 in PBS, blocked with 10% goat serum in PBS and subjected to immunohistochemistry staining with primary and secondary antibodies diluted in the blocking solution.

For immunolabelling the following antibodies at indicated dilutions were used: anti-Nestin (1:400; BD Bioscience), anti-Sox1 (1:100; R&D Systems), anti-Sox2 (1:200; Abcam), anti-Pax6 (1:200; DSHB), anti-Ki67 (1:200; Vector Labs), anti-TuJ1 (1:400; Covance), anti-Map2 (1:200; Millipore), anti-DCX (1:200; Millipore), anti-GFAP (1:200; Millipore), anti-O4 (1:50, Sigma-Aldrich), anti-GABA (1:200, Abcam), anti-vGlut1 (1:200; Millipore), anti-TH (1:100, Millipore), anti-Synaptophysin (1:100; Millipore), anti-PSD95 (1:200; Invitrogen), anti-vimentin (1:5000; Abcam), anti-S100β (1:1000; Sigma-Aldrich), anti-aquaporin 4 (AQP4, 1:100; Santa Cruz Biotechnology) and anti-excitatory amino acid transporter 2 (EAAT2, 1:100; Santa Cruz Biotechnology), secondary Alexafluorophore-conjugated antibodies (1:1000, Invitrogen). DNA was stained using Hoechst 33258 (1:10000, Invitrogen). All cells expressing a particular marker were counted manually and normalized to the total number of cells.

Microarray. mRNA was extracted from hiPSCs, hNSCs and derived cells using the RNAeasy kit (Quiagen) following manufacturer's recommendations. mRNA quantity and purity were determined by using a NanoDrop ND-1000 spectrophotometer (NanoDrop Technologies). Additional quality check was performed by the Agilent Bioanalyzer (Agilent). Gene expression profiles were generated using HumanGene 2.0ST arrays according to manufacturer's recommendations (Affymetrix).

Bioinformatics. Correspondence analysis (CoA) from the TIGR MeV (MultiExperimentViewer; http://www.tm4.org/mev/) expression analysis platform was performed on the whole transcriptome established by the HumanGene 2.0ST arrays after RMA normalization proposed by the Affymetrix Expression Console.

GeneOntolgy (GO) analysis was performed on the 1428 transcripts specifically differing hNSCs from parental hiPSCs and from filial hMLDCs by a 2-fold difference. Here, we used the GO–biological process analyzer implemented in the DAVID analysis platform (http://david.abcc.ncifcrf.gov/)[22]. GO terms and associated p-values (0.05 or lower) were then introduced into the REVIGO webserver[23] to establish network files. These files were than uploaded to the cytoscape software where the final GO-Network was built up (www.cytoscape.org)[24].

RT-qPCR. For quantification analysis, total RNA (mRNAs and miRNAs) was extracted from hiPSCs, hNSCs, human neurons (4 weeks of differentiation) and human astrocytes (6weeks of differentiation) by the RNAeasy kit (Quiagen) following manufacturer's recommendations. Gene expression levels were evaluated by the SYBR-Green Jump Start Taq Ready Mix (Sigma-Aldrich) following manufacturer's recommendations. Gene-related intensity levels were evaluated upon normalization with *GAPDH* levels. The following primers were used:

GAPDH: GTGGACCTGACCTGCCGTCT, GGAGGAGTGGGTGTCGCTGT
OCT4: CCTCACTTCACTGCACTGTA, CAGGTTTTCTTTCCCTAGCT
NANOG: TGAACCTCAGCTACAAACAG, TGGTGGTAGGAAGAGTAAAG
SOX2: CCCAGCAGACTTCACATGT, CCTCCCATTTCCCTCGTTTT
Ki67: ATACGTGAACAGGAGCCAG, CCTTGGAATCTTGAGCTTTCTC
SOX1: AATTTTATTTTCGGCGTTGC, TGGGCTCTGTCTCTTAAATTTGT
NESTIN: CTGGAGCAGGAGAAACAGG, TGGGAGCAAAGATCCAAGAC
PAX6: ATGTGTGAGTAAAATTCTGGGCA, GCTTACAACTTCTGGAGTCGCTA
GFAP: CTGCTCAATGTCAAGCTGG, AATGGTGATCCGGTTCTCC
MAP2: GGAGACAGAGATGAGAATTCCT, GAATTGGCTCTGACCTGGT
TH: GTGCTAAACCTGCTCTTCTC, TTCAAACGTCTCAAACACCT
SLC6A11 (GABA): CAACAACTGCTACAGGGAC, GAGAAGATGGCAAACCCAG
SLC17A7 (Glutamate transporter): CCATGACTAAGCACAAGACTC, AGATGACACCTCCATAGTGC.

Extraction of intracellular metabolites and Gas Chromatography-Mass Spectrometry. Astrocytes and MLD cultures were cultivated for 6 weeks in 12-well plates and washed with 1 ml of 0.9% NaCl and quenched with 0.2 ml −20 °C methanol. After adding an equal volume of 4 °C cold water, cells were collected with a cell scraper and transferred in tubes containing 0.2 ml −20 °C chloroform. The extracts were shaken at 1400 rpm for 20 min at 4 °C (Thermomixer Eppendorf) and centrifuged at 16,000 × g for 5 min at 4 °C. 0.2 ml of the upper aqueous phase was collected in specific glass vials with micro inserts and evaporated under vacuum at −4 °C using a refrigerated CentriVap Concentrator (Labconco).

Metabolite derivatization was performed using a Gerstel MPS. Dried polar metabolites were dissolved in 15 µl of 2% methoxyamine hydrochloride in pyridine at 40 °C under shaking. After 60 min an equal volume of MTBSTFA was added and held for 60 min at 40 °C. 1 µl sample was injected into an SSL injector at 270 °C in splitless mode. GC/MS analysis was performed using an Agilent 7890A GC equipped with a 30 m DB-35MS + 5m Duraguard capillary column. Helium was used as carrier gas at a flow rate of 1.5 ml/min. The GC oven temperature was held at 100 °C for 2 min and increased to 300 °C at 10 °C/min.

After 3 min, the temperature was increased to 325 °C. The GC was connected to an Agilent 5975C inert XL MSD, operating under electron ionization at 70 eV. The MS source was held at 230 °C and the quadrupole at 150 °C. The detector was operated in scan mode with mass range m/z 70–800. The total run time of one sample was 25.00 min. All GC/MS chromatograms were processed by using MetaboliteDetector[25]. Mass isotopomer distributions (MIDs) were determined and corrected for natural isotope abundance using MetaboliteDetector (Hiller *et al.*, 2009). For determination of MIDs the following ions were selected (Wegner *et al.*, 2014): Asparatate_3TBDMS: 418–427; Citrate_4TBDMS: 591–601; Glutamate_3TBDMS: 432–442; Serine_3TBDMS: 390–397; Glycine_2TBDMS: 246–252; Lactate_2TBDMS:261–269.

Electrophysiology. For electrophysiological recordings coverslips with hNSC derived neurons were transferred to a recording chamber mounted on an upright microscope (Zeiss, Oberkochen, Germany) and kept in a bath solution containing (in mM): NaCl 130, KCl 3, NaHCO3 10, CaCl2 1.5, MgCl2 1, Glucose 11, HEPES 10, pH 7.3 with NaOH. Patch pipettes with 2−4 M were filled with (in mM) K-gluconate 125, KCl 20, EGTA 0.5, MgATP 4, MgCl2 4, Na2GTP 0.3, HEPES 10, pH 7.4 with KOH. Measurements were done with an EPC10 amplifier and Patchmaster software (HEKA, Lambrecht, Germany). For puff-application of KCl or glutamate, a pipette with 15 µm tip diameter was placed 60–100 µm away from the recorded cell. Pressure ejection was controlled by a pico pump (PV830, WPI, Sarasota, FL).

Measurement of Glutamate Uptake. Astrocytes DIV 80–90 and HEK 293 cells were incubated for 10 minutes at 37 °C in basic media containing 50 M of L-glutamic acid (Sigma). Glutamate uptake was measured using a colorimetric kit (abcam) according to manufacturer's instructions. Absorbance measurements were normalized to total protein per culture well.

Mice. 12 week old male NOD/SCID mice were kept under standard conditions according to governmental rules and regulations. All experiments have been conducted according to the German Animal Welfare Act and have been approved by the responsible authorities (Landesamt für Natur, Umwelt und Verbraucherschutz Nordrhein-Westfalen). For each transplantation approach, 3 animals were used.

hNSC transplantation. For stereotactic injections, mice were under deep anesthesia (intraperitoneal injection of 17 µl of 2.5% Avertin per gram of body weight) and fixed into a stereotactic frame (Kopf). Three microlitres of cell suspension (in total: 1×10^5–2×10^5 cells) were injected into the lateral ventricle over 5 minutes using a Hamilton 7005KH 5µl syringe. Following stereotactic coordinates in relation to bregma were used: anteroposterior: 1.4 mm, mediolateral: ±0.84 mm, dorsoventral: −2.5 below skull. In order to control the hNSC fate after transplantation, we introduced an *in vitro* pre-differentiation step in our experimental set-up. At the first step, passage 6 or higher hNSCs were splitted in a 1:2 ratio. Three days later, the hNSC maintenance medium in one of the dishes was changed to neuronal differentiation medium, while the second dish was subjected to astroglial differentiation by replacing the maintenance medium by glial differentiation medium. After one week of pre-differentiation, 1×10^6 to 2×10^6 cells were transplanted into the brain of adult NOD/SCID mice. The cell fate was analyzed 6 additional weeks later.

Perfusion, sectioning and immunohistochemistry. Mice under deep anesthesia were perfused with 50 ml PBS following 50 ml 4% PFA/1 PBS solution. After dissection, isolated brains were post-fixed in 4% PFA/1 PBS solution over night at 4 °C. 40 µm sagittal brain sections were cut using a Vibratom (Leica VT 1200 S). Free-floating sections were permeabilized in Tris-buffered saline solution with 0.1M Tris, 150mM NaCl, pH 7.4/0.5% Triton-X 100/0.1% Na-Azide/0.1% Na-Citrate/5% normal goat serum (TBS+/+/+) for at least 1 h. The primary antibodies anti-Hu Nuclei (1:200; Millipore), anti-DCX (1:400; Abcam), anti-TuJ1 (1:600; Covance) and anti-GFAP (1:100; Millipore) were diluted in TBS+/+/+ and incubated for 48 h on a shaker at 4 °C. For immunofluorescence staining, secondary Alexa-fluorophore conjugated antibodies (Invitrogen) and Hoechst 33258 (1:10000, Invitrogen) were used. Sections were analyzed with a Zeiss LSM 710 confocal microscope.

Statistical analysis. Data presented are means ± SEM. Statistical significance was tested with Sigma Plot software. Results were denoted statistically significant when p values were < 0.05; number (n) of samples/repeats are given in the Results and Figure legends.

Results

Newly generated hNSCs conserved self-renewing characteristics. We maintained human iPSCs on mouse embryonic fibroblasts (MEFs) or under feeder free conditions, and treated them according to the scheme in Fig. 1a. As described previously[12], the neural induction of embryonic bodies from hiPSC (Fig. 1b,c) was achieved by inhibition of BMP and TGFß signaling[26,27]. Simultaneously, we administered CHIR99021 and Purmorphamine to stimulate the canonical WNT- and SHH-pathways[28,29]. These neural-induced embryonic bodies (Fig. 1c) were cultivated under defined conditions until neural tube like structures appear (Fig. 1d). Neural rosette-like structure formation was induced by supplementing the culture medium with bFGF[3] for four additional days (Fig. 1e). After re-plating, the cells were cultured

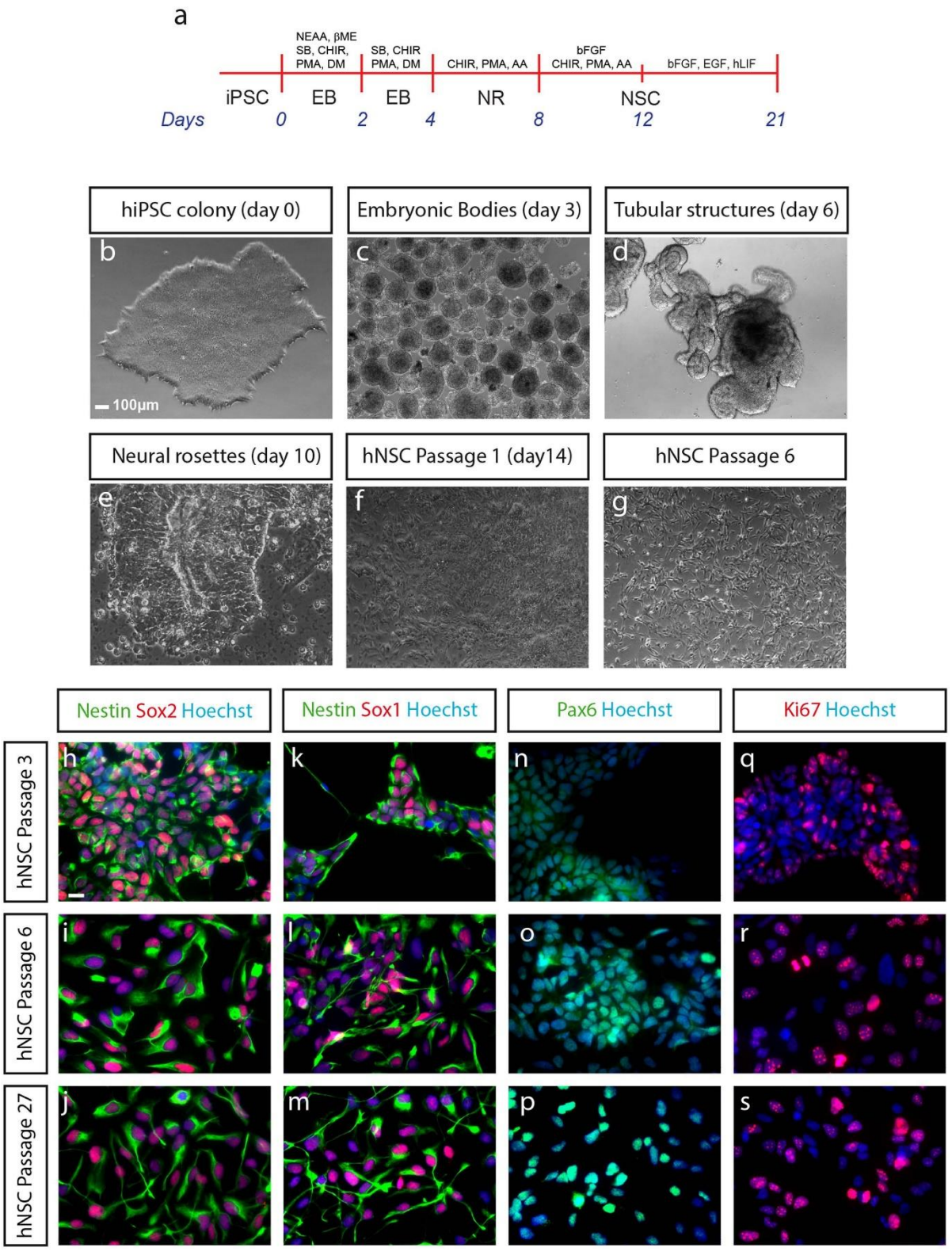

Figure 1. Generation of human neural stem cells (**a**) Schematic representation for directed differentiation of iPSC cells to hNSC. (**b–g**) Phase contrast of images of the generation of hNSC. (**b**) Feeder-free hiPSC. (**c**) Embryonic bodies after 3 days of differentiation. (**d**) Tube like structures after six days of differentiation. (**e**) Induction of neural rosette formation at day 10. (**f**) First passage of hNSCs at day 14 of hiPSC differentiation; (**g**) heterogeneous cell population becomes homogeneous after several passages. hNSC. (**h–s**) Immunofluorescence labeling of the neural stem cell markers Nestin, Sox2, Sox1 and Pax6 as well as of the cell cycle marker Ki67 of hNSCs at Passage 3 (**h**,**k**,**n**,**q**), Passage 6 (**i**,**l**,**o**,**r**) and Passage 27 (**j**,**m**,**p**,**s**). Scale bar 10 µm.

in presence of EGF, bFGF, N2, B27 and hLIF. Following the first passages, the initially heterogeneous cell clusters adopted a homogeneous morphology (Fig. 1f,g). Induction of differentiation into either the neuronal or the glial lineage (details see below) induced further changes in morphology.

One key characteristic of neural stem cells is their extensive self-renewal potential. This ability was evaluated by measuring the cell number over the first 21 passages following their generation. The resulting exponential growth curve showed stable proliferation rates over the 21 passages analyzed (Figure S2a). To confirm that generated hNSCs preserved self-renewing characteristics, we evaluated the presence of the stem cell markers Nestin, Sox2, Sox1 and Pax6 at early (passage 3 and 6) and late (passage 27) pas- sages (Fig. 1h–p). While Nestin, Sox1 and Sox2 showed very similar expression patterns, Pax6 displayed cytoplasmic labeling at lower passage numbers and more nuclear labeling at higher passages (Fig. 1n–p), which is in agreement with data on brain development[30]. Finally, we observed that hNSCs maintained proliferation characteristics, as demonstrated by the positive labeling of the cell cycle marker Ki67 across passages (Fig. 1q–s). These results demonstrate that generation and maintenance of hiPSC-derived hNSCs was achieved robustly, and that hNSCs maintained self-renewing characteristics over numerous passages.

hNSCs revealed distinct gene expression profile. In order to further characterize the generated hNSCs, we compared the mRNA transcriptome of hiPSCs, and hNSCs derived from these progenitors (Fig. 2). Additionally, we included differentiated cells, derived from these hNSCs in the analysis. Since the induced differentiation was undirected, multiple cell types were present in this population; consequently we consider this a multilineage differentiation (hMLDCs) (Figure S1). To minimize the interlineage differences existing between iPSC-lines generated from different individuals[31], we based our comparison on hiPSCs, hNSCs and hMLDCs derived from the same individual. The transcriptome-based correspondence analysis (CoA) of the three cell types demonstrated that hiPSCs, hNSCs and hMLDCs were characterized by distinct molecular expression signatures (Fig. 2a).

The paired comparison of hiPSCs and of hNSCs in a scatter blot highlights that neural-stem-cell-genes (Pax6, Sox1 and Nestin) were higher expressed in hNSCs when compared to their parental hiPSCs. Similarly, hNSCs showed a significant downregulation of the pluripotency genes Lin28a, Nanog and Oct4 (Fig. 2b and Figure S2b). RT-qPCR analysis comparing the expression levels of the pluripotency genes Oct4 and Nanog as well as the neural-stem-cell-gene Nestin between hiPSCs and hNSCs confirmed these data (Fig. 2c). Interestingly, the neural stem cell specific marker Nestin was found nearly absent in hiPSCs when compared to hNSCs. The marker Sox2, predicted to be strongly expressed within pluripo- tent[1] and neural stem cells[32], as well as the proliferation marker Ki67, exhibited similar expression levels within hiPSCs and hNSCs.

We further isolated 1428 transcripts that differed at least twofold between hNSCs, hiPSCs and hMLDCs. The resulting Gene Ontology (GO) analysis revealed that genes specifically expressed in hNSCs were mainly involved in the biological processes development, differentiation, neurogenesis and cell adhesion (Fig. 2d). In order to better decipher key mechanisms important for hNSC maintenance, we performed a network analysis on the "biological-process GO-terms" that were statistically associated with the 1428 enriched hNSCs genes. Within the GO-Network, we observed that the GO terms clus- tered as sub-networks that may be outlined as "Tissue development", "Cell growth and differentiation", "Neurogenesis and neuron development", "Regulation of catabolism and metabolism" and "Regulation of BMP signaling pathway" (Fig. 2e). We also compared the transcriptional profiles of hiPSCs, hNSCs and hMLDCs and identified the genes differentially regulated in the 3 groups (Table S1 and Figure S3). By this approach, we were able to define a unique expression signature that clearly distinguished hNSCs from less differentiated hiPSCs as well as from the more differentiated hMLDCs.

hNSCs differentiated into mature astrocytes. In the next step we wanted to demonstrate the ability of hNSCs to differentiate into astrocytes. The astrocytic differentiation medium consisted of the basic cultivation medium supplemented with 1%FCS. The most commonly used marker protein for astrocytic differentiation is GFAP. However, astrocytes positive for GFAP are considered to show a reactive phenotype while astrocytes negative for GFAP show a quiescent phenotype with protoplasmic morphology, as described previously[33]. We therefore used the additional markers S100β and vimentin to investigate astrocyte differentiation.

After 45–50 days of differentiation, we observed that nearly 100% of the cells were expressing S100β (Fig. 3a). After 60 days, some astrocytes showed GFAP immunoreactivity while all the cells expressed vimentin (Fig. 3b–d). S100ß was expressed in 100% of the cells also at this time point (Fig. 3f–h). The contamination with neurons was negligible as shown by the Tuj1 staining (Fig. 3e). We further observed that after 60 days of differentiation, some cells still expressed the proliferation marker Ki67 (Fig. 3g), indicating that they are able to proliferate, a capacity shared with primary astrocytes[34,35]. In support, loss of neural stem cell- and proliferation markers with simultaneous increase of glial markers was also observed by RT-qPCR. *Nestin* and *Ki67* were significantly downregulated upon 45 days of glial differentiation and we observed a massive increase in the expression levels of *GFAP* gene (Fig. 3i).

Remarkably, after 60 days of differentiation all astrocytes also expressed a basal level of AQP4 (Fig. 4a), a marker for the main water channel in the perivascular membranes, typically present in astrocytic end-feet in brain tissue. Additionally, they expressed the glutamate transporter EAAT2 (Fig. 4b) that is used by astrocytes *in situ* to remove glutamate from the extracellular space. This is a key function of mature

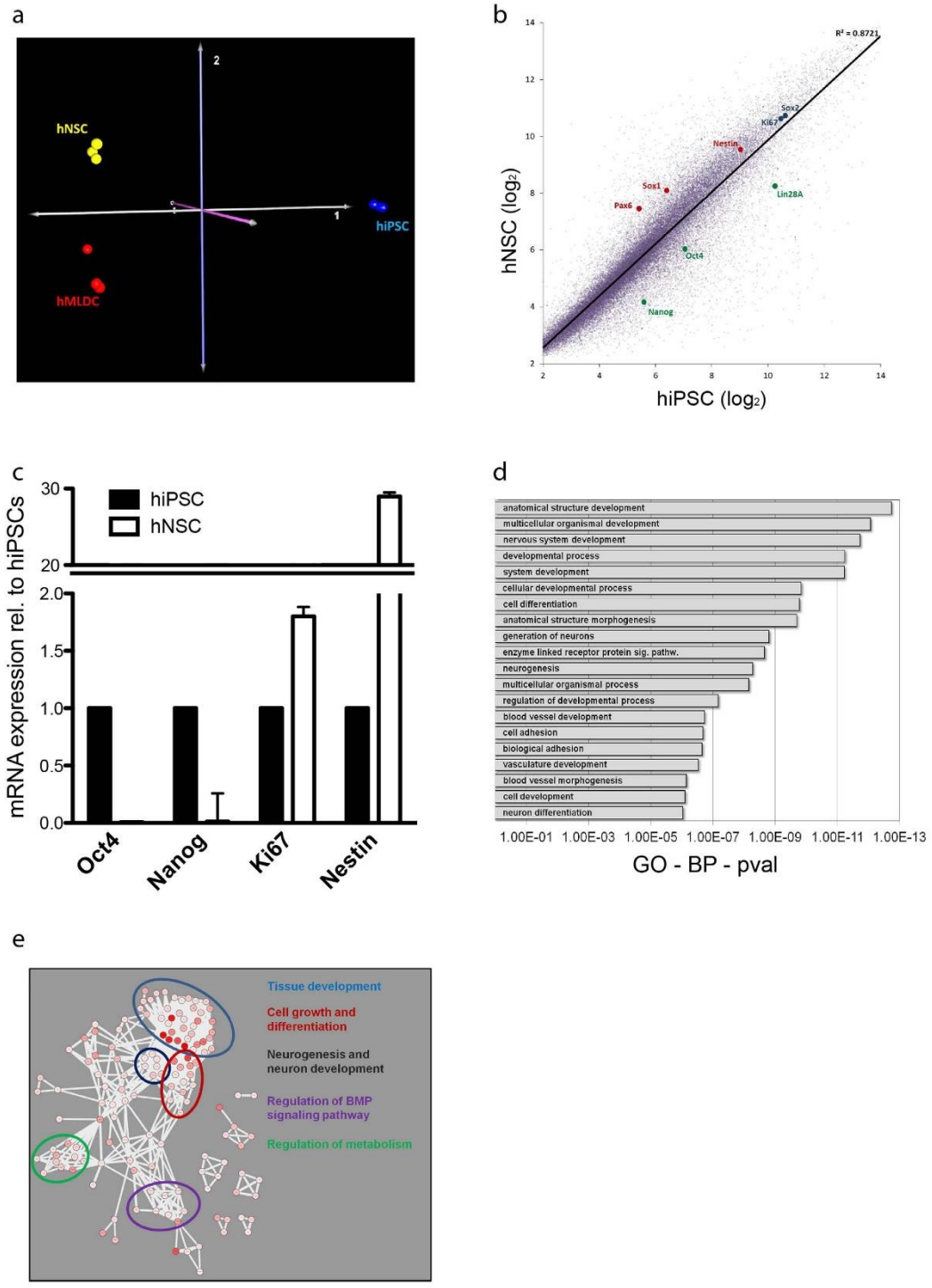

Figure 2. Molecular Characterization of hNSCs (**a**) Multi-Dimensional Scale analysis based on the mRNA transcription profiles of hiPSCs (blue), hNSCs (yellow) and hMLDCs (red). All profiled cell-types were generated from the same individual. (**b**) mRNA scatter blot of hiPSCs and hNSC; hNSC specific genes (red), hiPSC specific genes (green), genes observed in both cell types (black). (**c**) mRNA expression levels of OCT4, Nanog, Ki67, SOX2 and Nestin in hiPSC and hNSC quantified by RT-qPCR. (**d**) Gene Ontology analysis based on the 1428 genes specifically expressed in hNSCs when compared to hiPSCs and hMLDCs. (**e**) GO terms were subjected to a network analysis based on ReviGO (http://revigo.irb.hr/) and CytoScape (http://www.cytoscape.org/) softwares. The main GO sub-clusters are highlighted.

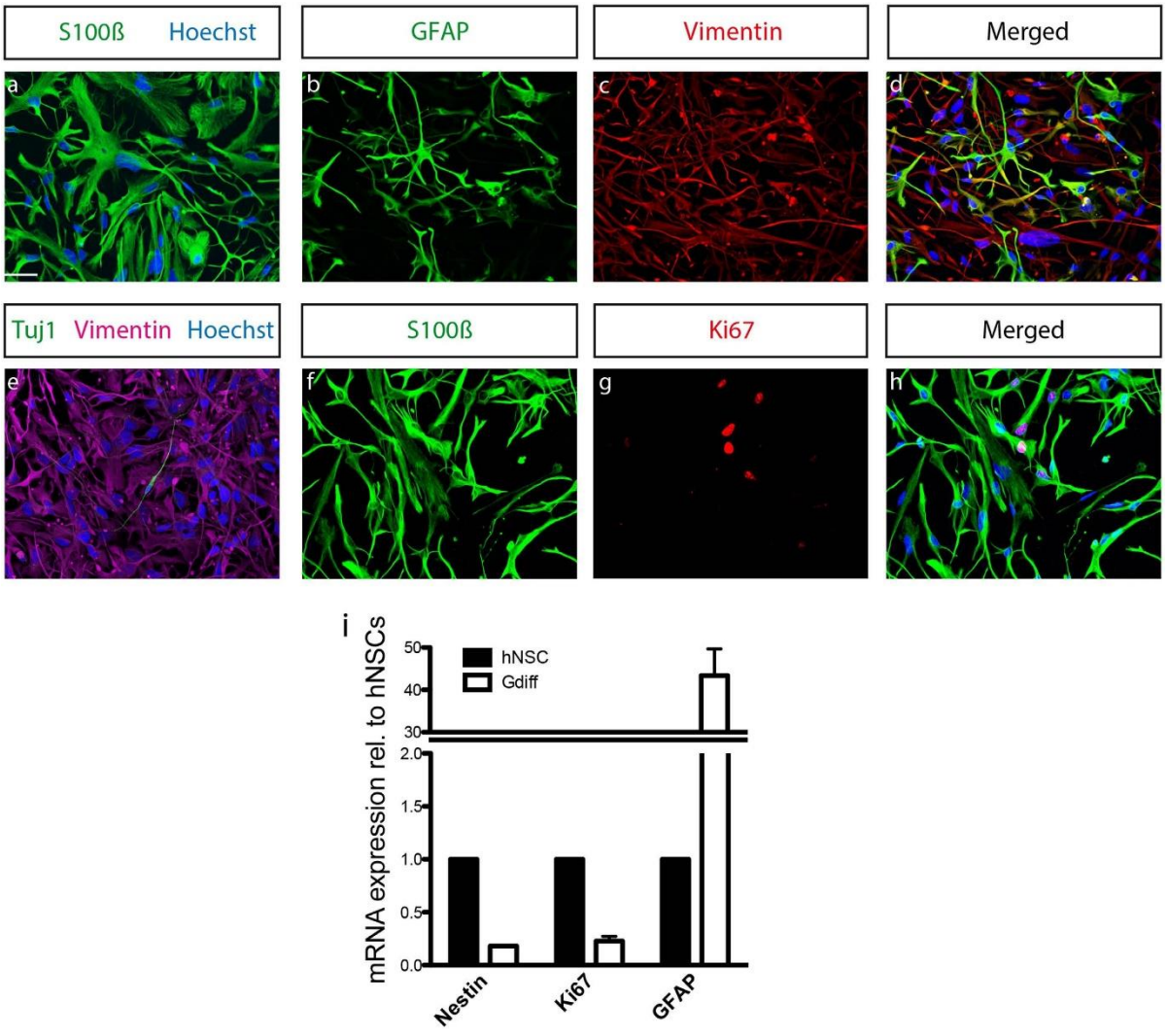

Figure 3. Rapid generation of hNSC derived astrocytes. Representative confocal images illustrating the expression of astrocytic markers (**a**) S100β after 50 days of differentiation, (**b–d**) GFAP-vimentin, (**e**) Tuj1-vimentin, (**f–h**) S100β-Ki67. (**i**) mRNA expression levels of *Nestin, Ki67, GFAP* in hNSC and astrocyte quantified by RT-qPCR.

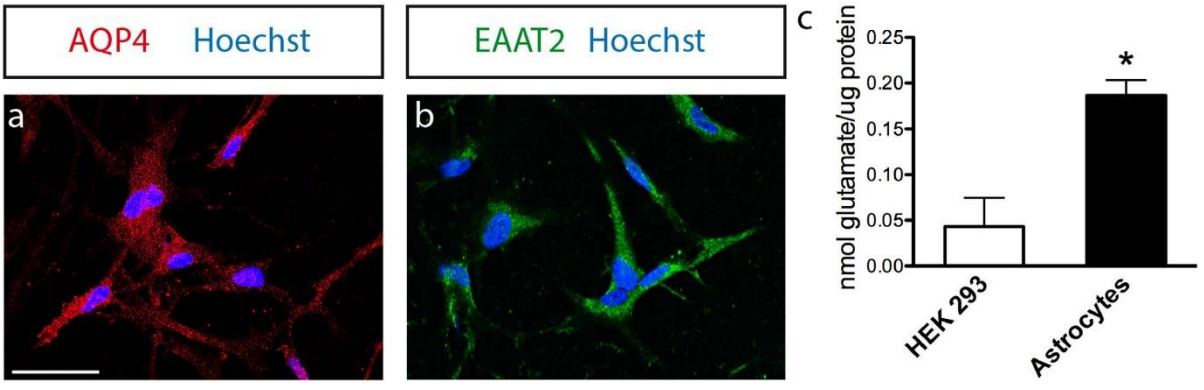

Figure 4. Astrocytes displayed mature functions. Representative confocal images illustrating the expression of astrocytic markers (**a**) AQP4 and (**b**) EAAT2 after 60 days of differentiation. Scale bars 50 µm.
(**c**) Glutamate up-take in astrocytes DIV 80–90 and HEK 293. Mean ± SEM; n = 3 indipendent experiments.

astrocytes[36] that was also confirmed by a glutamate uptake assay (Fig. 4c). Astrocytes differentiated for 80–90 days were able to transport glutamate intracellularly. We assessed HEK 293 as a cell type with no specific glutamate intake ability ($p = 0{,}016$, Student *t* test).

Our results demonstrate that by replacing the hNSC maintenance medium with the adequate differentiation medium it was possible to induce a robust and homogenous differentiation into astrocytes. The homogeneous immunoreactivity toward AQP4 and EAAT2 and the ability to transport glutamate suggest that hNSC-derived astrocytes reached a certain level of maturity and functionality.

Astrocytes showed increased pyruvate carboxylase activity and reduced serine biosynthesis. A hallmark of astrocytes is the presence and the relative high activity of the metabolic enzyme pyruvate carboxylase (PC)[37]. PC catalyzes the carboxylation of pyruvate to the tricarboxylic acid cycle (TCA) intermediate oxaloacetate. This reaction is important during anabolic processes to replenish the TCA cycle with oxaloacetate. To investigate the presence and the activity of pyruvate carboxylase in hNSCs derived astrocytes we used uniformly labeled [U-^{13}C]glucose to monitor the fate of glucose in astrocytes. Application of this stable isotope tracer results in isotopic enrichment in all metabolites downstream of the tracer (*e.g.* metabolites of the glycolysis and the TCA cycle). The isotopic enrichment can be measured using Gas Chromatography/Mass Spectrometry. In case pyruvate is oxidized via pyru- vate dehydrogenase to acetyl-coA the succeeding citrate molecule shows a mass enrichment by two (M2 isotopologue). In case of pyruvate carboxylation by PC the succeeding citrate molecule shows a mass enrichment by three (M3 isotopologue). M5 citrate isotopologues result from both, pyruvate dehydro- genase and PC activity (Fig. 5a).

Using this approach, we compared pure astrocyte cultures with multi-lineage differentiation cultures (MLDCs) and we observed increased PC activity in the pure astrocyte culture (17% enrichment vs. 4% enrichment of M3 aspartate) (Fig. 5b). We also observed increased M3 and M5 isotopologue abundance of citrate originating from M3 oxaloacetate as the precursor (Fig. 5c). To compare the amount of glucose contributing to the citrate pool, we calculated the total carbon contribution from glucose to citrate in both culture conditions (Fig. 5d). We determined 24% glucose carbon contribution to citrate in pure astrocyte cultures and only 15% glucose carbon contribution in MLDCs. This difference was also visible in glutamate (Fig. 5d,e). In summary, these data show increased PC activity and glucose derived carbon contribution into the TCA cycle in astrocytes compared to MLDCs.

Besides glucose, the amino acid glutamine represents the most important carbon source for cells. This is especially pronounced in proliferating cells or in any cell type with increased anabolic demands[38]. To evaluate the impact of glutamine to the TCA cycle of astrocytes we used uniformly labeled [U-^{13}C] glutamine and investigated the isotopic enrichment in citrate. In the astrocyte cultures we found that glutamine provided similar amounts of carbons for the synthesis of citrate as glucose (22%) (Fig. 5d). However, in MLDCs (where the glucose contribution was lower as in astrocytes) we found an increased contribution from glutamine (34%), probably to compensate for the decreased glucose contribution. In line with increased glutamine derived carbon contribution we also found higher M4 and M5 istopologue abundances of citrate (Fig. 5f).

Furthermore we identified also unexpected features of astrocyte metabolism compared to MLDCs. By using [U-^{13}C]glucose we found clear differences in the MID of serine. This non-essential amino acid can be derived from 3-phosphoglycerate, an intermediate of the glycolysis (Fig. 6a). As an alternative to *de novo* biosynthesis it can be taken up from the medium. Based on stable isotope experiments we found higher relative serine biosynthesis rates in MLDCs (24%) as in pure astrocyte cultures (5%) (Fig. 6b,c) where most serine originated from the medium (M0 isotopologue abundance). Interestingly, although we found at least 5% (astrocytes) and 24% (MLDCs) of relative glucose contribution to serine, there was very little labeling in glycine (Fig. 6d). This indicated that the equilibrium of the SHMT catalyzed reaction is far on the side of serine and that most glycine is taken up from the medium rather than being synthesized from glucose.

Similar to serine, we also found increased labeling in lactate (M3) in MLDCs (Fig. 6e). Lactate has an important role in maintaing the cytosolic redox balance of NADH/NAD$^+$. The reason for different lactate labeling patterns could be caused by two reasons: first, pure astrocyte cultures might consume more (unlabeled) pyruvate from the medium (present at 1mM concentration) resulting in higher M0 abundance and second, pyruvate and thus lactate might be produced from serine *via* serine dehydratase. Whether this function plays a role in glial metabolism needs further investigation.

hNSCs differentiated into various neuronal subtypes. Although we here focus on astrocyte differentiation, the ability to differentiate into neurons is a hallmark of NSCs and therefore needs to be evaluated for the characterization. To induce neuronal differentiation in our hNSC culture system a treatment with the factors BDNF (brain-derived neurotrophic factor), GDNF (glial cell line-derived neurotrophic factor), TGFB-3 (transforming growth factor beta-3), dbcAMP (dibutyryl-cAMP) and ascorbic acid was used. After 4 weeks of neuronal differentiation, derived cells showed positive labeling for early neuronal markers such as TuJ1 and Doublecortin (Figure S4a and b) as well as for the advanced matu- ration marker MAP2 (Figure S4c). The neuronal differentiation protocol enabled hNSCs to differenti- ate into GABAergic (GABA, 36.21%), glutamatergic (vGlut1, 40.34%) and dopaminergic neurons (TH, 12.68%) (Figure S4d–f), whereas differentiation into GFAP-positive cells was low (Figure S4g).

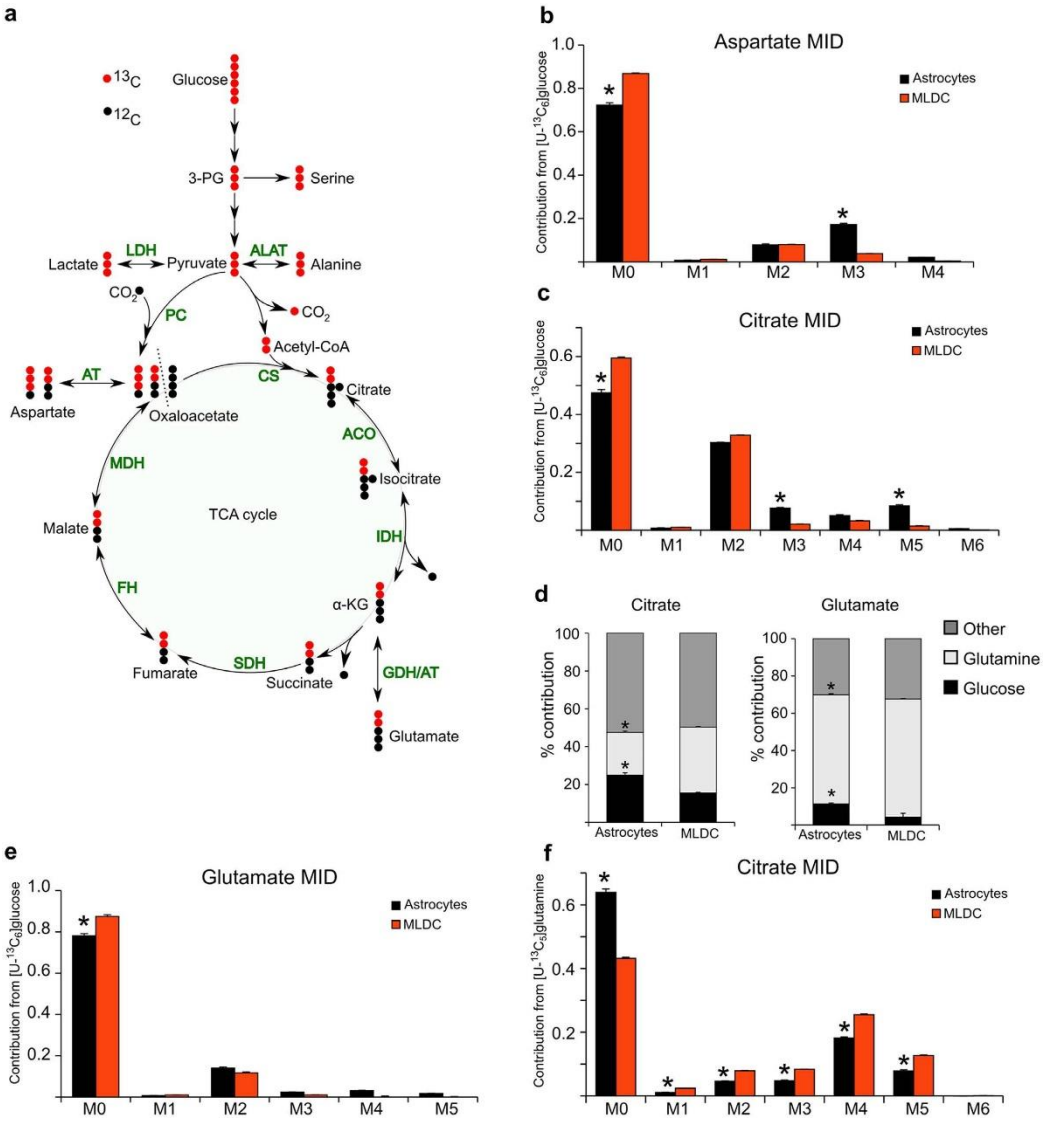

Figure 5. Stable isotope assisted metabolic profiling of hNSCs derived astrocyte. (**a**) Atom transition model of uniformly labeled [U-^{13}C]glucose. Glucose derived [U-^{13}C]pyruvate can enter the TCA cycle via pyruvate dehydrogenase (PDH) dependent oxidation of pyruvate to acetyl-coA. In this case citrate molecules show a mass increase by two (M2 isotopologue). Subsequent TCA cycle metabolites are also M2 isotopologues. As an alternative way to enter the TCA cycle pyruvate can be carboxylated by pyruvate carboxylase, resulting in oxaloacetate M3 isotopologues. The dotted line indicates the start and the end of the cycle. ALAT: alanine aminotransferase; LDH: lactate dehydrogenase; PC: pyruvate carboxylase; CS: citrate synthase; ACO: Aconitase; IDH: isocitrate dehydrogenase; GDH: glutamate dehydrogenase; AT: aminotransferase; SDH: succinate dehydrogenase; FH: fumarate hydratase; MDH: malate dehydrogenase. (**b–f**) Mass isotopomer distributions (MIDs) and carbon contributions. Cells were labeled for 24h prior extraction of intracellular metabolites and analysis by GC/MS. M1-M6 indicates the number of ^{13}C atoms incorporated into the metabolite. (**b**) MID of aspartate using [U-^{13}C]glucose as a tracer. (**c**) MID of citrate using [U-^{13}C]glucose as a tracer. (**d**) Calculated carbon contribution from gluocose, glutamine and other carbon sources (e.g. lipids, branched chain amino acids) to citrate (left) and glutamate (right). (**e**) MID of glutamate using [U-^{13}C]gl = 3 independent experiments in triplicate; p-value < 0.05.

To test these results at the mRNA level, we used RT-qPCR to quantitate expression of the neural stem cell marker Nestin, the proliferation marker Ki67, the neuronal marker MAP2, as well as the neuronal sub-type markers for GABAergic (GABA), glutamatergic (GLUT, vGlut1) and dopaminergic (TH) neurons. This analysis was performed in a comparison of hNSC under maintenance conditions and after 4 weeks of neuronal differentiation (Figure S4h). The results demonstrate that neural stem cell identity and proliferation capacities decreased with differentiation. At the same time, we observed

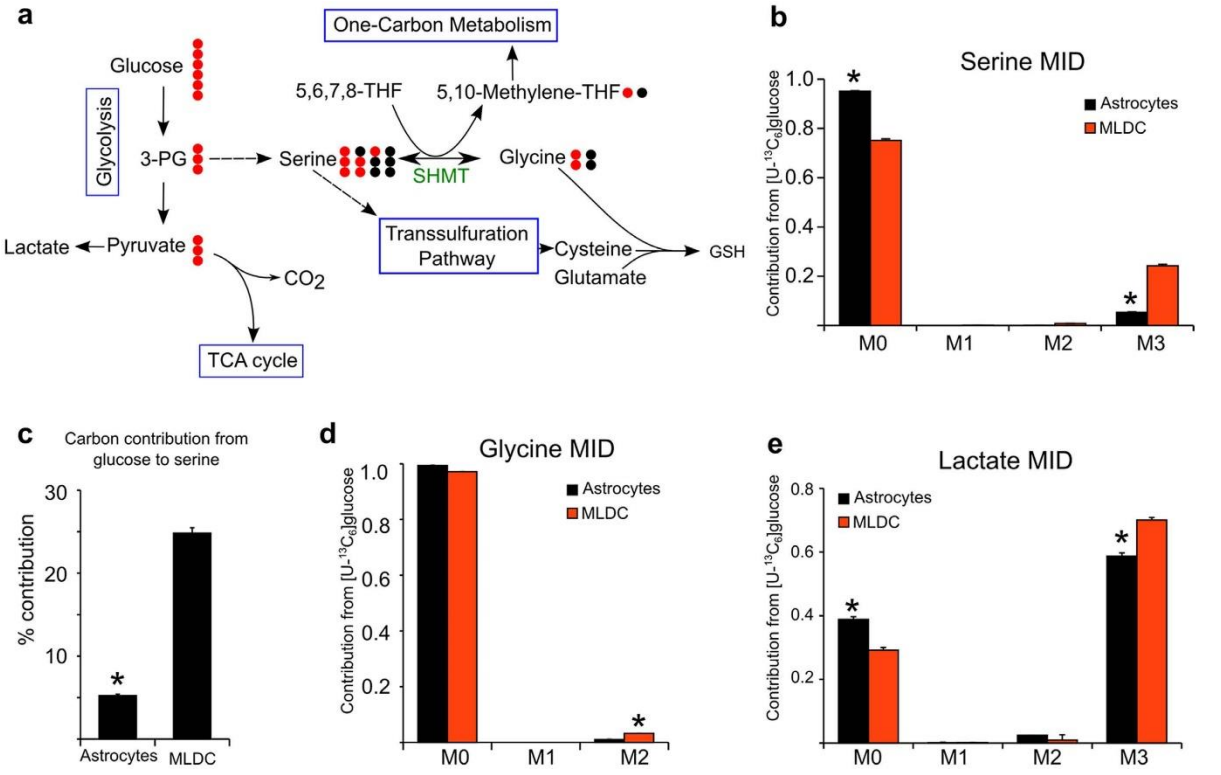

Figure 6. Stable isotope assisted metabolic profiling reveals differences in serine biosynthesis in hNSCs derived astrocytes and hNSCs derived MLDC. (**a**) Cartoon illustrating possible atom transitions for serine in respect to the reversibility of the enzyme serine hydroxy methyl transferase (SHMT) and potential metabolic fates for serine. The hydroxymethylgroup of serine is transferred on tetrahydrofolate resulting in M2 glycine isotopologues. In the reversible reaction serine can be M0, M1, M2 or again M3 depending on the combination of labeled and unlabeled metabolite. (**b**) MID of serine using [U-^{13}C]glucose as a tracer. (**c**) Carbon contribution of glucose to serine. Glutamine has no contribution to the serine pool (data not shown) (**d**) MID of glycine using [U-^{13}C]glucose as a tracer. (**e**) MID of lactate using [U-^{13}C]glucose as a tracer. Mean ±SEM, n = 3 independent experiments in triplicate; p-value < 0.05.

increased expression levels of MAP2, GABA, vGlut1 and TH (Figure S4h), indicating ongoing neuronal differentiation.

To examine whether these neurons were functional, we performed immunolabelling for synaptic markers after 4 weeks of differentiation. We reliably detected the pre- and postsynaptic markers synaptophysin and PSD95 (Figure S5a–d and S5e–h), consistent with the expression of a more mature neuronal phenotype. Next, we performed whole-cell patch-clamp recordings following standard pro- cedures. Under voltage clamp conditions, neurons showed a fast transient inward current in response to depolarizing voltage steps (-1.9 ± 0.4 nA, n = 30; Figure S5i) that was identified as a sodium (Na^+-) current by blocking its influx with 0.5 µM TTX (Figure S5j). The transient Na^+-current was followed by an outward current with partial inactivation, typical for a mixture of voltage activated potassium channels. This outward current included an A-current that was identified in 10 out of 12 cells tested with a pre-pulse protocol (data not shown). The input resistance of the induced neurons was 1.5 ± 0.2 GΩ (n = 33). The amount of sodium current as well as the input resistance are typical for mature neurons[39,40]. In current clamp recordings, cells showed spontaneous action potential (AP) firing, when depolarized to a membrane potential near −50 mV by current injection (Figure S5k). Depolarizing currents elicited APs with $+19 \pm 5$ mV peak potential (n = 15 cells; Figure S5l) and a width at half-maximal amplitude of 3.8 ± 0.1 ms (n = 10). While the generation of APs is an important aspect of the neuronal lineage, we observed no spontaneous postsynaptic currents in continuous voltage clamp recordings (>3 min per cell; n = 30). Similarly, evoked postsynaptic currents could not be elicited by moderate depolarization with KCl applied in bath solution (10 mM; n = 5) or by puffs with high KCl (150 mM; 1–5 s duration; n = 6) directly onto patched cells. In contrast, puff-application of glutamate (1 mM, 0.5 s) elicited inward currents (608 ± 362 pA; n = 4) under voltage clamp conditions (Figure S5m), or depolarizations to mem- brane potentials near 0 mV (n = 4) during current clamp (Figure S5n). These data indicate the presence of typical sodium channels and glutamate receptors in differentiated hNSCs cells, however, they also

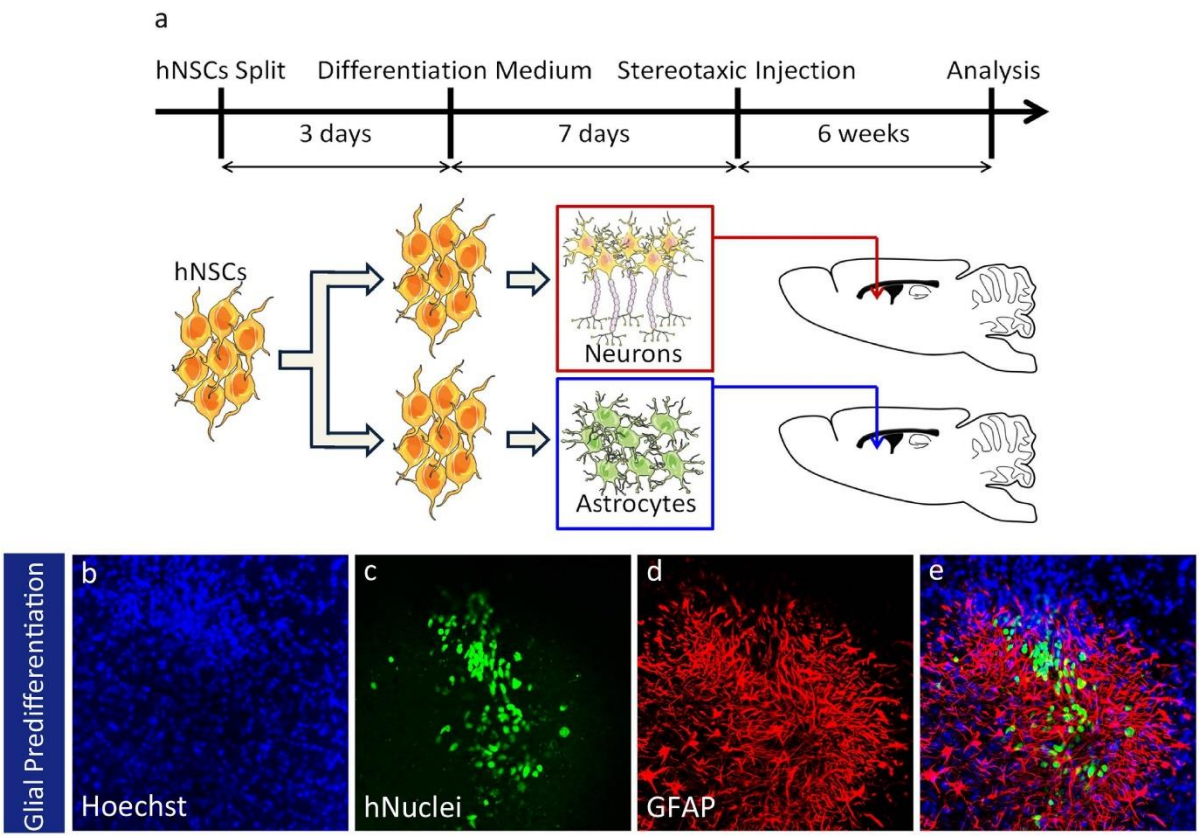

Figure 7. Transplantation of hNSC derived neurons and astrocytes in NOD/SCID mice. (**a**) Schematic representation of the protocol followed. hNSC were kept in maintenance medium for 3 days after splitting. Then the maintenance medium was switched to glial differentiation medium. Stereotactic injection into the subventricular zone of NOD/SCID mice was performed 7 days later. Representative images showing that clusters of GFAP positive cells formed by pre-differentiated hNSC (**b–e**). Drawings were produced using Servier Medical Art (www.servier.com; http://creativecommons.org/licenses/by/3.0/).

indicate that the synaptic release machinery is still incompletely developed, requiring more research into the specific factors regulating its differentiation.

Transplanted hNSCs survived and differentiated *in vivo*. Finally, we aimed at characterizing hNSC derived cells *in vivo*. The use of hiPSC-derived cells mandates that firstly, transplanted cells are devoid of tumor formation potential, and secondly, the transplanted cells are able to survive *in vivo*. Since the potential of tumor formation is inversely correlated to the degree of differentiation, we selected cells after 6 passages for transplantation because nearly all hNSCs were Nestin-positive and Oct4-/Nanog-negative at this time point. Stereotactic injection of self-renewing hNSCs into the subventricular zone of NOD/SCID mice was never followed by any tumoral growth. In total, 1×10^6 to 2×10^6 hNSCs were transplanted into the brain hemispheres of 9 mice. 3 mice were sacrificed after 6 weeks, 3 other mice were sacrificed after 3 month and the final 3 mice were sacrificed after 6 months. In none of these mice, we observed tumoral outgrowth.

To control cells fate after transplantation, hNSC were subjected to a pre-differentiation step. The cell fate was analyzed 6 additional weeks later (Fig. 7a). Since injected cells were of human origin, the transplant could be identified by immunofluorescence with a specific antibody directed against human nuclei (hNuc). Human NSCs that were neuronal pre-differentiated one week before transplantation, were able to survive and to differentiate into TuJ1 (Figure S6c) and Doublecortin (Figure S6g) positive neurons. hNSCs that were differentiated to astroglia for 1 week prior transplantation formed clusters of GFAP positive astrocytes (Fig. 7d).

These data demonstrate that pre-differentiation prior to transplantation can direct the fate of transplanted cells after grafting. The ability to define the fate of cells after transplantation is of outstanding importance for controlled cell replacement therapies. Thus the here described hNSC system may provide a basis for further investigations aiming at the development of strategies for future therapeutic approaches.

Discussion

In this manuscript, we describe a novel protocol for the generation of hNSCs from hiPSCs. This fate transition is achieved by the chronological administration of media with defined compositions. The here presented protocol is very robust and independent of any sorting method. In contrast to other protocols for the generation of human neural precursor cells, no small molecules were needed for keeping hNSCs under self-renewing condition[12,41–43]. Differently to previous studies where neural progenitors grow and proliferate as neurospheres[44] or neural rosettes[45], hNSCs were homogeneously maintained in a two-dimensional adherent cell system. Spontaneous differentiation of hNSC into other cell types was negligible. hLIF in the media blocked fate transition of hNSC into neuronal cells. Although hLIF has been reported to induce astrocytes differentiation in synergy with bone morphogenetic protein (BMP) 2 from mouse neuroepithelial cells[46], we did not detect significant amounts of GFAP-positive cells in the hNSC under maintenance condition. The beneficial effect of LIF has been previously observed in human neural progenitor cells in terms of prevention of apoptosis by inhibition of caspase 3 and 7 [47]. LIF also provided protection against reactive oxygen species and enhanced cell proliferation[47]. These effects have shown to be driven by the activation of JAK-STAT3 (Janus kinase-Signal transducer and activator of transcription 3) and MEK (MAPK/ERK kinase) pathways in non-neural stem cells such as mouse embryonic stem cells[48] and human neural progenitor cells[47].

The here described cells conserved the two main characteristics of neural stem cells, i.e. self-renewing and multi-linear differentiation capacities. Since they grow in homogenous cultures, these cells are an attractive tool for expression profiling, disease modeling and high content screenings. Besides their ability to differentiate into functional neurons, hNSCs differentiated into glial cells within a relatively short time period. In this study, we determined a gene expression profile that distinguishes hNSC from less differentiated hiPSC and more differentiated neurons and astrocytes. Since these profiles were generated from cells from the same individual (starting iPSC line), the degree of comparability is very high and the derived signatures should purely represent the differentiation status.

Several papers described the generation of human astrocytes from fetal or adult post-mortem central nervous system by the expansion of neuronal precursors[49,50]. This approach required 6 months to generate a pure population of astrocytes[51]. Other recent papers described the differentiation of astrocytes from iPSC with protocols requiring from 35 days[52] up to 4 months[53]. Importantly, the obtained populations seem to represent astrocytes just in a reactive form as shown by the almost 100% immunoreactivity for GFAP. Therefore, these cultures might not be suitable to completely model mature astrocyte functions or to mirror patho- and physiological conditions[33].

In the here presented study, the derivation of astrocytes was achieved by a cost-efficient media composition, which ensures a highly pure culture as shown by the negligible contamination with Tuj1 positive cells. Unlike other protocols[54], our protocol is simple and does not require any antibody-based sorting step of glia or neuronal progenitors. Remarkably, we were able to obtain a population of mature astrocytes both in a quiescent state with a protoplasmic morphology (negative for GFAP) as well as in a reactive phenotype characterized by GFAP expression. The expression of EAAT2 in all the cells and the ability to uptake glutamate strongly supported the acquisition of mature functions. The importance of this feature was highlighted by the different effects of immature and mature astrocytes on axonal regeneration[55,56].

The high pyruvate carboxylase activity confirmed the acquisition of metabolic specialization of hNSC-derived astrocytes as pyruvate carboxylation is an important anaplerotic reaction, specifically occurring in astrocytes[57,58]. Moreover, the relative glucose flux into the TCA cycle was higher in astrocytes resulting in higher glucose derived carbon contribution to glutamate[59]. Very interestingly, in astrocytes as well as MLDCs around 50% of the citrate carbons derived from other sources than glucose or glutamine. These other sources might be represented by lipid oxidation and/or degradation of amino acids such as branched chain amino acids. Compared to other cell lines 50% of carbons derived from alternative carbon sources is relatively high, at least at basic culture conditions and high oxygen tension (unpublished data). The reasons for that can be multiple and should be investigated in future research. Identifying the relevance of alternative carbon sources for glial specific metabolism could help for a better understanding of cell survival and integrity.

Particularly interesting is the role of serine as it represents an important metabolic intersection point to i) provide one-carbon units to the folate mediated one-carbon metabolism, to ii) serve as a precursor for the transsulfuration pathway to generate cysteine from serine and homocysteine and iii) as the precursor to produce the non-essential amino acid glycine. Serine and its connected metabolic pathways have been shown to be of special importance in neuronal oxidative stress conditions[60]. Astrocytes have an important supportive function in protecting neurons against oxidative stress by providing the antioxidant glutathione[61]. Glycine represents together with cysteine and glutamate one of the three amino acids that build the antioxidant glutathione.

Recently, the outstanding importance of astrocytes for neurological disease got into focus of several research approaches. As an example, it has been shown that astrocytes strongly contribute to the development of the Down syndrome[62]. Additionally, a recent study clearly demonstrated that transplantation of astrocytes was extremely beneficial in a rat model of Parkinson's disease[63]. Thus, the availability of an effective method to generate mature astrocytes, as described in this study, is of key importance for convincing disease-modeling studies and replacement therapy strategies. This is becoming a relevant field of investigation especially for neurodegenerative diseases such as Parkinson´s and Alzheimer´s disease.

References

1. Takahashi, K. & Yamanaka, S. Induction of pluripotent stem cells from mouse embryonic and adult fibroblast cultures by defined factors. *Cell* **126,** 663–676, doi: 10.1016/j.cell.2006.07.024 (2006).
2. Takahashi, K. *et al.* Induction of pluripotent stem cells from adult human fibroblasts by defined factors. *Cell* **131,** 861–872, doi: 10.1016/j.cell.2007.11.019 (2007).
3. Conti, L. & Cattaneo, E. Neural stem cell systems: physiological players or *in vitro* entities? *Nature reviews. Neuroscience* **11,** 176–187, doi: 10.1038/nrn2761 (2010).
4. Conti, L. *et al.* Niche-independent symmetrical self-renewal of a mammalian tissue stem cell. *PLoS biology* **3,** e283, doi: 10.1371/journal.pbio.0030283 (2005).
5. Wernig, M. *et al.* Neurons derived from reprogrammed fibroblasts functionally integrate into the fetal brain and improve symptoms of rats with Parkinson's disease. *Proceedings of the National Academy of Sciences of the United States of America* **105,** 5856–5861, doi: 10.1073/pnas.0801677105 (2008).
6. Liu, Z. *et al.* The tumourigenicity of iPS cells and their differentiated derivates. *Journal of cellular and molecular medicine* **17,** 782–791, doi: 10.1111/jcmm.12062 (2013).
7. Araque, A., Parpura, V., Sanzgiri, R. P. & Haydon, P. G. Tripartite synapses: glia, the unacknowledged partner. *Trends in neurosciences* **22,** 208–215 (1999).
8. Brockhaus, J. & Deitmer, J. W. Long-lasting modulation of synaptic input to Purkinje neurons by Bergmann glia stimulation in rat brain slices. *The Journal of physiology* **545,** 581–593 (2002).
9. Haydon, P. G. & Carmignoto, G. Astrocyte control of synaptic transmission and neurovascular coupling. *Physiological reviews* **86,** 1009–1031, doi: 10.1152/physrev.00049.2005 (2006).
10. Ota, Y., Zanetti, A. T. & Hallock, R. M. The role of astrocytes in the regulation of synaptic plasticity and memory formation. *Neural plasticity* **2013,** 185463, doi: 10.1155/2013/185463 (2013).
11. Di Giorgio, F. P., Carrasco, M. A., Siao, M. C., Maniatis, T. & Eggan, K. Non-cell autonomous effect of glia on motor neurons in an embryonic stem cell-based ALS model. *Nature neuroscience* **10,** 608–614, doi: 10.1038/nn1885 (2007).
12. Reinhardt, P. *et al.* Derivation and expansion using only small molecules of human neural progenitors for neurodegenerative disease modeling. *PloS one* **8,** e59252, doi: 10.1371/journal.pone.0059252 (2013).
13. Israel, M. A. *et al.* Probing sporadic and familial Alzheimer's disease using induced pluripotent stem cells. *Nature* **482,** 216–220, doi: 10.1038/nature10821 (2012).
14. Brennand, K. J. *et al.* Modelling schizophrenia using human induced pluripotent stem cells. *Nature* **473,** 221–225, doi: 10.1038/nature09915 (2011).
15. Soldner, F. *et al.* Generation of isogenic pluripotent stem cells differing exclusively at two early onset Parkinson point mutations. *Cell* **146,** 318–331, doi: 10.1016/j.cell.2011.06.019 (2011).
16. Morizane, A. *et al.* Direct comparison of autologous and allogeneic transplantation of iPSC-derived neural cells in the brain of a non-human primate. *Stem cell reports* **1,** 283–292, doi: 10.1016/j.stemcr.2013.08.007 (2013).
17. Payne, N. L. *et al.* Application of human induced pluripotent stem cells for modeling and treating neurodegenerative diseases. *New biotechnology* **32,** 212–228, doi: 10.1016/j.nbt.2014.05.001 (2015).
18. Inoue, H., Nagata, N., Kurokawa, H. & Yamanaka, S. iPS cells: a game changer for future medicine. *The EMBO journal* **33,** 409–417, doi: 10.1002/embj.201387098 (2014).
19. Geerts, H. Of mice and men: bridging the translational disconnect in CNS drug discovery. *CNS drugs* **23,** 915–926, doi: 10.2165/11310890-000000000-00000 (2009).
20. Barberi, T. *et al.* Neural subtype specification of fertilization and nuclear transfer embryonic stem cells and application in parkinsonian mice. *Nature biotechnology* **21,** 1200–1207, doi: 10.1038/nbt870 (2003).
21. Soundararajan, P., Lindsey, B. W., Leopold, C. & Rafuse, V. F. Easy and rapid differentiation of embryonic stem cells into functional motoneurons using sonic hedgehog-producing cells. *Stem cells* **25,** 1697–1706, doi: 10.1634/stemcells.2006-0654 (2007).
22. Huang da, W., Sherman, B. T. & Lempicki, R. A. Systematic and integrative analysis of large gene lists using DAVID bioinformatics resources. *Nature protocols* **4,** 44–57, doi: 10.1038/nprot.2008.211 (2009).
23. Supek, F., Bosnjak, M., Skunca, N. & Smuc, T. REVIGO summarizes and visualizes long lists of gene ontology terms. *PloS one* **6,** *e21800*, doi: 10.1371/journal.pone.0021800 (2011).
24. Cline, M. S. *et al.* Integration of biological networks and gene expression data using Cytoscape. *Nature protocols* **2,** 2366–2382, doi: 10.1038/nprot.2007.324 (2007).
25. Hiller, K. *et al.* MetaboliteDetector: comprehensive analysis tool for targeted and nontargeted GC/MS based metabolome analysis. *Analytical chemistry* **81,** 3429–3439, doi: 10.1021/ac802689c (2009).
26. Chambers, S. M. *et al.* Highly efficient neural conversion of human ES and iPS cells by dual inhibition of SMAD signaling. *Nature biotechnology* **27,** 275–280, doi: 10.1038/nbt.1529 (2009).
27. Kim, D. S. *et al.* Robust enhancement of neural differentiation from human ES and iPS cells regardless of their innate difference in differentiation propensity. *Stem cell reviews* **6,** 270–281, doi: 10.1007/s12015-010-9138-1 (2010).
28. Sineva, G. S. & Pospelov, V. A. Inhibition of GSK3beta enhances both adhesive and signalling activities of beta-catenin in mouse embryonic stem cells. *Biology of the cell/under the auspices of the European Cell Biology Organization* **102,** 549–560, doi: 10.1042/BC20100016 (2010).
29. Wu, X., Walker, J., Zhang, J., Ding, S. & Schultz, P. G. Purmorphamine induces osteogenesis by activation of the hedgehog signaling pathway. *Chemistry & biology* **11,** 1229–1238, doi: 10.1016/j.chembiol.2004.06.010 (2004).
30. Yan, Q. *et al.* Sumoylation activates the transcriptional activity of Pax-6, an important transcription factor for eye and brain development. *Proceedings of the National Academy of Sciences of the United States of America* **107,** 21034–21039, doi: 10.1073/pnas.1007866107 (2010).
31. Cahan, P. & Daley, G. Q. Origins and implications of pluripotent stem cell variability and heterogeneity. *Nature reviews. Molecular cell biology* **14,** 357–368, doi: 10.1038/nrm3584 (2013).
32. Qu, Q. & Shi, Y. Neural stem cells in the developing and adult brains. *Journal of cellular physiology* **221,** 5–9, doi: 10.1002/jcp.21862 (2009).
33. Roybon, L. *et al.* Human stem cell-derived spinal cord astrocytes with defined mature or reactive phenotypes. *Cell reports* **4,** 1035–1048, doi: 10.1016/j.celrep.2013.06.021 (2013).
34. Bardehle, S. *et al.* Live imaging of astrocyte responses to acute injury reveals selective juxtavascular proliferation. *Nature neuroscience* **16,** 580–586, doi: 10.1038/nn.3371 (2013).
35. Lundgaard, I., Osorio, M. J., Kress, B. T., Sanggaard, S. & Nedergaard, M. White matter astrocytes in health and disease. *Neuroscience* **276,** 161–173, doi: 10.1016/j.neuroscience.2013.10.050 (2014).
36. Huang, Y. H. & Bergles, D. E. Glutamate transporters bring competition to the synapse. *Current opinion in neurobiology* **14,** 346–352, doi: 10.1016/j.conb.2004.05.007 (2004).
37. Gamberino, W. C., Berkich, D. A., Lynch, C. J., Xu, B. & LaNoue, K. F. Role of pyruvate carboxylase in facilitation of synthesis of glutamate and glutamine in cultured astrocytes. *Journal of neurochemistry* **69,** 2312–2325 (1997).

38. Wise, D. R. & Thompson, C. B. Glutamine addiction: a new therapeutic target in cancer. *Trends in biochemical sciences* **35,** 427–433, doi: 10.1016/j.tibs.2010.05.003 (2010).
39. Belinsky, G. S., Moore, A. R., Short, S. M., Rich, M. T. & Antic, S. D. Physiological properties of neurons derived from human embryonic stem cells using a dibutyryl cyclic AMP-based protocol. *Stem cells and development* **20,** 1733–1746, doi: 10.1089/scd.2010.0501 (2011).
40. Pre, D. *et al.* A time course analysis of the electrophysiological properties of neurons differentiated from human induced pluripotent stem cells (iPSCs). *PloS one* **9,** e103418, doi: 10.1371/journal.pone.0103418 (2014).
41. Kim, D. S. *et al.* Highly pure and expandable PSA-NCAM-positive neural precursors from human ESC and iPSC-derived neural rosettes. *PloS one* **7,** e39715, doi: 10.1371/journal.pone.0039715 (2012).
42. Koch, P., Opitz, T., Steinbeck, J. A., Ladewig, J. & Brustle, O. A rosette-type, self-renewing human ES cell-derived neural stem cell with potential for *in vitro* instruction and synaptic integration. *Proceedings of the National Academy of Sciences of the United States of America* **106,** 3225–3230, doi: 10.1073/pnas.0808387106 (2009).
43. Li, W. *et al.* Rapid induction and long-term self-renewal of primitive neural precursors from human embryonic stem cells by small molecule inhibitors. *Proceedings of the National Academy of Sciences of the United States of America* **108,** 8299–8304, doi: 10.1073/pnas.1014041108 (2011).
44. Ebert, A. D. *et al.* EZ spheres: a stable and expandable culture system for the generation of pre-rosette multipotent stem cells from human ESCs and iPSCs. *Stem cell research* **10,** 417–427, doi: 10.1016/j.scr.2013.01.009 (2013).
45. Elkabetz, Y. *et al.* Human ES cell-derived neural rosettes reveal a functionally distinct early neural stem cell stage. *Genes & development* **22,** 152–165, doi: 10.1101/gad.1616208 (2008).
46. Nakashima, K., Yanagisawa, M., Arakawa, H. & Taga, T. Astrocyte differentiation mediated by LIF in cooperation with BMP2. *FEBS letters* **457,** 43–46 (1999).
47. Majumder, A. *et al.* Neurotrophic effects of leukemia inhibitory factor on neural cells derived from human embryonic stem cells. *Stem cells* **30,** 2387–2399, doi: 10.1002/stem.1201 (2012).
48. Anneren, C. Tyrosine kinase signalling in embryonic stem cells. *Clinical science* **115,** 43–55, doi: 10.1042/CS20070388 (2008).
49. Haidet-Phillips, A. M. *et al.* Astrocytes from familial and sporadic ALS patients are toxic to motor neurons. *Nature biotechnology* **29,** 824–828, doi: 10.1038/nbt.1957 (2011).
50. Verwer, R. W. *et al.* Mature astrocytes in the adult human neocortex express the early neuronal marker doublecortin. *Brain: a journal of neurology* 130, 3321–3335, doi: 10.1093/brain/awm264 (2007).
51. Krencik, R., Weick, J. P., Liu, Y., Zhang, Z. J. & Zhang, S. C. Specification of transplantable astroglial subtypes from human pluripotent stem cells. *Nature biotechnology* **29,** 528–534, doi: 10.1038/nbt.1877 (2011).
52. Emdad, L., D'Souza, S. L., Kothari, H. P., Qadeer, Z. A. & Germano, I. M. Efficient differentiation of human embryonic and induced pluripotent stem cells into functional astrocytes. *Stem cells and development* **21,** 404–410, doi: 10.1089/scd.2010.0560 (2012).
53. Juopperi, T. A. *et al.* Astrocytes generated from patient induced pluripotent stem cells recapitulate features of Huntington's disease patient cells. *Molecular brain* **5,** 17, doi: 10.1186/1756-6606-5-17 (2012).
54. Yuan, S. H. *et al.* Cell-surface marker signatures for the isolation of neural stem cells, glia and neurons derived from human pluripotent stem cells. *PloS one* **6,** e17540, doi: 10.1371/journal.pone.0017540 (2011).
55. Goldshmit, Y. *et al.* Fgf-dependent glial cell bridges facilitate spinal cord regeneration in zebrafish. *The Journal of neuroscience: the official journal of the Society for Neuroscience* **32,** 7477–7492, doi: 10.1523/JNEUROSCI.0758-12.2012 (2012).
56. Tom, V. J., Steinmetz, M. P., Miller, J. H., Doller, C. M. & Silver, J. Studies on the development and behavior of the dystrophic growth cone, the hallmark of regeneration failure, in an *in vitro* model of the glial scar and after spinal cord injury. *The Journal of neuroscience: the official journal of the Society for Neuroscience* **24,** 6531–6539, doi: 10.1523/JNEUROSCI.0994-04.2004 (2004).
57. Shank, R. P., Bennett, G. S., Freytag, S. O. & Campbell, G. L. Pyruvate carboxylase: an astrocyte-specific enzyme implicated in the replenishment of amino acid neurotransmitter pools. *Brain research* **329,** 364–367 (1985).
58. Amaral, A. I., Teixeira, A. P., Hakonsen, B. I., Sonnewald, U. & Alves, P. M. A comprehensive metabolic profile of cultured astrocytes using isotopic transient metabolic flux analysis and C-labeled glucose. *Frontiers in neuroenergetics* **3,** 5, doi: 10.3389/fnene.2011.00005 (2011).
59. Pardo, B. *et al.* Brain glutamine synthesis requires neuronal-born aspartate as amino donor for glial glutamate formation. *Journal of cerebral blood flow and metabolism: official journal of the International Society of Cerebral Blood Flow and Metabolism* **31,** 90–101, doi: 10.1038/jcbfm.2010.146 (2011).
60. Krug, A. K. *et al.* Transcriptional and metabolic adaptation of human neurons to the mitochondrial toxicant MPP(+). *Cell death & disease* **5,** e1222, doi: 10.1038/cddis.2014.166 (2014).
61. Dringen, R. Glutathione metabolism and oxidative stress in neurodegeneration. *European journal of biochemistry/FEBS* **267,** 4903 (2000).
62. Chen, C. *et al.* Role of astroglia in Down's syndrome revealed by patient-derived human-induced pluripotent stem cells. *Nature communications* **5,** 4430, doi: 10.1038/ncomms5430 (2014).
63. Proschel, C., Stripay, J. L., Shih, C. H., Munger, J. C. & Noble, M. D. Delayed transplantation of precursor cell-derived astrocytes provides multiple benefits in a rat model of Parkinsons. *EMBO molecular medicine* **6,** 504–518, doi: 10.1002/emmm.201302878 (2014).

Acknowledgements

The authors would like to thank Inga Werthschulte and Thea van Wuellen for excellent technical assistance. T.P. was supported by a Marie Curie Fellowship. The JCS lab is supported by the Fonds National de la Recherché (FNR) Luxembourg (CORE, C13/BM/5791363) a University Luxembourg Internal Research Project (MidNSCs) and the EU Joint Programme - Neurodegenerative Disease Research (JPND, SynSpread project). M.M. acknowledges support by the Deutsche Forschungsgemeinschaft (SFB629 TPB11).

Author Contributions

T.P., S.B. and J.M. designed and conducted the experiments, interpreted the data and drafted the manuscript. S.N., C.T., R.L.M., J.B. and M.S. conducted specific experiments, participated in the interpretation of data and contributed to the manuscript. M.M. and J.C.S. coordinated the study, designed the experiments, interpreted the data and participated in drafting the manuscript. All authors reviewed and approved the final manuscript.

Additional Information

Supplementary information accompanies this paper at http://www.nature.com/srep

Competing financial interests: The authors declare no competing financial interests.

How to cite this article: Palm, T. *et al.* Rapid and robust generation of long-term self-renewing human neural stem cells with the ability to generate mature astroglia. *Sci. Rep.* **5**, 16321; doi: 10.1038/srep16321 (2015).

Rapid and robust generation of long-term self-renewing human neural stem cells with the ability to generate mature astroglia

- Supplementary Information –

Thomas Palm[1*], Silvia Bolognin[2*], Johannes Meiser[2], Sarah Nickels[2], Claudia Träger[1], Ralf-Leslie Meilenbrock[1], Johannes Brockhaus[3], Miriam Schreitmüller[3], Markus Missler[3,4] and Jens Christian Schwamborn[1, 2]

*Equal contribution

[1] Stem Cell Biology and Regeneration Group, Institute of Cell Biology (ZMBE), Westfälische Wilhelms-Universität Münster, 48149 Münster, Germany

[2] Luxembourg Centre for Systems Biomedicine (LCSB), University of Luxembourg, Esch-Belval, Luxembourg

[3] Institute of Anatomy and Molecular Neurobiology, Westfälische-Wilhelms University, Münster, Germany

[4] Cluster of Excellence EXC 1003, Cells in Motion, CiM, Münster, Germany

Running Title: Generation and characterization of hNSCs and glia

Supplementary Figure Legends

Figure S1. Multilinear differentiation of hNSCs

Multilinear differentiation is achieved by culturing hNSCs in the basic medium, supplemented with 10% of FCS. Stem cells differentiated into TuJ1 positive neurons (a) and GFAP positive astrocytes (b).

Figure S2. Gene expression profiling of hNSCs

(a) Growth curve of hNSCs maintained under proliferative conditions over 21 Passages. (b) Paired analysis of the microarray based expression intensities of hiPSC and hNSCs associated genes.

Figure S3. Differential gene profiling between hiPSCs, hNSCs, and hMLDCs.

Transcriptional analysis and heat map correlation showing 2587 transcripts differentially regulated in hiPSCs, hNSCs and hMLDCs.

Figure S4. Derivation of functional neurons.

(a-f) Representative confocal images illustrating the expression of neuronal markers Tuj1 (a), DCX (b), MAP2(c), GABA-Tuj1 (d), vGlut1-Tuj1 (e) and TH-Tuj1 (f). (g) Quantification of the number of neurons positive for MAP2, Tuj1, vGLUT1, GABA, TH, GFAP. (h) mRNA expression levels of *Nestin*, *Ki67*, *MAP2*, *TH*, *GABA* and *GLUT1* in hNSC and neurons quantified by RT-qPCR.

Figure S5. hNSCs derived neurons develop synapses and electrophysiological activity.

(a-h) Representative confocal images illustrating the expression of neuronal markers synaptophysin (j), NCAM (k), PSD95 (n), Tuj1 (o). (i) Current-voltage protocol (-60 to +20 mV, 50 ms) shows fast inward current and slower outward currents. (j) The fast inward current is identified as Na^+-current by its sensitivity to TTX (0.5 µM; red trace). (k) In current clamp recordings cells fired spontaneous action potentials (APs), when the membrane potential was set to -50 mV. (l) Current steps (5 - 15 pA, 0.3 s) activated overshooting APs, stronger injections elicited series of APs with moderately declining amplitudes. (m) Puff-application of glutamate (1 mM) from a glas pipette (15 µm tipp diameter) placed 50 - 80 µm away from the recorded cell elicited an inward current when the cell was voltage clamped to -70 mV. (n) During current clamp, the cells depolarized in response to the glutamate puff.

Figure S6. Transplantation of hNSC derived neurons in NOD/SCID mice.

(a-h) Representative images of the subventricular zone showing that the pre-differentiated hNSC differentiate into Tuj1 (c) and Doublecortin (DCX) (g) positive cells.

Table S1. mRNA differentially expressed upon differentiation

List of mRNA differentially expressed between hiPSCs (group 1), hNSCs (group 2), and hMLDCs (group 3). Statistical analysis was performed using ANOVA followed by Bonferroni´s multiple comparison test.

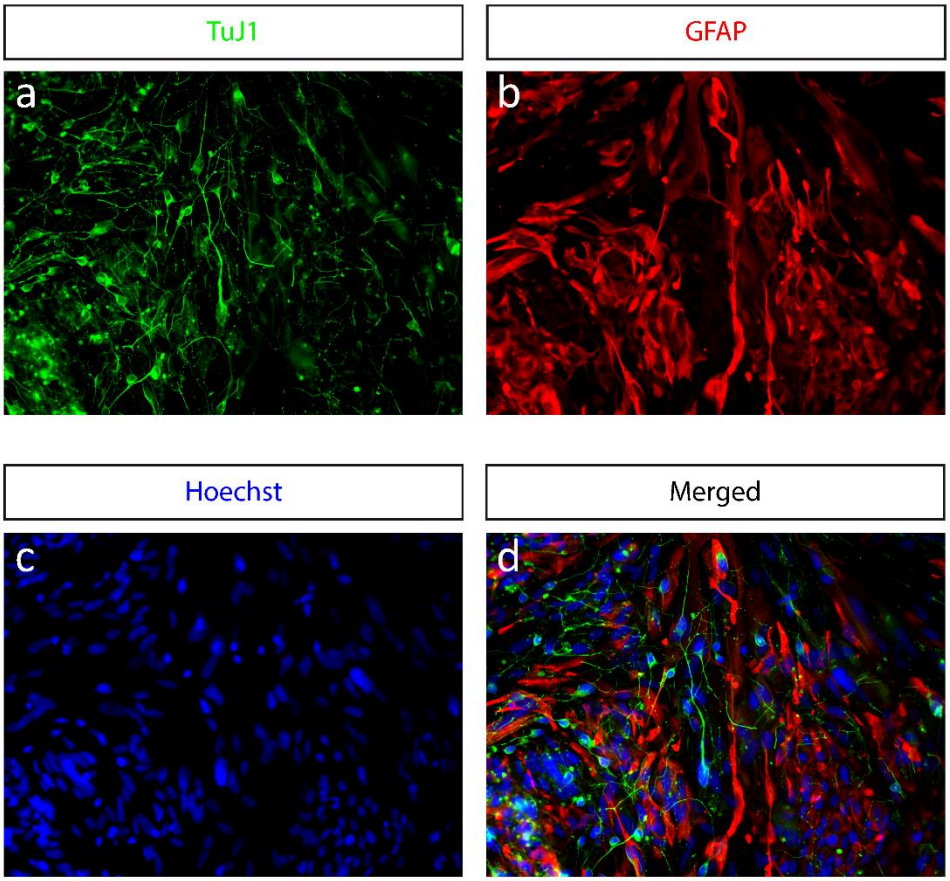

Figure S1

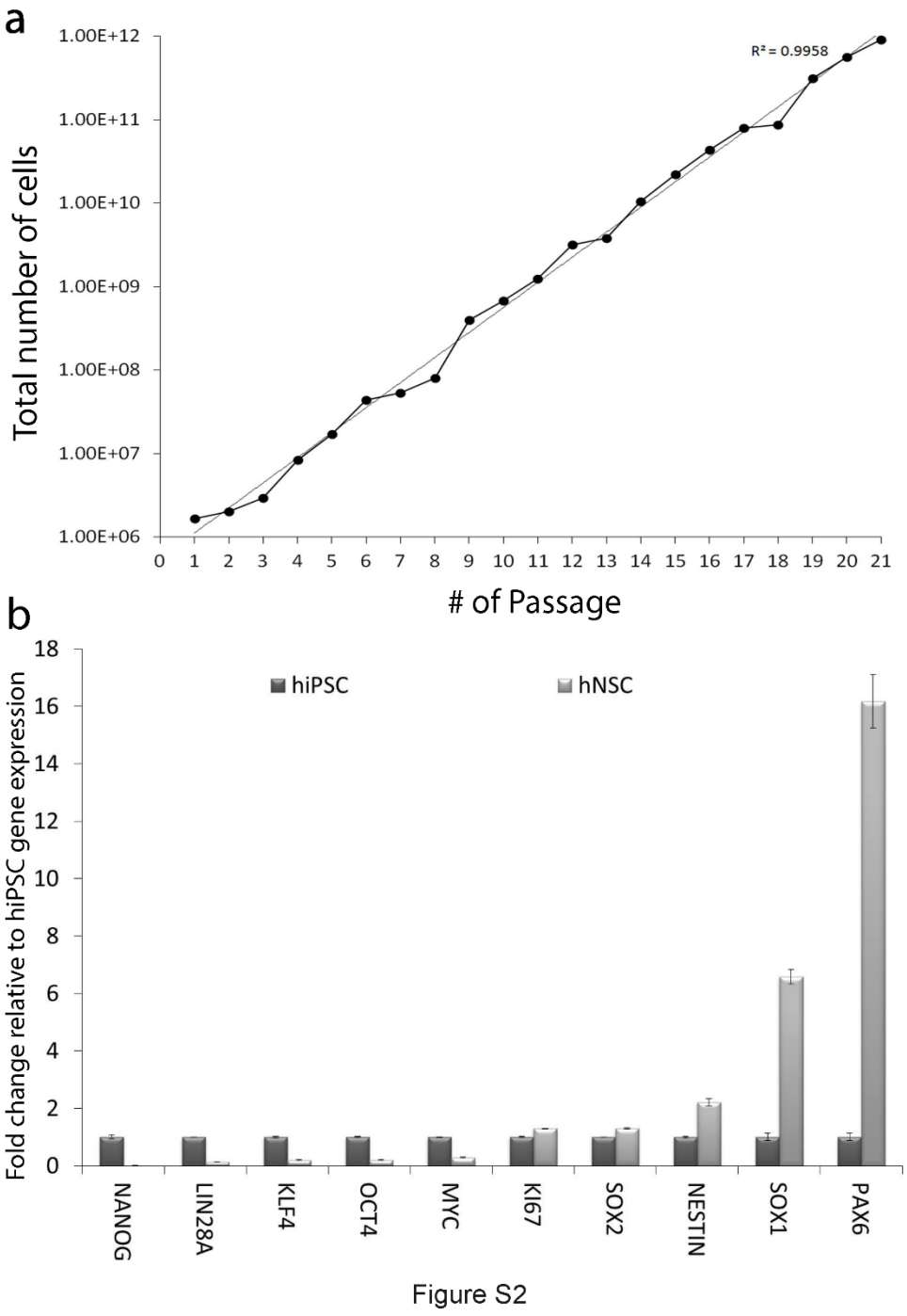
a
Total number of cells
1.00E+12
1.00E+11
1.00E+10
1.00E+09
1.00E+08
1.00E+07
1.00E+06
R² = 0.9958
0 1 2 3 4 5 6 7 8 9 10 11 12 13 14 15 16 17 18 19 20 21
# of Passage
b
Fold change relative to hiPSC gene expression
18
16
14
12
10
8
6
4
2
0
hiPSC
hNSC
NANOG
LIN28A
KLF4
OCT4
MYC
KI67
SOX2
NESTIN
SOX1
PAX6

Figure S2

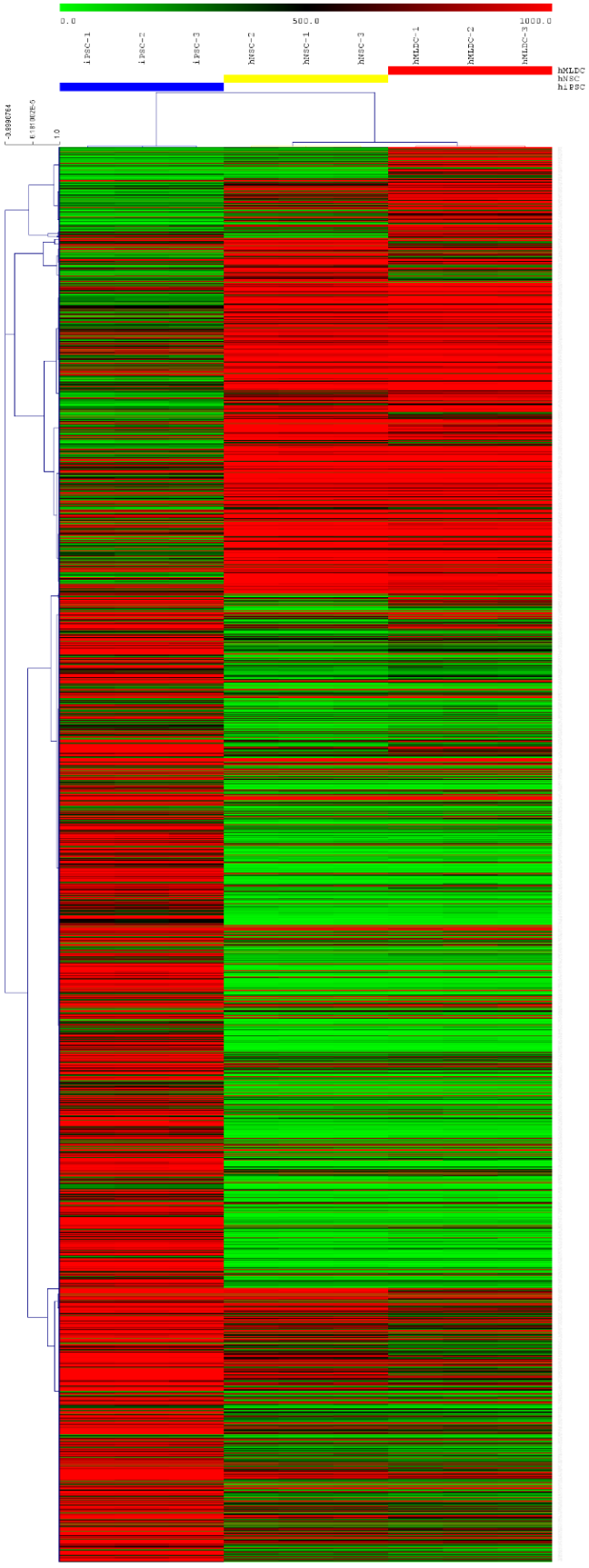
0.0
500.0
1000.0
hiPSC-1
hiPSC-2
hiPSC-3
hNSC-2
hNSC-1
hNSC-3
hMLDC-1
hMLDC-2
hMLDC-3
hMLDC
hNSC
hiPSC

Figure S3

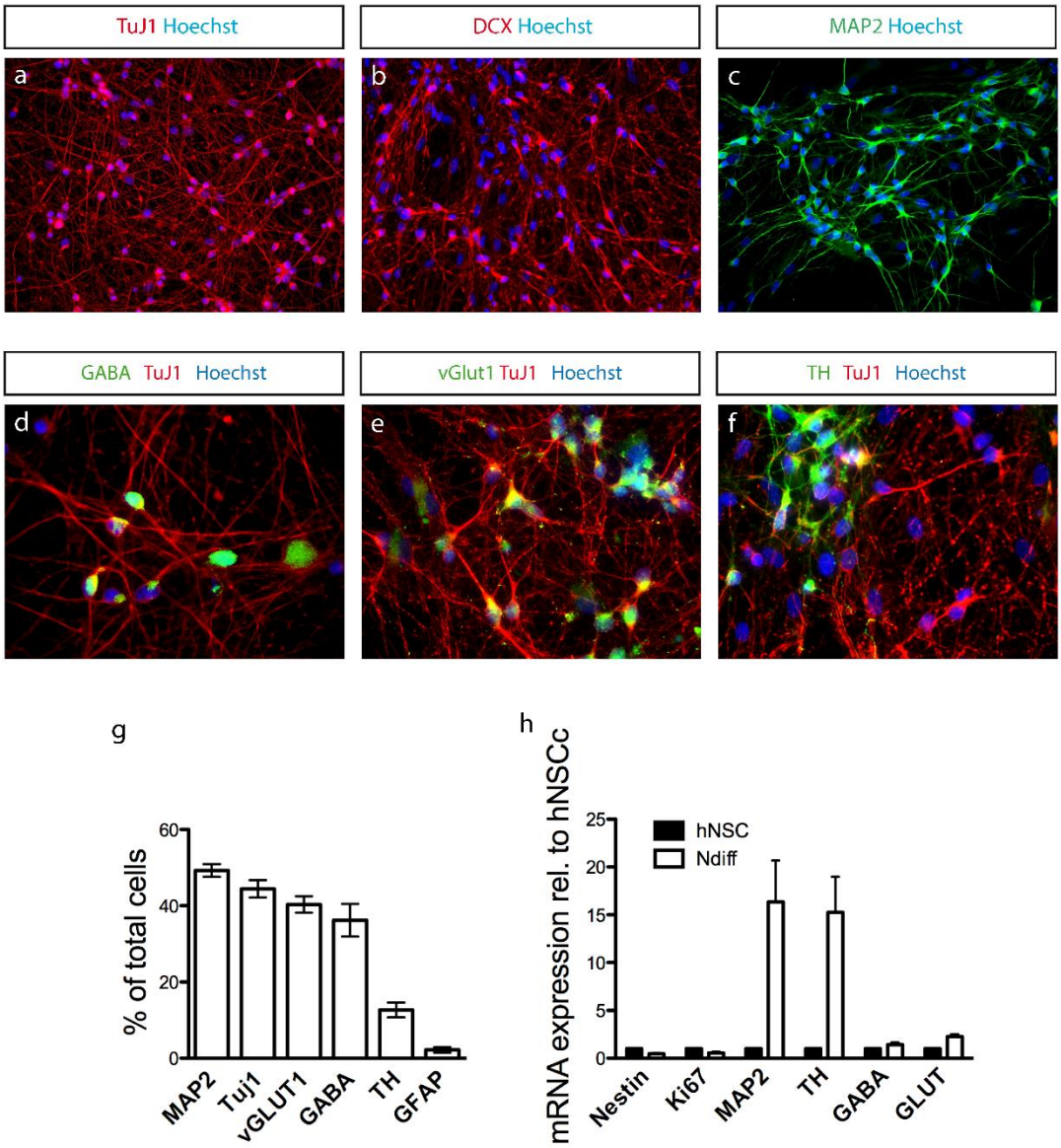
TuJ1 Hoechst
DCX Hoechst
MAP2 Hoechst
a
b
c
GABA TuJ1 Hoechst
vGlut1 TuJ1 Hoechst
TH TuJ1 Hoechst
d
e
f
g
% of total cells
60
40
20
0
MAP2
Tuj1
vGLUT1
GABA
TH
GFAP
h
mRNA expression rel. to hNSCc
25
20
15
10
5
0
hNSC
Ndiff
Nestin
Ki67
MAP2
TH
GABA
GLUT

Figure S4

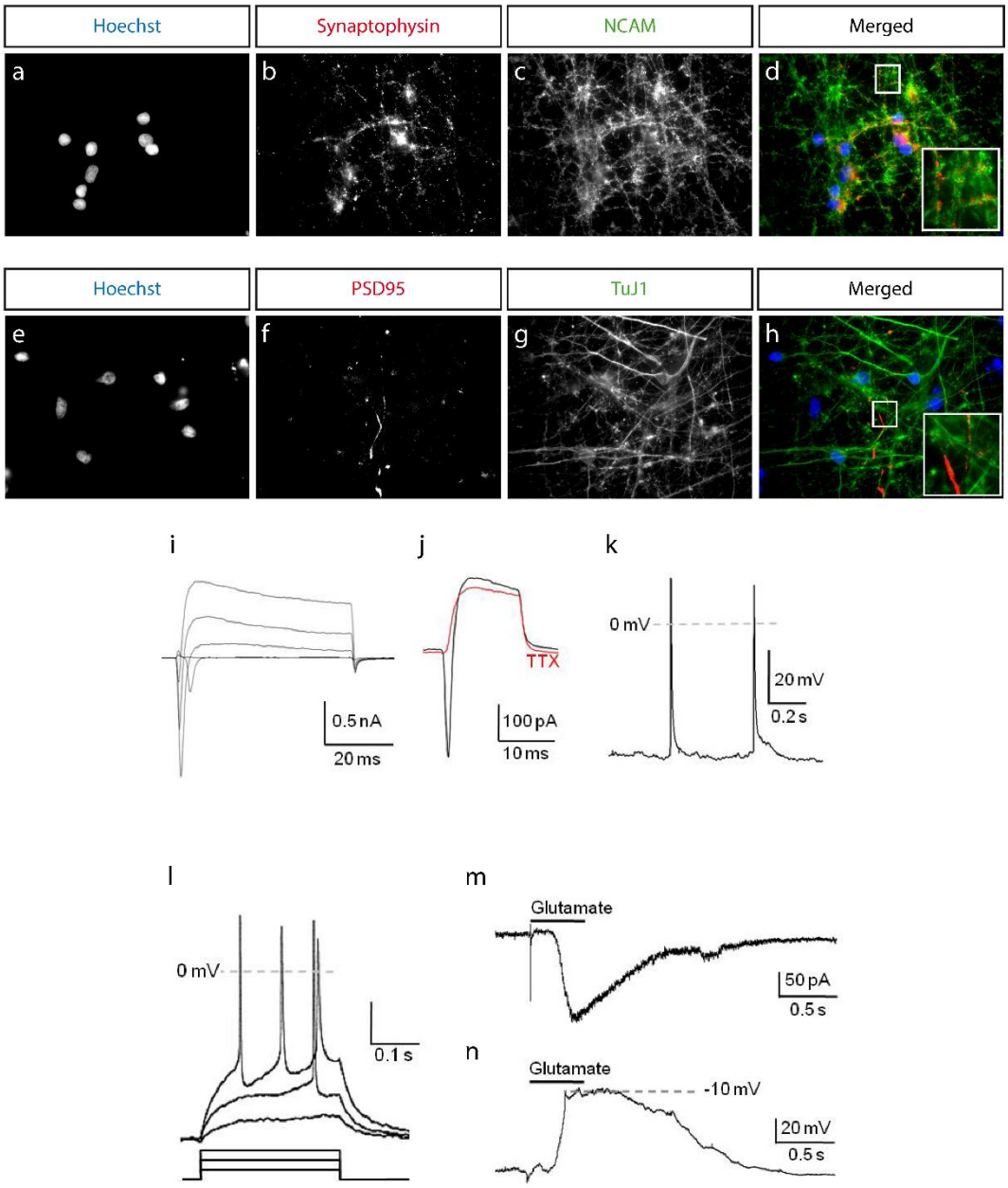
Hoechst
Synaptophysin
NCAM
Merged
a
b
c
d
Hoechst
PSD95
TuJ1
Merged
e
f
g
h
i
0.5 nA
20 ms
j
TTX
100 pA
10 ms
k
0 mV
20 mV
0.2 s
l
0 mV
0.1 s
m
Glutamate
50 pA
0.5 s
n
Glutamate
-10 mV
20 mV
0.5 s

Figure S5

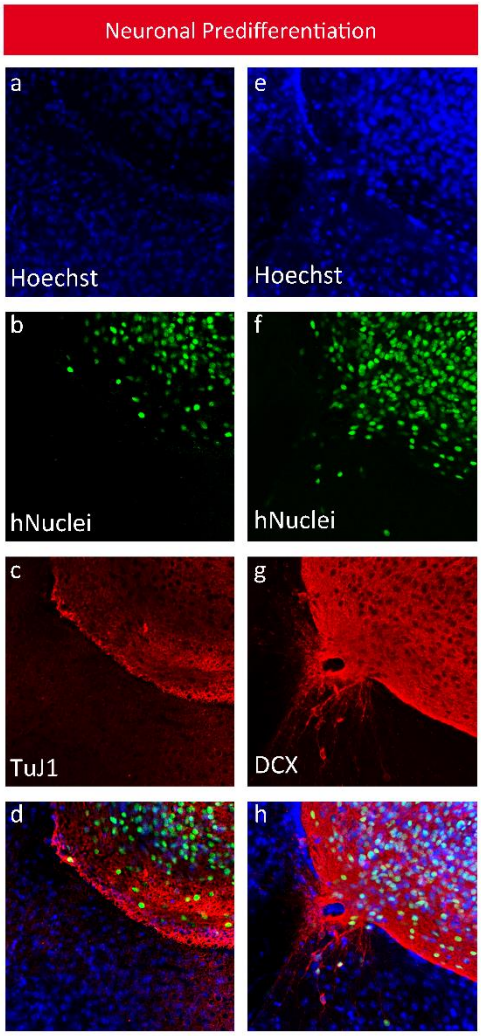

Figure S6

Table S1: https://www.nature.com/articles/srep16321

2 Publication II

FACS assisted CRISPR-Cas9 genome editing facilitates Parkinson's disease modeling

Jonathan Arias-Fuenzalida[1,4,7,*] , Javier Jarazo[1,7,*], Xiaobing Qing[1], Jonas Walter[1], Gemma Gomez-Giro[1,3], Sarah Louise Nickels[1,2], Holm Zaehres[3,4], Hans Robert Schöler[3,6], Jens Christian Schwamborn[1]

*These authors equally contributed to the article

[1]Luxembourg Centre for Systems Biomedicine (LCSB), Developmental and Cellular Biology, University of Luxembourg, L-4362, 7 avenue des Hauts-Fourneaux,

[2]Luxembourg Life Science Research Unit (LSRU), Systems Biology, University of Luxembourg, L-4362 Belvaux, Luxembourg

[3]Max Planck Institute for Molecular Biomedicine, Department of Cell and Developmental Biology, Röntgenstrasse 20, 48149 Münster, Germany

[4]Graduate School of Biostudies, Kyoto University, Kyoto 606-8502, Japan

[5]Ruhr-University Bochum, Medical Faculty, Department of Anatomy and Molecular Embryology, 44801 Bochum, Germany

[6]Westphalian Wilhelms University Münster, Medical Faculty, 48149 Münster, Germany

Stem Cell Reports 2017, under revision

2.1 Preface

Gene editing is defined as the technique used to insert, delete, or replace site-specific DNA fragments within the genome of an organisms or cell. Gene editing has broad applications in research and biotechnology. The most prominent role of gene editing for *in vitro* disease modeling is its use for loss and gain of function experiments as for instance creating or deleting a mutation. Especially in PD, it becomes more and more important to use isogenic controls, due to the multifactoriality of the disease and the discovery of new genetic causes and risk loci. Isogenic controls that only differ in one mutation are used in order to exclude the influences from the genetic background and to discover the underlying mechanisms of the disease. With the discovery of the newest tool, the CRISPR-Cas9 genome editing technology, it became possible to conduct precise, targeted genomic modulation in a cost-efficient and less time-consuming manner compared to previous approaches. Nevertheless, some hurdles remain, such as the effort of clonal screening and the exclusion of random integration and non homologous end joining (NHEJ). In this paper, we described a fluorescence-assisted editing technique that allows the differentiation between correctly edited clones, and non-edited, or randomly integrated ones, through simple fluorescent staining. This deterministic approach allows fast and efficient clone screening and expansion, and therefore represents a valuable tool for generating isogenic controls to study PD. Using this method, we could show that cell lines with inserted mutations in α-SYN manifest typical PD-associated phenotypes, such as mitochondrial deficiencies.

My contribution to this publication was limited to the provision and interpretation of the microarray data depicted in Figure 5b. Moreover, I edited the manuscript and within my main project, I worked with isogenic control cell lines.

FACS assisted CRISPR-Cas9 genome editing facilitates Parkinson's disease modeling

Jonathan Arias-Fuenzalida [1,2,7], Javier Jarazo [1,7], Xiaobing Qing [1], Jonas Walter [1] Gemma Gomez-Giro [1,4], Sarah Louise Nickels [1,3], Holm Zaehres [4,5], Hans Robert Schöler [4,6], Jens Christian Schwamborn [1]

[1] Luxembourg Centre for Systems Biomedicine (LCSB), Developmental and Cellular Biology, University of Luxembourg, L-4362, 7 avenue des Hauts-Fourneaux, Luxembourg

[2] Graduate School of Biostudies, Kyoto University, Kyoto 606-8502, Japan

[3] Life Science Research Unit (LSRU), Systems Biology, University of Luxembourg, L-4367, 6 avenue du swing, Luxembourg

[4] Max Planck Institute for Molecular Biomedicine, Laboratory of Cell and Developmental Biology, Roentgenstrasse 20, Muenster, Germany

[5] Ruhr-University Bochum, Medical Faculty, Department of Anatomy and Molecular Embryology, 44801 Bochum, Germany

[6] Westphalian Wilhelms University Muenster, Medical Faculty, 48149 Muenster, Germany

[7] These authors equally contributed to the article

Correspondence should be addressed to J.C.S. (jens.schwamborn@uni.lu)

Abstract

Genome-editing and human induced pluripotent stem cells hold great promises for the development of isogenic disease models and the correction of disease-associated mutations for isogenic tissue therapy. CRISPR-Cas9 has emerged as a versatile and simple tool for engineering human cells for such purposes. However, the current protocols to derive genome-edited lines require the screening of a great number of clones to obtain one free of random integration or on-locus NHEJ containing alleles. Here we describe an efficient method to derive biallelic genome-edited populations by the use of fluorescent markers. We call this technique FACS Assisted CRISPR-Cas9 Editing (FACE). FACE allows the derivation of correctly edited clones carrying a positive selection fluorescent module, and the exclusion of non-edited, random integrations and on-target allele NHEJ-containing cells, from the correctly edited polyclonal population. Here we derived a set of isogenic lines containing Parkinson's disease associated mutations in α-Synuclein, and present their comparative phenotypes.

Graphical abstract

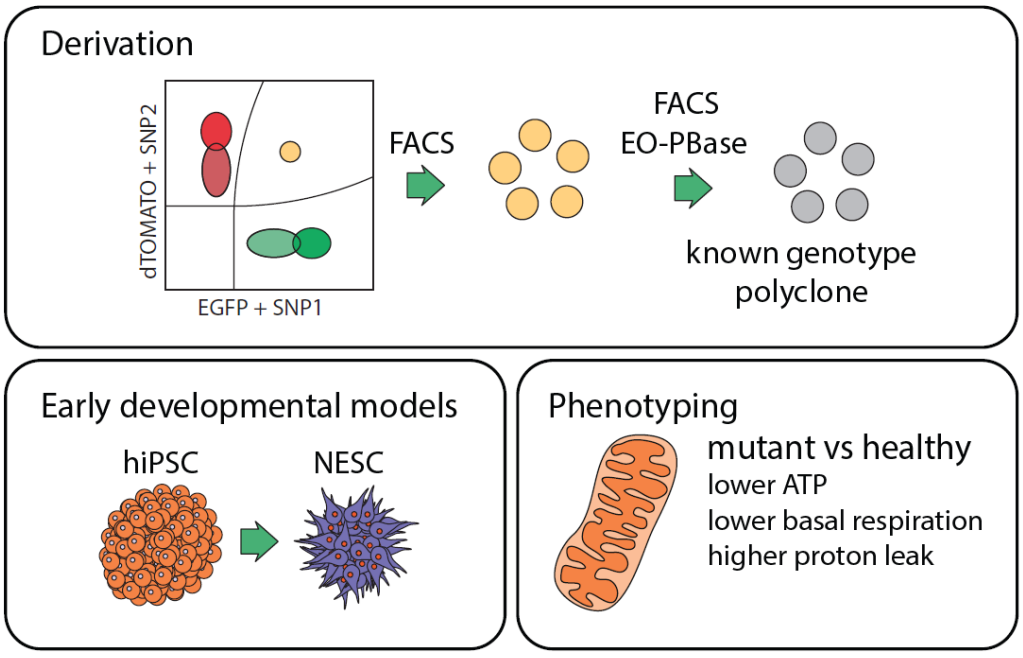

Introduction

Parkinson's disease (PD) is a multifactorial neurodegenerative disorder characterized by rigidity, bradykinesia, postural instability, and resting tremor (Barker et al., 2015; Lotharius and Brundin, 2002). A portion of the PD cases result from autosomal dominant mutations in the *SNCA* gene, which encodes α-Synuclein. Physiologically, α-Synuclein is implicated in synaptic transmission and vesicle transport, while in pathological conditions it is part of protein aggregates known as Lewy bodies and Lewy neurites (Goedert et al., 2013). Patients carrying mutations in the *SNCA* gene suffer from early onset of PD. Mutations in *SNCA* include increase in gene dosage (Devine et al., 2011) and heterozygous missense mutations such as p.A30P and p.A53T (Bendor et al., 2013; Soldner et al., 2011). The mutations in *SNCA* can account for up to 15% of the familial early onset PD cases (Bozi et al., 2014; Pankratz and Foroud, 2007).

Importantly, genome editing tools can assist in parsing PD phenotypes. CRISPR-Cas9 reliability as an editing tool has been extensively validated by whole genome sequencing of edited lines (Kim et al., 2015; Veres et al., 2014). Furthermore, Cas9 specificity has been improved with high-fidelity variants (Kleinstiver et al., 2016; Slaymaker et al., 2016). However, eliminating uncertainties in genotype outcomes of edited lines has remained challenging. Screening of correctly edited clones is a labor-consuming process that entails the selection of on-target knock-in clones and the exclusion of random integrations, on-target indels, and second allele indel events. To leverage the power of genome editing tools in the evaluation of polygenic diseases such as PD, it is necessary to overcome such labor and time consuming limitations. Hence, the fast generation of genome-edited populations carrying a known genotype outcome is highly necessary.

Results

Deterministic genotype outcomes in multiple loci for the generation of isogenic lines. The use of two donors containing fluorescent protein reporters (EGFP or dTOMATO) associated with defined SNP allelic variants creates outcomes of known genotypes (**Figure 1A** and **E**): heterozygous (population 1A), homozygous healthy (population 1B) and homozygous pathogenic (population 1C) (**Figure 1E**). One-step biallelic targeting occurs with a mean frequency of 37.5 percent using dsDNA donor vectors (**Supplemental table 1**). In our system, donor vectors for *SNCA* (exon 2 and exon 3) were cloned with an internal positive selection module containing EGFP or dTOMATO, and a negative selection module containing tagBFP in the backbone outside the homology arms (**Figure 1A**). The combination of donors was designed according to the desired genotype outcome (**Figure 1E**). For the heterozygous *SNCA* mutations rs104893878 (p.A30P) and rs104893877 (p.A53T), combinations were chosen containing mutant and wild type donors (**Figure 1E** population 1A and **S1**). In the case of SNCAe2 a mutant donor ($EGFP^{pos}$) carried the transversion c.88g>c, and in the case of SNCAe3, the donor carried the transition c.209g>a ($EGFP^{pos}$). For each locus a corresponding wild type donor ($dTOMATO^{pos}$) was also included to obtain the heterozygous combination (**Figure 1E**). Similar expression levels of reporters were observed from each allele in *SNCA* on chromosome 4, as evidenced by the double positive population in the FACS plots (**Figure 1D**). In order to test whether similar expression levels could be observed in other genomic regions, exon 5 of the gene encoding PTEN-induced putative kinase (PINK1) on chromosome 1 was targeted. In contrast to *SNCA* mutant PD patients, *PINK1* PD patients are homozygotes or compound heterozygotes (Ishihara-Paul et al., 2008). Hence, for PINK1e5 both donors ($EGFP^{pos}$) and ($dTOMATO^{pos}$) carried the pathogenic transversion c.1197t>a (**Figure 1E** population 1C). By FACS, the biallelic targeted population separated clearly from the other genotype populations (**Figure S6**) as it did for *SNCA* (**Figure 1D**). Together, these results validate our approach to target both alleles of a gene of interest in different genomic regions.

Repetitive elements reduce on-target genome editing efficiency by increasing random integration. We introduced silent point mutations in one or several PAM sequences of donors to shield the template from Cas9-induced linearization and to avoid linear DNA induced random integration (**Figure S1A**). Properly targeted alleles are thus shielded from secondary Cas9 cleavage events eliminating the risk of on-target indels (Merkle et al., 2015) (**Figure S1A**). Two weeks after electroporation, each edited population was expanded up to $15x10^6$ puromycin-resistant and fluorescent protein positive cells. The inclusion of tagBFP in the negative selection module allowed us to quantify, visualize, and exclude random integration events (**Figure 1A-B**, **1F**). The tagBFP negative selection module avoids by-stander toxicity or incomplete negative selection from systems such as thymidine kinase (Ruby and Zheng, 2009). The percentage of $tagBFP^{pos}$ random integration ranged from 5.8-14.6% for SNCAe2, from 42.6-64.2% for SNCAe3, and from 27.2-30.4% for PINK1e5 (**Figure 1B**, **1F** and **Figure S2A-C**). The extent of random integration correlated with the type and proportion of repetitive elements present in the homology arms of the donors. We assessed random integration using donors for six genomic regions with known repetitive element composition, and tested twelve sgRNAs. The loci that we evaluated include chromosome 1 (PINK1 exon 5), chromosome 4 (*SNCA* exon 2 and exon 3), and additionally chromosome 16 (ceroid lupofuscinosis 3, CLN3 exon 5-8, exon 10-13 and exon 14-15) (**Figure S2G**). For the analysis we performed a linear optimization model of the form Ax=b (**Figure S2H**). The matrix A corresponded to the frequency of repetitive elements in the homology arms (**Figure S2G**). The vector x corresponded to the type of repetitive elements present in the analyzed dataset (**Figure S2G**), and a variable of all non-included repetitive elements (upsilon). The vector b corresponded to the experimentally measured random integration level, given by the percentage of $TagBFP^{pos}$ cells (**Figure S2A-F**). Based on this we derived a model to predict random integration frequency intrinsic to the composition of repetitive elements in the homology arms (**Figure S2H-I**). The solution allows assigning weight coefficients to each repetitive element. The value of each weight coefficient indicates which repetitive element contributes the most to the random integration frequency observed. The solution space is constrained for a maximum of

100% random integration and sequence length physical boundaries for each repetitive element. The optimization solution indicates that the most relevant repetitive elements correspond to the Short Interspersed Nuclear Elements (SINE) family, specifically Alu and Mir (**Figure S2H-I**).

FACS purification increases speed and yield of isogenic derivation. For the on-target (tagBFP^{neg}) cells the ratio of EGFP to dTOMATO was ~50% in all cases analyzed, which is consistent with a comparable efficiency for both donors (**Figure 2A**, **2C** and **Figure S6D**). The initial percentage of double positive EGFP^{pos} dTOMATO^{pos} cells ranged from a mean 2.15% for SNCAe2, 3.4% for SNCAe3 to 3.75% for PINK1e5 (**Figure 2C** and **Figure S6D**). Quantifications were conducted independently using different sgRNAs (**Figure 2C** and **Figure S6D**). One sorting step yields a population of up to 3x10^5 EGFP^{pos} dTOMATO^{pos} cells (**Figure 2B**, **2D**). The gating position of the double positive population afforded nearly complete purity with either only one sorting step or a two-stage sorting for yield and subsequently for purity (**Figure 2E**, **Figure S6E** and **Figure S9B**). Although it is possible to isolate the single channel double positive EGFP$^{pos/pos}$ or dtOMATO$^{pos/pos}$ populations (population type 2) (**Figure 1C-D, 1G** and **Figure 2C**) using the FSC-A dimension, there is an extensive overlap with the indel-bearing single positive population (population type U) (**Figure 1G** and **Figure S4**). A high frequency of NHEJ events was detected in the non-targeted allele of the single positive population (population type U), hence purification of the double positive EGFP$^{pos/pos}$ or dtOMATO$^{pos/pos}$ populations presents a risk of co-purifying the overlapping indel bearing cells (**Figure S4D-E**). In this combination of events, only the biallelic EGFP^{pos} dTOMATO^{pos} group offers a deterministic genotype outcome. Sanger sequencing of biallelic targeted *SNCA* mutations demonstrated the heterozygous integration of the pathogenic SNP rs104893878 (p.A30P) and rs104893877 (p.A53T) in each polyclone (**Figure 2F-G**), the homozygous integration of the edited PAM, and the transition from genome to positive selection module (**Figure 2F-G**). Isolation of single clones from the polyclonal populations and sequencing

allows the analysis of the composition and a quantified assessment of the specificity of the process (**Figure 2H** and **Figure S3**).

Transposase mediated generation of footprint-free isogenic lines. The positive selection modules in each double-positive polyclone were excised using a codon-optimized hyperactive and excision-only (R372A/K375A) variant of the piggybac transposase (Li et al., 2013b; Yusa et al., 2011) (**Figure 3D-E**). Even though the excision-only variant presents an activity of 0.85 times that of WT (**Figure 3B-C**), it is preferred as it lacks the reintegration cycle of WT variants (Li et al., 2013a). The heterozygous SNCAe2 and SNCAe3 EGFP^{pos} dTOMATO^{pos} polyclonal populations were transfected with *in vitro*-transcribed mRNA encoding excision-only transposase. Subsequently, the excised EGFP^{neg} dTOMATO^{neg} population was sorted (**Figure 3D-E** and **Figure S9C**). Using the excision-only variant and two transfection steps, we observed average excision efficiencies of 3.65% for SNCAe2, 2.15% for SNCAe3, and 6.5% for PINK1e5 (**Figure 3D** and **Figure S6F**). A second sorting step, to purify cells that underwent selection module removal, yielded up to 2.5x10^6 EGFP^{neg} dTOMATO^{neg} SNP knocked-in cells (**Figure S9C**). In the FACS analysis, it is possible to observe transition states for single-copy excision and complete removal of both selection modules (**Figure 3A**, **3D-E** and **Figure S6F**). We observed a curved continuous population shifting from the double-positive EGFP^{pos} dTOMATO^{pos} quadrant to the double-negative EGFP^{neg} dTOMATO^{neg} quadrant in all cases. Sanger sequencing of the *SNCA* targeted and transposed genomic region demonstrated the heterozygous integration of the pathogenic SNP rs104893878 (p.A30P) and rs104893877 (p.A53T) in each polyclone (**Figure 3F-G**). Isolation of single cell derived clones from the PAM shielded polyclones and sequencing permitted quantification of their composition and therefore an assessment of the specificity of the process (**Figure 3H** and **Figure S5**). In our selected polyclones and the composition analysis, the positive selection modules were excised, the edited SNPs remained, and the edited PAM sites remained in the non-coding sequence (**Figure S1A** and **S5D-E**). The minimal timeframe required for each step is indicated in **Figure S9**. Karyotype assessment was conducted for each polyclone and parental control

(**Figure S8A-C**). Pluripotency of lines was assessed by immunostaining for OCT4, SOX2, TRA1-81 and SSEA4 (**Figure S8D-E**).

***SNCA* mutants present early mitochondrial impairment.** In order to validate the edited *SNCA* lines, a phenotypic characterization was conducted (**Figure 4**). Isogenic iPS cells were differentiated into neuroepithelial stem cells (NESCs) (Reinhardt et al., 2013) (**Figure 4A** and **Figure S7A-B**). NESCs typically express the *SNCA* transcript at 0.86 and 0.7 times the level of *GAPDH* and *TUBG1*, respectively (**Figure 4B** and **Figure S7C**). Western blot analysis indicated a similar protein level of monomeric α-Synuclein for all genotypes (**Figure 4C**). Extracellular energy flux analyses were conducted for parental healthy NESCs, and mutant isogenic α-Synuclein p.A30P and p.A53T NESCs (**Figure 4D**). Cells expressing the α-Synuclein mutation p.A53T showed a significantly reduced maximal respiration capacity compared to the parental isogenic control (**Figure 4D-F**). Moreover, both the p.A30P and p.A53T α-Synuclein mutant NESCs showed comparatively reduced energy performance, manifested by a lower basal respiration, ATP production, and non-mitochondrial respiration (**Figure 4D-F**).

Discussion

Overall, FACE constitutes a robust method to achieve deterministic genotype outcomes for the generation of isogenic cell lines. The selection of biallelic editing events ensure a defined genotype. It should be noted that, due to transient disruption of the coding sequence, this approach is restricted to genes with non-essential function in the target cell type. The use of a fluorescent negative selection module to exclude random integration events allows sorting of clearer isolated biallelic populations, compared with similar approaches (Eggenschwiler et al., 2016). However, potential limitations are that the positive selection modules could be subjected to position-effect variegation (including promotor silencing), additionally plasmid break points within random integrated plasmids in the promoter or fluorescent protein cassette

cannot be fully excluded. Finally, silencing of promotors for the fluorescent proteins might occur. Nevertheless, usage of the fluorescent markers expedite the selection, reducing the timescale in comparison to potential position-effect variegation (Norrman et al., 2010). It should be noted that editing approaches that use either ssDNA or dsDNA could be subjected to cleavage within non-functional or functional sequences. The advantage of dsDNA approaches in comparison to ssDNA are its flexibility to carry larger cargos, in order to deposit designer-insertions, designer-deletions or selection modules. In addition, larger sequences of donors are easier to detect by conventional methods in comparison to short ssDNA. Similarly, potential imperfect integration of dsDNA donor templates can be readily detected by simple methods as PCR, in comparison to ssDNA based methods.

Conventional derivation of single nucleotide mutations, not associated with a direct selection phenotype or selection marker, can require screening an average 911 ± 375 clones and using 8.8 ± 5.9 sgRNAs (Paquet et al., 2016). Conversely, early elimination of undesirable outcomes obviates the need to perform extensive colony screening and results in a faster, more efficient derivation process. Thus, FACE constitutes an attractive alternative to conventional methods. The efficiency of homology directed repair is influenced by the length of the homology arms used (Hasty et al., 1991). Others and we use homology arms of ~1kbp, which provides a balance between efficiency and specificity (Hockemeyer et al., 2011). The sequence conversion from endogenous genome to that carried in donor templates extend from ~400bp in dsDNA donors (Elliott and Jasin, 2001; Elliott et al., 1998) to ~30bp in ssDNA donors (Paquet et al., 2016). Hence, it is of critical importance to include the edited bases close to the dsDNA break point and close to the positive selection module unit, independently of the length of homology arms or the type of template used. Post-knock-in and post-transposition clonal composition analysis confirmed that FACE enables the derivation of polyclones, and significantly reduces the screening efforts, if individual clones are needed. On the other hand, the derivation of edited polyclones presents the advantage of avoiding the risk inherent with clone-specific biases. Extensive expansion, required for clonal derivation, is reported to subject cells to culture aberrations (Jahreiss et al., 2008; Ma et al., 2015; Martins-Taylor and

Xu, 2012). It is widely accepted that single cell passaging for any type of cell culture application, including the here described process of FACS based enrichment, imposes an unavoidable risk of genome instability (Chan et al., 2008). The derivation of polyclones reduces the culture time needed for each step, since sufficient material is available earlier. Karyotype analysis of the edited lines demonstrated that the process did not induce chromosomal abnormalities when compared with the parental line. Previous reports also support the possibility of achieving low incidence of modification with genome editing tools (Lorenz et al., 2017; Veres et al., 2014).

In order to protect the dsDNA donor template from Cas9 induced linearization and to avoid post-integration cleavage of targeted sequences, we introduced silent mutations in the PAM sequences. This requires special attention to design, in order to introduce the edited-PAM in a non-coding sequence or as a silent mutation. Others and we have successfully exploited this mechanistic insight to protect post-integration targeted sequences from secondary cleavage events (Inui et al., 2014; Paquet et al., 2016). Similarly, design considerations are needed to identify adjacent transposase excision sequences (TTAA), or to generate a de novo TTAA sequence in non-coding regions or by silent editions. Protocol optimization for the use of an excision-only transposase variant (Li et al., 2013b) allowed the derivation of footprint-free isogenic sets for disease modeling. We were able to observe transition states that represent the removal of one or both positive selection modules. The transition populations presented a curve pattern that accounts for dissimilar stability of the fluorescent proteins (Snapp, 2009) and transcripts after the CDS module was removed.

The influence of repetitive elements on the efficiency of genome editing has been reported previously (Ishii et al., 2014). Recognizable repetitive elements constitute up to ~45% of the human genome (Lander et al., 2001). Repetitive elements in human can be classified in four families: short interspersed elements (SINE), long interspersed elements (LINE), LTR retrotransposons and DNA transposons. Each category present multiple sub-families. Using linear optimization modeling, we determined that in our dataset the repetitive elements of SINE family, Alu and Mir, contribute the most to random integration events. These repetitive

elements have 1.5 million copies and constitutes ~13% of the human genome (Lander et al., 2001). Although this discrete dataset does not include all existing human repetitive elements, it demonstrates their direct contribution to random integration. Other aspects as the composition of repetitive elements, and distance to the dsDNA break point, might also modulate the frequency of random integration. Our data confirm previous reports that repetitive elements act as templates for off-target homologous recombination (Ishii et al., 2014). These sequences should be avoided when designing homology arms in order to enhance the on-target recombination and edition.

In Summary, we generated an isogenic set of human *SNCA* mutants for PD specific cellular modeling. The set carries disease-associated mutations p.A30P and p.A53T in the *SNCA* gene. Using human NESCs, an early neurodevelopment model, we observed energy metabolism phenotypes that previously only have been described in *SNCA* p.A30P mutant differentiated neurons (Ryan et al., 2013). This demonstrates the applicability of the here described approach for the generation of disease relevant models. We envision that FACE could be efficiently implemented for automated high throughput genome editing, enabling fast phenotype assessment in the future.

Experimental procedures

Stem cell culture and electroporation. The following human induced pluripotent stem (iPS) cells reprogrammed with non-integrative episomal methods were used: A13777 (Gibco cat no. A13777) from female cord blood-derived $CD34^{pos}$ cells. Cell lines were cultured in Essential 8 medium (Thermo Fisher cat no. A1517001) on laminin521 (Biolamina) or matrigel. Cells were normally dissociated with accutase (Thermo Fisher cat no. A1110501) and plated in media containing ROCK inhibitor Y27632 (Sigma cat no. Y0503) at 10µM for 24h after dissociation. Cells were subjected to positive selection with puromycin (Sigma cat no. P9620) at a concentration of 0.5µg/mL as shown in Figure S9. Cells were electroporated using 4D-

Nucleofector System (Lonza) and a 4D kit for human dermal fibroblast (Lonza cat no. V4XP). Parental pre-electroporation line presents micro-duplication 20q11.21.

Construction of sgRNA vectors and donor plasmids. Cas9 target sequences with predicted high catalytic activity were selected (Doench et al., 2014) (**Figure S1**) and cloned into pX330 vector (Addgene 42230) as previously described (Ran et al., 2013). Primers used are indicated in **Supplemental table 3**. The donor vectors were pDONOR-SNCAe2-WT (Addgene 85845), pDONOR-SNCAe2-A30P (Addgene 85846), pDONOR-SNCAe3-WT (Addgene 85847), pDONOR-SNCAe3-A53T (Addgene 85848) and pDONOR-PINK1e5-I368N (Addgene 86154) in EGFP and dTOMATO containing versions. Homology arms were assembled by conventional methods (Gibson, 2011) on donor scaffold pDONOR-tagBFP-PSM-EGFP (Addgene 100603) and pDONOR-tagBFP-PSM-dTOMATO (Addgene 100604).

In vitro RNA transcription and mRNA transfection. The coding sequence of codon-optimized hyperactive transposase Piggybac from *Trichoplusia ni* (Yusa et al., 2011) and the excision-only mutant (Li et al., 2013b) were amplified to incorporate the T7 promoter. Primers used are indicated in **Supplemental table 3**. The PCR product was used as template for in vitro transcription with a mMESSAGE mMACHINE T7 kit (Thermo Fisher cat no. AM1344) according to the manufacturer's protocol. The transcript was poly-adenylated with a Poly(A) tailing kit (Thermo Fisher cat no. AM1350) and purified with a MEGAclear transcription clean-up kit (Thermo Fisher cat no. AM1908). The transcript quality was evaluated with a Bionalayzer RNA 6000 nano (Aglient cat no. 5067-1511). Transfection was performed with Stemfect RNA transfection kit (Stemgent cat no. 00-0069) according to the manufacturer's protocol.

Fluorescent Activated Cell Sorting. FACS was conducted using sterile line sorting on a baseline and CST calibrated BD FACS ARIA III. Drop delay calibrations were ensured prior to each sample. For all human iPS cells an 85µm nozzle, a yield or purity sorting mask and

neutral density filter 2.0 were used. Cells were pre-separated with 35µm and 20µm strainers (Corning cat no. 352235 and Miltenyi cat no. 130-101-812). Sorting was conducted with single cell exclusive gating hierarchies on FSC and SSC wide and high (**Figure S6A**). Use of strainers and single cell gating is highly recommended (**Figure S6B**). For efficiency analysis, live cells were quantified by SYTOX Blue Dead Cell Stain (Thermo Fisher cat no. S34857).

Characterization of polyclones. Composition of polyclones was assessed by sub-cloning. Single cell clones were expanded and genomic DNA extracted using QuickExtract solution (Epicentre cat no. QE09050). Clones were genotyped for the left homology arm junction, right homology arm junction, and WT junction as indicated in **Figure S3** and **Figure S5**, using primers in **Supplemental table 3**. PCR products of the left homology arm were used for Sanger sequencing of subclones of SNCAe2(A30P) 632 polyclone and SNCAe3(A53T) 636 polyclone as shown in **Figure S3**. The WT junction was used for Sanger sequencing of subclones of transposed SNCAe2(A30P) 632 polyclone and transposed SNCAe3(A53T) 636 polyclone as shown in **Figure S5**.

Microarray Karyotype. Genomic DNA from the pre-electroporation parental, and isogenic polyclones was purified using GenElute Blood genomic DNA Kit (Sigma cat no. NA2020). Samples were processed at Bonn Univesity Life&Brain genomics facility using Illumina iScan technology (Illumina).

Immunostaining. Cells were fixed on PFA and permeabilized on PBS triton-X 0.2%. For characterizing human iPS cells, primary antibodies used were OCT4 (Santa Cruz cat no. sc-5279) dilution 1:100, TRA1-81 (Millipore cat no. MAB4381) dilution 1:50, SOX2 (Abcam cat no. ab97959) dilution 1:100 and SSEA4 (Millipore cat no. MAB4304) dilution 1:50. Secondary antibodies used were donkey anti-mouse alexa fluor 488 (Thermo Fisher cat no. A-21202) and donkey anti-rabbit alexa fluor 488 (Thermo Fisher cat no. A-21206), both at dilution 1:1000. For characterizing NESCs, primary antibodies used were NESTIN (BD cat no.

611659) dilution 1:600 and SOX2 (Abcam cat no. ab97959) dilution 1:200. Secondary antibodies used were donkey anti-mouse 488 (Thermo Fisher cat no. A-21202) and donkey anti-rabbit 647 (Thermo Fisher cat no. A-31573), both at dilution 1:1000. For nuclear staining, Hoechst-33342 (Thermo Fisher cat no. 62249) was used at dilution 1:1000. Images were acquired in an inverted microscope (Zeiss Axio ObserverZ1).

NESCs differentiation and culture. Induced pluripotent stem cells were clustered on aggrewell plates (Stem cell technologies cat no. 27845) for 12 hours. Embryoid bodies were transferred to ultra-low attachment plates and differentiated with the program in **Figure 4A**. Briefly, cells were cultured on KO-DMEM (Gibco cat no. 10829018) supplemented with 20% knock-out serum replacement (Gibco cat no. A3181501), 2mM glutamax (Gibco cat no. 35050061), 1x non-essential amino acids (Gibco cat no.11140035), 1µM dorsomorphine (Sigma cat no. P5499), 3µM CHIR99021 (Sigma cat no. SML1046) and 0.5µM purmorphamine (Sigma cat no. SML0868). From day three onwards, cells were cultured on DMEM-F12: neurobasal media (1:1) supplemented with N2 (Gibco cat no. 17502048), B27 without vitamin A (Gibco cat no. 12587001) and 2mM glutamax. For day three and four, media was supplemented with 10µM SB431542 (Sigma cat no. S4317). From day five onwards, the culture was maintained with 150µM ascorbic acid (Sigma cat no. A5960), 3µM CHIR99021 and 0.5µM purmorphamine. At day six, embryoid bodies were dissociated with accutase and plated on laminin211 (Biolamina) or matrigel coated plates.

Extracellular energy flux analysis. NESCs were plated on Seahorse XFe96 assay plates (Aglient) at a density of 65k cells per well and the oxygen consumption rate was quantified in a Seahorse XFe96 Analyzer. Four baseline measurements were performed before any treatment injection. Three measurements were performed after each injection as shown in **Figure 4**. Final concentrations of compounds were 1µM for oligomycin (Sigma cat no. 75351), FCCP (Sigma cat no. C2920), antimycin A (Sigma cat no. A8674) and rotenone (Sigma cat

no. R8875). DNA was quantified using CyQUANT kit (Thermo Fisher cat no. C7026) and normalization based on DNA content as previously described (Silva et al., 2013).

Western Blotting. For western blot analysis of NESCs total protein, an antibody against α-Synuclein (C-20)-R (Santa Cruz cat no. sc-7011) was used at a dilution of 1:100, and an antibody against GAPDH (abcam cat no. ab9485) was used at a dilution of 1:1000 overnight. Blots were developed using anti-rabbit IgG HRP-linked secondary antibody (GE Healthcare Life Sciences cat no. NA934V) and west-pico chemiluminescent substrate (Thermo Fisher cat no. 34080). Membranes were imaged in a Raytest Stells system with exposure of 30s for both α-Synuclein and GAPDH.

Microarray. RNA was extracted from healthy control NESCs using quiazol (Qiagen cat no. 79306) and miRNeasy (Qiagen cat no. 217004). Samples were processed at the EMBL Genomics Core Facility using Affymetrix human Gene 2.0 arrays. Results were processed using GC-RMA analysis.

Figure legends

Figure 1. Biallelic integration of fluorescent protein containing donors permits deterministic genotype outcomes. (**A**) Donor vectors contain a fluorescent positive selection module expressing EGFP or dTOMATO and a negative selection module expressing tagBFP to facilitate selection of targeted integration events. Positive selection modules contain puromycin resistance gene (Puro). (**B**) Representative example of SNCAe3 636 polyclone. Random integration tagBFP^{pos} cells are excluded from the correctly edited on-target cells (tagBFP^{neg}). (**C**) Theoretical distribution of populations for non-random outcomes as in **E-G**. (**D**) Representative example of SNCAe3. On-target EGFP^{pos} and dTOMATO^{pos} cells include homozygous populations, EGFP^{pos}/EGFP^{pos} and dTOMATO^{pos}/dTOMATO^{pos} (type 2), and heterozygous populations of undefined second-allele state EGFP^{pos}/WT-NHEJ or dTOMATO^{pos}/WT-NHEJ (type U). (**E**) Outcomes of the derived population are defined according to donor vector design. Knock-in (KI). (**F**) The tagBFP negative selection module allows removal of random integration events, assisting in the derivation of defined outcomes. (**G**) Single-channel populations present an overlap between the defined homozygous and heterozygous second allele indel-bearing populations.

Figure 2. FACS purification increases the speed and yield of isogenic derivation (**A**) Gating structure and population types for the knock-in, purification, and excision strategy. (**B**) Single cell gating structures yields high purity biallelic edited cells. (**C**) Post selection sorting of double-positive biallelic edited cells for SNCAe2 and SNCAe3 using independent sgRNAs (sgRNA630, sgRNA632, sgRNA634 or sgRNA636). FACS plots are represented with 2 percent contour lines. For SNCAe3, sgRNA 636 is included dot plot to show the distribution of 1.2 percent of Q2. (**D**) Representative EGFP^{pos}dTOMATO^{pos} culture after sorting. Biallelic edited cells generate homogenous knock-in cultures. (**E**) Yield-purity and purity-purity sorting strategies permit the generation of a homogenous biallelic knock-in population. (**F**) Sanger sequencing chromatogram of polyclone SNCAe2(A30P) 632 knock-in. Knock-in (KI). (**G**)

Sanger sequencing chromatogram of polyclone SNCAe3(A53T) 636 knock-in. (**H**) Analysis of the polyclone composition as in **Figure S3**.

Figure 3. Transposase mediated excision of positive selection modules. (**A**) Schematic representation of the transition states for excision. The transition is recapitulated in the excision of **D-E** and **Figure S6F**. Puromycin resistance gene (Puro). (**B**) Optimization of conditions for transposase mediated excision. Representative histograms for excision of the positive selection module using wild type (WT) and excision-only (EO) transposase variants and one to three transfection steps. (**C**) Quantification of the excision efficiency shown in **B**. Each condition represents three replicates. For transposase optimization assays, the $EGFP^{pos}$ populations type 2 + type U were used. Significance determined by a one-way ANOVA. Significance level * $p<0.05$. (**D**) Two transfection steps of excision-only transposase results in removal of the positive selection module for SNCAe2 and SNCAe3. Purification of $EGFP^{neg}dTOMATO^{neg}$ yields footprint-free edited lines. (**E**) Cultures after transposase transfection for SNCAe2 present single and double positive selection module removal events (in arrows) as shown in **A**. (**F**) Sanger sequencing chromatogram of transposed polyclone SNCAe2(A30P) 632 and parental control. (**G**) Sanger sequencing chromatogram of transposed polyclone SNCAe3(A53T) 636 and parental control. (**H**) Analysis of the respective polyclone composition as in **Figure S5**.

Figure 4 Edited *SNCA* isogenic lines present PD associated phenotypes. (**A**) NESCs differentiation protocol. (**B**) Microarray expression level for *SNCA*, *TUBG1*, and *GAPDH* in healthy control NESCs. (**C**) Western blot subsequent to denaturing SDS-PAGE for α-Synuclein and GAPDH, for NESCs. (**D**) Wave plot of oxygen consumption rates for the α-Synuclein isogenic set. Each wave corresponds to three biological replicates. SD of the sample is included. (**E**) Maximal respiration, proton leak, basal respiration, ATP production, and non-mitochondrial respiration for the α-Synuclein isogenic set in **D**. (**F**) Radar plot of fold changes for extracellular energy flux analysis performance in **D**. Significance levels

correspond to the higher p-value assigned to a mutant per category. Significance determined by unpaired Student's t-test. Significance levels are *p<0.05, **p<0.01 and ***p<0.001.

Author contributions

J.AF. and J.J. established the FACS sorting purification system. J.AF. and X.Q. established the transposase excision system. J.AF. and J.J. established the IVT system. J.AF., X.Q., J.J. and G.GG. performed cloning of constructs. J.AF. and J.J. performed genome editing of the lines. J.AF. and G.GG. performed random integration analysis. J.AF. and J.J. differentiated cultures. J.AF., J.W. and J.J. performed extracellular energy flux analysis. S.N. performed microarray experiments. J.AF and S.N. performed gene expression analysis. J.AF. and G. GG. performed blots. J.C.S., H.Z. and H.S. supervised. J.AF. and J.C.S. wrote the manuscript and organized display items. All the authors read and agreed to the final version of the manuscript.

Competing financial interests. J.C.S. is shareholder of Braingineering Technologies sarl. J.AF., J.J., X.Q., and J.C.S. are inventors on a patent application (LU92964).

Acknowledgments

We would like to thank Prof. F. Zhang from the McGovern Institute for Brain Research for providing the Cas9 vector. We acknowledge G. Preciat for valuable feedback on optimization. We acknowledge Prof. J. Hejna, E. Berger and S. Bolognin for their valuable comments on the manuscript. This project was supported by the LCSB pluripotent stem cell core facility. J.J., J.W., and X.Q. were supported by fellowships from the FNR (AFR, Aides à la Formation-Recherche). G.GG. was supported by NCL-Stiftung. J.J. is supported by Pelican award from the Fondation du Pelican de Mie et Pierre Hippert-Faber supported. This is an EU Joint Programme-Neurodegenerative Disease Research (JPND) project (INTER/JPND/14/02; INTER/JPND/15/11092422). Further support comes from the SysMedPD project which has

received funding from the European Union's Horizon 2020 research and innovation programme under grant agreement No 668738.

References

Barker, R.A., Drouin-Ouellet, J., and Parmar, M. (2015). Cell-based therapies for Parkinson disease-past insights and future potential. Nature reviews Neurology *11*, 492-503.

Bendor, J.T., Logan, T.P., and Edwards, R.H. (2013). The function of alpha-synuclein. Neuron *79*, 1044-1066.

Bozi, M., Papadimitriou, D., Antonellou, R., Moraitou, M., Maniati, M., Vassilatis, D.K., Papageorgiou, S.G., Leonardos, A., Tagaris, G., Malamis, G.*, et al.* (2014). Genetic assessment of familial and early-onset Parkinson's disease in a Greek population. European journal of neurology *21*, 963-968.

Chan, E.M., Yates, F., Boyer, L.F., Schlaeger, T.M., and Daley, G.Q. (2008). Enhanced plating efficiency of trypsin-adapted human embryonic stem cells is reversible and independent of trisomy 12/17. Cloning and stem cells *10*, 107-118.

Devine, M.J., Ryten, M., Vodicka, P., Thomson, A.J., Burdon, T., Houlden, H., Cavaleri, F., Nagano, M., Drummond, N.J., Taanman, J.W.*, et al.* (2011). Parkinson's disease induced pluripotent stem cells with triplication of the alpha-synuclein locus. Nature communications *2*, 440.

Doench, J.G., Hartenian, E., Graham, D.B., Tothova, Z., Hegde, M., Smith, I., Sullender, M., Ebert, B.L., Xavier, R.J., and Root, D.E. (2014). Rational design of highly active sgRNAs for CRISPR-Cas9-mediated gene inactivation. Nature biotechnology *32*, 1262-1267.

Eggenschwiler, R., Moslem, M., Fraguas, M.S., Galla, M., Papp, O., Naujock, M., Fonfara, I., Gensch, I., Wahner, A., Beh-Pajooh, A.*, et al.* (2016). Improved bi-allelic modification of a transcriptionally silent locus in patient-derived iPSC by Cas9 nickase. Scientific reports *6*, 38198.

Elliott, B., and Jasin, M. (2001). Repair of double-strand breaks by homologous recombination in mismatch repair-defective mammalian cells. Molecular and cellular biology *21*, 2671-2682.

Elliott, B., Richardson, C., Winderbaum, J., Nickoloff, J.A., and Jasin, M. (1998). Gene conversion tracts from double-strand break repair in mammalian cells. Molecular and cellular biology *18*, 93-101.

Gibson, D.G. (2011). Enzymatic assembly of overlapping DNA fragments. Methods in enzymology *498*, 349-361.

Goedert, M., Spillantini, M.G., Del Tredici, K., and Braak, H. (2013). 100 years of Lewy pathology. Nature reviews Neurology *9*, 13-24.

Hasty, P., Rivera-Perez, J., and Bradley, A. (1991). The length of homology required for gene targeting in embryonic stem cells. Molecular and cellular biology *11*, 5586-5591.

Hockemeyer, D., Wang, H., Kiani, S., Lai, C.S., Gao, Q., Cassady, J.P., Cost, G.J., Zhang, L., Santiago, Y., Miller, J.C.*, et al.* (2011). Genetic engineering of human pluripotent cells using TALE nucleases. Nature biotechnology *29*, 731-734.

Inui, M., Miyado, M., Igarashi, M., Tamano, M., Kubo, A., Yamashita, S., Asahara, H., Fukami, M., and Takada, S. (2014). Rapid generation of mouse models with defined point mutations by the CRISPR/Cas9 system. Scientific reports *4*, 5396.

Ishihara-Paul, L., Hulihan, M.M., Kachergus, J., Upmanyu, R., Warren, L., Amouri, R., Elango, R., Prinjha, R.K., Soto, A., Kefi, M.*, et al.* (2008). PINK1 mutations and parkinsonism. Neurology *71*, 896-902.

Ishii, A., Kurosawa, A., Saito, S., and Adachi, N. (2014). Analysis of the role of homology arms in gene-targeting vectors in human cells. PloS one *9*, e108236.

Jahreiss, L., Menzies, F.M., and Rubinsztein, D.C. (2008). The itinerary of autophagosomes: from peripheral formation to kiss-and-run fusion with lysosomes. Traffic *9*, 574-587.

Kim, D., Bae, S., Park, J., Kim, E., Kim, S., Yu, H.R., Hwang, J., Kim, J.I., and Kim, J.S. (2015). Digenome-seq: genome-wide profiling of CRISPR-Cas9 off-target effects in human cells. Nature methods *12*, 237-243, 231 p following 243.

Kleinstiver, B.P., Pattanayak, V., Prew, M.S., Tsai, S.Q., Nguyen, N.T., Zheng, Z., and Joung, J.K. (2016). High-fidelity CRISPR-Cas9 nucleases with no detectable genome-wide off-target effects. Nature *529*, 490-495.

Lander, E.S., Linton, L.M., Birren, B., Nusbaum, C., Zody, M.C., Baldwin, J., Devon, K., Dewar, K., Doyle, M., FitzHugh, W.*, et al.* (2001). Initial sequencing and analysis of the human genome. Nature *409*, 860-921.

Li, M.A., Pettitt, S.J., Eckert, S., Ning, Z., Rice, S., Cadinanos, J., Yusa, K., Conte, N., and Bradley, A. (2013a). The piggyBac transposon displays local and distant reintegration preferences and can cause mutations at noncanonical integration sites. Molecular and cellular biology *33*, 1317-1330.

Li, X., Burnight, E.R., Cooney, A.L., Malani, N., Brady, T., Sander, J.D., Staber, J., Wheelan, S.J., Joung, J.K., McCray, P.B., Jr.*, et al.* (2013b). piggyBac transposase tools for genome engineering. Proceedings of the National Academy of Sciences of the United States of America *110*, E2279-2287.

Lorenz, C., Lesimple, P., Bukowiecki, R., Zink, A., Inak, G., Mlody, B., Singh, M., Semtner, M., Mah, N., Aure, K.*, et al.* (2017). Human iPSC-Derived Neural Progenitors Are an Effective Drug Discovery Model for Neurological mtDNA Disorders. Cell stem cell.

Lotharius, J., and Brundin, P. (2002). Pathogenesis of Parkinson's disease: dopamine, vesicles and alpha-synuclein. Nature reviews Neuroscience *3*, 932-942.

Ma, H., Folmes, C.D., Wu, J., Morey, R., Mora-Castilla, S., Ocampo, A., Ma, L., Poulton, J., Wang, X., Ahmed, R.*, et al.* (2015). Metabolic rescue in pluripotent cells from patients with mtDNA disease. Nature *524*, 234-238.

Martins-Taylor, K., and Xu, R.H. (2012). Concise review: Genomic stability of human induced pluripotent stem cells. Stem cells *30*, 22-27.

Merkle, F.T., Neuhausser, W.M., Santos, D., Valen, E., Gagnon, J.A., Maas, K., Sandoe, J., Schier, A.F., and Eggan, K. (2015). Efficient CRISPR-Cas9-mediated generation of knockin human pluripotent stem cells lacking undesired mutations at the targeted locus. Cell reports *11*, 875-883.

Norrman, K., Fischer, Y., Bonnamy, B., Wolfhagen Sand, F., Ravassard, P., and Semb, H. (2010). Quantitative comparison of constitutive promoters in human ES cells. PloS one *5*, e12413.

Pankratz, N., and Foroud, T. (2007). Genetics of Parkinson disease. Genetics in medicine : official journal of the American College of Medical Genetics *9*, 801-811.

Paquet, D., Kwart, D., Chen, A., Sproul, A., Jacob, S., Teo, S., Olsen, K.M., Gregg, A., Noggle, S., and Tessier-Lavigne, M. (2016). Efficient introduction of specific homozygous and heterozygous mutations using CRISPR/Cas9. Nature *533*, 125-129.

Ran, F.A., Hsu, P.D., Wright, J., Agarwala, V., Scott, D.A., and Zhang, F. (2013). Genome engineering using the CRISPR-Cas9 system. Nature protocols *8*, 2281-2308.

Reinhardt, P., Glatza, M., Hemmer, K., Tsytsyura, Y., Thiel, C.S., Hoing, S., Moritz, S., Parga, J.A., Wagner, L., Bruder, J.M.*, et al.* (2013). Derivation and expansion using only small molecules of human neural progenitors for neurodegenerative disease modeling. PloS one *8*, e59252.

Ruby, K.M., and Zheng, B. (2009). Gene targeting in a HUES line of human embryonic stem cells via electroporation. Stem cells *27*, 1496-1506.

Ryan, S.D., Dolatabadi, N., Chan, S.F., Zhang, X., Akhtar, M.W., Parker, J., Soldner, F., Sunico, C.R., Nagar, S., Talantova, M.*, et al.* (2013). Isogenic human iPSC Parkinson's model shows nitrosative stress-induced dysfunction in MEF2-PGC1alpha transcription. Cell *155*, 1351-1364.

Silva, L.P., Lorenzi, P.L., Purwaha, P., Yong, V., Hawke, D.H., and Weinstein, J.N. (2013). Measurement of DNA concentration as a normalization strategy for metabolomic data from adherent cell lines. Analytical chemistry *85*, 9536-9542.

Slaymaker, I.M., Gao, L., Zetsche, B., Scott, D.A., Yan, W.X., and Zhang, F. (2016). Rationally engineered Cas9 nucleases with improved specificity. Science *351*, 84-88.

Snapp, E.L. (2009). Fluorescent proteins: a cell biologist's user guide. Trends in cell biology *19*, 649-655.

Soldner, F., Laganiere, J., Cheng, A.W., Hockemeyer, D., Gao, Q., Alagappan, R., Khurana, V., Golbe, L.I., Myers, R.H., Lindquist, S.*, et al.* (2011). Generation of isogenic pluripotent stem cells differing exclusively at two early onset Parkinson point mutations. Cell *146*, 318-331.

Veres, A., Gosis, B.S., Ding, Q., Collins, R., Ragavendran, A., Brand, H., Erdin, S., Cowan, C.A., Talkowski, M.E., and Musunuru, K. (2014). Low incidence of off-target mutations in individual CRISPR-Cas9 and TALEN targeted human stem cell clones detected by whole-genome sequencing. Cell stem cell *15*, 27-30.

Yusa, K., Zhou, L., Li, M.A., Bradley, A., and Craig, N.L. (2011). A hyperactive piggyBac transposase for mammalian applications. Proceedings of the National Academy of Sciences of the United States of America *108*, 1531-1536.

Figures

Figure 1

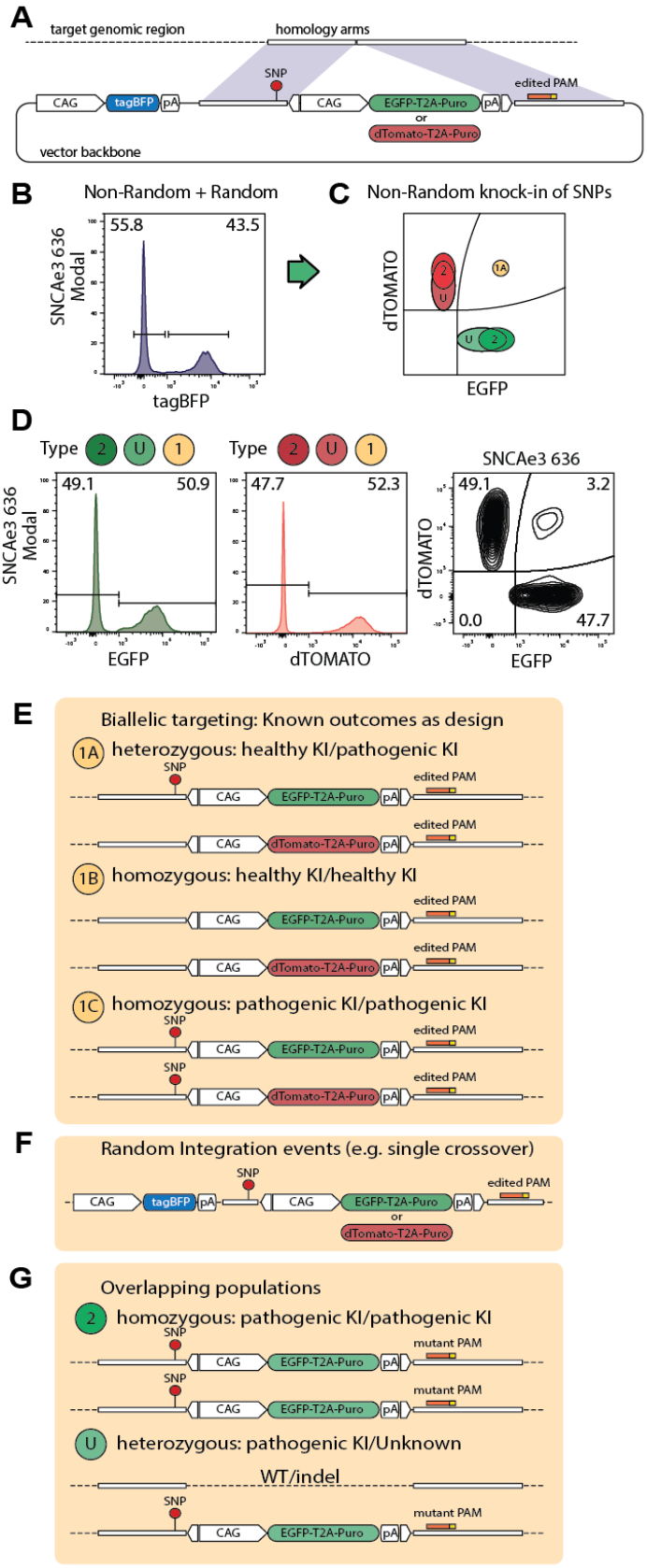

Figure 2

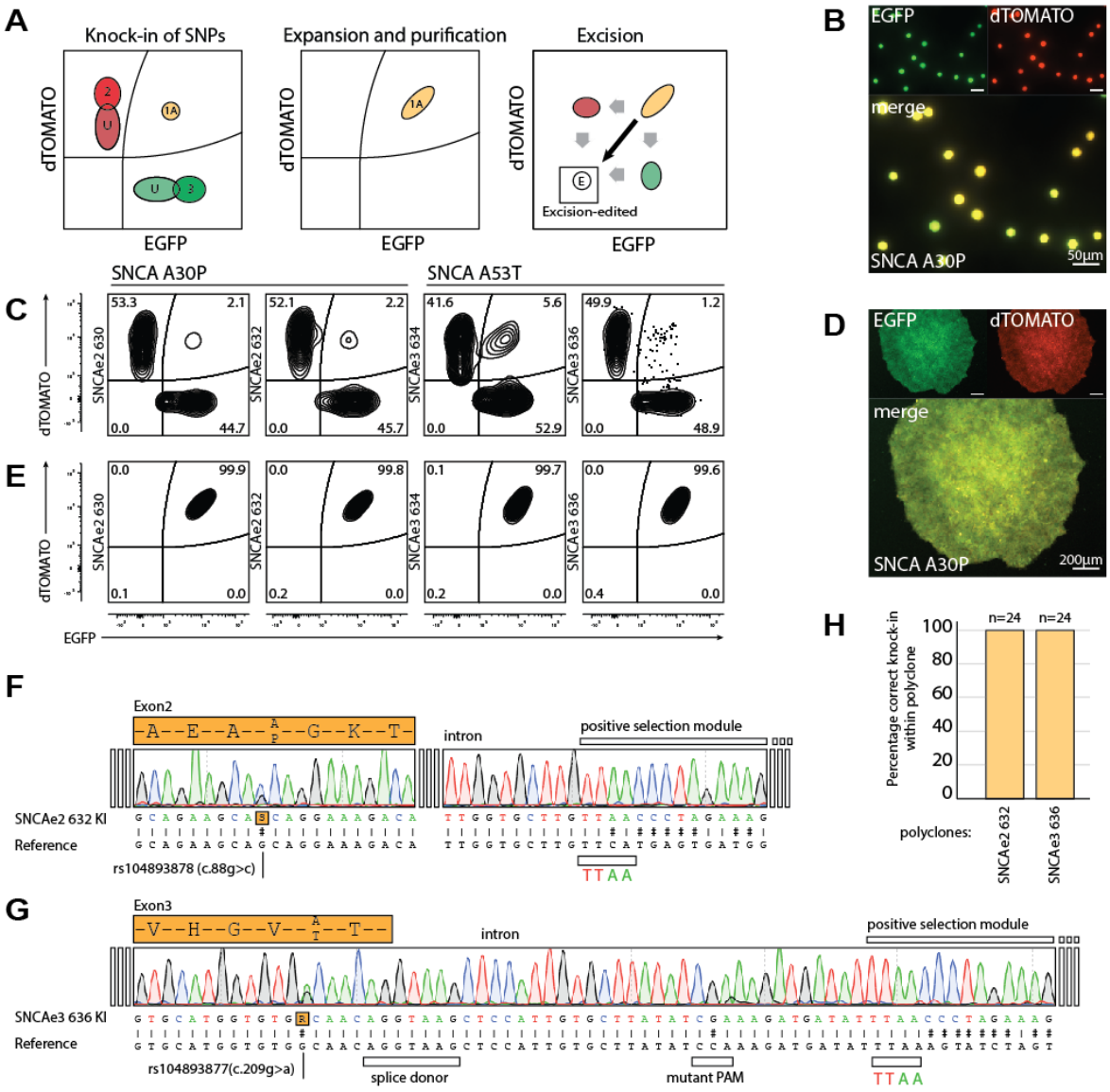
A
Knock-in of SNPs
Expansion and purification
Excision
dTOMATO
EGFP
Excision-edited
B
EGFP
dTOMATO
merge
SNCA A30P
50µm
C
SNCA A30P
SNCA A53T
SNCAe2 630
SNCAe2 632
SNCAe3 634
SNCAe3 636
53.3
2.1
0.0
44.7
52.1
2.2
45.7
41.6
5.6
52.9
49.9
1.2
48.9
D
EGFP
dTOMATO
merge
SNCA A30P
200µm
E
99.9
99.8
99.7
99.6
F
Exon2
intron
positive selection module
SNCAe2 632 KI
Reference
rs104893878 (c.88g>c)
TTAA
G
Exon3
intron
positive selection module
SNCAe3 636 KI
Reference
rs104893877(c.209g>a)
splice donor
mutant PAM
TTAA
H
Percentage correct knock-in within polyclone
n=24
n=24
polyclones:
SNCAe2 632
SNCAe3 636

Figure 3

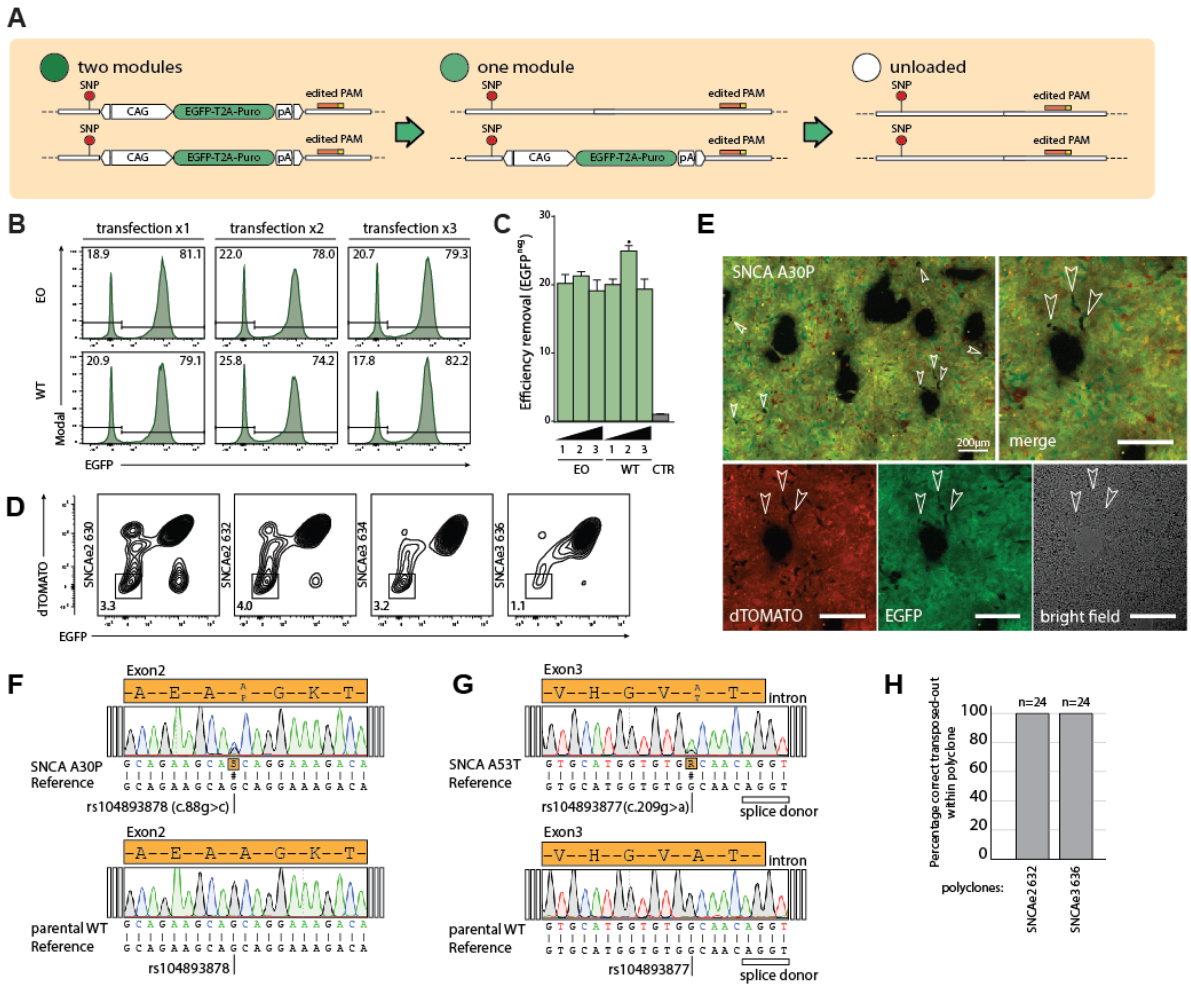
A
two modules
one module
unloaded
SNP
CAG
EGFP-T2A-Puro
pA
edited PAM
B
transfection x1
transfection x2
transfection x3
EO
WT
Modal
EGFP
18.9
81.1
22.0
78.0
20.7
79.3
20.9
79.1
25.8
74.2
17.8
82.2
C
Efficiency removal (EGFP neg)
1 2 3 1 2 3
EO
WT
CTR
D
dTOMATO
EGFP
SNCAe2 630
SNCAe2 632
SNCAe3 634
SNCAe3 636
3.3
4.0
3.2
1.1
E
SNCA A30P
200µm
merge
dTOMATO
EGFP
bright field
F
Exon2
-A--E--A--A--G--K--T-
SNCA A30P
Reference
rs104893878 (c.88g>c)
parental WT
Reference
rs104893878
G
Exon3
-V--H--G--V--A--T--
intron
SNCA A53T
Reference
rs104893877(c.209g>a)
splice donor
parental WT
Reference
rs104893877
H
Percentage correct transposed-out within polyclone
n=24
n=24
polyclones:
SNCAe2 632
SNCAe3 636

Figure 4

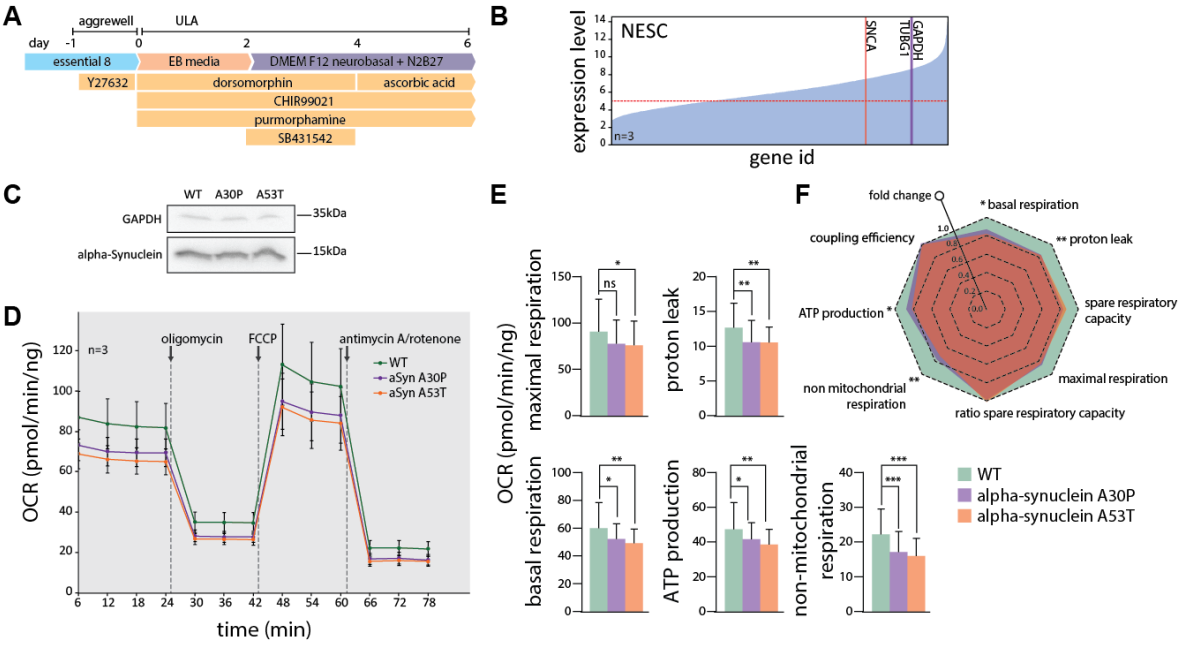
A
aggrewell
ULA
day -1 0 2 4 6
essential 8
EB media
DMEM F12 neurobasal + N2B27
Y27632
dorsomorphin
ascorbic acid
CHIR99021
purmorphamine
SB431542
B
NESC
SNCA
GAPDH
TUBG1
expression level
n=3
gene id
C
WT A30P A53T
GAPDH
35kDa
alpha-Synuclein
15kDa
D
n=3
oligomycin
FCCP
antimycin A/rotenone
WT
aSyn A30P
aSyn A53T
OCR (pmol/min/ng)
time (min)
E
OCR (pmol/min/ng)
maximal respiration
proton leak
basal respiration
ATP production
non-mitochondrial respiration
ns
F
fold change
* basal respiration
** proton leak
spare respiratory capacity
maximal respiration
ratio spare respiratory capacity
non mitochondrial respiration
ATP production
coupling efficiency
WT
alpha-synuclein A30P
alpha-synuclein A53T

FACS assisted CRISPR-Cas9 genome editing facilitates Parkinson's disease modeling

- Supplemental Information -

Jonathan Arias-Fuenzalida [1,2,7], Javier Jarazo [1,7], Xiaobing Qing [1], Jonas Walter [1] Gemma Gomez-Giro [1,4], Sarah Louise Nickels [1,3], Holm Zaehres [4,5], Hans Robert Schöler [4,6], Jens Christian Schwamborn [1]

[1] Luxembourg Centre for Systems Biomedicine (LCSB), Developmental and Cellular Biology, University of Luxembourg, L-4362, 7 avenue des Hauts-Fourneaux, Luxembourg

[2] Graduate School of Biostudies, Kyoto University, Kyoto 606-8502, Japan

[3] Life Science Research Unit (LSRU), Systems Biology, University of Luxembourg, L-4367, 6 avenue du swing, Luxembourg

[4] Max Planck Institute for Molecular Biomedicine, Laboratory of Cell and Developmental Biology, Roentgenstrasse 20, Muenster, Germany

[5] Ruhr-University Bochum, Medical Faculty, Department of Anatomy and Molecular Embryology, 44801 Bochum, Germany

[6] Westphalian Wilhelms University Muenster, Medical Faculty, 48149 Muenster, Germany

[7] These authors equally contributed to the article

Correspondence should be addressed to J.S. (jens.schwamborn@uni.lu)

Supplemental Figure legends

Figure S1. **Cleaving region design. Related to Figure 1**. (**A**) Schematic representation of *SNCA* exon 2 and *SNCA* exon 3 indicating the binding site of the sgRNAs tested (**Supplemental table 3**), disease-associated SNPs, and PAM edited bases.

Figure S2. Repetitive elements decrease on-target efficiency and increase random integration events. Related to Figure 1. Flow cytometry histogram for tagBFP: **(A)** *SNCA* exon 2 sgRNA 630 and 632, **(B)** *SNCA* exon 3 sgRNA 634 and 636, **(C)** *PINK1* exon 5 sgRNA 517 and 526, **(D)** CLN3 exon 14-15 sgRNA 788, 789 and 909, **(E)** CLN3 exon 5-8 sgRNA 781 and 783, and **(F)** CLN3 exon 10-13 sgRNA 561 and 563. **(G)** Distribution and type of repetitive elements in the homology arms of the dsDNA donors for SNCAe2, SNCAe3, PINK1e5, CLN3e5-6, CLN3e10-13 and CLN3e14-15. **(H)** Predictive model for random integration. The predictive model *PR* uses the matrix of repetitive element frequency in the homology arms *A*, the repetitive elements vector *x,* and the observed incidence of tagBFP^{pos} random integration *b*. The mathematical model generates coefficients for each repetitive element and the constant of the system for random integration prediction. **(I)** The space of non-zero coefficients derived from **H**: SINE Alu and SINE Mir, allows inferring expected random integration frequencies.

Figure S3. Quantification of polyclone composition and efficiency post-knock-in. Related to Figure 2. (**A**) Schematic representation of the genomic structure after knock-in and genomic structure after transposition. Positive selection module (PSM), left homology arm (LHA) and right homology arm (RHA). The binding sites of the genotyping primers are represented (**Supplemental table 3**), as well as the left homology arm junction, right homology arm junction, and WT junction. (**B**) Genotyping PCR products of 24 clones derived from the polyclone SNCAe2(A30P) 632, and WT control. (**C**) Genotyping PCR products of 24 clones derived from the polyclone SNCAe3(A53T) 636, and WT control. (**D**) Representation of the left homology arm junction of SNCAe2 including the SNP rs104893878 and PSM

interface. Sanger sequencing chromatograms of 24 clones derived from the polyclone SNCAe2(A30P) 632 as in **B**. Chromatograms show the transversion *SNCA* c.88g>c and the TTAA interface to the PSM. Knock-in (KI). (**E**) Representation of the left homology arm junction of SNCAe3 including the SNP rs104893877 and PSM interface. Sanger sequencing chromatograms of 24 clones derived from the polyclone SNCAe3(A53T) 636 as in **C**. Chromatograms show the transition *SNCA* c.209g>a and the TTAA interface to the PSM. Knock-in (KI).

Figure S4. **Single fluorescent protein homozygous clones (type 2) present high overlap with heterozygous indel-bearing clones (type U)**. **Related to Figure 2**. (**A**) Homozygous and heterozygous dTOMATO^{pos} SNCAe2 clones were analyzed by FACS. The histogram (left) confirms the overlap in the 2D-fluorescent cytometry map (right). (**B**) Schematic representation of overlapping populations as in **Figure 1G**. Knock-in (KI). (**C**) Type U (one copy integration) and type 2 (two copy integration) single cell clones also present high overlap in the FSC-A dimension. Clone type U population overlaps 26.1% with the gate established by the type 2 clone. (**D**) Sequencing of the non-targeted allele amplified from the type U population presents a high frequency of indels as indicated by a set of Sanger sequencing reads (n=20) for SNCAe2 and SNCAe3 type U. (**E**) Representative chromatogram for an indel bearing non-targeted allele of the type U population. Cas9 cleavage site indicated in arrow.

Figure S5. Quantification of polyclone composition and efficiency post-transposition. Related to Figure 3. (**A**) Schematic representation of the genomic structure after knock-in and genomic structure after transposition. Positive selection module (PSM), left homology arm (LHA) and right homology arm (RHA). The binding sites of the genotyping primers are represented (**Supplemental table 3**), as well as the left homology arm junction, right homology arm junction, and WT junction. (**B**) Genotyping PCR products of 24 clones derived from the transposed polyclone SNCAe2(A30P) 632, pre-removal polyclone, and WT control. (**C**) Genotyping PCR products of 24 clones derived from the transposed polyclone

SNCAe3(A53T) 636, pre-removal polyclone, and WT control. (**D**) Representation of the WT junction of SNCAe2 including the SNP rs104893878, and the TTAA interface to the genomic region. Sanger sequencing chromatograms of 24 clones derived from the transposed polyclone SNCAe2(A30P) 632. Chromatograms show the transversion *SNCA* c.88g>c and the TTAA interface to the genomic region. (**E**) Representation of the WT junction of SNCAe3 including the SNP rs104893877, and the TTAA interface to the genomic region. Sanger sequencing chromatograms of 24 clones derived from the transposed polyclone SNCAe3(A53T) 636. Chromatograms show the transition *SNCA* c.209g>a and the TTAA interface to the genomic region.

Figure S6. **Single cell gating structure and biallelic editing of PINK1e5**. **Related to Figure 2 and Figure 3**. (**A**) Hierarchical single cell gating structure of SSC and FSC wide and high for single cell preparations of PINK1e5(I368N) 517 polyclone. (**B**) Preparation of cells with a cell strainer and single cell gating structure is essential to ensure high quality sorting. Scale bar 25µm. (**C**) Gating structure and population types for knock-in, purification, and excision strategy. (**D**) Post selection sorting of double-positive biallelic edited cells for PINK1e5, using independent sgRNAs (sgRNA 517 and sgRNA 526). FACS plots are represented with 2 percent contour lines. (**E**) Purity-purity sorting allows the generation of a homogenous biallelic knock-in population. (**F**) excision-only transposase expression removes the positive selection module for PINK1e5. (**G**) Parental WT control.

Figure S7. **Differentiation, protein, and transcriptional level analysis of NESCs**. **Related to Figure 4**. (**A**) Differentiation of induced pluripotent stem cells to NESCs in 3D culture as shown in **Figure 4A**. (**B**) Immunostaining of NESCs for the neurepithelial stem cell markers NESTIN and SOX2. Scale bar 50µm. (**C**) Relative expression of *SNCA* mRNA with respect to *TUBG1* and *GAPDH* transcripts in microarray expression analysis in **Figure 4B**.

Figure S8. Microarray karyotype and pluripotency of parental and isogenic lines. Related to Figure 2 and Figure 3. (**A**) Microarray karyotype analysis of the parental line before electroporation, (**B**) polyclone 6321421 *SNCA* p.A30P and (**C**) polyclone 6361868 *SNCA* p.A53T. (**D**) Immunostaining for the pluripotency markers OCT4, TRA1-81, SOX2 and SSEA4 for parental control, (**E**) polyclone 6321421 *SNCA* p.A30P and (**F**) polyclone 6361868 *SNCA* p.A53T. Scale bar 200µm.

Figure S9. Minimal timeframe required for editing. Related to Figure 1, Figure 2 and Figure 3. (**A**) Schematic representation of conventional sgRNA testing experiment. Activity of sgRNA is validated and ranked based on colony counts at day 10. Puromycin (Puro) and ROCK inhibitor Y27632 (Y). (**B**) A minimum of three passages and 25 days are needed for knock-in process. Sorting strategies of yield/purity or purity/purity can be implemented. Puromycin (Puro) and ROCK inhibitor Y27632 (Y). (**C**) A minimum of four passages and 20 days are needed for transposition process. Sorting strategy of yield/purity is recommended. ROCK inhibitor Y27632 (Y).

Supplementary Tables

Supplementary Table 1. Biallelic targeting frequency

Polyclone sample	Frequency composed biallelic[a]	Frequency single channel biallelic[b]	Frequency total biallelic[c]
SNCAe3 636	0.032	0.179	0.390
SNCAe2 630	0.021	0.145	0.311
SNCAe2 632	0.022	0.148	0.319
SNCAe3 634	0.056	0.237	0.529
SNCAe3 636	0.012	0.110	0.231
PINK1e5 517	0.033	0.182	0.396
PINK1e5 526	0.042	0.205	0.452
Mean total			**0.375**

[a]Frequency composed biallelic is defined as the experimentally measured $EGFP^{pos}dTOMATO^{pos}$ population.
[b]Frequency of single channel biallelic represents separately the $EGFP^{pos}EGFP^{pos}$ and $dTOMATO^{pos}dTOMATO^{pos}$ population, calculated as $\sqrt{\text{frequency composed biallelic}}$.
[c]Frequency total biallelic correspond to $\text{frequency composed biallelic} + 2 * \text{frequency of single channel biallelic}$.

Supplementary Table 2. *SNCA* polyclones summary

Polyclone	PAM shielded	sgRNA	FACS % non-random	FACS % composed biallelic knock-in	% correct genotype post-knock-in (n correct/total)	FACS % transposition	% correct genotype post-transposition (n correct/total)
SNCAe2(A30P) 632	YES	632	94.1	2.2	100 (24/24)	4.0	100 (24/24)
SNCAe3(A53T) 636	YES	636	56.8	1.2	100 (24/24)	1.1	100 (24/24)
SNCAe2(A30P) 630	NO	630	85.1	2.1	Not determined	3.3	Not determined
SNCAe3(A53T) 634	NO	634	34.2	5.6	Not determined	3.2	Not determined

Supplementary Table 3. Oligonucleotides used in this study

Primer	Sequence (5' to 3')	Region (Purpose)
SNCAe2_F1 (no1615)	gaggagtcggagttgtggagaag	SNCAe2 (Genotyping)
SNCAe2_R1 (no1616)	ttcccccactgatctatgttgaagag	SNCAe2 (Genotyping)
SNCAe3_F1 (no1617)	actgaaaaatccaacattagagagg	SNCAe3 (Genotyping)
SNCAe3_R1 (no1036)	ccagaacttgccacatgctt	SNCAe3 (Genotyping)
ITR_R1 (no861)	agatgtcctaaatgcacagcg	ITR (Genotyping)
ITR_F1 (no1310)	cgtcaattttacgcatgattatctttaac	ITR (Genotyping)
SNCAe2 (no1065)	tccgtggttaggtggctaga	SNCAe2 (Sequencing)
SNCAe3 (no1034)	gggccccggtgttatctcat	SNCAe3 (Sequencing)
T7-transposase_F (no1673)	gaaattaatacgactcactataggg ccgccaccatgggcagcagcctggac	transposase CDS (T7 fusion IVT)
Transposase_R (no1693)	ggcaaacaacagatggctgg	transposase CDS (IVT)
SNCAe2_628F	caccggtaaaggaattcattagcca	synthetic (sgRNA cloning)
SNCAe2_629F	caccgggactttcaaaggccaagga	synthetic (sgRNA cloning)
SNCAe2_630F	caccggctgctgagaaaaccaaaca	synthetic (sgRNA cloning)
SNCAe2_631F	caccgagggtgttctctatgtaggt	synthetic (sgRNA cloning)
SNCAe2_632F	caccgggtgcttgttcatgagtgat	synthetic (sgRNA cloning)
SNCAe3_633F	caccgtatatcctaaaactagaaga	synthetic (sgRNA cloning)

SNCAe3_634F	caccgtgtaggctccaaaaccaagg	synthetic (sgRNA cloning)
SNCAe3_635F	caccgatctttggatataagcacaa	synthetic (sgRNA cloning)
SNCAe3_636F	caccggatactttaaatatcatctt	synthetic (sgRNA cloning)
SNCAe3_637F	caccgatacttgccaagaataatga	synthetic (sgRNA cloning)
SNCAe2_628R	aaactggctaatgaattcctttacc	synthetic (sgRNA cloning)
SNCAe2_629R	aaactccttggcctttgaaagtccc	synthetic (sgRNA cloning)
SNCAe2_630R	aaactgtttggttttctcagcagcc	synthetic (sgRNA cloning)
SNCAe2_631R	aaacacctacatagagaacaccctc	synthetic (sgRNA cloning)
SNCAe2_632R	aaacatcactcatgaacaagcaccc	synthetic (sgRNA cloning)
SNCAe3_633R	aaactcttctagttttaggatatac	synthetic (sgRNA cloning)
SNCAe3_634R	aaacccttggttttggagcctacac	synthetic (sgRNA cloning)
SNCAe3_635R	aaacttgtgcttatatccaaagatc	synthetic (sgRNA cloning)
SNCAe3_636R	aaacaagatgatatttaaagtatcc	synthetic (sgRNA cloning)
SNCAe3_637R	aaactcattattcttggcaagtatc	synthetic (sgRNA cloning)
U6_F	gagggcctatttcccatgattcc	U6 (sequencing)

Supplementary Figures

Figure S1

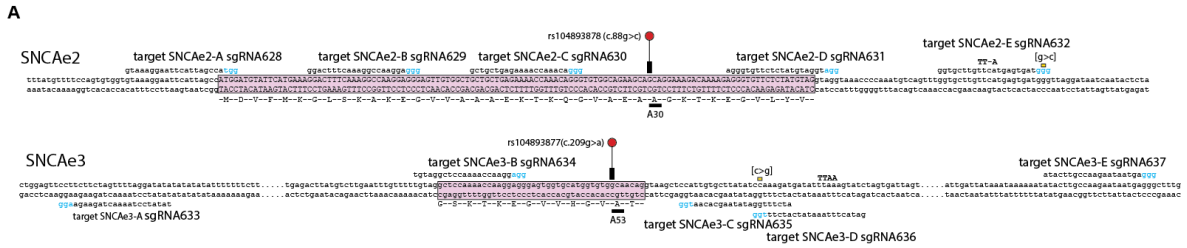

Figure S2

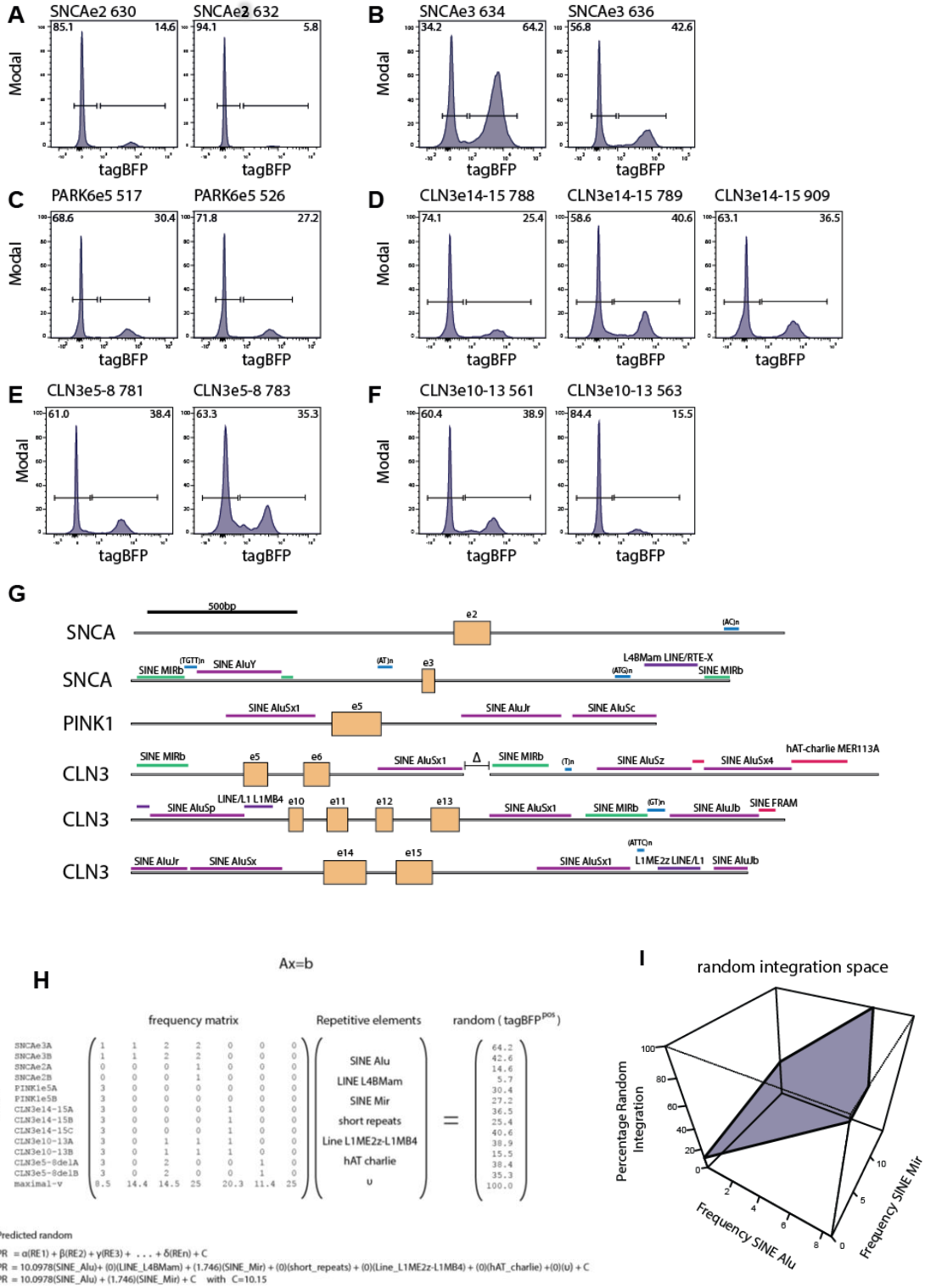
A
SNCAe2 630
SNCAe2 632
B
SNCAe3 634
SNCAe3 636
C
PARK6e5 517
PARK6e5 526
D
CLN3e14-15 788
CLN3e14-15 789
CLN3e14-15 909
E
CLN3e5-8 781
CLN3e5-8 783
F
CLN3e10-13 561
CLN3e10-13 563
Modal
tagBFP
G
500bp
SNCA
PINK1
CLN3
H
Ax=b
frequency matrix
Repetitive elements
random (tagBFP POS)
Loci
SINE Alu
LINE L4BMam
SINE Mir
short repeats
Line L1ME2z-L1MB4
hAT charlie
υ
Predicted random
PR = α(RE1) + β(RE2) + γ(RE3) + . . . + δ(REn) + C
PR = 10.0978(SINE_Alu)+ (0)(LINE_L4BMam) + (1.746)(SINE_Mir) + (0)(short_repeats) + (0)(Line_L1ME2z-L1MB4) + (0)(hAT_charlie) +(0)(υ) + C
PR = 10.0978(SINE_Alu) + (1.746)(SINE_Mir) + C with C=10.15
I
random integration space
Percentage Random Integration
Frequency SINE Alu
Frequency SINE Mir

Figure S3

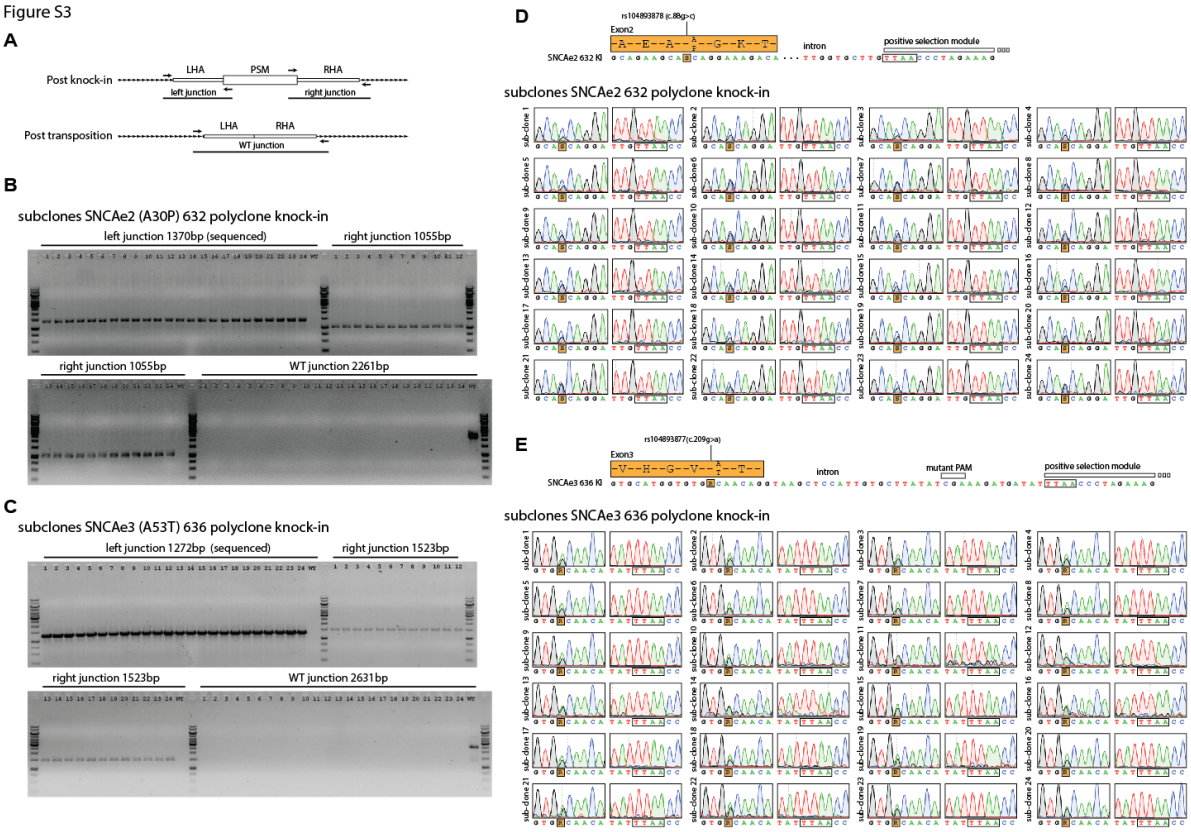

Figure S4

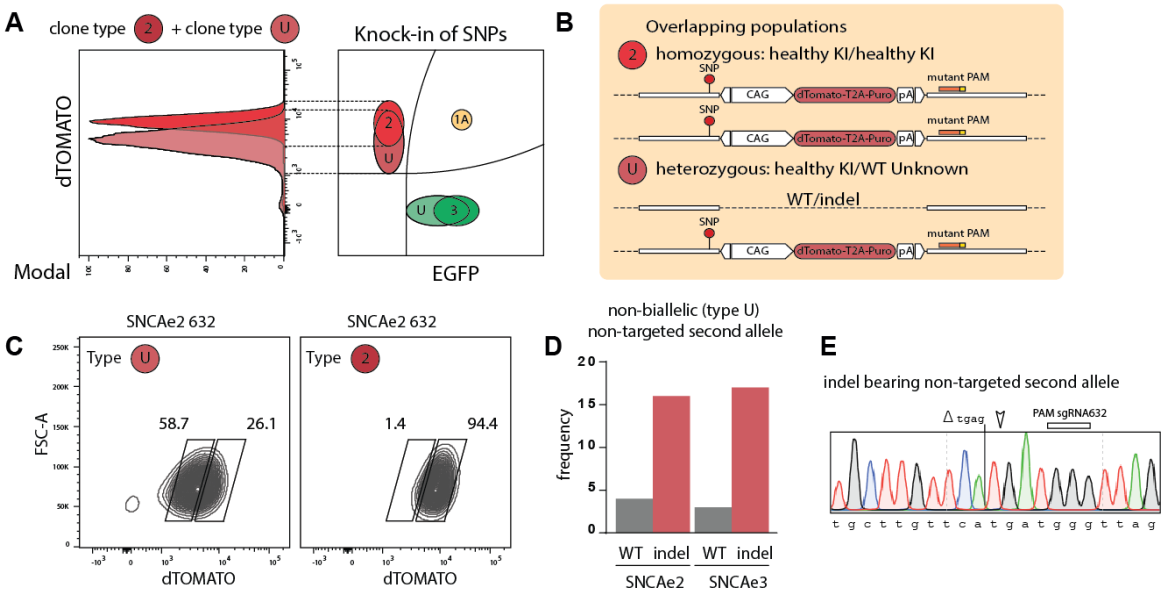

Figure S5

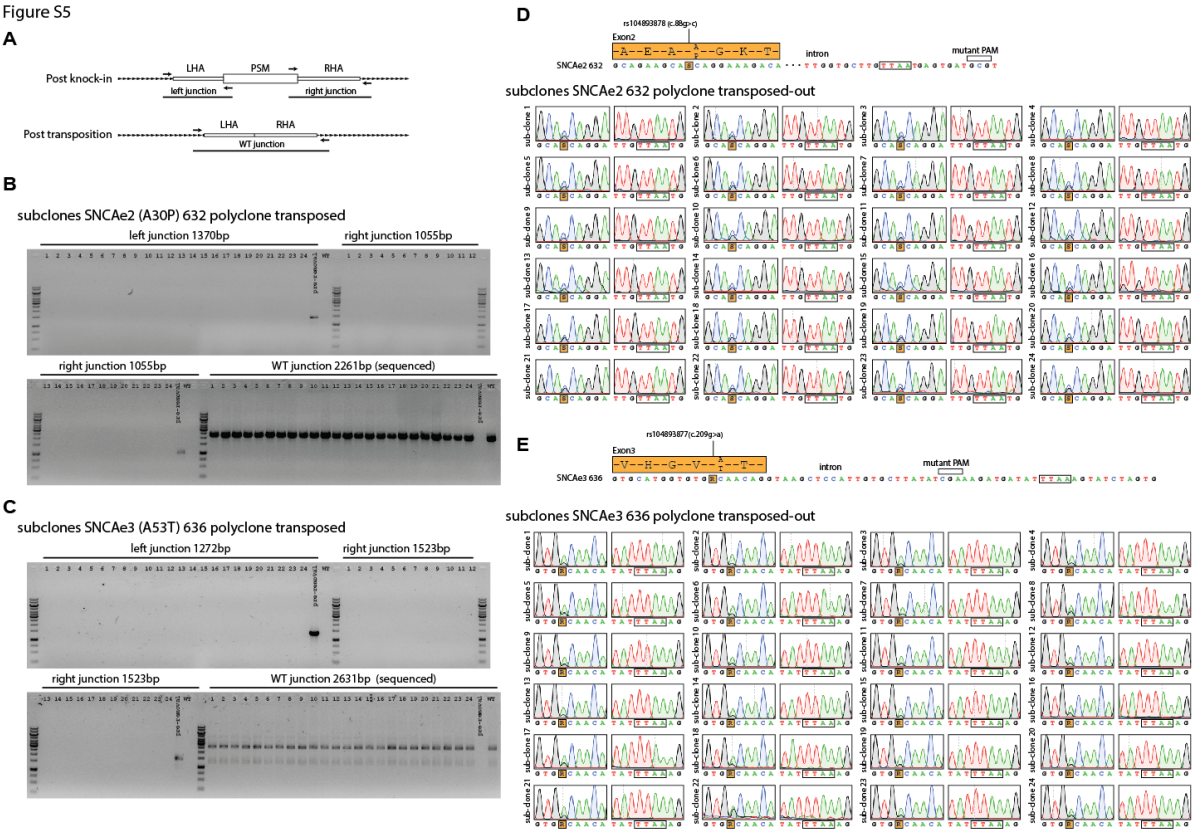

Figure S6

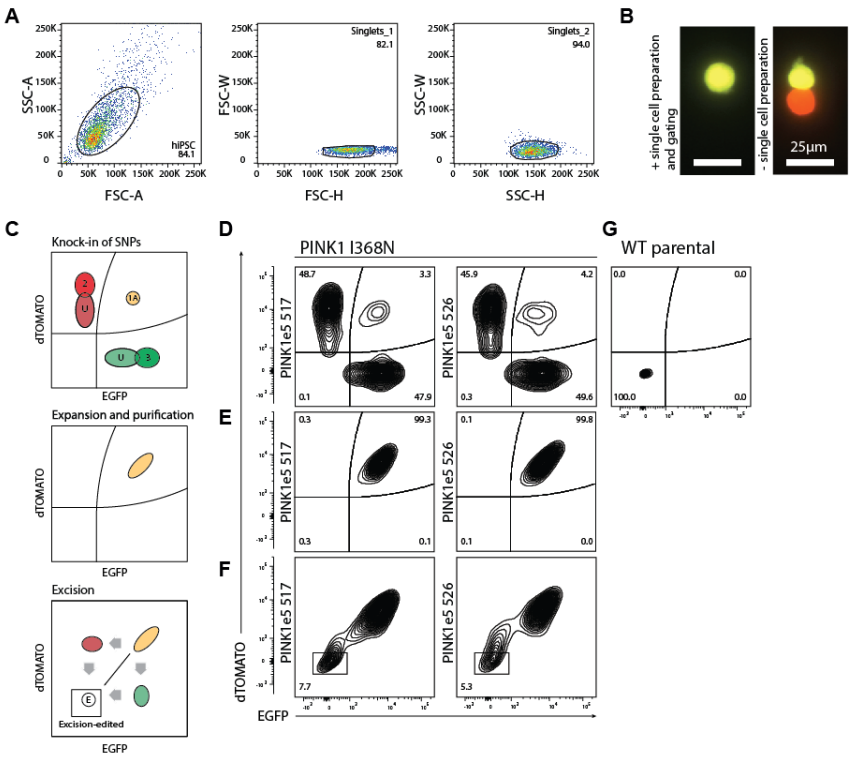

Figure S7

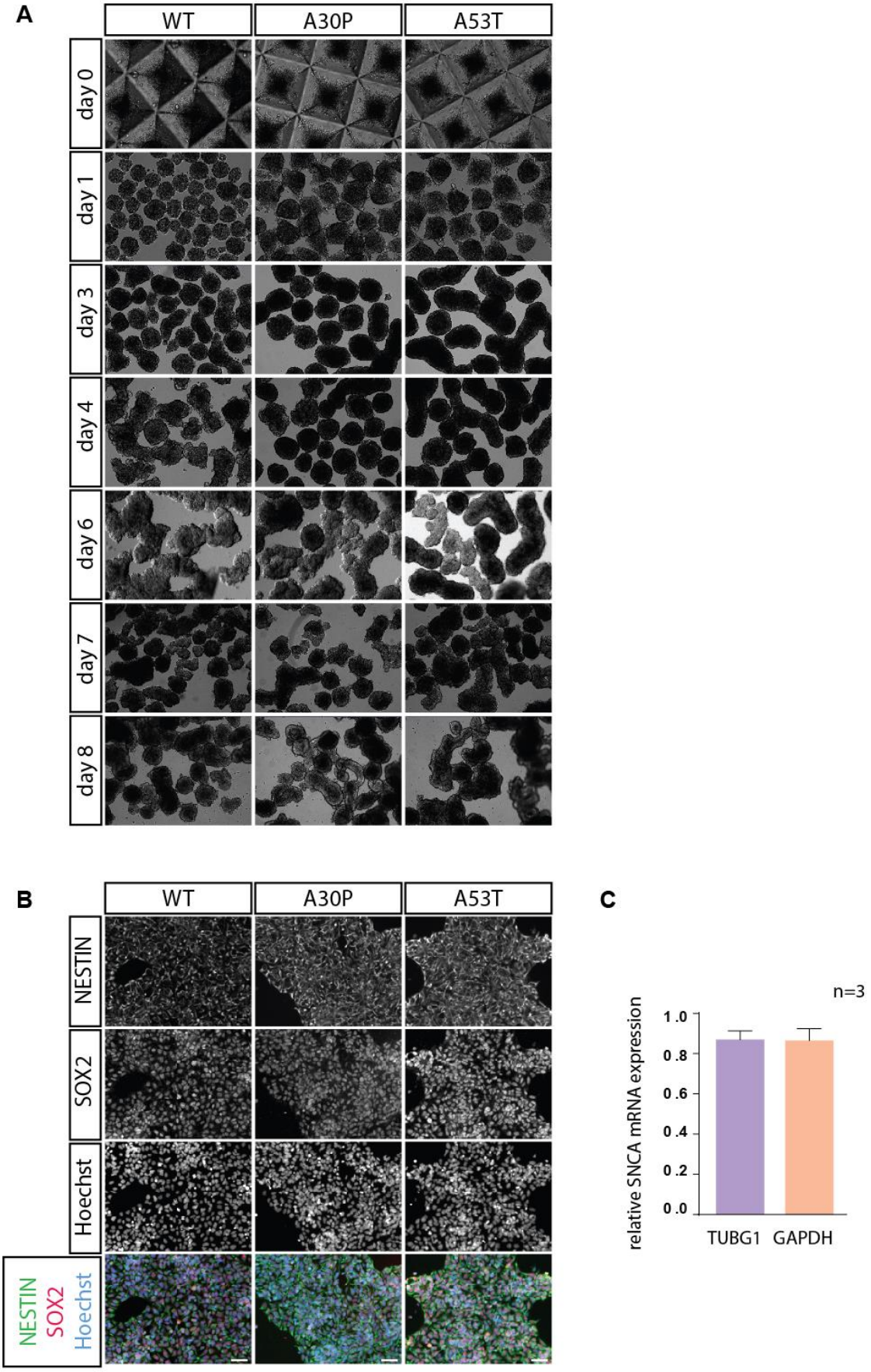
A
WT
A30P
A53T
day 0
day 1
day 3
day 4
day 6
day 7
day 8
B
WT
A30P
A53T
NESTIN
SOX2
Hoechst
NESTIN
SOX2
Hoechst
C
n=3
relative SNCA mRNA expression
1.0
0.8
0.6
0.4
0.2
0.0
TUBG1
GAPDH

Figure S8

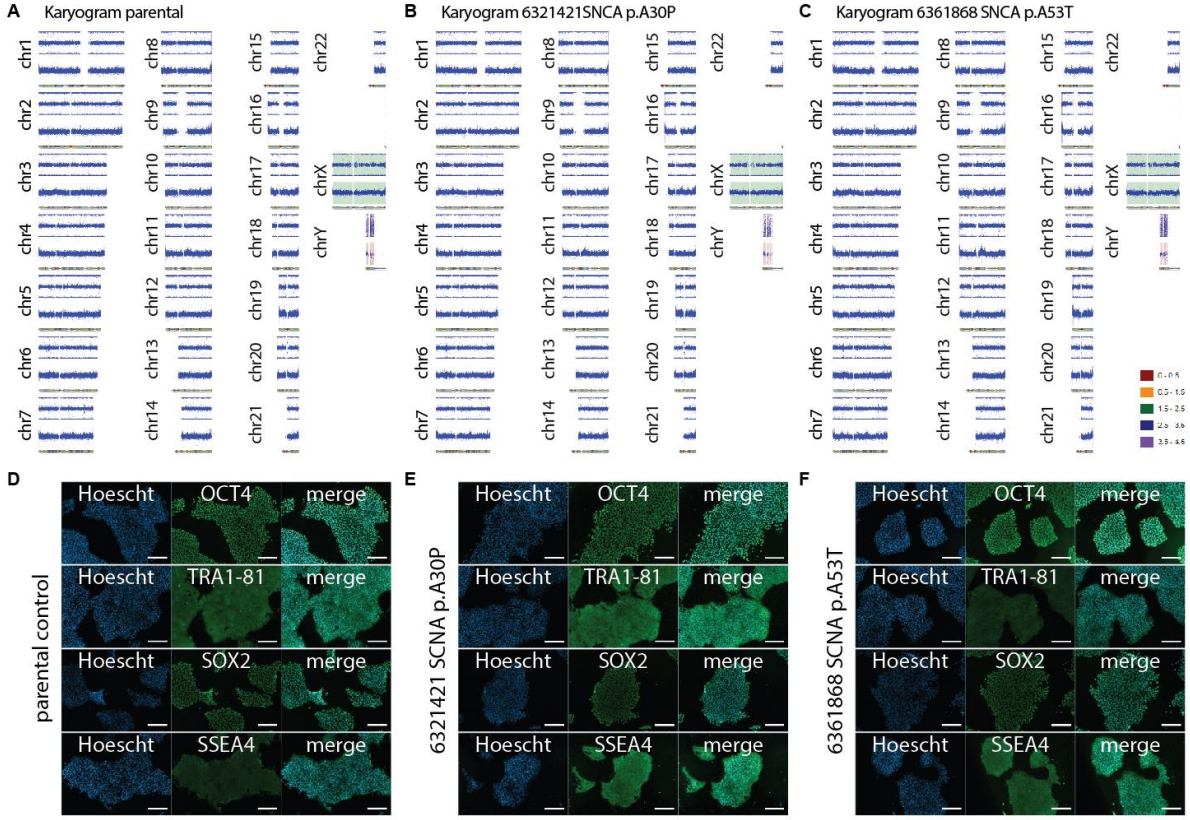

Figure S9

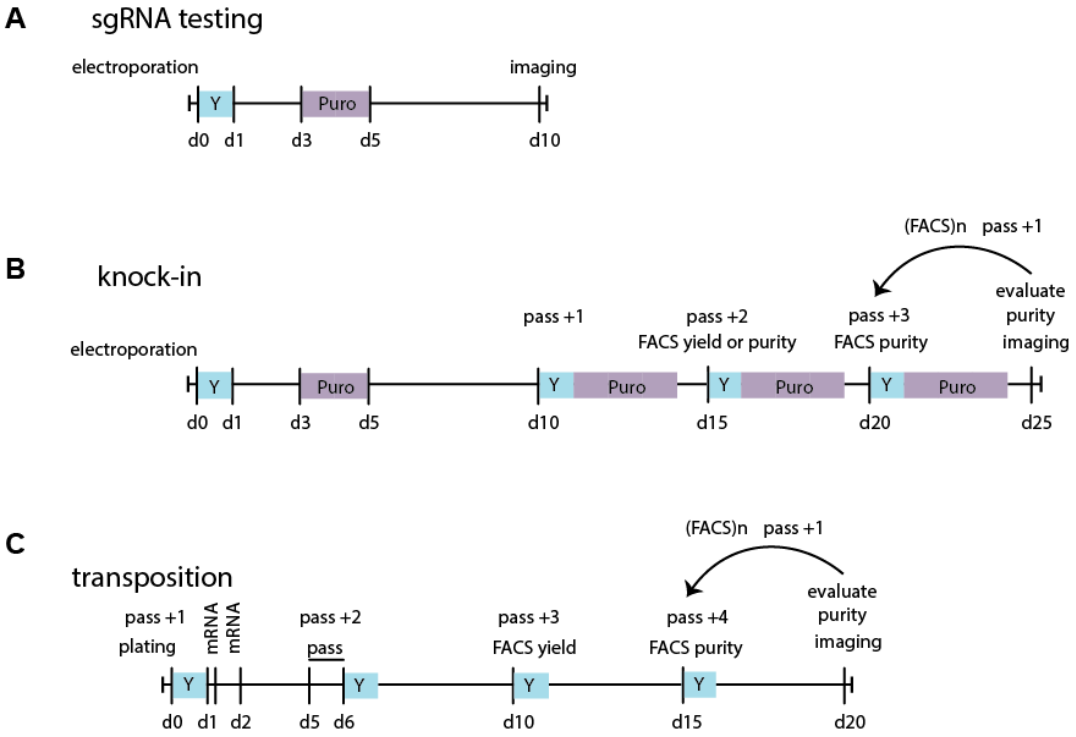

3 Publication III

The Parkinson's disease patient's genetic background complements LRRK2-G2019S pathogenicity in human neuroepithelial stem cells

Sarah Louise Nickels[1,2], Jonas Walter[1], Silvia Bolognin[1], Christian Jaeger[1], Xiaobing Qing[1], Johan Tisserand[1], Javier Jarazo[1], Kathrin Hemmer[1], Amy Harms[3], Paul M.A. Antony[1], Enrico Glaab[1], Thomas Hankemeier[3], Christine Klein[4], Lasse Sinkkonen[2], Thomas Sauter[2], Jens Christian Schwamborn[1,*]

[1]Luxembourg Centre for Systems Biomedicine (LCSB), University of Luxembourg, L-4367 Belvaux, Luxembourg
[2]Life Sciences Research Unit (LSRU), Systems Biology, University of Luxembourg, L-4367 Belvaux, Luxembourg
[3]Leiden Academic Centre for Drug Research (LACDR), Analytical Biosciences, Leiden University, NL-2333 CC Leiden, Netherlands
[4] Institute of Neurogenetics, University of Lübeck, D-23538 Lübeck, Germany

Developmental Cell 2017, submitted

3.1 Preface

Parkinson's disease is a complex progressive neurodegenerative disorder with multiple genetic contributions. The disease is characterized by the loss of dopaminergic neurons within the substantia nigra. Evidence suggests that PD has a neuro-developmental component, meaning that the predisposition to suffer from PD is probably already determined during embryogenesis. The most prevalent mutation, within LRRK2, namely LRRK2-G2019S, is linked to familial and sporadic cases of PD and different polymorphisms are associated with its age of onset. LRRK2-G2019S has, amongst other things, been linked to impaired neurogenesis, supporting the developmental contribution to disease manifestation. Due to the multiple origins of PD, the incomplete penetrance of LRRK2-G2019S and the high variability of its phenotypes, we hypothesize that modifiers within the patient's genetic background act as susceptibility factors for developing PD. Here, we analyzed 19 different iPSC-derived NESC lines originating from human patients or healthy donors. Isogenic control lines were used to differentiate between LRRK2-G2019S-dependent and genetic background specific phenotypes. Furthermore, transcriptomic and metabolomic data were acquired in order to analyze the underlying mechanisms of the phenotypes and to identify potential genetic modifiers. We demonstrate that LRRK2-G2019S patient lines are altered in cell death, proliferation, mitosis, and protein expression. However, the changes are only partly LRRK2-G2019S dependent, highlighting the contribution of the PD patient genetic background. Transcriptomic analysis identified misregulated genes, such as serine racemase (*SRR*), that are likely to be responsible for the observed phenotypes and might act as genetic modifiers. By using the enzymatic product of SRR, D-serine, we were able to rescue the LRRK2-G2019S dependent and independent phenotypes. Furthermore, serine metabolism was not only impaired in NESCs, but also in the blood plasma of LRRK2-G2019S carriers. The identification of a novel susceptibility factor within the patient's genetic background could lead to new strategies for diagnostics and therapy.

This publication is the result of my main project, and except for the help, supervision, and collaborations stated in the author contributions, all the practical work, as well as the biological interpretation, was performed by myself.

The Parkinson's disease patients' genetic background complements LRRK2-G2019S pathogenicity in human neuroepithelial stem cells

Sarah Louise Nickels[1,2], Jonas Walter[1], Silvia Bolognin[1], Christian Jaeger[1], Xiaobing Qing[1], Johan Tisserand[1], Javier Jarazo[1], Kathrin Hemmer[1], Amy Harms[3], Paul M.A. Antony[1], Enrico Glaab[1], Thomas Hankemeier[3], Christine Klein[4], Lasse Sinkkonen[2], Thomas Sauter[2], Jens Christian Schwamborn[1,*]

[1]Luxembourg Centre for Systems Biomedicine (LCSB), University of Luxembourg, L-4367 Belvaux, Luxembourg

[2]Life Sciences Research Unit (LSRU), Systems Biology, University of Luxembourg, L-4367 Belvaux, Luxembourg

[3]Leiden Academic Centre for Drug Research (LACDR), Analytical Biosciences, Leiden University, NL-2333 CC Leiden, Netherlands

[4] Institute of Neurogenetics, University of Lübeck, D-23538 Lübeck, Germany

*Correspondence: Jens C. Schwamborn, Luxembourg Centre for Systems Biomedicine (LCSB), University of Luxembourg, 6, avenue du Swing, L-4367 Belvaux, Luxembourg; E-mail: jens.schwamborn@uni.lu

GAPHICAL ABSTRACT

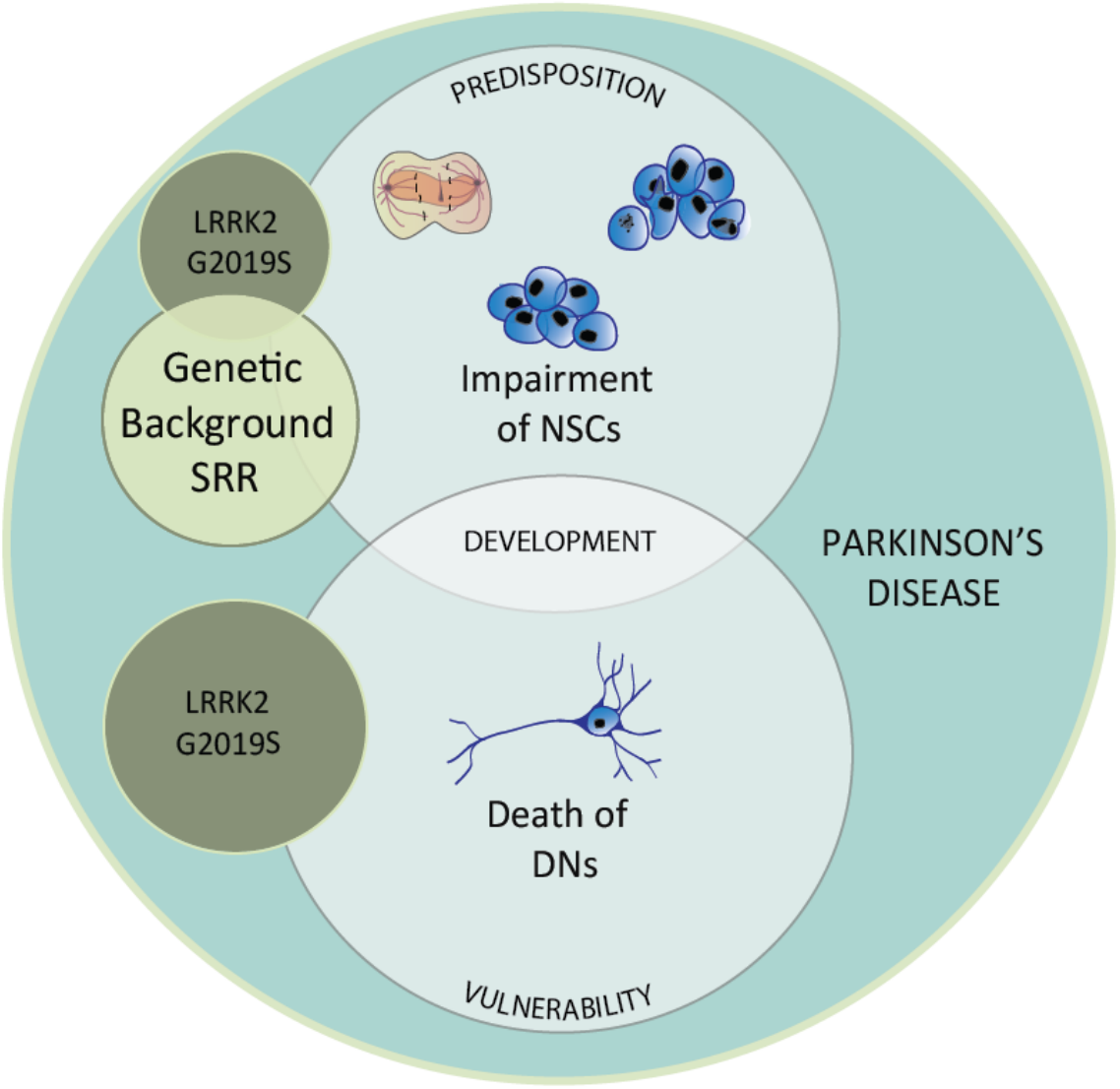

RESULTS III

SUMMARY

Parkinson's disease (PD) has a neuro-developmental component with multiple genetic predispositions. The most prevalent mutation, LRRK2-G2019S is linked to familial and sporadic PD. Based on the multiple origins of PD and the incomplete penetrance of LRRK2-G2019S, we hypothesize that modifiers in the patient genetic background act as susceptibility factors for developing PD. To assess the developmental component of LRRK2-G2019S pathogenesis, we used 19 human iPSC-derived neuroepithelial stem cell lines (NESCs). Isogenic controls distinguish between LRRK2-G2019S dependent and independent cellular phenotypes. LRRK2-G2019S patient and healthy mutagenized lines showed altered NESC self-renewal. Within patients, phenotypes were only partly LRRK2-G2019S dependent, suggesting a significant contribution of the genetic background. We identified serine racemase (*SRR*) as a novel patient-specific, developmental, genetic modifier contributing to the aberrant phenotypes. Its enzymatic product, D-serine, rescued altered NESC renewal. Susceptibility factors in the genetic background, such as SRR, could be new targets for early PD diagnosis and treatment.

KEYWORDS

Parkinson's disease, LRRK2-G2019S, Neural stem cells, Genetic background, Susceptibility factor, Serine racemase.

HIGHLIGHTS

- Impaired stem cell self-renewal and viability in LRRK2-G2019S PD patient NESC lines
- PD associated phenotypes partly depend on the genetic background
- Identification of serine racemase (*SRR*) as a susceptibility factor
- Serine is increased in G2019S carriers and D-serine rescues cellular phenotypes

INTRODUCTION

Parkinson's disease (PD) is the second most common neurodegenerative disease. Pathophysiologically, PD is characterized by the loss of midbrain dopaminergic neurons (DN) in the *Substantia Nigra pars compacta* (*SNpc*) and by the inclusion of misfolded proteins, such as α-synuclein (α-SYN), within Lewy bodies[1–4]. The first symptoms of PD only occur after a reduction of approximately 50% of DN innervation[5]. The triggers that lead to the onset of PD and finally to the irreversible DN degeneration are poorly understood and thus, PD pathogenesis remains largely elusive with no effective disease modifying treatment.

Besides neurodegeneration, we hypothezise that PD carries a strong neuro-developmental component, meaning that the predisposition to suffer from PD in later stages of life may already be determined during embryogenesis. Indeed, a high number of PD-associated genes are expressed and directly involved in neuronal development[6]. Additionally, accumulating evidence suggests that PD associated genes deregulate neural stem cells and impair neurogenesis[7–10]. These dysfunctions might unavoidably lead to deficiencies during the development of the central nervous system, e.g., α-synuclein (*Snca*) knock-out mice showed a reduced number of DNs in the *SNpc* during embryonic development[11]. Furthermore, the age of onset of clinically detectable motor symptoms is highly variable, including juvenile and late onset cases, and previous evidences suggests that also seemingly idiopathic (iPD) cases have a genetic contribution[12–15].

PD has been proposed to encompass different multifactorial diseases, with similar phenotypic outcome[16]. Multiple genetic predispositions can cause similar parkinsonian phenotypes and symptoms. Currently, mutations in six genes have been unequivocally identified to cause monogenic forms of PD that are phenotypically more or less similar to iPD [17] and 28 GWAS risk loci were found to increase the risk to develop PD[12]. The most common mutation that causes autosomal dominant PD is a glycine to serine substitution at position 2019 (G2019S) in the leucine-rich-repeat-kinase-2 (LRRK2)[18,19]. *LRRK2* is of special interest as its mutations are the monogenetic cause of familial PD and 1-2% of the sporadic

cases, without familial history, could be linked to the G2019S mutation[20,21]. Furthermore, a small nucleotide polymorphism in the *LRRK2* gene was shown to act as common risk modifier for developing PD[12]. Epidemiologic studies suggest that the age of onset between individuals carrying LRRK2-G2019S is highly variable, that there are gender-specific variations, and that different ethnicities show higher prevalences than others[22–24]. These observations suggest that genetic variants within the patients' specific genetic background may underlie this variability. For instance, polymorphisms contribute to the variability in PD-associated phenotypes and are directly linked to the age of onset of LRRK2-G2019S-induced pathogenesis[25–28]. This high individual variability may explain why asymptomatic carriers exist, why the penetrance of LRRK2-G2019S is age-dependent, and why the LRRK2 phenotypic spectrum is practically indistinguishable from that of iPD[20,29,30].

Pathogenic LRRK2 impairs a wide range of cellular functions including protein trafficking and degradation, cytoskeletal integrity, cell death, proliferation, synaptogenesis, and differentiation[31]. Previous studies suggest that LRRK2 has an impact on neural stem cell proliferation and integrity and plays a role in neurogenesis[7,10,32–36]. Furthermore, *LRRK2* expression is enhanced in the ventricular and sub-ventricular zone of the developing mouse brain during neurogenesis[37]. This suggests a possible link between LRRK2, impaired neurogenesis, and the onset or progression of PD, and corroborates the hypothesis of a developmental contribution to the disease manifestation[6].

The high variability of LRRK2-G2019S associated phenotypes and the heterogeneity of idiopathic PD indicate that also in patients suffering from monogenic PD the genetic background may play a major role. Specifically, genetic modifiers could act as susceptibility factors for manifesting PD. To explore this hypothesis, we investigated human PD patient specific, iPSC derived neuroepithelial stem cells (NESCs). To differentiate between LRRK2-G2019S dependent phenotypes and genetic background-specific changes, isogenic control lines were used[10,27,38]. The identification of phenotypes in LRRK2-G2019S PD patient-specific hNESCs will allow us to gain new insights into the importance of neural stem cell deregulations in PD pathogenesis and development. Finally, analysing the patients' genetic background

enables us to discover susceptibility factors that may control disease-related cellular phenotypes and predispose to PD. These novel genetic modifiers could potentially be used as biomarkers for early diagnosis or as personalized therapeutic targets for precision medicine.

RESULTS

Generation and quality control of hNESCs derived from iPSCs

In this study, we use 19 different hNESC lines derived from induced pluripotent stem cells (iPSCs) using small molecules[39]. The iPSCs were derived from fibroblasts of six healthy individuals (H1, H2, H3, H4, H5 and H6) and five patients with PD carrying the LRRK2-G2019S mutation (P1, P1.1, P2, P3, P4, P5 and P6) (**Fig. 1a**). The different genetic backgrounds raised the need to account for the genetic variability. Three of the iPSC lines were newly derived from fibroblasts (H5, P5, and P6) and characterized for pluripotency marker expression and genomic integrity (**Supplementary Fig. 1a-c**). From this pool of iPSCs six isogenic control lines were generated. Three were gene-corrected (P1GC, P1.1GC and P2GC) and in three healthy lines the LRRK2-G2019S mutation was introduced (H1G2019S, H3G2019S and H6.1G2019S) (**Fig. 1a**)[27]. The insertion of G2019S into the healthy cell lines H3 and H6.1 was performed by CRISPR-Cas9 gene editing (**Supplementary Fig. 2**). The other lines were previously generated using Zinc Finger Nucleases (Reinhardt et al., 2013b). Isogenic lines were generated to distinguish the phenotypes caused by the LRRK2-G2019S mutation from those driven by the genetic background. All 19 hNESC lines express the neural stem cell markers SOX2, NESTIN, SOX1 and PAX6 (**Fig. 1b** and **Supplementary Fig. 3a-b**). Moreover, sequencing of the LRRK2-G2019S region confirmed the genotypes (**Fig. 1c** and **Supplementary Fig. 3c**).

Neuronal differentiation of patient specific stem cells recapitulates well-established LRRK2-G2019S dependent phenotypes *in vitro*

Previously LRRK2-G2019S was shown to impair neurogenesis by inducing cell death, neurite shortening and inceasing α-SYN levels in DNs[27]. In order to validate our *in vitro* disease model, we first investigated

whether these established LRRK2-G2019S induced phenotypes could be recapitulated in our neuronal cultures. After induction of neuronal differentiation, the quantification of pyknotic nuclei, α-SYN, and DN complexity confirmed these phenotypes (**Fig. 1d-f**). DNs were identified by positive immunoreactivity with anti-tyrosine hydroxylase (TH) antibodies. In 14-day-old neurons derived from patient hNESCs, we observed a significant increase in the area of pyknotic nuclei (Hoechst) and α-SYN compared to neurons from healthy individuals (**Fig. 1d**, **e**). Furthermore, neurite complexity, represented by the number of nodes and links in neurites of TH immunoreactive neurons was significantly decreased in patient lines, in accordance with reduced neurite outgrowth (**Fig. d**, **e**). Importantly, insertion of the LRRK2-G2019S mutation into healthy lines consistently recapitulated the presumed cell death and DN complexity phenotypes, while gene correction rescued them, suggesting that LRRK2-G2019S causes the observed phenotypes (**Fig. 2f**).

LRRK2-G2019S causes changes in α-SYN and TAU levels in patient NESC lines

After recapitulating known cellular phenotypes in DNs, we were interested whether we could detect PD-relevant differences, already at the stem cell level in NESCs. PD is characterized as a synucleinopathy with Lewy body inclusions, however, multiple studies suggest that TAU protein aggregations also play a role in PD progression[1,40,41]. Based on this, we investigated whether α-SYN and TAU protein expression levels were already affected in patient-specific NESCs. Western blot analysis revealed the presence of α-SYN and TAU monomers in NESCs (**Fig. 2a-b**). Since patient-derived neurons showed increased α-SYN levels (**Fig. 1d-e)** and since LRRK2-G2019S increased α-SYN and TAU levels in DNs[27], we investigated whether this increase was already present in patient-specific NESCs. However, due to inter-individual variability, no significant difference in the global levels of α-SYN and TAU was found between cell lines from healthy controls and patients. Moreover, the introduction of G2019S into healthy lines was insufficient to induce a significant increase in the expression of α-SYN or TAU. By contrast, when comparing patient lines with mutation corrected isogenic controls, a significant increase of α-SYN and TAU levels was found in the mutation carrying cells (**Fig. 2a**, **b**).

Patient cell lines show impaired stem cell self-renewal

To further investigate cellular phenotypes in neural stem cells, we addressed proliferation and cell death. MTT assay derived growth curves revealed reduced cell viability or metabolic activity of the patient cell lines compared to the healthy ones (**Fig. 2d**). To assess whether this decrease was linked to lower proliferation rates, we stained for the mitosis marker phospho-histone3 (PH3). In the patient-derived lines, less cells were undergoing cell division as compared to healthy controls (**Fig. 2c** and **e**). Additionally, immunostainings for cleaved caspase3 (CC3) and for pyknotic nuclei revealed increased cell death and apoptosis in patient-derived lines (**Fig. 2c** and **e**).

PD-associated phenotypes are partially genetic background-dependent: The LRRK2-G2019S mutation is sufficient but not necessary to alter cell death and proliferation

Next, we investigated whether the altered proliferation and increased cell death phenotypes were indeed caused by the LRRK2-G2019S mutation. For this purpose, we made use of NESC lines from healthy individuals, in which the mutation was introduced. In these lines, we were able to detect phenotypes similar to the ones observed in patient lines (**Fig. 2f-h**). However, correcting the mutation in patient derived lines did not rescue the phenotypes (**Fig. 2f-h**). This observation suggests that in the patient-derived lines, the genetic background is contributing significantly to the phenotypes. Altogether, these results show that both the LRRK2-G2019S mutation itself, introduced into the healthy background, as well as the patient genetic background can reduce proliferation and increase cell death in human NESCs. This observation further highlights the complexity of the PD-specific phenotypes and their underlying causes.

Stratification of LRRK2-G2019S dependent and independent phenotypes

To investigate whether the observed phenotypes are LRRK2-G2019S- or genetic background-dependent, we repeated the proliferation and cell death assays in the presence of the LRRK2 kinase inhibitor CZC-25146[42]. Previously, CZC-25146 was shown to rescue LRRK2-G2019S induced apoptosis in DNs[42]. In PD patient-derived NESCs, however, increased cell death and decreased mitosis were not

rescued by inhibiting LRRK2-kinase activity, suggesting that these changes are not induced by modified LRRK2 functionality (**Fig. 3a**, **b**). This observation is in agreement with the previous finding that the gene-correction of LRRK2-G2019S was not sufficient to rescue these phenotypes (**Fig. 2f-h**) and further emphasizes the important contribution of the genetic background. Moreover, inhibiting LRRK2 in patient compared to gene-corrected cells had as expected no effect (**Suplementary Fig. 5** and **Table 1**). In contrast, both LRRK2-G2019S-dependent increased cell death and reduced mitosis, caused by the introduction of the LRRK2-G2019S mutation into healthy NESCs, can be rescued by treatment with CZC-25146 (**Fig. 2a**, **c**).

Identification of potential susceptibility factors in the patient's genetic background

Based on the observation that cellular phenotypes depend on the information carried by the patient's genetic background, we aimed at identifing responsible genes. For this purpose, we performed a gene expression analysis via whole transcriptome microarray profiling. The obtained microarray data confirmed that deregulation of the hNESC transcriptome is mainly influenced by the patient's genetic background. Differential expression analysis using the RankProduct approach[43] identified only two shared significantly differentially expressed genes (DEGs) across all compared conditions (estimated percentage of false positive predictions ≤ 0.05) (**Fig. 4a** and **Supplementary Table 2**). These comparisons include Healthy vs. Patients (H vs. P); Healthy vs. Healthy with introduced LRRK2-G2019S mutation (H vs. HG2019S) and Patients vs. Patients after correction of the LRRK2-G2019S mutation (P vs. PGC). This observation suggests a limited contribution of LRRK2-G2019S alone to changes in gene expression. Furthermore, a meta-analysis[44] of both isogenic groups (H vs HG2019S and P vs PGC) revealed only 63 significant DEGs upon insertion of the mutation and 69 DEGs upon gene correction (**Fig. 4a**). To investigate which genes could act as possible genetic modifiers accounting for the patients' genetic background-dependent phenotypes, we evaluated differential gene expression between healthy and patient lines. We identified 865 DEGs (**Fig. 4a**). The top 75 most significant candidates are represented in a heat map (**Fig. 4b**). Interestingly, we found 3 genes that have been linked to PD before; ADP ribosylation factor-like GTPase 17a and b *(ARL17a*, *ARL17b)* and coiled-coil-helix-coiled-coil-helix

domain containing 2 (*CHCHD2)* (**Fig. 4c**). Moreover, an enrichment analysis for functions and diseases was performed using Ingenuity Pathway Analysis. Strikingly, this pathway analysis strongly highlighted several development processes as significantly altered between healthy and patient lines (**Fig. 4d**). Notably, both isogenic groups (H vs HG2019S and P vs PGC) shared common genes with healthy versus patients (H vs P) comparisons, indicating that LRRK2-G2019S has a context-specific influence on the differences in gene expression between healthy and patient lines (**Fig. 4a** and **Supplementary Table 2**). For instance, homeobox B1 (*HOXB1)*, one of the identified genes involved in neural development, was differentially expressed between healthy and patient-derived lines, and gene correction rescued its expression in the context of the patient-specific background (**Fig. 4f**). Furthermore, upon insertion of the mutation, similar functions as between healthy individuals and patients were enriched (**Fig. 4e**). Finally, we identified novel candidate genes from the top 75 most significant DEGs that were involved in pathways potentially relevant for PD, where they may act as the sought-after genetic modifiers (**Fig. 4g**). Among these genes we consider serine racemase (*SRR*), dnaJ heat shock protein family member C15 (*DNAJC15*) and glutathione peroxidase 7 (*GPX7)* as the most promising candidates (**Fig. 4g**).

Serine metabolism is deregulated in LRRK2-G2019S patients and patient cell lines

From the DEGs, SRR qualified as a major genetic modifier candidate for PD, because serine metabolism has previously been described in several neurodegenerative diseases[45–47]. Additionally, SRR was previously shown to act as a regulator of apoptosis and necrosis, and its product D-serine (**Fig. 5b**) induces proliferation, migration, and differentiation of neural stem cells[48,49]. Thus, deregulation of serine metabolism in patient-derived lines might contribute to the observed cellular phenotypes. RT-qPCR for *SRR* validated the reduced expression in patient cell lines (**Fig. 5a**). As SRR catalyzes the conversion between L-serine and D-serine, we investigated intracellular levels of L-serine in the NESC cultures (**Fig. 5b**, **c**). Consistent with the reduced SRR expression, the patient lines showed increased levels of L-serine compared to the healthy lines (**Fig. 5c**). Interestingly, the most decreased amino acid in patients was phospho-serine, the precursor metabolite of serine (**Fig. 5c**). To further investigate the importance of serine metabolism in PD, we analysed the serine levels in the blood plasma of 25 healthy

individuals, 25 idiopathic PD patients, and 5 PD patients with the LRRK2-G2019S mutation. (**Fig. 5d**). Interestingly, we observed that LRRK2-G2019S carriers indeed showed increased blood serine levels compared to healthy individuals. Striklingly, this difference was not seen in idiopathic PD patients (**Fig. 5d**).

D-serine, the enzymatic product of SRR, rescues LRRK2-G2019S-independent and -dependent phenotypes

We hypothesized that the reduced levels of SRR lead to increased levels of serine and a deficiency in the conversion to D-serine (**Fig. 5b**). Based on the described function of D-serine in neural stem cells, we further hypothesized that the deficiency in D-serine production might contribute to the observed cellular phenotypes, and consequently, the effects may be rescued through treatment with D-serine. Indeed, treatment with 100 µM D-serine led to the complete rescue of the proliferation and cell death phenotypes in PD patient-derived cells (**Fig. 6a**, **b** and **Supplementary Fig. 5** and **Supplementary Table 1**). Interestingly, this rescue is specific for the neural stem cell-related phenotypes. No rescue of the neuronal phenotypes was achievable through D-serine treatment (**Supplementary Fig. 4**). Furthermore, on the stem cell level, not only the phenotypes in patient-derived cells, but also the ones resulting from the insertion of the LRRK2-G2019S mutation into healthy cells were rescued by D-serine treatment (**Fig. 6a**, **c**). Based on these results, we propose that D-serine supplementation or treatment with SRR activators might have therapeutic applications in PD.

DISCUSSION

iPSC-derived patient specific lines with their isogenic controls are state-of-the-art *in vitro* models to study neurodegenerative diseases. Importantly, iPSC technology has opened up the possibility to recapitulate physiologically relevant patient-specific changes in neural cells without ethical objections[50]. Moreover, as PD-associated phenotypes are susceptible to genetic background variations, the use of gene-edited isogenic control lines enables accounting for individual genetic differences

between patients[10,38]. In this study, the use of iPSC-derived neuroepithelial stem cells allowed us to investigate the role of the PD-associated LRRK2-G2019S mutation and the contribution of the patient's genetic background in neural development.

We first conclusively showed that our disease model can indeed recapitulate well-established neuronal phenotypes induced by LRRK2-G2019S, as described in the literature[27]. Thus, we were able to reproduce in neurons patient specific, LRRK2-G2019S-dependent increases in cellular death and decreases in neurite complexity. The observation that α-SYN expression was increased in the patient neurons but not in a LRRK2-G2019S dependent manner might be due to the fact that we assessed general volumes of α-SYN, not specifically within TH-positive neurons. Nevertheless, the observed phenotypes prove the functionality of the here-used stem cell lines for *in vitro* disease modelling of PD.

With regards to our hypothesis that PD may have a developmental component, we have demonstrated that neuroepithelial stem cells derived from PD patients carrying the LRRK2-G2019S mutation already show significant alterations in cell death and proliferation. The phenotypes of increased cell death, and reduced mitosis, are both indicators of functionally relevant neural stem cell deregulations. Regarding the role of LRRK2 in NESCs, we showed that introducing LRRK2-G2019S into healthy lines is sufficient to induce the described neural stem cell phenotypes. Furthermore, inhibiting the kinase activity rescued the G2019S-induced phenotypes. This suggests that LRRK2 might indeed be necessary for maintaining the balance between self-renewal and cell death in NESCs. Additionally, correcting the LRRK2-G2019S mutation within patient-specific lines significantly decreased the expression of both disease-associated proteins aSYN and TAU, highlighting the role of LRRK2-G2019S in the context of the patient-specific background. Intriguingly, altered a-SYN and TAU protein expressions were the only phenotypes rescuable by gene correcting LRRK2-G2019S in NESCs in the patient-specific background. Furthermore, on the genetic level, we were able to identify only few significant DEGs underlying the LRRK2-G2019S dependent deregulations and only two of them were common between both isogenic

groups. The two shared genes were *LOC105377261* and *ROCK1P1*, a pseudogene, suggesting that, as shown before, LRRK2-G2019S alone has no major direct effects on gene expression[51].

By contrast, multiple sources of evidence, discussed below, suggest that in the physiologically relevant disease-associated model of patient-derived cell lines, the changes are highly dependent on the patient genetic background and less on the mutation itself. We demonstrated that gene-correction of G2019S as well as LRRK2 kinase inhibition were unable to rescue reduced proliferation and increased cell death. Importantly, we identified significant DEGs that may account for the genetic background-related phenotypes. *ARL17a* and *B* are involved in protein trafficking and represent known risk loci for PD and progressive supranuclear palsy[12,52–55]. Additionally, we identified several genes from the rab GTPases (*RAB32, RAB33a, RAB31, RAB9A* and *RAB38*) involved in endosomal protein trafficking, which most likely have major implications in LRRK2-G2019S induced PD pathogenesis[56,57]. Furthermore, *CHCHD2*, a mitochondrial nuclear retrograde regulator has been shown to cause autosomal dominant PD[58]. Interestingly, 4 of the top 75 candidates accounting for genetic differences of patient neural stem cells have already been identified in a transcriptome analysis before. *CHCHD2*, *NNAT*, *PTGR1* and *ID1* are together upregulated in iPSC derived DNs carrying the four PD causing mutations *SNCA*, *GBA*, *LRRK2*, and *PARK2* [59]. Together with our data this suggests that the patient genetic background plays an important role in the development of PD and that a single mutation is, at least in some cases, not sufficient to explain disease manifestation[59]. Furthermore, these results support the utility of neural stem cells to detect PD-relevant changes in gene expression.

Pathway analysis confirmed that developmental genes are altered between healthy and patient cell lines, corroborating a developmental contribution to PD. Enriched gene clusters regulating neural development, including components of the OCT family, HOX genes, PAX genes and of the NOTCH pathway were identified. Interestingly, significant alterations in *HOXB1* between patient and healthy individuals were rescued upon gene correction, making it an interesting target for future analysis.

Although proportionally, few genetic changes are LRRK2-G2019S dependent, a statistical meta-analysis[44] of the two inserted and the three gene-corrected cell lines identified 63 DEGs (FDR<0.05) upon insertion of the mutation and 69 DEGs (FDR<0.05) upon gene correction. Interestingly, genes that were differentially expressed upon insertion were again enriched in the functional annotations of cellular-, nervous system-, tissue-, embryonic- and organismal- development. Moreover, cellular growth and proliferation was one of the top significant enriched functions, possibly explaining the proliferation alteration observed upon G2019S insertion. The overlap between all three comparisons clearly shows that similar genes are modulated upon LRRK2-G2019S insertion or correction as between healthy and patient individuals. However, a clear context-specific separation of the LRRK-G2019S mutation within the healthy and the patient background could be observed, highlighting the strong contribution of the genetic background and necessity of isogenic controls in studies using patient derived samples. The context-dependent role of LRRK2-G2019S within the different genetic backgrounds emphasizes the complexity and heterogeneity of PD and suggests that background specific modifiers complement LRRK2-G2019S pathogenicity.

SRR represents a novel gene that might act as genetic modifier and has never been directly associated with PD before. D-serine, the enzymatic product of serine racemase, rescued the LRRK2-G2019S-independent but also dependent deregulations in patient stem cells. Interestingly, no effect was observed on neuronal phenotypes, highlighting that in our *in vitro* model deficiencies in D-serine are stem cell-specific. However, in a previous meta-analysis of *post mortem* transcriptomics data from the *SNpc* brain region of PD patients and unaffected controls, SRR was also identified to be significantly reduced in PD[60]. This result is in agreement with results from patient's blood plasma, where we observe an increase in serine levels in the LRRK2-G2019S carriers. The decrease in SRR expression most probably leads to an accumulation in intracellular serine levels as observed in affected NESCs, which potentially leads to increased secretion into the medium *in vitro* or the blood stream *in vivo*. Interestingly, idiopathic PD cases did not show differences in serine levels, highlighting that there must be an interplay between the PD patient background-related impairment in serine metabolism and the LRRK2-G2019S

mutation. This indicates that a deficiency in D-serine, due to impaired serine conversion, might lead to neurological dysfunctions. The data presented here suggest the potential value of D-serine as a complementary treatment for PD and its use as an early preventive strategy. Consistent with this, SRR was shown to promote neuronal stem cell proliferation and differentiation by acting on NMDAR and Ca+ regulation, as well as through ERK1/2-CREB and GSK-3b signalling[49]. Interestingly, deregulation of ERK1/2 dependent pathways has been described before in iPSC-derived DNs[27].

Overall, this study highlights the importance of selecting the appropriate model to study PD and demonstrates the influence of the highly variable patient genetic background on PD pathogenesis. The similar phenotypes observed by both SRR decrease and LRRK2-G2019S introduction might be explained by the nature of the phenotypes. Both proliferation and cell death are crucial characteristics of stem cell maintenance and as such might be influenced by a multitude of pathways. Furthermore, the fact that D-serine rescues not only the PD background-dependent phenotypes but also LRRK2-G2019S-induced differences indicates that LRRK2-G2019S contributes to the PD genetic background-induced phenotypes. The hypothesis that there must be an interplay between LRRK2-G2019S and serine metabolism is strenghtened by the fact that only LRRK2-G2019S carriers show increased serine blood plasma levels. A convergence into the same pathway or an interplay between LRRK2 and SRR cannot be excluded. Regardless of the causal factors, reduced proliferation and increased cell death of neural stem cells have significant consequences for *in vivo* neurogenesis. Moreover, in healthy lines, LRRK2-G2019S alone might be sufficient to cause PD-associated phenotypes *in vitro,* whereas several factors might be required for disease manifestation *in vivo*. Our study consolidates the idea that PD is a multi-variant polygenic disease where different genetic modifiers influence the phenotypes. The fact that LRRK2 alone is not responsible for the investigated NESC impairments, could have major implications on PD therapeutic strategies in G2019S carriers that currently mainly focus on inhibiting LRRK2 kinase activity. In this study, we demonstrate that serine racemase is a novel factor involved in the contribution of the patient genetic background to the LRRK2-G2019S induced pathogenesis. Its role as a potential

susceptibility factor for PD in patient neural stem cells suggests that SRR, and L/D-serine may serve as new therapeutic targets or potential biomarkers for early diagnosis.

Here, we show that the patient's genetic background has major implications in PD pathogenesis. We discover a developmental genetic modifier that acts as a susceptibility factor within the Parkinson's disease genetic background of neural stem cells and might predispose LRRK2-G2019S carriers to develop PD. Reduced expression of SRR, in combination with LRRK2-G2019S, contributes to PD-associated phenotypes. Furthermore, the results presented here might help to explain the incomplete penetrance and the variable age of onset and progression of LRRK2-G2019S carriers. Identifying a susceptibility factor in neural epithelial stem cells that can be used as a blood biomarker offers the potential for very early diagnosis, stratification, and treatment.

EXPERIMENTAL PROCEDURES

Generation of iPSCs and gene editing

iPSC reprogramming and gene editing details can be found in the Supplemental Experimental Procedures.

Neural stem cell derivation and culture

NESCs were generated by small molecule patterning[39]. Cells were cultured on Matrigel-coated plates in N2B27 (Neurobasal, DMEM-F12 (1:1), P/S, L-glutamine, B27 (1:100), N2 (1:200) (Invirogen)) freshly supplemented with 3 µM CHIR-99021 (Axon Medchem), 0.75 µM purmorphamine (Enzo Life Science) and 150 µM ascorbic acid (Sigma). Typically for maintenance cells were splitted 1:10 every 7 days using Accutase.

Neuronal differentiation

NESCs were seeded in duplicates at 10,000 cells into a Cell Carrier-96 Black, glass bottom plate from Perkin Elmer covered with Matrigel. Differentiation was initiated at day 2 after seeding by adding differentiation media consisting in N2B27 freshly supplemented with 10 ng/ml hBDNF (Peprotech), 10 ng/ml hGDNF (Peprotech), 500 µM dbcAMP (Peprotech), 200 µM ascorbic acid (Sigma), and 1 ng/ml TGF-β3 (Peprotech). Additionally, 1 µM purmorphamine (Enzo Life Science) was added for an additional 6 days. Cells were differentiated in total for 14 days.

Immunocytochemistry

Detailed protocol for Immunostaining by CC3, Hoechst, PH3, TH, TUJ1 and α-SYN can be found in the Supplementary Experimental Procedures.

Image analysis of NESC cultures

5-10 images per coverslip were collected using a Zeiss Confocal microscope. Images were converted into JPEG using ZEN lite (Zeiss) after best fit and gamma was set to 0.6 to reduce variabilities in single cell intensity. Nuclei counting of Hoechst staining was performed with Image J. Images were reduced

in size to 500 pixels, made binary and counted by ITCN plugin using the following settings width 13, minimum distance 26. CC3, pyknotic nuclei, and PH3 were hand counted.

High troughput image analysis of neuronal cultures

10 images were randomly acquired per well using Opera High Content Screening Microscope (Perkin Elmer). The custom image analysis algorithm developed in-house automates 3 key steps: mosaic stitching, segmentation of nuclei and TH positive neurons, and the analysis of neuronal branching in TH positive cells including the extraction of morphometric features (nodes and links). For nucleus segmentation, a foreground image was computed by convolving the raw Hoechst channel with a gaussian filter of size 10 and standard deviation 2. For the background image, a gaussian filter of size 60 and standard deviation 20 was used. The difference was computed by subtracting the background from the foreground. To identify pyknotic nuclei based on their fluorescence intensity, the raw Hoechst channel was preprocessed via average filtering with a square shaped structuring element of side length 5. Pixels with values above 400 were classified as pyknotic nuclei pixels. For the segmentation of DNs, the raw TH channel was convolved with a gaussian filter of size 10 and standard deviation 1. For refining the mask, connected components with less than 100 pixels were removed. To leverage the morphometric analysis of DNs, the surface of the 3D TH mask was defined via erosion of the TH mask with a structuring element corresponding to a pixel and its 6 connected neighborhood. Skeletonization of the TH mask has been performed using established methods (Kerschnitzky et al., 27624977) which allowed us to identify nodes and links.

Statistical analysis of NESC cultures

For immunocytochemistry, the number of CC3- and PH3- positive cells as well as the number of pyknotic nuclei were normalized to the total amount of cells (Hoechst). For H-P comparisons the percentage of the healthy control lines, as shown in **Table 1**, was set to 1. Each bar represents 6 cell lines with 3 biological replicates. Data is represented as Mean ± SEM. GRUBB's outlier test with α=0.1 followed by a Student's t-test have been performed on raw data. For isogenic comparisons, cell lines were

normalized within isogenic controls. The percentage of the healthy and gene-corrected lines, as shown in **Table 1**, was set to 1. For healthy and patient gene-edited lines, each bar represents 3 cell lines with 3 biological replicates. Data is represented as Mean ± SEM. One-sample t-test and GRUBB's outlier test with α=0.1 were performed on normalized data.

Statistical analysis of neuronal cultures

For neuronal cultures, the volume of pyknosis and the volume synuclein were normalized to the total volume of cells (Hoechst). For H-P comparisons the healthy control lines were set to 1. Each bar represents 6 cell lines with 4 biological replicates. Within replicates each experiment was normalized to H1 to account for inter plate variabilities. Data is represented as Mean ± SEM. GRUBB's outlier test with α=0.1 followed by a Student's t-test has been performed on raw data. For isogenic comparisons, cell lines were normalized within isogenic controls. Healthy and gene corrected lines were set to 1. For WT lines, each bar represents 6 cell lines (3H and 3PGC) with 4 biological replicates. For G2019S lines, each bar represents 6 cell lines (3P and 3HG2019S) with 4 biological replicates. Data is represented as Mean ± SEM. One-sample t-test and GRUBB's outlier test with α=0.1 were performed on normalized data.

For neuronal complexity the volume of nodes and links of TH-positive neurons were normalized to the total volume of TH. For H-P comparisons, the healthy control lines were set to 1. Each bar represents the total number of nodes and links for 6 cell lines with 4 biological replicates. Within replicates, each experiment was normalized to H1 to account for inter-plate variabilities. Data is represented as Mean ± SEM. Iterative GRUBB's outlier test with α=0.1 followed by a t-test have been performed on raw data. For isogenic comparisons, cell lines were normalized within isogenic controls. Healthy and gene corrected lines were set to 1. For WT lines, each bar represents 6 cell lines (3H and 3PGC) with 4 biological replicates for both measurements nodes and links. For G2019S lines, each bar represents 6 cell lines (3P and 3HG2019S) with 4 biological replicates for both measurements nodes and links. Data

is represented as mean ± SEM. One-sample t-test and iterative GRUBB's outlier test with α=0.1 were performed on normalized data.

MTT colometric cell viability assay

Cells were seeded at 20,000 cells per 96 well in triplicates. 100 µl of fresh media with 0.5 mg/ml MTT salt (the tetrazolium salt MTT (3-(4,5-dimethylthiazol-2-yl)-2,5-diphenyl tetrazolium bromide) (Sigma) [61] were added for 3h at day 1, 3 and 6. Reaction was stopped by removing the media and disrupting cells in 100 µl in dimethy-sulfoxyde (DMSO) (Sigma). DMSO w/o cells was used as a blank. Optical density (OD) was measured at all three time points at 450 nm using a microplate reader.

Protein analysis

Protocols for protein extraction, of α-SYN and TAU Western blotting and analysis can be found in the Supplemental Experimental Procedures. For healthy versus patient comparison each bar represents 6 cell lines with 3 biological replicates; Mean ± SEM. *p<0.05 according to t-test, GRUBB's outlier test with α=0.1. For isogenic comparisons for the insertion of the mutation each bar represents 2 cell lines with 3 biological replicates and for the gene correction each bar represents 3 cell lines with 3 biological replicates; Mean ± SEM. *p<0.05 according to one-sample t-test, GRUBB's outlier test with α=0.1.

Chemical treatments

For LRRK2 inhibition, cells were treated one day after seeding with 0.5 µM CZC-25146 (Millipore) in DMSO for 5 days. Same amount of DMSO without Inhibitor was used as a control. For D-serine complementation cells wert treated 1 day after seeding for the following 5 days with 100 µm D-serine (Sigma). For neuronal cultures cells were treated directly after seeding with 100 µm D-serine for 16 days.

Microarray sample preparation and analysis

Cells were seeded at 150,000 cells per 12-well plate for 6 days. RNA was extracted after metabolite extraction. 3 interphases were combined, resuspended in Qiazol and extracted using miRNA easy kit following the manufacturer's instructions (Qiagen). Samples were processed with EMBL Genomics Core

Facility using Affymetrix Human Gene 2.0 arrays. The raw CEL-files were pre-processed using the GC-RMA procedure[62] and differential expression across the biological conditions of interest was analysed in the R statistical programming framework (R Development Core Team 2011) using the RankProduct method[43]. Heat map dendrograms were created using average linkage hierarchical clustering with the Euclidean distance metric. Differential expression meta-analyses across multiple comparisons of biological conditions were conducted using the weighted p-value combination approach by Marot et al. [44].

RT-qPCR

SRR microarray results were validated by RT-qPCR (Agilent AriaMx). cDNA was produced by the High-Capacity RNA-to-cDNA™ Kit (Invitrogen) using 0.5 µg RNA. TaqMan SRR primer probe set (Thermo Scientific) and TaqMan Gene Expression Master Mix (Thermo Scientific) was mixed with 1 µl of cDNA. The running protocol consisted in 2 min 50°C, 10 min 95°C, followed by 40x cycles of 15 s 95°C and 1 min 60°C.

Metabolite extractions and amino acid measurements

For metabolite extraction cells were seeded in technical triplicates at 200,000 cells per well on a 12-well plate. Polar metabolites were extracted using a liquid-liquid extraction protocol. First, cells were washed with 0.9% NaCl, then 200 µl methanol and 200 µl water were added. The cells were scraped and transferred into 200 µl chloroform. The mixture was vortexed and incubated for 20 min at 4°C, 1400 rpm (Eppendorf Thermomixer). Then, the mixture was centrifuged at 21,000 xg for 5 min and 4°C. 150 µl of the polar phase were transferred into a GC glass vial with micro insert. Solvents were evaporated in a rotary vacuum evaporator at -4°C until dry. The study has been performed according to the quality system of the Biomedical Metabolomics Facility Leiden[63], see supplementary material, and methods. For statistical analysis technical triplicates of each cell line underwent GRUBB's outlier test with α=0.1, followed by averaging technical triplicates of each cell line within biological replicates. An additional GRUBB's outlier test with α=0.1 was performed on the three biological replicates of each

cell line. A Students t-test was performed for each amino acid independently. No correction for multiple comparision was performed.

Blood plasma metabolite extraction, derivatization, GC-MS measurement, and data processing

Polar plasma metabolites were extracted using a liquid-liquid extraction protocol. First, 20 µl plasma were added to 100 µl methanol and 20 µl water. The water fraction contains three internal standards: 20 µg/ml U^{13c}-Ribitol (Omicron Biochemicals), 10 µg/ml Pentanedioic-d_6 acid (C/D/N Isotopes), and 20 µg/ml Tridecanoic-d_{25} acid (C/D/N Isotopes). After adding 50 µl chloroform, the monophasic mixture was vortexed and incubated for 5 min at 4°C and 1400 rpm (Eppendorf Thermomixer). For phase separation, 50 µl chloroform and 50 µl water were added and vortexed for 1 min. Then, the mixture was centrifuged at 21,000 xg for 5 min and 4°C. 140 µl of the polar phase were transferred into a GC glass vial with micro insert. Solvents were evaporated in a rotary vacuum evaporator at -4°C until dry. Derivatization and GC-MS analyses in full scan mode were carried out as described previously[64]. All GC-MS chromatograms were processed using the Metabolite Detector software, v3.020151231Ra[65]. The software package supports automatic deconvolution of all mass spectra. Compounds were annotated by retention time and mass spectrum. The data set was normalized by internal standards.

ACKNOWLEDGMENTS

The JCS lab is supported by the Fonds National de la Recherche (FNR) (CORE, C13/BM/5791363) and by a University Luxembourg Internal Research Project grant (MidNSCs). JW, JJ, and XQ are supported by fellowships from the FNR (AFR, Aides à la Formation-Recherche) and SN has a doctoral school position from the Doctoral School in Systems and Molecular Biomedicine of University of Luxembourg. This is an EU Joint Programme - Neurodegenerative Disease Research (JPND) project. Further support comes from the SysMedPD project which has received funding from the European Union's Horizon 2020 research and innovation programme under grant agreement No 668738. This project was supported by the LCSB pluripotent stem cell core facility and the LCSB metabolomics platform. We thank Xiangyi

Dong for her assistance in the laboratory. CK is supported by the DFG through FOR2488 (P1). We thank Prof. A. Schwambach from the University of Hannover for providing us with a reprogramming vector. We thank Thomas Palm and Peter Reinhardt for deriving hNESC. We thank the Wellcome Trust Sanger institute, its funders, collaborators and Life Tech limited for supporting us with cell lines. We thank Prof. Dr. Thomas Gasser from the Universitätsklinikum Tübingen, Prof. Dr. Hans R. Schöler from the Max-Planck-Gesellschaft and Dr. Jared Sterneckert from the CRTD for providing us with cell lines. We thank the NINDS repository for providing cell lines. We also thank the private donors who support our work at the LCSB. Microarrays were performed with EMBL GeneCore genomics core facility. We thank Aurélien Ginolhac for the preliminar microarray analysis. Bioinformatics analyses presented in this paper were carried out in part using the HPC facilities of the University of Luxembourg (see http://hpc.uni.lu). Amino acid measurements were performed at the LACDR, Analytical Biosciences, Leiden University.

AUTHOR CONTRIBUTIONS

S.L.N. cultured hNESC, performed and designed experiments, prepared the Fig.s and wrote the original draft. J.W., J.J. X.Q., and K.H. provided iPSCs and hNESCs. X.Q. gene edited iPSCs and derived hNESCs. J.W. and J.J. reprogrammed iPSC and derived hNESC. E.G. performed the microarray analysis, and prepared Fig.s. J.T performed immunostainings of neuronal cultures. P.A and S.B developed and ran the scripts for hightroughput analysis with the OPERA. C.J performed blood plasma metabolite extractions, GC-MS and analysed the data. A.H and T.H. performed amino acid measurements. C.S provided blood plasma. S.B, J.T, C.J. P.A, E.G, C.K, L.S, and T.S revised the manuscript. L.S and T.S helped to initiate the project, supervised it, and analysed results. J.C.S. conceived and supervised the project, designed the experiments and revised the manuscript.

REFERENCES

1. Spillantini, M. G. *et al.* Alpha-synuclein in Lewy bodies. *Nature* 388, 839–840 (1997).
2. Goedert, M., Spillantini, M. G., Del Tredici, K. & Braak, H. 100 years of Lewy pathology. *Nat Rev Neurol* 9, 13–24 (2013).
3. Tretiakoff. Contribution a L'étude de L'anatomie Pathologique de Locus Niger de Soemmerling. *Univ. Paris, Paris.* (1919).
4. Hasseler, R. Zur pathologie der paralysis agitans und des postencephalitschen Parkinsonismus. *J. Psychol. Neurol.* 48, 387–476 (1938).
5. Scherman, D. *et al.* Striatal dopamine deficiency in parkinson's disease: Role of aging. *Ann. Neurol.* 26, 551–557 (1989).
6. Le Grand, J. N., Gonzalez-Cano, L., Pavlou, M. A. & Schwamborn, J. C. Neural stem cells in Parkinson's disease: A role for neurogenesis defects in onset and progression. *Cell. Mol. Life Sci.* 72, 773–797 (2014).
7. Paus, M. *et al.* Enhanced dendritogenesis and axogenesis in hippocampal neuroblasts of LRRK2 knockout mice. *Brain Res.* 1497, 85–100 (2013).
8. Marxreiter, F., Regensburger, M. & Winkler, J. Adult neurogenesis in Parkinson's disease. *Cell. Mol. Life Sci.* 70, 459–73 (2013).
9. Winner, B., Kohl, Z. & Gage, F. H. Neurodegenerative disease and adult neurogenesis. *Eur. J. Neurosci.* 33, 1139–51 (2011).
10. Liu, G.-H. *et al.* Progressive degeneration of human neural stem cells caused by pathogenic LRRK2. *Nature* 491, 603–7 (2012).
11. Garcia-Reitboeck, P. *et al.* Endogenous alpha-synuclein influences the number of dopaminergic neurons in mouse substantia nigra. *Exp. Neurol.* 248, 541–545 (2013).
12. Nalls, M. A. *et al.* Genetic comorbidities in parkinson's disease. *Hum. Mol. Genet.* 23, 831–841 (2014).
13. Kitada, T. *et al.* Mutations in the parkin gene cause autosomal recessive juvenile parkinsonism. *Nature* 392, 605–608 (1998).
14. Köroğlu, Ç., Baysal, L., Cetinkaya, M., Karasoy, H. & Tolun, A. DNAJC6 is responsible for juvenile parkinsonism with phenotypic variability. *Park. Relat. Disord.* 19, 320–324 (2013).
15. Sánchez-Danés, A. *et al.* Disease-specific phenotypes in dopamine neurons from human iPS-based models of genetic and sporadic Parkinson's disease. *EMBO Mol. Med.* 4, 380–95 (2012).
16. Dick, F. D. *et al.* Environmental risk factors for Parkinson's disease and parkinsonism: the Geoparkinson study. *Occup. Environ. Med.* 64, 666–72 (2007).
17. Marras, C. *et al.* Motor and nonmotor heterogeneity of LRRK2-related and idiopathic Parkinson's disease. *Mov. Disord.* 31, 1192–1202 (2016).
18. Zimprich, A. *et al.* Mutations in LRRK2 cause autosomal-dominant parkinsonism with pleomorphic pathology. *Neuron* 44, 601–607 (2004).
19. Paisán-Ruíz, C. *et al.* Cloning of the gene containing mutations that cause PARK8-linked Parkinson's disease. *Neuron* 44, 595–600 (2004).
20. Healy, D. G. *et al.* Phenotype, genotype, and worldwide genetic penetrance of LRRK2-associated Parkinson's disease: a case-control study. *Lancet Neurol.* 7, 583–590 (2008).
21. Berg, D., Schweitzer, K. J. & Leitner, P, E. Al. Type and frequency of mutations in the LRRK2 gene

in familial and sporadic Parkinson's disease*. *Brain* 128, 3000–3011 (2005).

22. Cilia, R. *et al.* LRRK2 mutations in Parkinson's disease: Confirmation of a gender effect in the Italian population. *Park. Relat. Disord.* 20, 911–914 (2014).
23. Hentati, F. *et al.* LRRK2 parkinsonism in Tunisia and Norway: A comparative analysis of disease penetrance. *Neurology* 83, 568–569 (2014).
24. Ozelius, L. J. *et al.* LRRK2 G2019S as a cause of Parkinson's disease in Ashkenazi Jews. *N. Engl. J. Med.* 354, 424–425 (2006).
25. Golub, Y. *et al.* Genetic factors influencing age at onset in LRRK2-linked Parkinson disease. *Parkinsonism Relat. Disord.* 15, 539–541 (2009).
26. Botta-Orfila, T. *et al.* Age at onset in LRRK2-associated PD is modified by *SNCA* variants. *J. Mol. Neurosci.* 48, 245–247 (2012).
27. Reinhardt, P. *et al.* Genetic correction of a LRRK2 mutation in human iPSCs links parkinsonian neurodegeneration to ERK-dependent changes in gene expression. *Cell Stem Cell* 12, 354–67 (2013).
28. Trinh, J. & Farrer, M. Advances in the genetics of Parkinson disease. *Nat. Rev. Neurol.* 9, 445–54 (2013).
29. Gatto, E. M. *et al.* The LRRK2 G2019S mutation in a series of Argentinean patients with Parkinson's disease: Clinical and demographic characteristics. *Neurosci. Lett.* 537, 1–5 (2013).
30. Lesage, S. *et al. LRRK2* G2019S as a Cause of Parkinson's Disease in North African Arabs. *N. Engl. J. Med.* 354, 422–423 (2006).
31. Wallings, R., Manzoni, C. & Bandopadhyay, R. Cellular processes associated with LRRK2 function and dysfunction. *FEBS J.* 282, 2806–2826 (2015).
32. Winner, B. *et al.* Adult neurogenesis and neurite outgrowth are impaired in LRRK2 G2019S mice. *Neurobiol. Dis.* 41, 706–16 (2011).
33. Bahnassawy, L. *et al.* The parkinson's disease-associated LRRK2 mutation R1441G inhibits neuronal differentiation of neural stem cells. *Stem Cells Dev.* 22, 2487–96 (2013).
34. Schulz, C. *et al.* Leucine-rich repeat kinase 2 modulates retinoic acid-induced neuronal differentiation of murine embryonic stem cells. *PLoS One* 6, e20820 (2011).
35. Milosevic, J. *et al.* Emerging role of LRRK2 in human neural progenitor cell cycle progression, survival and differentiation. *Mol. Neurodegener.* 4, 25 (2009).
36. Gonzalez-cano, L., Menzl, I., Tisserand, J., Nicklas, S. & Jens, C. Parkinson ' s disease associated mutant LRRK2 mediated inhibition of miRNA activity is antagonized by TRIM32 .
37. Zechel, S., Meinhardt, A., Unsicker, K. & von Bohlen und Halbach, O. Expression of leucine-rich-repeat-kinase 2 (LRRK2) during embryonic development. *Int. J. Dev. Neurosci.* 28, 391–399 (2010).
38. Soldner, F. *et al.* Generation of Isogenic Pluripotent Stem Cells Differing Exclusively at Two Early Onset Parkinson Point Mutations. *Cell* 146, 318–331 (2011).
39. Reinhardt, P. *et al.* Derivation and expansion using only small molecules of human neural progenitors for neurodegenerative disease modeling. *PLoS One* 8, e59252 (2013).
40. Polymeropoulos, M. H. *et al.* Mutation in the α-Synuclein Gene Identified in Families with Parkinson's Disease Mutation in the α-Synuclein Gene Identified in Families with Parkinson's Disease. *Science (80-.).* 276, 2045–2047 (1997).
41. Wszolek, Z. K. *et al.* Autosomal dominant parkinsonism associated with variable synuclein and tau pathology. *Neurology* 62, 1619–1622 (2004).

42. Ramsden N, Perrin J, Ren Z, Lee BD, Zinn N, Dawson VL, Tam D, Bova M, Lang M, Drewes G, Bantscheff M, Bard F, Dawson TM, H. C. Chemoproteomics-based design of potent LRRK2-selective lead compounds that attenuate Parkinson's disease-related toxicity in human neurons. *ACS Chem. Biol.* 6, 1021–1028 (2011).

43. Breitling, R., Armengaud, P., Amtmann, A. & Herzyk, P. Rank products: A simple, yet powerful, new method to detect differentially regulated genes in replicated microarray experiments. *FEBS Lett.* 573, 83–92 (2004).

44. Marot, G., Foulley, J. L., Mayer, C. D. & Jaffrézic, F. Moderated effect size and P-value combinations for microarray meta-analyses. *Bioinformatics* 25, 2692–2699 (2009).

45. Sasabe, J. *et al.* D-serine is a key determinant of glutamate toxicity in amyotrophic lateral sclerosis. *EMBO J.* 26, 4149–59 (2007).

46. Fujii, K. *et al.* Serine racemase binds to PICK1: potential relevance to schizophrenia. *Mol. Psychiatry* 11, 150–7 (2006).

47. Morita, Y. *et al.* A Genetic Variant of the Serine Racemase Gene Is Associated with schizophrenia. *Biol. Psychiatry* 61, 1200–1203 (2007).

48. Canu, N., Ciotti, M. T. & Pollegioni, L. Serine racemase: A key player in apoptosis and necrosis. *Front. Synaptic Neurosci.* 6, 1–15 (2014).

49. Huang, X. *et al.* D-Serine regulates proliferation and neuronal differentiation of neural stem cells from postnatal mouse forebrain. *CNS Neurosci. Ther.* 18, 4–13 (2012).

50. Takahashi, K. & Yamanaka, S. Induction of Pluripotent Stem Cells from Mouse Embryonic and Adult Fibroblast Cultures by Defined Factors. *Cell* 126, 663–676 (2006).

51. Devine, M. J. *et al.* Pathogenic LRRK2 mutations do not alter gene expression in cell model systems or human brain tissue. *PLoS One* 6, e22489 (2011).

52. Allen, M. *et al.* Gene expression, methylation and neuropathology correlations at progressive supranuclear palsy risk loci. *Acta Neuropathol.* 132, 1–15 (2016).

53. Chai, C. & Lim, K.-L. Genetic insights into sporadic Parkinson's disease pathogenesis. *Curr. Genomics* 14, 486–501 (2013).

54. Höglinger, G. U. *et al.* Identification of common variants influencing risk of the tauopathy progressive supranuclear palsy. *Nat. Genet.* 43, 699–705 (2011).

55. Latourelle, J. C., Dumitriu, A., Hadzi, T. C., Beach, T. G. & Myers, R. H. Evaluation of Parkinson Disease Risk Variants as Expression-QTLs. *PLoS One* 7, (2012).

56. Steger, M. *et al.* Phosphoproteomics reveals that Parkinson's disease kinase LRRK2 regulates a subset of Rab GTPases. *Elife* 5, (2016).

57. Waschbüsch, D. *et al.* LRRK2 transport is regulated by its novel interacting partner Rab32. *PLoS One* 9, (2014).

58. Funayama, M. *et al.* CHCHD2 mutations in autosomal dominant late-onset Parkinson's disease: A genome-wide linkage and sequencing study. *Lancet Neurol.* 14, 274–282 (2015).

59. Momcilovic, O. *et al.* Derivation, characterization, and neural differentiation of integration-free induced pluripotent stem cell lines from Parkinson's disease patients carrying *SNCA*, LRRK2, PARK2, and GBA mutations. *PLoS One* 11, 1–26 (2016).

60. Glaab, E. & Schneider, R. Comparative pathway and network analysis of brain transcriptome changes during adult aging and in Parkinson's disease. *Neurobiol. Dis.* 74, 1–13 (2015).

61. Mosmann, T. Rapid colorimetric assay for cellular growth and survival: Application to proliferation and cytotoxicity assays. *J. Immunol. Methods* 65, 55–63 (1983).

62. WU, Z. & IRIZARRY, R. A. Stochastic Models Inspired by Hybridization Theory for Short Oligonucleotide Arrays ZHIJIN. *J. Comput. Biol.* 12, 882–893 (2005).

63. Noga, M. J. *et al.* Metabolomics of cerebrospinal fluid reveals changes in the central nervous system metabolism in a rat model of multiple sclerosis. *Metabolomics* 8, 253–263 (2012).

64. Jäger, C., Hiller, K. & Manuel, B. Metabolic Profiling and Quantification of Neurotransmitters in Mouse Brain by Gas Chromatography-Mass Spectrometry. *Curr. Protoc. Mouse Biol.* 333–342 (2016).

65. Hiller, K. *et al.* MetaboliteDetector: comprehensive analysis tool for targeted and nontargeted GC/MS based metabolome analysis. *Anal. Chem.* 81, 3429–3439 (2009).

FIGURE LEGENDS

Fig. 1. The *in vitro* disease model recapitulates well established phenotypes in neuronal cultures carrying LRRK2-G2019S.

(**a**) Summary of cell lines: information about age of sampling and sex (F or M) of the patients (P) and healthy donors (H) as well as the source of the cell line. (**b**, **c**) Quality controls. (**b**) Representative images of stem cell protein expression NESTIN and SOX2 and neuroectoderm marker expression PAX6 and SOX1 for quality control of hNESCs. Hoechst was used for nuclei staining. (**c**) Representative images of hNESC genotyping. Cell lines were sequenced for the LRRK2-G2019S heterozygous point mutation G>A. (**d-f**) Neuronal differentiation potential and phenotyping. (**d**) Representative images of neuronal cultures, stained with ß-tubulin3 (TUJ1), tyroxine hydroxylase (TH) and α-SYN. Neurons derived from patients show significantly more pyknotic nuclei, increased α-SYN levels as neurons derived from healthy donors, N=6, n=4, (**d**, **e**). Furthermore patient dopaminergic neurons (TH+) show lower complexity (nodes and links) compared to healthy individuals, N=6, n=8 (**d**, **f**). (**e**, **f**) Quantification of (**d**). Data is represented as Mean ± SEM. *p≤0.05, **p≤0.01 according to t-test, (iterative) GRUBB's outlier test α=0.1. (**c**) The phenotypes are LRRK2-G2019S dependent. Data is represented as Mean ± SEM. *p≤0.05 according to t-test, (iterative) GRUBB's outlier test with α=0.1.

Fig. 2. Phenotypes in patient compared to healthy hNESCs and their respective isogenic controls.

(**a**, **b**) Patient lines have increased α-SYN and TAU protein levels compared to their gene-corrected counterparts. Representative Western blot images and quantification for the 17 given cell lines for α-SYN and TAU. Protein levels were normalized to ponceau red. (**c**) Representative immunofluorescent images of patient compared to healthy individuals. Patient-derived hNESCs show decreased mitosis (phospho-histone3) and increased cell death, pyknosis (white stars) and apoptosis (cleaved caspase3). (**d**) The growth curve of hNESCs was determined by MTT assay after 1, 3 and 6 days. Each bar represents 6 cell lines with 5 biological replicates. Data is represented as Mean ± SEM. *p≤0.05 according to 2-way

ANOVA, GRUBB's outlier test with α=0.1. (**e**) Quantification of (**c**). Data is represented as Mean ± SEM. *p≤0.05 according to t-test, GRUBB's outlier test with α=0.1 N=6, n=3.

(**f**) Representative immunofluorescent images of mutagenized healthy hNESCs. Introduction of LRRK2-G2019S into healthy cell lines is sufficient to induce the patient-specific phenotypes such as an increase in pyknosis (Hoechst), apoptosis (CC3) and a reduction in mitosis (PH3), whereas gene correcting LRRK2-G2019S within the PD patient related genetic background is unable to rescue the observed phenotypes. (**g**) Quantification of (**f**). Data is represented as Mean ± SEM. *p≤0.05, **p≤0.01, ***p≤0.001, according to one-sample t-test, GRUBB's outlier test α=0.1, N=3, n=3. (**h**) The growth curve of hNESCs was determined by MTT assay after 1, 3, and 6 days. For healthy lines each bar represents 2 cell lines with 3 biological replicates. For patient lines each bar represents 3 cell lines with 5 biological replicates; Mean ± SEM. *p<0.05 according to 2-way RM-ANOVA followed by Sidak's multiple comparison.

See also **Supplementary Table 1** and **Supplementary Fig. 5**.

Fig. 3. LRRK2 inhibition rescues LRRK2 dependent phenotypes but not the patient genetic background related differences.

(**a**) Representative immunofluorescent images of hNESCs stained with Hoechst, PH3, and CC3 after treatment with 0.5 µM LRRK2 kinase inhibitor CZC-25146 in DMSO. (**b**) Quantification of (**a**). Inhibition of LRRK2-G2019S is not rescuing cell death or reduced mitosis in patient cell lines. (**c**) Quantification of (**a**). The mutation-induced phenotype in healthy lines, however, can be rescued by inhibiting LRRK2. For isogenic healthy lines each bar represents 3 cell lines with 3-4 biological replicates; Mean ± SEM. *p≤0.05, **p≤0.01, *** p≤0.001 according to one-sample t-test, GRUBB's outlier test with α=0.1.

See also **Supplementary Table 1** and **Supplementary Fig. 5**.

Fig. 4. Identification of genes deregulated in LRRK2-G2019S carriers that might act as susceptibility factors within the patient genetic background to contribute to the observed phenotypes.

(**a**) Venn Diagramm showing overlap of DEGs between all three comparisons (H vs P, H vs HG2019S and P vs PGC). Comparisons are based on Rank Product differential expression analysis, FDR≤0.05. (**b**)

Heatmap of top 75 DEGs between H vs P comparison, RankProduct differential expression analysis, FDR≤0.05. (**c**) DEGs previously associated with PD, Rank Product differential expression analysis, FDR≤0.05. Each dot represents one cell line out of 3 biological replicates. (**d**) Developmental gene *HOXB1* in H vs P and P vs PGC. RankProduct differential expression analysis, FDR<0.05. (**e**) Top 6 enriched functions between H vs P and H vs HG2019S from gene enriched analysis (Inguenity Pathway analysis) of RankProduct differential expression analysis, FDR≤0.05. (**f**) Differentially expressed target genes from top 75 candidates that qualify as genetic modifiers. RankProduct differential expression analysis, FDR≤0.05. Each dot represents one cell line out of 3 biological replicates. Red dots represent gene edited lines where the mutation has been introduced (H plot) or gene corrected (P plot) that cluster with their respective genetic background.

See also **Supplementary Table 2.**

Fig. 5. Serine metabolism is deregulated in the LRRK2-G2019S patient genetic background.

(**a**) Validation of *SRR* expression by RT-qPCR. The healthy lines were set to 1. Each bar represents 6 cell lines with 3 biological replicates; Mean ± SEM. *p≤0.05 according to Student's t-test. (**b**) SRR converts L-serine to D-serine. (**c**) Intracellular metabolite levels of hNESCs show increased serine levels in patients compared to healthy individuals. Each bar represents 6 cell lines with 3 biological replicates; log fold change of mean ± SEM. *p≤0.053 according to t-test, no multiple comparison. GRUBB's oulier test was performed within each of the three technical replicates and on the 3 biological replicates for each cell line α=0.1. (**d**) Serine levels in patient blood plasma are increased in LRRK2-G2019S carriers compared to healthy individuals and idiopathic PD cases. Mean ± SEM. *p≤0.0532 according to t-test, GRUBB's oulier test with α=0.1.

Fig. 6. D-serine treatment is rescuing LRRK2-G2019S dependent and independent phenotypes.

(**a**) Representative immunofluorescent images of hNESCs stained with Hoechst, phospho-histone3, and cleaved caspase3 after treatment with 100 µM D-serine for 6 days. (**b**) Quantification of (**a**). D-serine rescues cell death and mitosis in patient cell lines; Mean ± SEM. *p<0.05 according to t-test, GRUBB's

outlier test α=0.1. (**c**) Quantification of (**a**). D-serine rescues cell death and mitosis in LRRK2-G2019S mutagenized cell lines; Mean ± SEM. *p<0.05 according to one-sample t-test, GRUBB's outlier test with α=0.1. For CC3 each bar represents 2 cell lines with 4 biological replicates.

See also **Supplementary Fig. 4** and **5** and **Supplementary Table 1.**

FIGURES

a

Healthy (WT)	Isogenic CTRLs	Age of sampling	Sex	References
H1	H1G2019S	81	F	iPSCs Reinhardt et al., 2013
H3	H3G2019S	46	M	iPSCs BOBSC-T6/8_B1 Cambridge
H2	---	53	F	iPSCs Reinhardt et al., 2013
H4	---	55	M	iPSCs Coriell GM23338
H5	---	68	F	FB Coriell ND34769
H6	---	Cord	F	iPSCs Gibco A13777
H6.1	H6.1G2019S	Cord	F	iPSCs Gibco A13777

Patients (G2019S)	Isogenic CTRLs	Age of sampling	Sex	References
P1	P1GC	81	F	iPSCs Reinhardt et al., 2013
P1.1	P1.1GC	81	F	iPSCs Reinhardt et al., 2013
P2	P2GC	54	F	iPSCs Reinhardt et al., 2013
P4*	---	79	M	iPSCs Coriell ND35367
P5	---	66	F	FB Coriell ND33879
P6	---	51	F	FB Gasser Lab

*homozygous

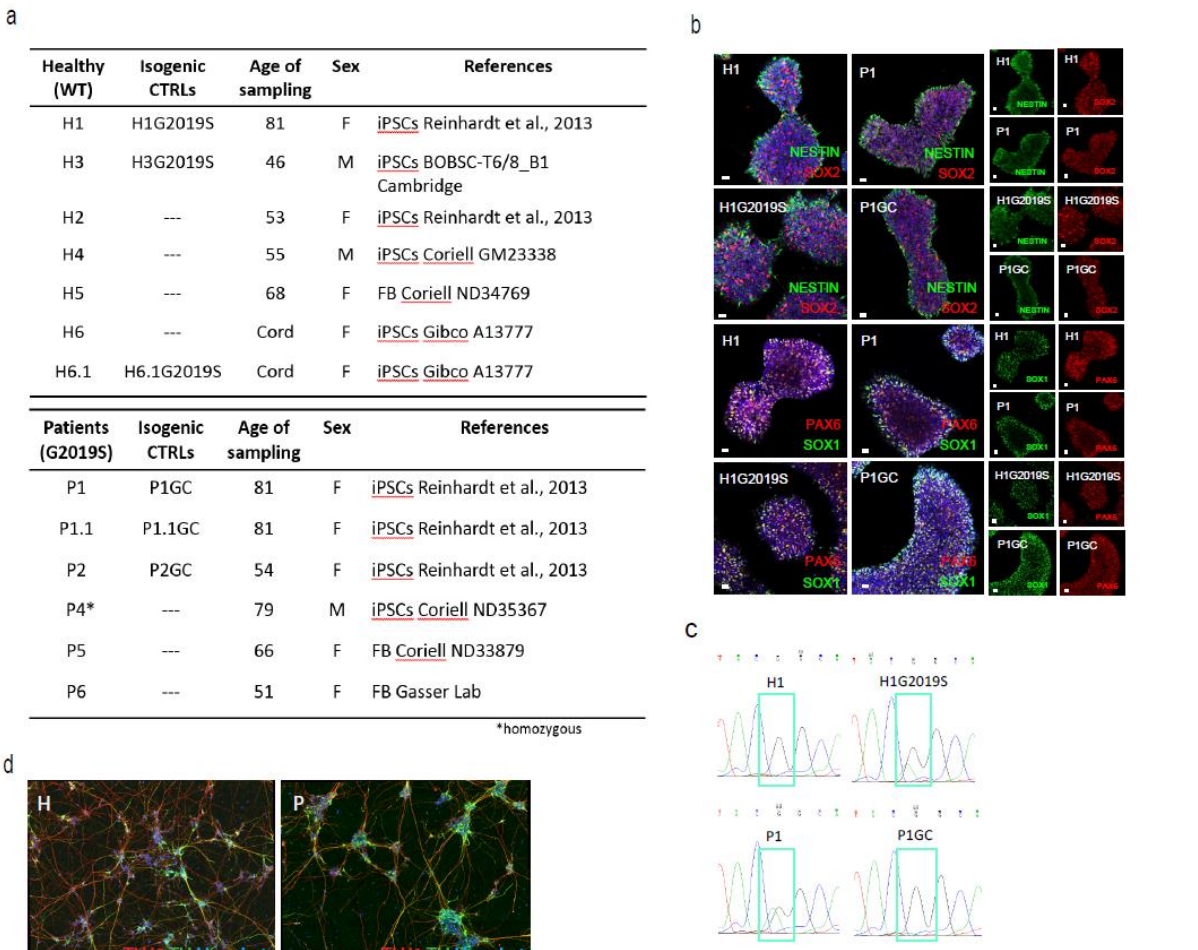

Figure 1 Model implementation

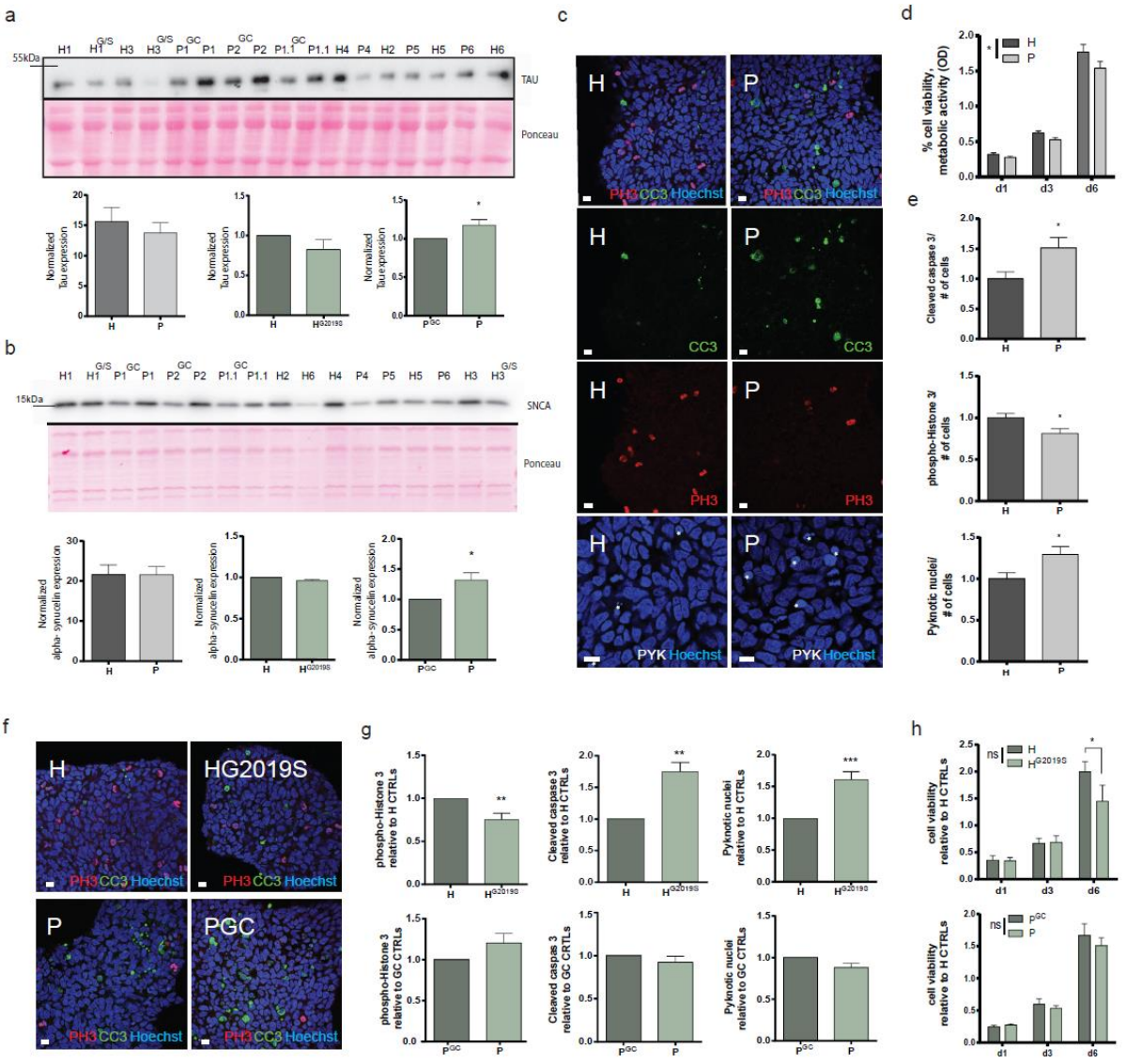

Figure 2 Phenotypes in hNESCs

a

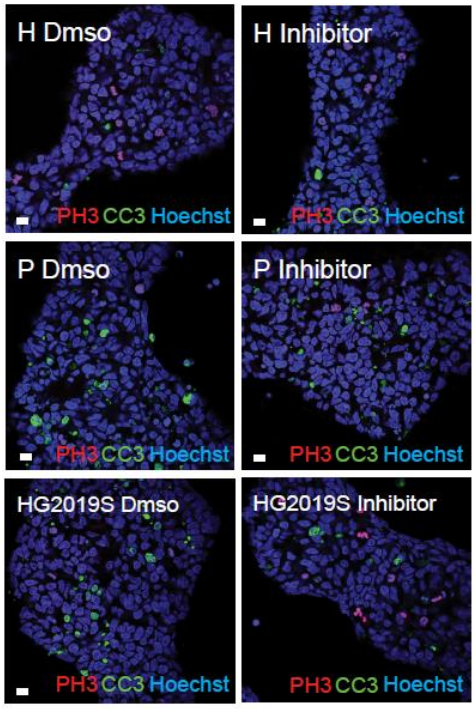

b

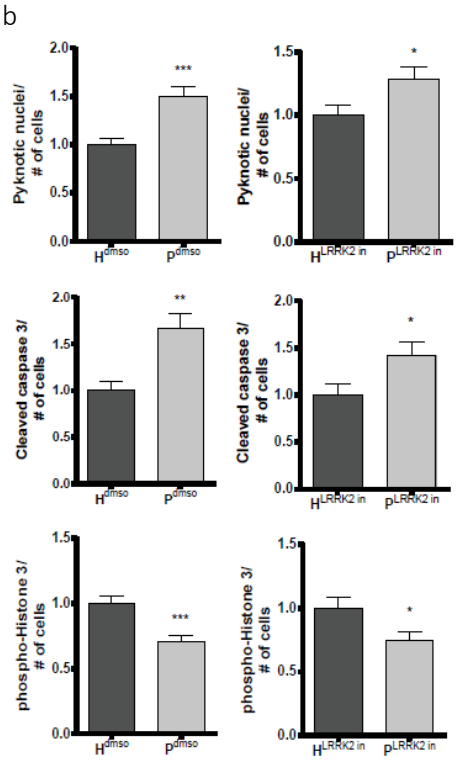

c

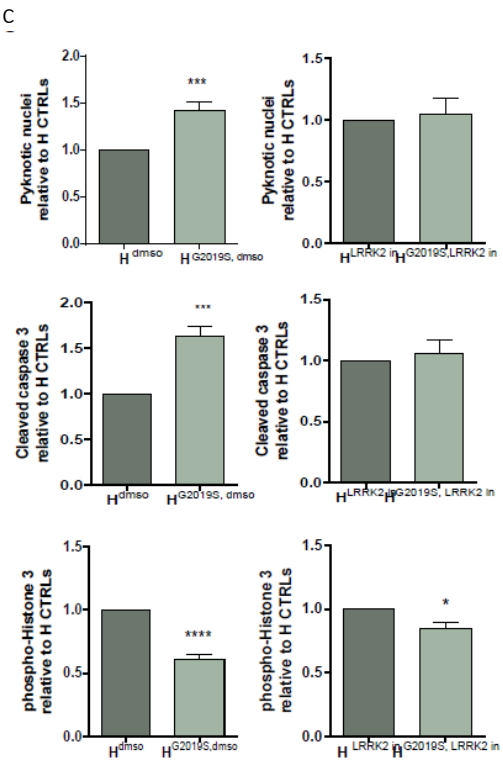

Figure 3. LRRK2 kinase Inhibitor

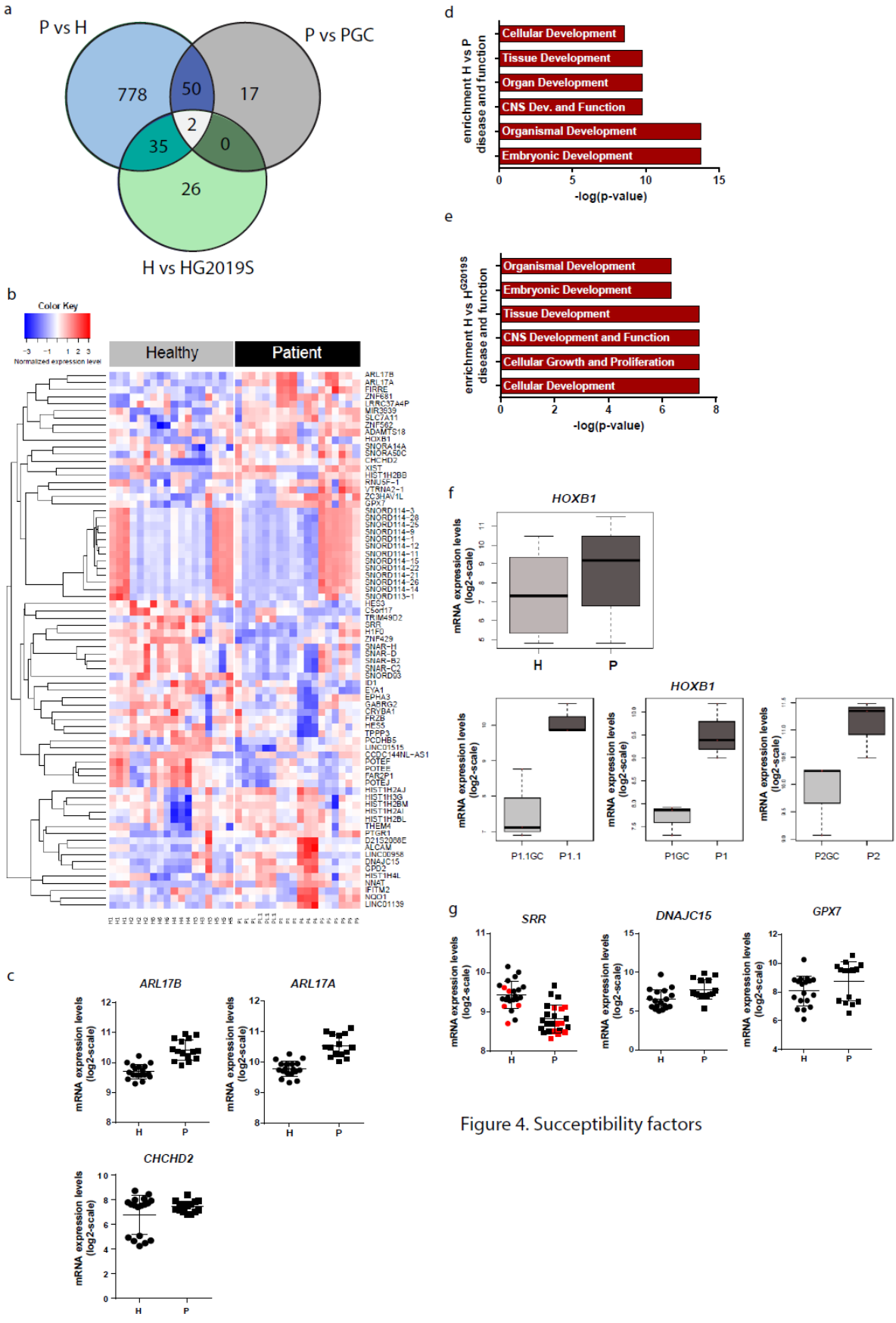

Figure 4. Succeptibility factors

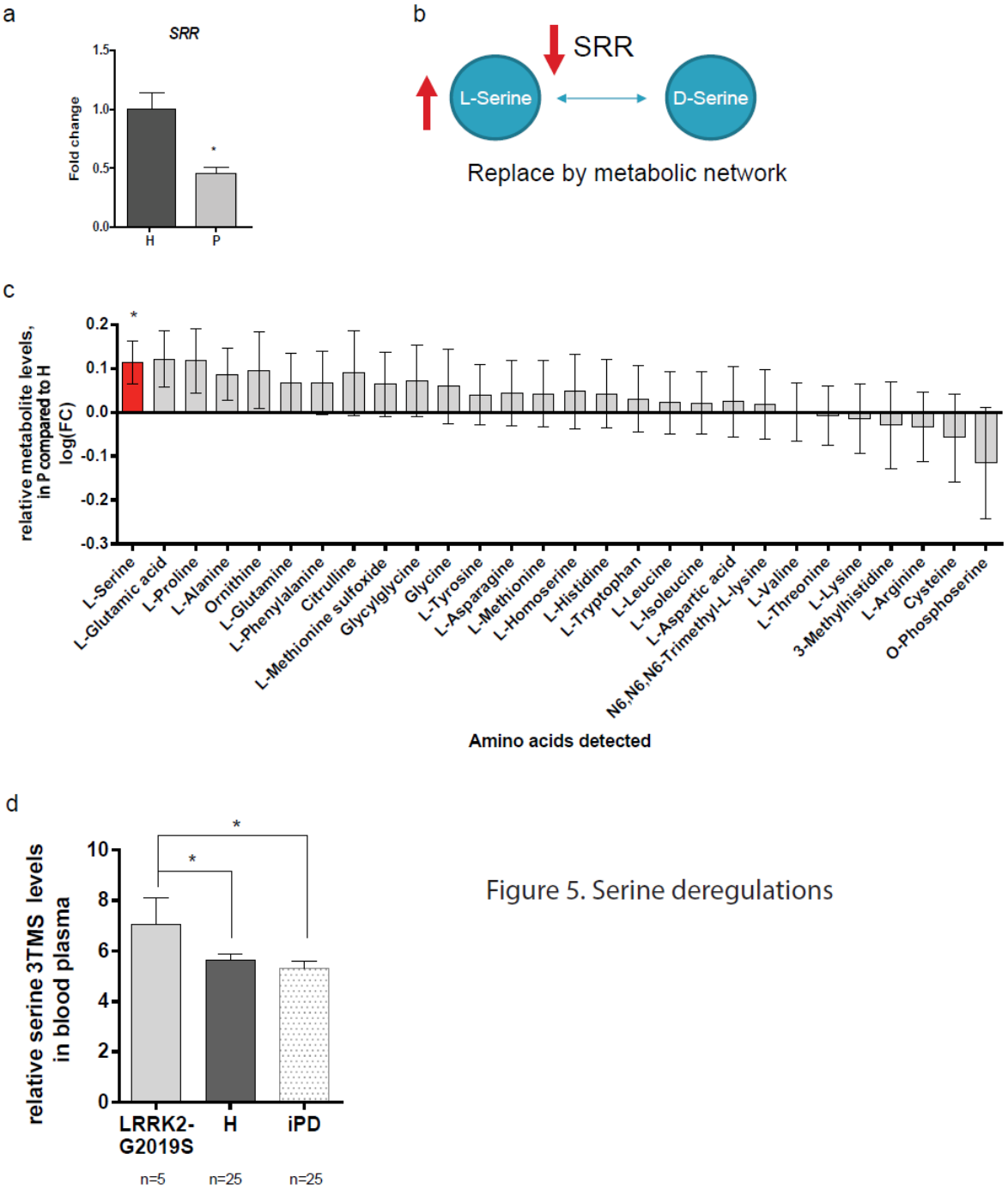

Figure 5. Serine deregulations

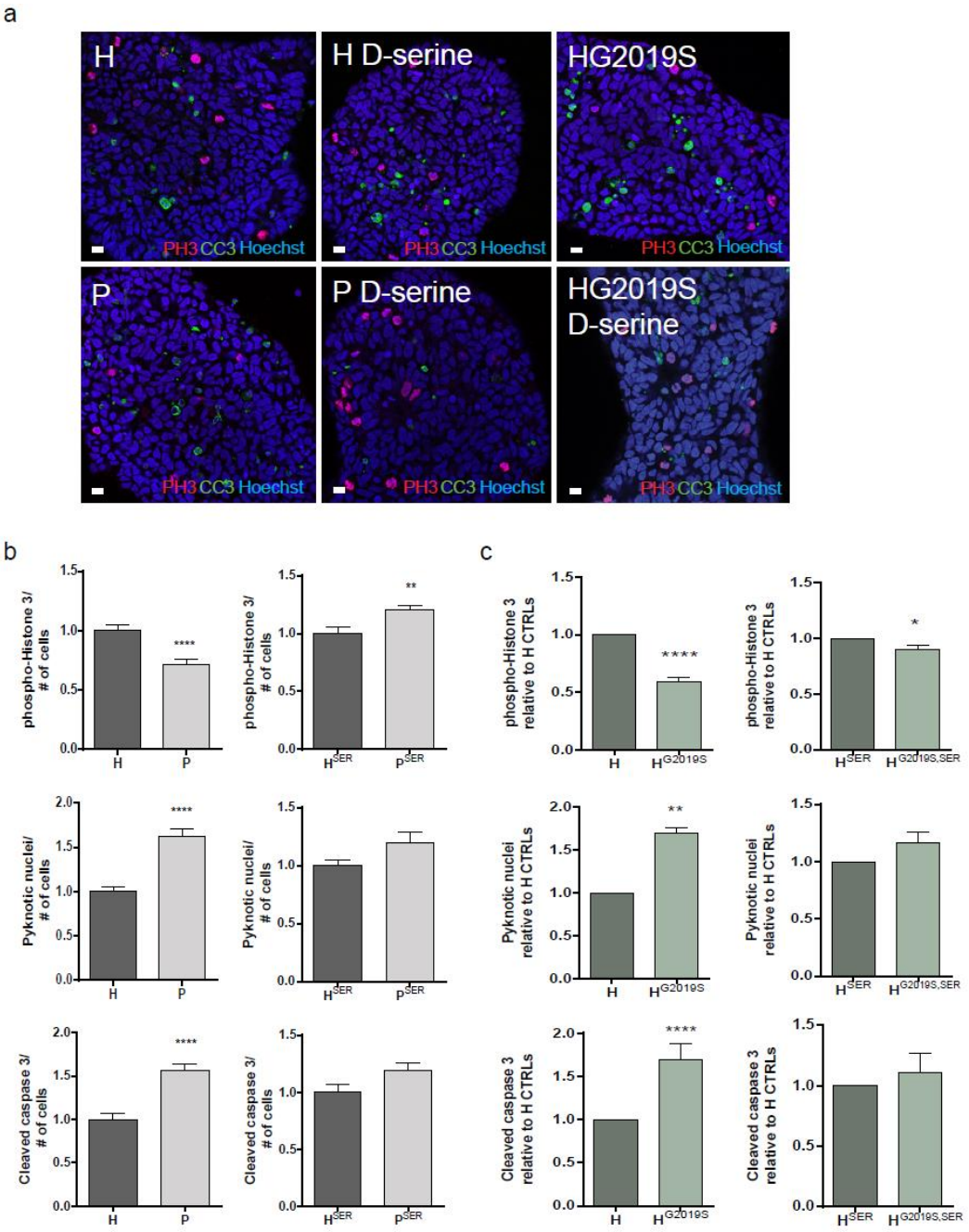

Figure 6 D-Serine rescue

SUPPLEMENTAL MATERIAL

SUPPLEMENTARY FIGURE LEGENDS

Supplementary Figure 1. iPSC quality controls of clones derived from fibroblasts. (**a**) ND34769, H5. (**b**) ND35367, P5. (**c**) Gasser lab, H3. Representative images by immunocytochemistry for pluripotency marker expression TRA-1-81, OCT4, TRA-1-60, SOX2, SSEA4 and NANOG (**a**- **c**). Chromosomes were counted using Dapi staining. Alkaline phosphatase staining shows pluripotency (**a**- **c**). Related to **Fig. 1**.

Supplementary Figure 2. CRISPR-Cas9 gene editing of H3 and H1. Strategy for introducing G6054A (protein: G2019S) mutation on the LRRK2 locus using CRISPR-Cas9 and piggyBac technologies in human iPSCs. A positive and negative double selection cassette was driven by CAG promoter to enrich edited cells and to remove the cassette afterwards. Junction PCR reactions (P1+P2, P3+P4) were used to detect the homologous recombination-driven targeted integration and piggyBac transposase-driven excision of the selection cassette. Edited LRRK2-G2019S site was confirmed by Sanger sequencing. Related to **Fig. 1**.

Supplementary Figure 3. Quality controls of all 21 cell lines. (**a**, **b**) Stem cell and neuroectoderm marker expression for quality control of hNESCs. (**a**) hNESCs were stained for NESTIN and SOX2 protein expression. (**b**) Representative image of PAX6 and SOX1 protein expression. Hoechst was used for nuclei staining. (**c**) Complete hNESC genotyping. Cell lines were sequenced for the LRRK2-G2019S heterozygous point mutation G>A. Note that P4 cells are derived from a homozygous carrier. Related to **Fig. 1**.

Supplementary Figure 4. D-Serine is not rescuing neuronal phenotypes. (**a**) Treatment with 100 µM D-serine is not rescuing decreased neuronal complexity, increased α-SYN levels, and pyknosis in DNs from P vs H comparisons and isogenic controls (G2019S vs WT comparisons). Data is represented as Mean ±

SEM. *p≤0.05, **p≤0.01, ***p≤0.001, ****p≤0.0001 according to t-test, (iterative) GRUBB's outlier test α=0.1. Related to **Fig. 1** and **6**.

Supplementary Figure 5. Representation of raw non normalized comparisons of phenotyping apoptosis, pyknosis, and mitosis shown in Table 1. PYK=number of pyknotic nuclei over the total amount of cells, CC3=number of cleaved caspase3 positive nuclei normalized to the total amount of cells and PH3=number of phospho-histone3 positive nuclei over the total amount of cells. Quantifications were done under control (untreated), DMSO, inhibitor (CZC-25146), and D-serine conditions. For D-serine a second in parallel seeded untreated control condition (USC) was used. Raw values represent the non-normalized percentage of the respective staining compared to the total amount of cells. For H-P comparisons GRUBB's outlier's test α=0.1 was performed (N=6, n=3). For isogenic comparisons (iso) the outlier test was performed on normalized data as for instance $H1^{G2019S}$/H1 (N=3, n=3). The statistical significance between each comparison can be found in **Table 1**, *p≤ 0.05 after t- or paired t-test. Related to **Fig. 2c-g** and **Fig. 3** and **6**.

Supplementary Table 1. Raw non normalized values of phenotyping apoptosis, pyknosis, and mitosis. Percentage of pyknosis, apoptosis, and mitosis in healthy and patient lines or in isogenic lines under untreated conditions or DMSO and the different treatments CZC-25146 (CZC) or D-serine (Ser). Data is represented Mean ± StD; p-values are assessed according to t-test or paired t-test. For H-P comparisons raw data was analysed after GRUBB's outlier's test α=0.1 by t-test, (n=17 or 18). For isogenic comparisons paired t-test (e.g. H1 vs $H1^{G2019S}$) was performed on raw data after outlier removal using the normalized data ($H1^{G2019S}$/H1), GRUBB's outlier's test α=0.1 (n=9 or 8). Visualization of the numbers can be seen in **Supplementary Fig 5**. Related to **Fig. 2c-g** and **Fig. 3** and **6**.

Supplementary Table 2. Overlap of DEGs between different conditions H-P, H-HG2019S, and P-PGC. Overlaps are represented within the Venn diagram **Fig. 4a**. Related to **Fig. 4**.

SUPPLEMENTAL EXPERIMENTAL PROCEDURES

Generation of iPSCs and gene editing

iPSC generation from primary human fibroblasts was performed using lentiviral transduction. The lentiviral particles for this were produced based on a published system[1,2]. Reprogramming itself was performed according to the manufacturer's protocol for TeSR™-E7™ (Stem cell Technologies). Appearing clones were picked and expanded on Geltrex® Matrix (Thermo Fisher Scientific). Clones were further characterized using Alkaline Phosphatase staining. 40 cycle RT-PCR was performed to verify the inactivity of the reprogramming cassette (data not shown), immunocytochemistry to verify the expression of pluripotency markers (OCT4, SOX2, NANOG, Tra1-60, Tra1-81, and SSEA4). Further, chromosome spreads were performed, 50 spreads were counted to ensure the right number of chromosomes per cell.

Immunocytochemistry

Cells were seeded in duplicates at either 10.000 per 96 well plate (neurones) or at 80,000 per 24 well plate (hNESCs) on Matrigel-coated glass bottom plates (Perkin Elmer) or glass coverslips. Cells were fixed after 6 days of maintenance or 14 days of differentiation using 4% paraformaldehyde in phosphosaline buffer (PBS) for 12 min. Permeabilization was done with 0.1% Triton-X100 in PBS. Cells were blocked 1h at RT with 10% FCS in PBS and incubated at 4°C o/n with primary antibody in blocking solution. Primary antibodies used for hNESCs were phospho-histone3 (ms Cell signalling) 1:200, and cleaved caspase3 (rb Cell Signalling) 1:200. Neurons were incubated with the appropriate dilution of primary antibody 1:1000 rabbit anti-TH (ab112, Abcam), 1:1000 chicken anti-TUJ1 (AB9354, Millipore), 1:400 mouse anti-α-synuclein (NBP1-05194, Novus Biologicals). Incubation with secondary antibodies was done for 1h at RT using goat anti-rabbit Alexa Fluor ®488, goat anti-mouse Alexa Fluor®568, goat anti-mouse Alexa Fluor®647, goat anti-chicken Alexa Fluor ®568 (Thermo Fisher Scientific) 1:1000 and Hoechst33342 (Themo Fisher Scientific) 1:10000 in 10% FCS. All washing steps were performed using 1xPBS.

Protein analysis

Proteins were extracted from 10 cm dishes after 6 days of maintenance. Cells were lysed using protein lysis buffer (0.2% Triton-X100, 1xProtease inhibitor cocktail (Roche) and 1xPhosphatase Inhibitor Cocktail V (Millipore) for 30 min at 4°C. The lysates were centrifuged for 30 min at 13000 rpm at 4°C and quantified using BCA essay. Proteins were diluted to 1.4 mg/ml, mixed with 6x loading dye and cooked for 3 min. Samples were size separated by electrophoresis on 7.5-12% NuPAGE Bis-Tris gradient gels according to the manufacturer's protocol (Invitrogen). Nitrocellulose membrane transfer was done using iBlot (Invitrogen). Membranes were stained with Ponceau S (Sigma) and blocked for 1h at RT with 5% milk, 0.2% Tween in PBS. Primary antibody incubation was done at 4°C o/n with ms α-SYN (Santa Cruz) 1:100, and ms TAU-1 (Millipore) 1:400 respectively. Detection was done by incubation for 1h at RT with horseradish peroxidase conjugated secondary antibodies (GE Healthcare) and enhanced chemiluminescence (ECL) kit (GE Healthcare). Images were taken using Stella and analysed with Image J.

Amino acid measurements

For derivatization and LC-MS/MS analyses the cell extract samples were reconstituted in 50 µl of methanol. Original samples were randomized and run in 3 batches which included calibration lines and blanks. The amine platform covers amino acids and biogenic amines employing an Accq-tag derivatization strategy adapted from the protocol supplied by Waters. 10 µL of each sample was spiked with an internal standard solution and taken to dryness in a speedvac. 23 isotopically labeled internal standards were used in the amine profiling platform including Ser_C13N15. The residue was reconstituted in borate buffer (pH 8.5) with AQC reagent. After reaction, the vials were transferred to an autosampler tray and cooled to 4°C until the injection. 1.0 µL of the reaction mixture was injected into the UPLC-MS/MS system. Chromatographic separation was achieved by an ACQUITY UPLC System (Waters, Etten-Leur, the Netherlands) on an Accq-Tag Ultra column (Waters) with a flow of 0.7 ml/min over a 11 min gradient. The UPLC was coupled to electrospray ionization on a triple quadrupole mass spectrometer (AB SCIEX Qtrap 6500). Analytes were detected in the positive ion mode and monitored

in Multiple Reaction Monitoring (MRM) using nominal mass resolution. Acquired data were evaluated using MultiQuant Software for Quantitative Analysis (AB SCIEX, Version 3.0.2), by integration of assigned MRM peaks and normalization using proper internal standards. For analysis of amino acids their 13C15N-labeled analogues were used. For other amines, the closest-eluting internal standard was employed. Blank samples were used to correct for background. After internal standard correction 39 amines complied with the acceptance criteria. Since the peaks were integrated and visually inspected as criteria were set: a signal to noise ratio over 3 and no or low blank effect. For these compounds no outliers or batch effect was observed.

SUPPLEMENTARY REFERENCES

1. Worringer, K. a *et al.* The let-7/LIN-41 Pathway Regulates Reprogramming to Human Induced Pluripotent Stem Cells by Controlling Expression of Prodifferentiation Genes. *Cell Stem Cell* 14, 40–52 (2014).
2. Warlich, E. *et al.* Lentiviral Vector Design and Imaging Approaches to Visualize the Early Stages of Cellular Reprogramming. *Mol. Ther.* 19, 782–789 (2011).

SUPPLEMENTARY FIGURES AND TABLES

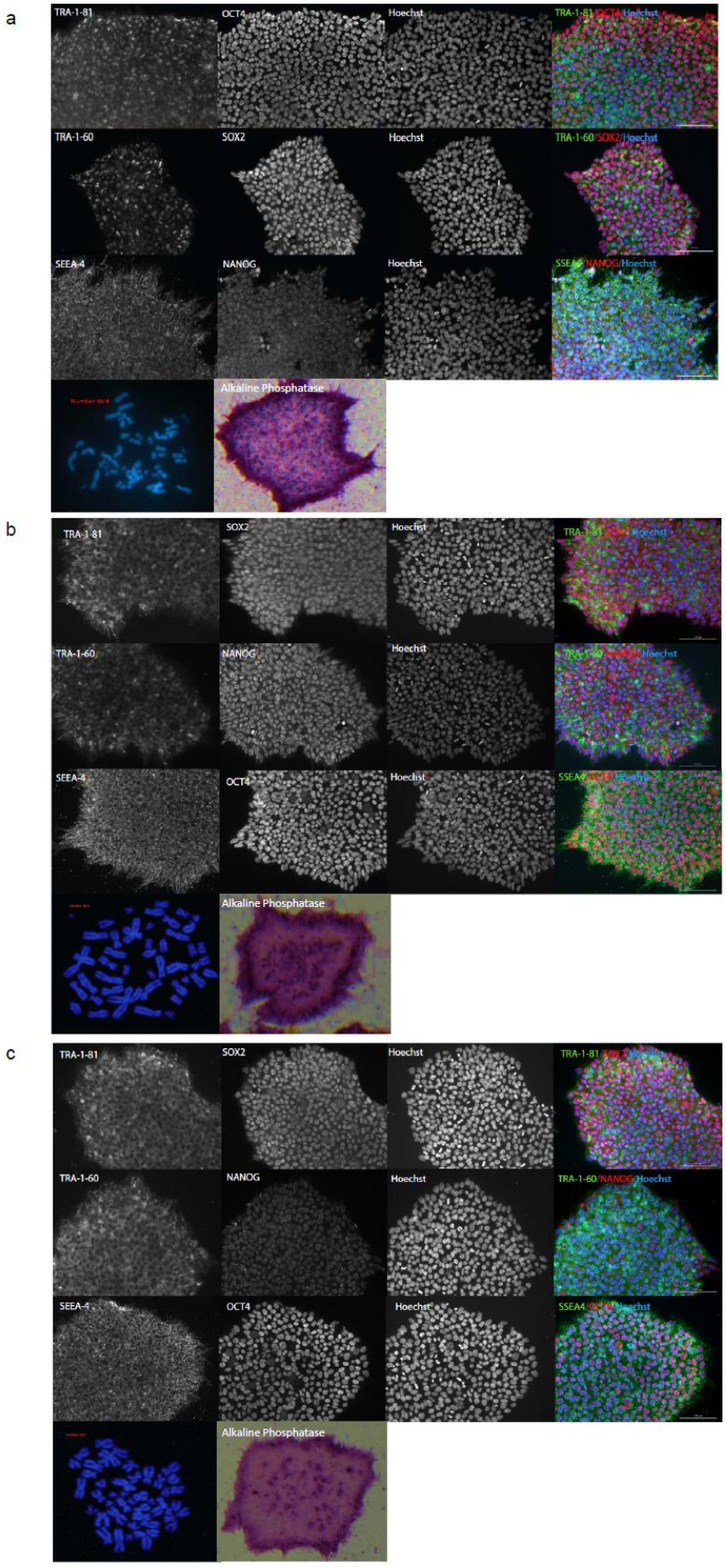

Supplementary Figure 1

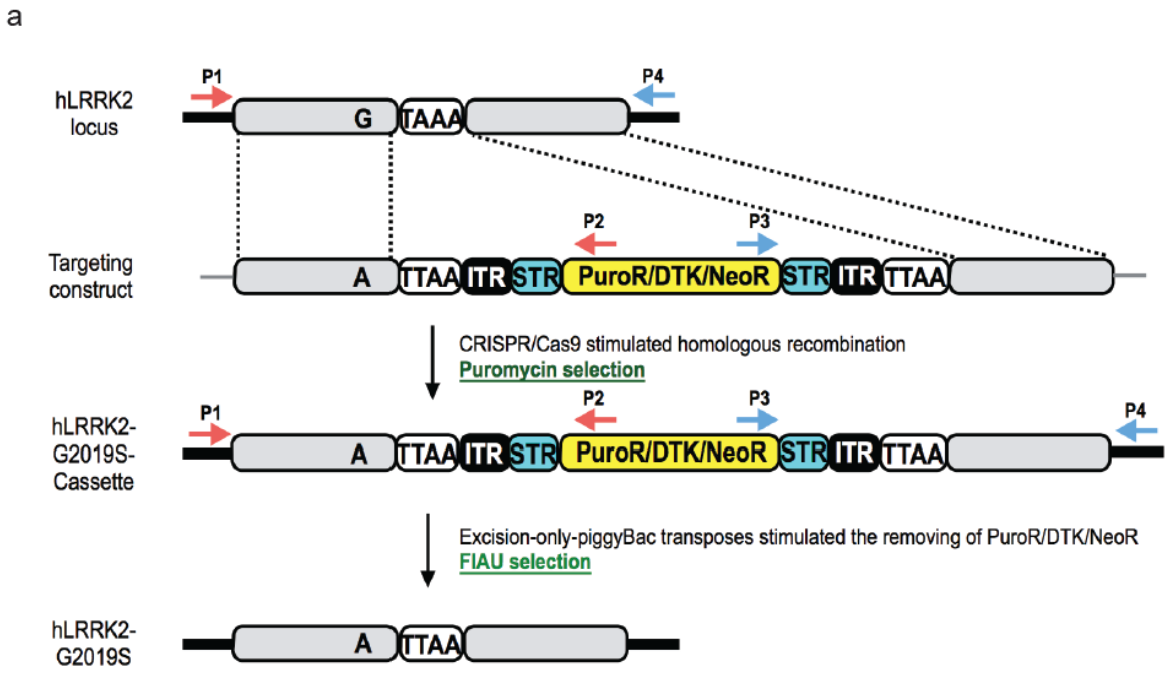

Supplementary Figure 2

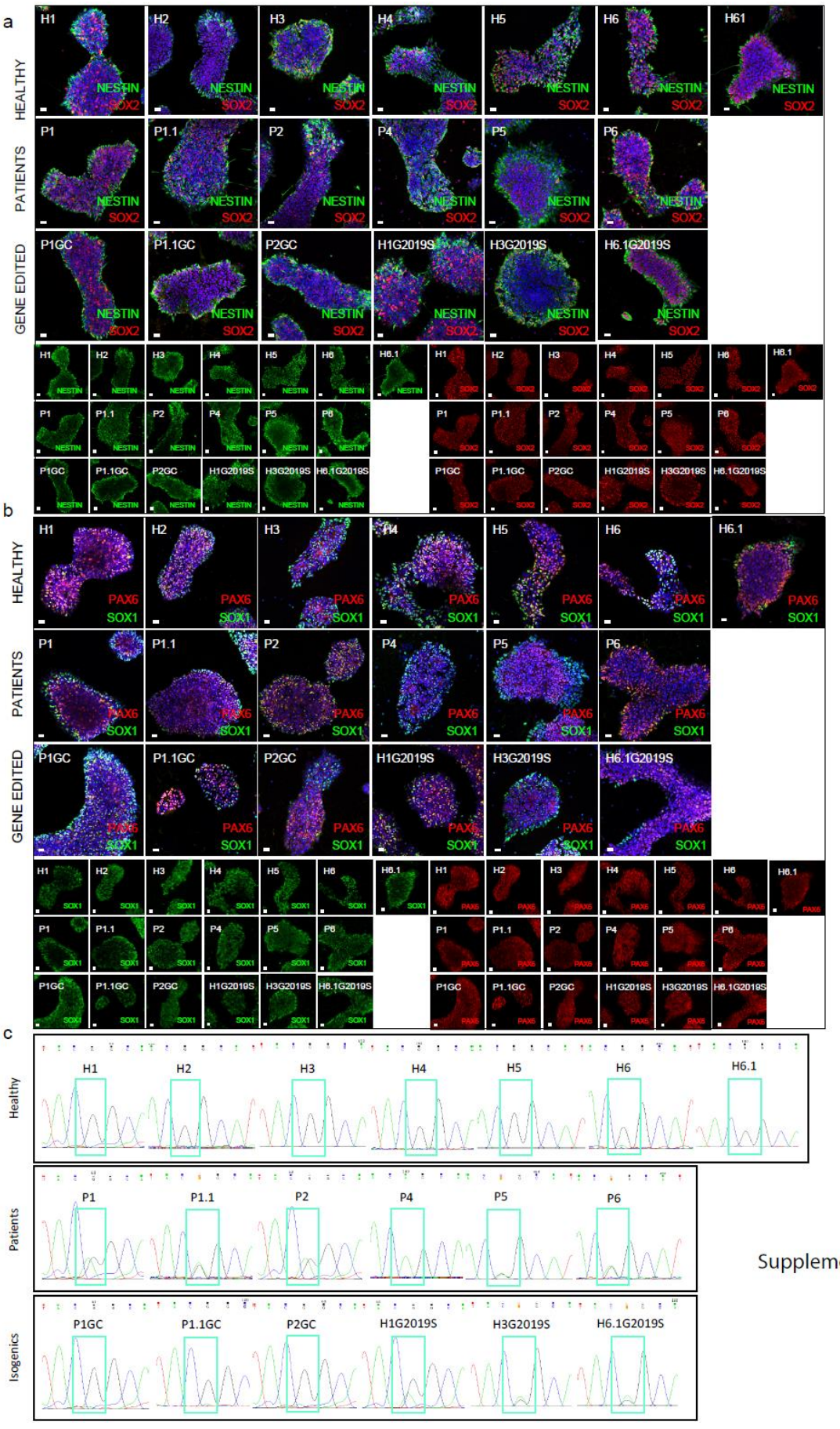

Supplementary Figure 3

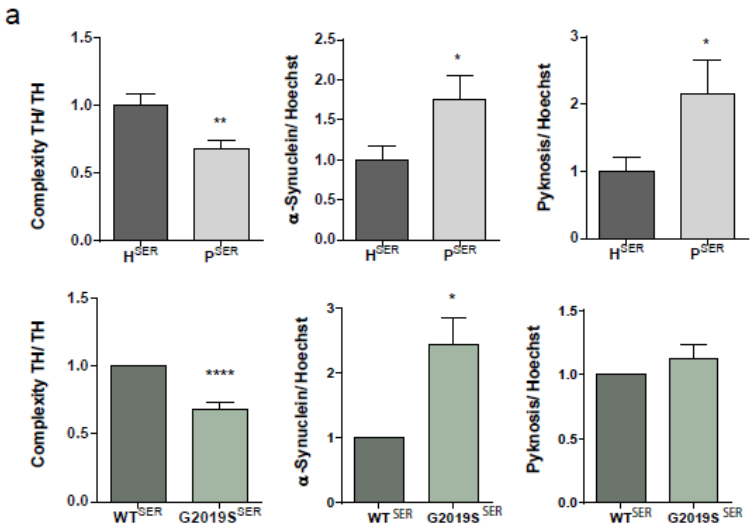

Supplementary Figure 4

Supplementary Figure 5

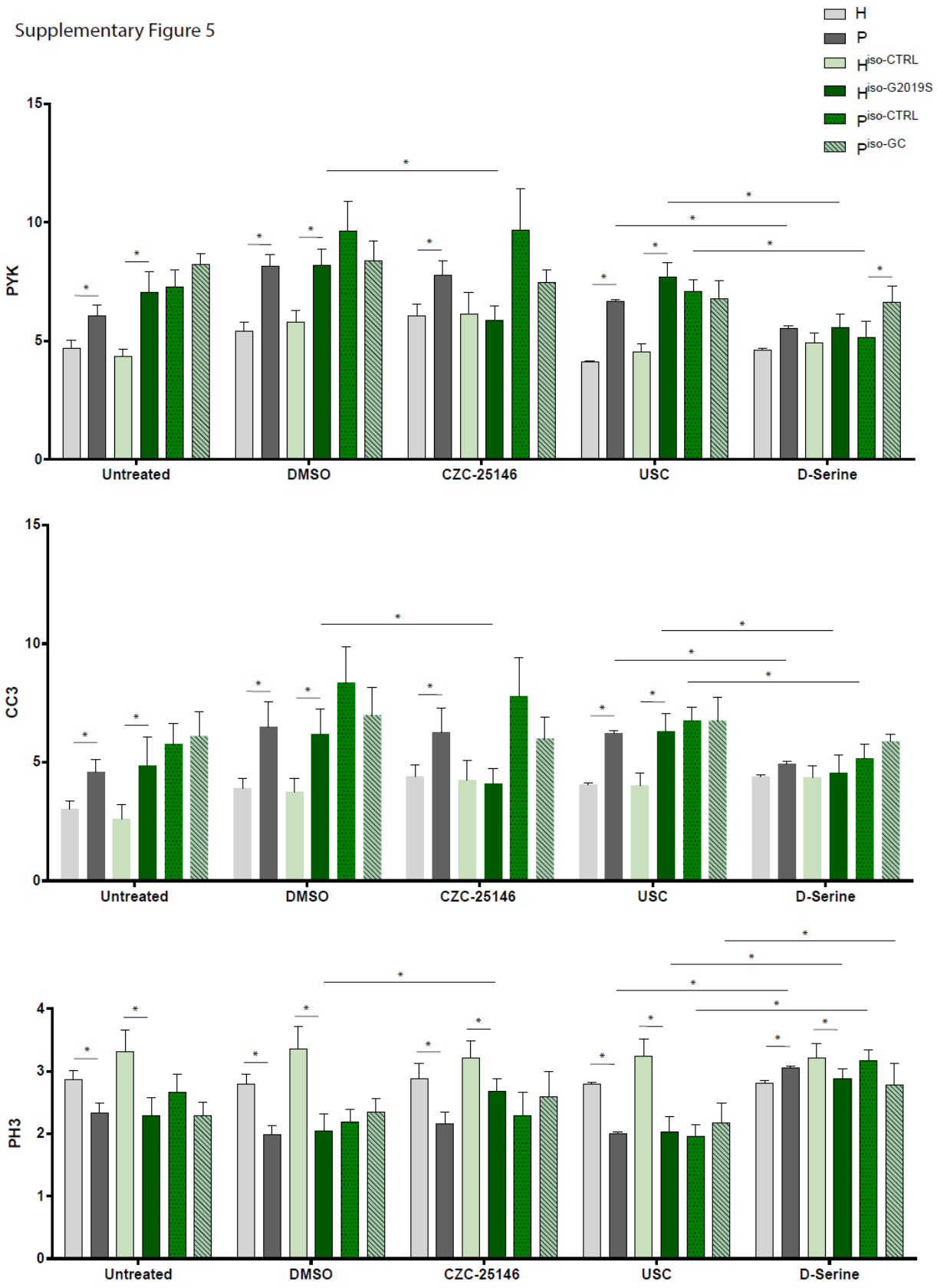

Supplementary Table 1. Raw values

	H-P Untreated (FIG 1e)		
	H (M±StD)	P (M±StD)	t-test
PYK	4.68% ± 1.47%	6.06% ± 1.87%	0.023
CC3	3.02% ± 1.48%	4.58% ± 2.23%	0.019
PH3	2.86% ± 0.62%	2.33% ± 0.68%	0.018

	H-P DMSO (FIG 3b)			H-P CZC-25146 (in DMSO) (FIG 3b)		
	H (M±StD)	P (M±StD)	t-test	H (M±StD)	P (M±StD)	t-test
PYK	5.42% ± 1.57%	8.15% ± 2.15%	0.0001	6.07% ± 1.96%	7.78% ± 2.48%	0.026
CC3	3.90% ± 1.73%	6.50% ± 2.55%	0.0012	4.40% ± 2.12%	6.24% ± 2.58%	0.027
PH3	2.80% ± 0.63%	1.99% ± 0.57%	0.0004	2.88% ± 1.03%	2.16% ± 0.81%	0.030

	H-H CZC-25146 vs DMSO			P-P CZC-25146 vs DMSO		
	H (CZC M±StD)	H (DMSO M±StD)	paired t-test	P (CZC M±StD)	P (DMSO M±StD)	paired t-test
PYK	6.07% ± 1.96%	5.42% ± 1.57%	0.3471	7.78% ± 2.48%	8.15% ± 2.15%	0.5874
CC3	4.40% ± 2.12%	3.90% ± 1.73%	0.2393	6.24% ± 2.58%	6.50% ± 2.55%	0.8109
PH3	2.88% ± 1.03%	2.80% ± 0.63%	0.8564	2.16% ± 0.81%	1.99% ± 0.57%	0.2607

	H-P Untreated serine ctrl (USC) (FIG 6b)			H-P D-Serine (FIG 6b)		
	H (M±StD)	P (M±StD)	t-test	H (M±StD)	P (M±StD)	t-test
PYK	4.10% ± 0.24%	6.68% ± 0.31%	< 0.0001	4.61% ± 0.25%	5.54% ± 0.39%	0.052
CC3	4.06% ± 0.29%	6.21% ± 0.33%	< 0.0001	4.39% ± 0.35%	4.94% ± 0.28%	0.2299
PH3	2.80% ± 0.13%	2.00% ± 0.12%	< 0.0001	2.61% ± 0.16%	3.05% ± 0.14%	0.0419

	H-H D-Serine vs USC			P-P D-Serine vs USC		
	H (Ser M±StD)	H (M±StD)	paired t-test	P (Ser M±StD)	P (M±StD)	paired t-test
PYK	4.61% ± 0.25%	4.10% ± 0.24%	0.0645	5.54% ± 0.39%	6.68% 0.31%	0.0004
CC3	4.39% ± 0.35%	4.06% ± 0.29%	0.0924	4.94% ± 0.28%	6.21% ± 0.33%	< 0.0001
PH3	2.61% ± 0.16%	2.80% ± 0.13%	0.1954	3.05% ± 0.14%	2.00% ± 0.12%	0.0002

	Iso Untreated (FIG 1g)		
	H (M±StD)	HG2019S (M±StD)	paired t-test
PYK	4.33% ± 0.77%	7.05% ± 2.14%	0.0012
CC3	2.60% ± 1.51%	4.84% ± 2.99%	0.0064
PH3	3.31% ± 0.84%	2.29% ± 0.48%	0.0068
	PGC (M±StD)	P (M±StD)	paired t-test
PYK	8.22% ± 1.15%	7.27% ± 1.79%	0.054
CC3	6.09% ± 2.54%	5.76% ± 2.14%	0.432
PH3	2.29% ± 0.52%	2.67% ± 0.70%	0.179

	Iso DMSO (FIG 3c)			Iso CZC-25146 (in DMSO) (FIG 3c)		
	H (M±StD)	HG2019S (M±StD)	paired t-test	H (M±StD)	HG2019S (M±StD)	paired t-test
PYK	5.81% ± 1.17%	8.17% ± 1.69%	0.0013	6.13% ± 2.27%	5.87% ± 1.45%	0.7152
CC3	3.74% ± 1.38%	6.17% ± 2.64%	0.0011	4.23% ± 2.11%	4.10% ± 1.60%	0.8246
PH3	3.36% ± 0.88%	2.05% ± 0.64%	0.0002	3.21% ± 0.67%	2.68% ± 0.48%	0.0202
	PGC (M±StD)	P (M±StD)	paired t-test	PGC (M±StD)	P (M±StD)	paired t-test
PYK	8.38% ± 2.05%	9.64% ± 3.05%	0.067	7.45% ± 1.29%	9.68% ± 4.28%	0.177
CC3	6.99% ± 2.84%	8.35% ± 3.70%	0.188	6.01% ± 2.23%	7.76% ± 4.06%	0.230
PH3	2.34% ± 0.55%	2.18% ± 0.54%	0.504	2.59% ± 1.01%	2.29% ± 0.91%	0.470

	Iso CZC-25146 vs DMSO			Iso CZC-25146 vs DMSO		
	H (CZC M±StD)	H (DMSO M±StD)	paired t-test	P (CZC M±StD)	P(DMSO M±StD)	paired t-test
PYK	6.13% ± 3.37%	5.81% ± 1.17%	0.628	9.68% ± 4.28%	9.64% ± 3.05%	0.9684
CC3	4.23% ± 2.11%	3.74% ± 1.38%	0.305	7.76% ± 4.06%	8.35% ± 3.70%	0.562
PH3	3.36% ± 0.88%	3.21% ± 0.67%	0.8476	2.29% ± 0.91%	2.18% ± 0.54%	0.6353
	HG2019S (CZC M±StD)	HG2019S (DMSO M±StD)	paired t-test	PGC (CZC M±StD)	PGC (DMSO M±StD)	paired t-test
PYK	5.87% ± 1.45%	8.17% ± 1.69%	0.0068	7.45% ± 1.29%	8.38% ± 2.05%	0.1488
CC3	4.10% ± 1.64%	6.17% ± 2.64%	0.0098	6.01% ± 2.23%	6.99% ± 2.84%	0.2295
PH3	2.68% ± 0.48%	2.05% ± 0.64%	0.0063	2.59% ± 1.01%	2.34% ± 0.55%	0.5081

	Iso USC (FIG 6c)			Iso D-Serine (FIG 6c)		
	H (M±StD)	HG2019S (M±StD)	paired t-test	H (M±StD)	HG2019S (M±StD)	paired t-test
PYK	4.54% ± 0.85%	7.70% ± 1.48%	<0.0001	4.90% ± 1.02%	5.58% ± 1.33%	0.1515
CC3	4.02% ± 1.34%	6.28% ± 1.89%	0.0035	4.35% ± 1.23%	4.53% ± 1.87%	0.7888
PH3	3.24% ± 0.66%	2.03% ± 0.59%	<0.0001	3.22% ± 0.54%	2.88% ± 0.49%	0.0462
	PGC (M±StD)	P (M±StD)	paired t-test	PGC (M±StD)	P (M±StD)	paired t-test
PYK	6.77% ± 1.92%	7.10% ± 1.13%	0.7114	6.63% ± 1.63%	5.19% ± 1.64%	0.0415
CC3	6.76% ± 2.43%	6.73% ± 1.44%	0.9798	5.87% ± 0.76%	5.17% ± 1.46%	0.314
PH3	2.17% ± 0.80%	1.96% ± 0.45%	0.3658	2.78% ± 0.86%	3.17% ± 0.42%	0.3087

	Iso D-Serine vs USC			Iso D-Serine vs USC		
	H (Ser M±StD)	H (M±StD)	paired t-test	P (Ser M±StD)	P(M±StD)	paired t-test
PYK	4.90% ± 1.02%	4.54% ± 0.85%	0.4055	5.19% ± 1.64%	7.10% ± 1.13%	0.00110
CC3	4.35% ± 1.23%	4.02% ± 1.34%	0.1600	5.17% ± 1.46%	6.73% ± 1.44%	0.0068
PH3	3.22% ± 0.54%	3.24% ± 0.66%	0.2497	3.17% ± 0.42%	1.96% ± 0.45%	0.0014
	HGS (Ser M±StD)	HGS (M±StD)	paired t-test	PGC (Ser M±StD)	PGC (M±StD)	paired t-test
PYK	5.58% ± 1.33%	7.70% ± 1.48%	0.0003	6.63% ± 1.63%	6.77% ± 1.92%	0.82290
CC3	4.53% ± 1.87%	6.28% ± 1.89%	0.0024	5.87% ± 0.76%	6.76% ± 2.43%	0.1569
PH3	2.88% ± 0.49%	2.03% ± 0.59%	0.0045	2.78% ± 0.86%	2.17% ± 0.80%	0.0053

Table 2. DEGs

OVERLAP P-H vs H-HG2019S: 35 DEG	OVERLAP P-H vs PGC-P: 50 DEG	OVERLAP H-P vs H-HG2019S vs P-PGC: 2 DEG
ADAMTS3	ADAMTS18	LOC105377261
ANGPT1	ADRA2A	ROCK1P1
DAAM1	AMOT	
DKK1	CCDC125	
ELL2	CNPY1	
HHIP	DDX11L10	
IGFBPL1	DUX4L25	
JAG1	EPHA3	
LGR5	FAR2P3	
LINC00648	FIRRE	
LOC100130976	HES3	
LOC101929518	HIST1H2BB	
LOC101929563	HIST1H3C	
MEIS2	HIST1H4A	
MIR1252	HOXB1	
MIR365A	ID1	
MIR4712	LINC01198	
MIRLET7A2	LOC101928307	
NEUROD4	LOC105373202	
NEUROG3	LOC105375161	
NNAT	LOC105378798	
NRCAM	LRRC34	
PCDH15	MIR548AM	
PCDH8	NAV3	
PPP1R3C	OR5H1	
SNORA14A	PPP1R14C	
SNORA60	PPP1R1A	
SNORD53	REXO1L1P	
SP5	SHISA6	
SPON1	SNORA11	
TCEAL7	SNORA74A	
TEX15	SNORD115-11	
TRDC	SNORD115-17	
TRDJ1	SNORD115-20	
ZIC2	SNORD115-22	
	SNORD115-39	
	SNORD115-42	
	SNORD115-44	
	SNORD115-5	
	SNORD115-6	
	SNORD115-9	
	TPPP3	
	VTRNA1-3	
	VTRNA2-1	
	ZC3HAV1L	
	ZNF229	
	ZNF429	
	ZNF506	
	ZNF558	
	ZNF667-AS1	

DISCUSSION

DISCUSSION

A - NSC MODELS FOR STUDYING PD AND THEIR DIFFERENTIATION POTENTIAL

In this thesis, four different cellular models were used or generated for potential disease modeling. We used NESCs and DNs to model PD, and generated NSCs and astrocytes for future disease modeling. All four cell lines are interdependent and derived from iPSCs. The advantages and limits of iPSC usage for disease modeling have already been highlighted in the introduction. In short, iPSCs represent an ethically, accessible and personalized tool, which allows the recapitulation of the complexity of neurological diseases. iPSCs make it possible to generate different neural cell types coming from the same patient to study them independently or together in order to get a global overview of the disease. Furthermore, together with their isogenic controls, iPSCs represent a very promising tool to address the divergent genetic contributions to PD. In contrast, non-genetic factors, such as environment and age, can't or can only be insufficiently recapitulated in an iPSC derived *in vitro* disease model. Another limitation is the derivation of homogenous cultures that are functionally active and recapitulate the *in vivo* situation. As described in section 2.4.1, different *in vitro* neural stem cell models have already been generated from ESCs or iPSCs. Here the focus is put first on the NESC model (the smNPCs) and the newly derived NSCs in order to discuss advantages, optimization possibilities and their developmental state. In a second step, their differentiation into astrocytes and DNs as well as the homogeneity, functional maturity and potential uses of the generated cultures will be discussed.

Isogenic hNESCs represent a physiologically relevant cell model for studying PD. They are patient-specific, committed to the neural lineage and can efficiently differentiate into DNs (Reinhardt *et al*. 2013b). The first step in generating and using an *in vitro* disease model is a proper characterization of the cell type identity. The NESCs represent cells from the developing neural plate as described by Reinhardt *et al*. in 2013b. In contrast to other NSC models with equally high differentiation potential, the NESCs can be stably maintained for more than 40 passages (Conti and Cattaneo, 2010; Reinhardt et al., 2013b). The expression of the typical NESC markers SOX1, PAX6, SOX2, and NESTIN confirms their neuro-epithelial identity (see section 2.4.2). The usage of a stable NESC line makes their handling easier and their maintenance cheaper compared to iPSCs. Furthermore, their commitment to the neural lineage provides them with a physiologically relevant advantage over iPSCs. The NESCs qualify, for instance, as DN precursor cells as they are able to differentiate into TH positive DNs (Reinhardt et al., 2013b). Additionnaly, the pre-differentiation of iPSCs into NSCs in general, permits a faster and more homogenous differentiation (Palm et al., 2015). As neural stem cell deregulations have been described

in PD pathogenesis the characteristics highlighted here make the NESCs an ideal model to study development and to address the contribution of developmental deficiencies to neurological diseases, such as LRRK2-G2019S induced PD (see section 2.2.2). The developmental contribution to PD will be further discussed in chapter D.

The NESC model was, as described, derived from iPSCs using small molecules. The patterning of NESCs *in vitro* by SHH and WNT activation and by dual SMAD inhibition provides them with a NPBSC-like identity. As described in section 2.1.1, during development, the SHH signals from the notochord and WNT signals from the surrounding non-neuronal ectoderm keep NESCs at the neural plate border in a specific state, which allows them to differentiate into cells from the CNS and PNS. At that stage, BMP signals are still inhibited in order to induce neurulation. The NESC model was shown to robustly differentiate into neurons from the PNS, meaning that as described, they retain neural crest cell properties (Reinhart *et al*. 2013). This is consistent with the expression of PAX6, which *in vivo* has a dorso–ventral gradient with highest expression at the roof plate of the developing neural tube. *In vivo* neural crest cell segregation is happening within the developing roof plate, which means the model is showing dorsalized properties. In contrast to these dorsalized properties, the NESCs are also able to differentiate into DNs, which, during development, are derived from the midline of the neural plate, which is a ventralized region giving rise to the floor plate. During development, the cells in this region of the neural plate, mainly depend on SHH signals as described in section 2.1.2, but never come into direct contact with the signals of the non-neuronal ectoderm, as the NPBSCs do. These ambiguities demonstrate that *in vitro* stem cell models are not completely recapitulating the *in vivo* situation. Due to the absence of tempo-structural limitations, the *in vitro* stem cell model used here has a much higher plasticity and differentiation potential than its *in vivo* counterpart. Redefining the patterning *in vitro* to a more ventralized NESC identity might increase the percentage of DNs and lead to a purer and more homogenous, differentiated culture for future studies (Smits *et al*., 2017 unpublished).

The generation of NSCs from NESCs further extended the possibilities for disease modeling and studying PD. During *in vivo* development, after neurulation, early NESCs give rise to rosette-like structures within the neural tube that elongate and align radially to become radial glial cells in the fetal brain (see 2.2.1). The NSC model used here was derived from NESCs by cultivating them in the presence of the mitogens EGF and FGF-2, as described for RGCs, and by providing them with LIF and fetal calf serum (FCS). As the NSCs are derived from the NESCs, they typically exhibit more mature characteristics, thus corresponding to a later developmental stage. The NSCs possess several RGC properties, such as an elongated morphology and the potential to efficiently generate mature astrocytes (see section 2.2.2). In contrast, however, to mature RGCs, they still express SOX1 (Casarosa *et al*., 2013). Hence, they can be considered an intermediate state between NESCs and RGCs, similar to the pluripotent stem cell

derived lt-hESNSCs, described in section 2.4.1 (Conti and Cattaneo, 2010; Falk *et al*., 2012; Koch *et al*., 2009). Based on these characteristics, the NSCs typically represent cells of the developing neural tube. However, unlike lt-hESNSCs, they do not form rosette-like structures anymore, a typical neural tube characteristic. Thus, as they share common features with RGCs and lt-hESNSCs, they were situated within Figure 15, at a later stage of neural tube development. Similar to the NESCs, the NSCs can be robustly expended and maintained. When comparing NESCs to NSCs, although clear morphological differences could be observed, the same classical markers SOX1, SOX2, NESTIN and PAX6 were used for their characterization. As the NSCs were derived from NESCs, it is obvious that they correspond to a later developmental stage. Nevertheless, in order to characterize their specific developmental origin, we could have stained for RGC-specific markers as described in section 2.4.2 or lt-hESNSC neurodevelopmental markers such as, dachshund homolog 1 (DACH1), nuclear receptor subfamily 2 group F member 1 (NR2F1), LIM domain only 3 (LMO3), or doublesex and mab-3 related transcription factor 3 (DMRT3) (Koch *et al*., 2009).

Besides disease modelling, both NSC and NESC models could be used for drug testing and therapeutic strategies. Due to the low regeneration potential of the CNS, a promising treatment option for neurodegenerative diseases consists in neural stem cell transplantations in order to replace the degenerated neurons. We showed in paper II that after pre-patterning NSCs *in vitro* into either the neuronal or glial lineage, they survived and differentiated into mature astrocytes and neurons in an *in vivo* mouse model (Palm et al., 2015). Thus, the generated NSCs could potentially be used for future *in vivo* studies and autologous stem cell replacement therapies.

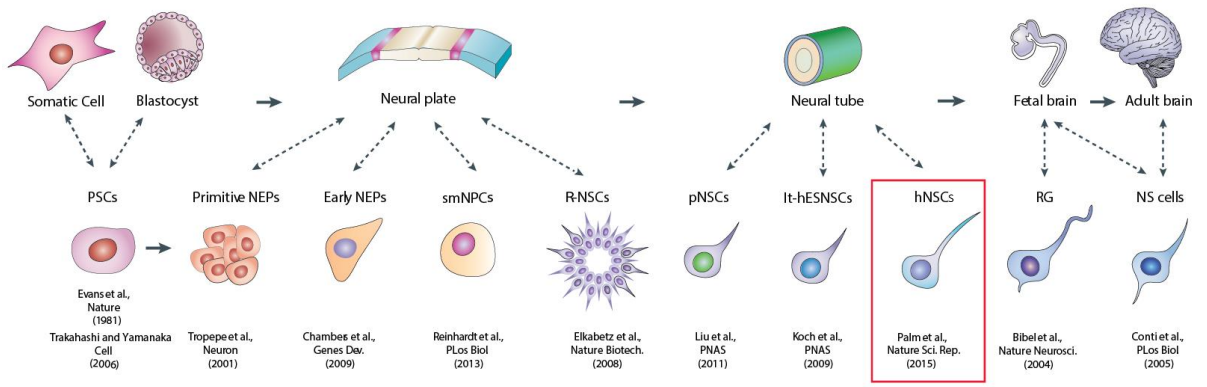

Figure 15. NSC populations that can be generated *in vitro* and their *in vivo* counterpart (II). Modified from Conti *et al.,* 2010. hNSCs generated in paper I were situated between lt-hESNSCs and RGCs in order to fit their developmental stage and *in vivo* counterpart. The paper giving their first description is cited below.

Wheras neural stem cells are highly homogenous, their differentiation can generate different amounts of neurons, atrocytes and oligodendrocytes depending on their developmental state and the differentiation protocol used. In this study, we used the NESCs to generate neurons and DNs as well as NSCs to mainly produce astrocytes. Compared to stem cells, differentiated cultures have higher

diversity, complexity and interaction possibilities. Compared to NESCs or NSCs, neuronal cultures offer, in particular, the advantage that they represent the most prominent cell type affected in PD. Moreover, studying the early steps of differentiation into DNs is essential to assess the contribution of developmental deregulations to PD. As described in section 2.3, neurogenesis was shown to be affected in PD and in particular LRRK2-G2019S deregulates proper neuritogenesis. Hence, the production of a pure homogenous culture of DNs is one of the main objectives for modeling PD. In our model system, DN generation was induced by SHH signals, mimicking *in vivo* the signals of the notochord and floor plate. Furthermore, TGF-ß, BDNF and GDNF mimic the external morphogene gradients that DNs are exposed to in the developing brain (see section 2.1.2). In addition, ascorbic acid (AA) and db-cAMP are both generally used for neuronal differentiation. AA reduces oxidative stress and cAMP induces signals that enhance neuronal differentiation (Halliwell, 1996; Sánchez *et al.,* 2004). The number of DNs was assessed by TH expression. TH is the rate-limiting enzyme in dopamine production and is widely used as marker for DNs. It should be noted that TH expression is no guarantee for the functionnality of DNs and dopamine production. Also nor- and adrenergic neurons express TH for noradrenaline and adrenaline production from dopamine (White, 2012). Nevertheless, TH expression is the best established marker for DN characterization and the effort to detect dopamine secretion is very laborious. Ideally, a more in-depth analysis, by staining for the producer and receptors of dopamine uptake and release such as AADC, vesicle monoamine transporter type 2 (VMAT2) and dopamine transporter (DAT), should complement TH expression when establishing a DN model system (White, 2012). Besides the characterization of DNs, their quantification allows the assessment of culture homogeneity. The amount of TH-positive DNs generated in this study was around 15%, when normalized to the total amount of TUJ1-positive neurons (see appendix 1.5), which is rather low compared to the 70% described in the original paper (Reinhardt *et al*. 2013b). This differences might be due to different environmental culture conditions, length of differentiation, handling and individual cell line variations. Moreover, different quantification techniques were used: whereas Reinhardt *et al*. (2013b) counted the number of double-positive nuclei, we quantified the whole neuronal network. In addition, the total amount of TH positive cells within the original study was only 35%, showng they had a considerable number of undifferentiated cells. As we used immunocytochemistry to identify TH positive DNs in this study, homogenous cultures were not necessary. Nevertheless, pure cultures represent a huge advantage for PD modeling and homogenous DN derivation strategies are needed. Thus, protocol optimizations are indispensable, in particular for techniques that require a large amount of cells, such as high throughput approaches. DN differentiation is not only dependent on the differentiation protocol, but also on the starting material. As described above, a more restricted ventralized pattenered precursor cell might enhance DN differentiation (Smits *et al*., 2017

unpublished). In addition, cell sorting techniques – although associated with high cellular waste – and single cell approaches could help address the issue. In contrast, heterogenous cultures might have the advantage that they better exhibit the *in vivo* situation where the physiological environment plays a major role. However, as discussed briefly below, to closer recapitulate the *in vivo* situation, a three dimensional differentiation, reminiscent of the embryonic development, is required. Similar to the stem cell models, neurons could be used – besides for disease modeling – for drug testing and autologous cell replacement strategies.

In addition to the loss of DNs, the importance of astrocytes within neurodegenerative diseases is well established. In PD, astrocytes play a role in neuroprotection through the clearance of extracellular α-SYN, the release of trophic factors, and the supply in antioxidants such as glutathione (Barres, 2008; Deleidi and Gasser, 2013) (as described in section 1.1.4 and 2.1.3). However, they can also be involved in neurodegeneration through pro-inflammatory cytokine and adenosine release, where the latter may increase PD patient's movement disorders (Rappold and Tieu, 2010). Moreover, astrocytes play an important role in DN differentiation (see section 2.1.3). Given the important roles of astrocytes for neurons in general and the special needs and susceptibility of DNs, minor variations in astrocytic support could lead to major consequences in DN survival. Compared to other brain regions, the midbrain has rather low levels of astrocytes (Mena and García de Yébenes, 2008), reinforcing the hypothesis that proper astrocyte support and a tightly regulated balance between pro and anti-survival functions is highly needed for DN differentiation and survival. A therapeutic strategy would consist in targeting astrocytes to modulate DN survival by increasing the pro-survival- and decreasing the pro-inflammatory response, as described in section 1.1.4 (Rappold and Tieu, 2010). Furthermore, where neuro-inflammation is the trigger causing PD and not the result of the disease, targeting astrocytic behavior *in vivo* could be used as prevention strategy. Therefore, drugs modulating astrocytic behavior need to be tested on *in vitro* cultures. For instance, preventing reactive astrocytes or scar formation could dramatically increase the potential for regeneration strategies. Furthermore, due to their high plasticity, astrocytes have an inherent potential for therapeutic transplantation strategies. They are able to transdifferentiate and induce endogenous neurogenesis (Song et al., 2002). Astrocytes can, for instance, dedifferentiate into RG-like cells to give rise to new neurons (Robel *et al.*, 2011). Thus, studying astrocytes and their differentiation from NSCs is essential towards understanding and modulating PD.

In this study, we differentiated mature metabolic active astrocytes that can be used for future PD modeling. The astrocytes were generated using 1% FCS, an undefined cocktail of various differentiation factors. Higher concentrations of FCS induced multilineage differentiation, showing that neurogenesis depends on the availability of neurotrophic factors within the cocktail. Prior studies deriving astrocytes

from iPSCs used defined factors such as EGF, FGF and ciliary neurotrophic factor (CNTF), but mostly generated glial fibrillary acidic protein (GFAP) positive reactive astrocytes (Chandrasekaran et al., 2016). Again, similarly as for the NESCs, the prepatterning of iPSCs into NSCs permitted a more homogenous differentiation. We were able to distiguish between quiescent and reactive astrocytes, which have different physiological functions. Mature markers for quiescent astrocytes are S100 calcium binding protein B (S100ß) and aquaporin 4 (AQP4), whereas reactive astrocytes express additionnaly high levels of GFAP (Robel *et al.,* 2011). Vimentin, another glial intermediate filament was shown to be expressed in mature and non-mature astrocytes as well as in reactive once (Bramanti *et al.,* 2010). We showed that we had a higher number of quiescent astrocytes, which mimics the physiological situation in the brain, where the reactive astrocytes mainly occur upon inflammation and scar formation. Identifying the exact components inducing and modulating astrocyte differentiation could further improve *in vitro* disease models. Here, the activation of the pyruvate carboxylase (PC) pathway highlights the functionality of the generated astrocytes. PC activity is important in mature astrocytes to replenish the TCA cycle during anabolic processes and was shown to facilitate the production of glutamate and glutamine (Gamberino *et al*., 1997). The glutamate and glutamine cycle between astrocytes and neurons is highly important for neurotransmission. Neurons use the glutamine provided by astrocytes in order to produce the neurotransmitter glutamate. Once released into the synaptic cleft, high extracellular concentrations of glutamate are toxic for the neurons. This surplus of released glutamate is taken up through the major glutamate transporter excitotoxicity amino acid transporter 2 (EAAT2), and recycled by the astrocytes (Niciu *et al.,* 2013). In line with PC activity, we observed the expression of EAAT2 within mature astrocytes and a decrease in glutamine usage for catabolic processes compared to multilineage differentiation cultures (MLDCs). The highlighted characteristics show that we generated a functionally active mature astrocyte model that should be used for PD modeling in order to further elucidate the role of astrocytes in PD and discover new treatment strategies.

Besides for studying the general roles of astrocytes in PD, the above highlighted benefits of our mature astrocyte model in glutamate shuttling and synaptic transmission could be worth studying in astrocytic and neuronal co-cultures with mutations causing PD. Glutamatergic neurotransmission, especially through N-methyl-D-aspartate receptors (NMDARs) is mediating and modulating synaptic transmission throughout the motor circuit of the basal ganglia (Johnson *et al*., 2009). As will be discussed below, NMDAR neurotransmission plays a role in PD pathogenesis. Within NMDARs, glutamate neurotransmission is supported by cofactors such as D-serine and glycine (Cummings and Popescu, 2015; Shleper, 2005). We could show that in our model, astrocytes use glycine, which they take up from the media, to produce serine instead of de novo synthesizing it from glucose. Interestingly, it was shown that astrocytes not only stimulate NMDAR signaling in neurons through glutamine transfer, but they

also modulate synaptic activity and memory by releasing the co-neurotransmitter D-serine (Henneberger *et al*., 2010; Panatier *et al*., 2006). Moreover, serine metabolism plays an important role in several neurodegenerative diseases, as will be highlighted in chapter C. Besides serine, the uptake of glycine from the media could be important to produce glutathione, one of the neuroprotective factors secreted by astrocytes in order to reduce oxidative stress in neurons. The fact that compared to MLDCs, our model is able to recapitulate different behaviors of astrocytes in terms of pyruvate carboxylase expression, glutamine, glycine, and serine metabolism makes it a very promising tool for studying NMDAR signaling in PD. Furthermore, as we showed that D-serine plays a role in NSC renewal in PD, it should be studied throughout different cell types and models, as will be discussed in chapter C.

Besides for studying NMDAR signaling in co-cultures, astrocytes are a promising tool for augmenting the complexity of purely neuronal disease models in order to imitate a more realistic *in vivo* situation. As already mentioned above, *in vitro* disease models never recapitulate the complexity of *in vivo* neuronal development and therefore only represent a model system. A major hurdle is the reproduction of the complex three-dimensional environment and the resulting morphogen gradients of embryonic development. The latest advances in the domain have attempted to tackle this problem by successfully generating three-dimensional cellular structures called organoids that mimic embryonic development. The increased complexity of this model system highly improved the functionality of human iPSC derived neuronal cultures and clearly represents the future of PD modeling (Monzel *et al*., 2017).

B - THE ROLE OF LRRK2-G2019S IN NSCs AND NEUROGENESIS

Our aim was to analyze the role of LRRK2-G2019S in healthy individuals and PD patient derived isogenic controls. The use of iPSC-derived cell lines in order to study LRRK2-G2019S enables us to analyze the role of the mutation in a physiologically relevant environment. This environment consists on the one hand of the genomic profile of a physiologically significant, in this case neuronally committed, cell type and on the other hand of the patient genetic background. As highlighted above, both NESCs and DNs represent valid neurological models for studying PD. The developmental component of PD and the contribution of the genetic background to the disease will be discussed in more detail in the following sections. Here, the focus is on the role of LRRK2-G2019S in NSCs and DNs in order to gain new insights on the physiological and pathogenic role of LRRK2 at the cellular level.

In NESCs and DNs, LRRK2-G2019S is sufficient to increase cell death. The role of LRRK2-G2019S in neurodegeneration was extensively studied, and different pathways through which LRRK2-G2019S

might induce cellular death, as described in section 1.2.2, have been reported before. LRRK2 has been shown to increase cell death in iPSC derived DNs and degenerate iPSC derived NSCs (Reinhardt *et al*., 2013a; Sánchez-Danés *et al*., 2012; Nguyen *et al*., 2011; Liu *et al*., 2012b). In contrast to DNs, the degeneration of NSCs, however, has only been indirectly described. Liu *et al*. (2012b) showed that LRRK2-G2019S degenerates the nuclear envelope of NSCs and increases apoptosis, but only upon proteasomal inhibition. Furthermore, Milosevic *et al*. (2009) assessed human neuronal precursor cell death, but only showed an increase of apoptosis upon LRRK2 knock-down and not LRRK2-G2019S expression. Hoeglinger *et al*. (2004) depicted a reduced number of NSCs in the SVZ, OB, and DG of human brains, but was contradicted by Van den Bergen *et al*. (2005) and no assessment of cell death was performed. The only study showing increased cell death in NSCs was from Bahnassawy *et al*. (2013) for cells carrying the R1441G mutation. Additionally, in that study, in contrast to Milosevic's observations, KO of LRRK2 rescued cells rather than inducing cell death. In this thesis, we are the first to report an increase in apoptosis and pyknosis in human NESCs upon the LRRK2-G2019S mutation. It seems that the gain of function of LRRK2 by the two most prominent pathogenic mutations increases, in both cases, cellular death, whereas the loss of function might have different effects depending on the model system used. The LRRK2-G2019S induced stem cell death observed during our work might be sufficient to cause impairments in neurogenesis. Similarly, we were able to show that the cell death phenotype persists in neuronal cultures, meaning that LRRK2-G2019S impairs neuronal development by increasing cellular death. Impairments in neurogenesis upon LRRK2-G2019S have been described before by several authors, but have to my knowledge never been linked to cell death (Schulz *et al*., 2011; Winner *et al*., 2011a). The effects of LRRK2-G2019S on cellular death in neuronal and NESC cultures are depicted as reduced neurogenesis and increased cell stress in Figure 16, to complement the phenotypes described in literature.

The increase observed in NESC death goes hand in hand with reduced cellular growth and mitosis. Here, we showed that LRRK2-G2019S is sufficient to reduce mitosis and cellular growth in cells from healthy individuals. In contrast to such increases in cell death, decreases in NSC proliferation have been reported before. Winner *et al*. (2011) reported a lower number of proliferating cells in the DG and SVZ of LRRK2-G2019S transgenic mice. Furthermore, Hoeglinger *et al*. (2004) showed that dopamine depletion reduces precursor cell proliferation in mice, and post-mortem brains of PD patients have fewer precursor cells compared to healthy controls. Additionally, human LRRK2-G2019S carrying iPSCs show lower colony forming capacities at higher passages (Liu *et al*., 2012b). In contrast, LRRK2 KO mice showed no change of neural precursor cell proliferation in the DG, and *in vitro* LRRK2 KO or LRRK2-R1441G mutation of mNSCs does not alter stem cell proliferation (Bahnassawy *et al*., 2013; Paus *et al*., 2013). Although Milosevic and colleagues reported a reactivation of the cell cycle in neural progenitors

with LRRK2 knock-down, it ultimately led to cell death and not proliferation. The described effect of LRRK2 on cell cycle activity could, however, explain why mitosis is affected in the LRRK2-G2019S carrying cells. Another speculation is that differences in mitosis could be linked to microtubule deficiencies. TAU protein levels, for instance, were shown to be increased in patient lines compared to gene-corrected ones. Besides mitosis, we used an MTT assay to assess cellular growth curves through the number of metabolic active cells. The MTT assay represents an indirect viability assay that measures the capacity of cells to convert the MTT salt to formazan, a reaction that depends on functional mitochondria. Given that mitochondria might be impaired in PD (see section 1.1.4), the assay might recapitulate defects in mitochondria rather than cell viability in general. The LRRK2-G2019S mutation was shown to increase mitochondrial fragmentation, and mitochondrial impairments might be responsible for neurite shortening (Su and Qi, 2013). Interestingly, in our cells, mitochondrial defects have previously been reported (Walter *et al*, 2017 unpublished). Nevertheless, as defects in mitochondrial function normally lead to reduced stress tolerance resulting in increased cell death, or reduced proliferation, the measurements ultimately represent a similar outcome. Taken together, the previous data and ours regarding LRRK2-G2019S indicate that the G2019S mutation in LRRK2 decreases cellular growth of neural stem cells, either by reducing viability or by directly decreasing mitosis and preventing proliferation. This decrease, however, might be indirect as prior LRRK2 KO studies did not show any self-renewal deficiencies. Moreover, in this study, the LRRK2-G2019S mutation was shown to be sufficient to reduce proliferation in healthy lines, but gene-correcting LRRK2-G2019S did not rescue the phenotypes in patients, as will be further discussed in chapter D.

A second phenotype assessed in NESCs and neurons was the amount of α-SYN. α-SYN is the main component of LBs and although a direct interaction between both proteins is still the source of some controversy, the LRRK2-G2019S mutation was shown to increase its expression (Sánchez-Danés *et al*., 2012; Reinhardt *et al*., 2013a; Nguyen *et al*., 2011). We were able to observe a LRRK2-G2019S-dependent increase in α-SYN within patient NESCs compared to their gene-corrected counterparts. In consonance with this findigs, TAU protein expression was shown to increase α-SYN aggregation, and we detected a LRRK2-G2019S dependent increase of TAU in patient NESCs (Badiola *et al*., 2011). The differences in NESCs were only visible at the level of isogenic controls because of the high variation between cell lines. Reinhardt *et al*. (2013a) showed similar G2019S-dependent increases in α-SYN levels in DNs and was unable to detect differences in non-isogenic cultures, because of high inter-individual variations in healthy controls. In contrast to the observations in the NESCs and the DNs assessed by Reinhardt *et al*. (2013a), we detected a global increase of α-SYN in neurons within the patient lines, but could not link it to LRRK2-G2019S. This discrepancy might be due to the fact that different neuronal subcultures were analyzed. In the case of Reinhardt *et al*. (2013a), they focused on DNs alone, whereas

we assessed global α-SYN levels within TH positive and negative neurons. Similar to us, others, have also previously demonstrated differences between healthy lines and patient ones. For instance, Sánchez-Danes *et al*. (2012) and Nguyen *et al*. (2011) showed increases in α-SYN levels in neurons from patients compared to healthy controls, but did not use isogenic controls to assess the dependency on LRRK2-G2019S. Nevertheless, Sánchez-Danes *et al*. (2012) most likely also observed a LRRK2-G2019S-dependent increase of α-SYN, as no difference for idiopathic PD cases was observed. Moreover, similar to Reinhardt *et al*, (2013a), they evaluated TH positive DNs only. It can be concluded that LRRK2-G2019S has most probably an effect on α-SYN expression within patient NESCs and DNs. Furthermore, the importance of individual variations, isogenic controls, and cell model homogeneity were highlighted once again.

Impairments of NESCs, such as cell death and α-SYN levels, were shown to persist in DNs, suggesting that neurogenesis is affected. Furthermore, in developing DNs (day14), LRRK2-G2019S reduces neurite complexity. This was shown before by Winner *et al*. (2011), MacLeod *et al*. (2006) and Sánchez-Danes *et al*. (2012), who demonstrated reduced dendritic length and a lower amount of branching points in transgenic mice, rat neurons, and iPSC-derived DNs, respectively. Similarly, LRRK2 KO mice showed longer dendrites and more branching points (Paus *et al*., 2013). This phenotype is very clearly LRRK2-G2019S-dependent, without any divergences in different cellular models, and the gain and loss of function of LRRK2 behave as expected in opposite directions. Decreases in neuronal complexity could be explained by deregulated TAU protein levels as already depicted in patient NESCs. Deficiencies in the microtubule network have previously been observed in LRRK2-G2019S mice and accompanied by reduced neurotransmission (Melrose *et al*., 2010). Furthermore, in drosophila, Lin *et al*. (2010) directly linked the neurite shrinkage caused by LRRK2-G2019S to hyper-phosphorylation and mis-localizations of the TAU protein. Others showed TAU aggregations within LRRK2-G2019S neurites (MacLeod *et al*., 2006; Schwab and Ebert, 2015). Given the importance of microtubules in neurite formation, trafficking, and maintenance as well as the role of neurofibrillary tangles in PD, the hypothetical explanation of linking TAU protein expression to reduced neurite length might be justified. Further validation and assessments in DNs will be needed. Another explanation for this phenotype might be the well-established role of LRRK2 in the modulation of the actin cytoskeleton as described in section 1.2.2 (Parisiadou et al., 2010). The reduced complexity of neurites is highlighted as reduced neuritogenesis in Figure 16.

As described in the introduction, the actual role of LRRK2 is still elusive, nevertheless, the effects of LRRK2-G2019S on NESCs and DNs seem to complement. As described in the introduction, LRRK2 interacts with microtubules, mitochondria's and α-SYN, and reduces neuritogenesis and stem cell proliferation (see section 1.2.2). α-SYN, and to a lesser degree also TAU aggregations as well as

mitochondrial deficits, are thought to be a major cause of DN cell death in PD. In NESCs, we were able to show that α-SYN and TAU augment. Moreover, cellular death, impaired mitosis and proliferation or mitochondrial activity can already be observed in patient NESCs. Consequently, the stem cell phenotypes unavoidably effect proper neuronal differentiation and might lead to DN atrophy. Interestingly, most of the phenotypes, such as increased cell death, α-SYN levels and, in a less obvious way, TAU accumulation or mitochondrial deficiencies and neuronal complexity, can be found in NESCs and in the DNs. This observation shows that LRRK2-G2019S potentially induces cell death independently of the cell type or differentiation status. Preliminary results from our lab confirm this observation within the astrocyte model (Bolognin *et al*., 2017 unpublished). Furthermore, NESCs as well as DNs carrying LRRK2-G2019S show major mitochondrial and neurogenic deficiencies emphasizing the persistence of the phenotypes and their participation in neuronal development (Walter *et al*., 2017 unpublished). Overall, it seems that LRRK2-G2019S has a wide comprehensive spectrum of actions and that PD is a multifactorial disease where more than one pathway and cell type is affected. It should be noted that we are the first to show that LRRK2-G2019S is able to affect human stem cells reminiscent of a developmental stage, which will be further elaborated in chapter D.

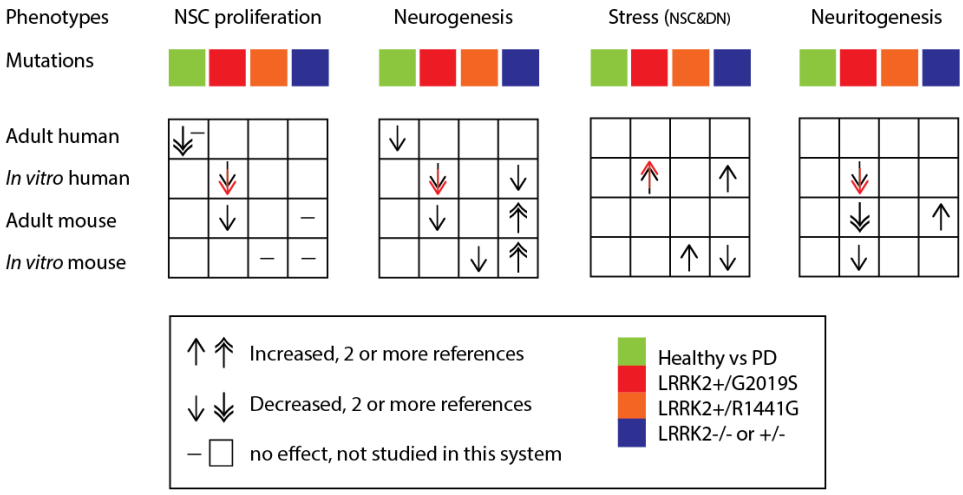

Figure 16. The role of LRRK2 in NSC maintenance and differentiation as well as comparisons between the healthy and diseased adult human brain (II). (Bahnassawy *et al*., 2013; B Winner *et al*., 2011; Schulz *et al*., 2011; Paus *et al*., 2013; Liu *et al*., 2012b; Milosevic *et al*., 2009; Höglinger *et al*., 2004; Van Den Berge *et al*., 2011; Curtis *et al*., 2007a; MacLeod *et al*., 2006; Plowey *et al*., 2008). Nickels *et al*., 2017 under submission in red arrows.

C - SUSCEPTIBILITY FACTORS WITHIN THE PD GENETIC BACKGROUND OF NSCs

Isogenic control lines as elaborated in section 2.4.1 nicely recapitulate the genetic contributions to the disease manifestations *in vitro*. They make it possible to differ between variabilities related to the genetic background, such as polymorphisms and susceptibility factors, and the underlying monogenetic cause of the disease. As it is well known that the PD patient genetic background plays a major role in the pathogenesis (see section 1.2.1 and 1.2.2), the use of background matched controls is indispensable in studying PD. Therefore, advances in CRISPR-Cas9 gene editing technologies are of major importance. As presented in paper II, we generated a deterministic genotyping method that prevents random integration and represents a fast and labor-reduced method for gene editing. By using gene-edited isogenic controls to study PD pathogenesis, we demonstrated that the phenotypes we observed are only partially dependent on LRRK2-G2019S, meaning that the PD patient genetic background is a significantly contributing factor (see paper III and chapter B). In particular, the NESC phenotypes of increased cell death and reduced proliferation in the patient cell lines were not rescuable by gene correcting LRRK2-G2019S. LRRK2-G2019S is sufficient to induce the phenotypes in the healthy lines, but LRRK2-G2019S is not necessary to preserve the phenotypes in patient lines. This shows that there must be susceptibility factors within the patient genetic background responsible for the observed deregulations, as will be extensively discussed below. Moreover, this loss of necessity has the connotation that once induced, PD is a progressive disease where the triggers and susceptibilities change over time. One might speculate that LRRK2-G2019S leads to epigenetic modifications during development that are not rescuable within the adult fibroblast derived NSCs – provided a somatic memory exists and these changes occur in a similar way during CNS development in order to be PD relevant. Furthermore, the phenotypic dependency on LRRK2-G2019S is different in neurons compared to stem cells. While in neurons, the phenotypes are rescuable by gene-correcting G2019S, in NESCs they are not. Hence, LRRK2-G2019S shows a cell-type-specific penetrance (e.g. pyknotic nuclei in DNs vs NESCs), meaning that different cell types might have different compensatory mechanisms, and that LRRK2-G2019S influences different pathways in different cellular models (e.g. mitosis vs neuronal complexity). Moreover, in DNs, LRRK2-G2019S alone causes more pronounced, mutation-dependent, phenotypes than in NESCs. Within DNs cell death, neuritogenesis, and probably also α-SYN, are inducible and rescuable by modulating LRRK2-G2019S. The question arises whether more pronounced or more mutation-dependent automatically means more severe. In NESCs, LRRK2-G2019S does not act alone, which makes this developmental PD associated phenotype a much more complex driver of the disease compared to the straight-forward effect of LRRK2-G2019S on DN neurodegeneration. The cell type specific differences and dependencies, once again highlight the complexity of the disorder and the

concept of a more complicated driver underlying the disease manifestations does justice to the extent of PD.

In this study, we discovered several potential susceptibility factors that might contribute to the observed phenotypes. We identified genes such as *NTS, RAB32, GPX7, ARL17a* and *b, CHCHD2, DNAJC15* and *SRR,* which all have the potential to modulate PD (paper III and appendix 1.4). Neurotensin (*NTS*) was differentially upregulated in patients and was shown to interact with dopamine (St.-Gelais *et al*., 2006) (appendix 1.4). NTS is involved in dopaminergic pathological events, such as PD, where its upregulation compensates for the loss of DNs (St.-Gelais *et al*., 2006). Interestingly, it is also secreted in the intestine, where it is responsible for inhibiting intestinal contractions (Furness *et al*., 2013). It should be noted that constipation is one of the early occurring non-motor symptoms of PD. Moreover, we identified RAB32, which is involved in the protein trafficking pathway, melanosome formation, pathogen engulfment, mitochondrial fission and fusion events and regulates the transport of LRRK2 (see section 1.1.4) (Haile *et al*., 2017; Ohbayashi *et al*., 2017; Waschbüsch *et al*., 2014). Thus, *RAB32* represents an ideal candidate for further studies. ADP ribosylation factor like GTPase 17a and b (ARL17a and b), two other promising candidates involved in protein trafficking, represent risk loci associated with MAPT (TAU) induced PD, through GWAS (Simón-Sánchez *et al*., 2009). Moreover, an SNP in *ARL17a* has been linked to PD and *ARL17b* correlates with progressive supranuclear palsy (Allen *et al*., 2016; Nalls *et al*., 2014). Furthermore, different proteins involved in mitochondrial related stress and ROX species formation stood out as interesting candidates for further studies. Glutathione peroxidase 7 (GPX7) is, as all peroxidases, mainly reducing, H_2O_2 into water and oxidizing glutathione, one of the main antioxidant within cells, in order to protect the cells from oxidative stress. As oxidative stress is an important factor of PD (see section 1.1.4 and chapter A) an upregulation of *GPX7* in some of the patients might counteract reactive oxygen species production. Moreover, mutations in coiled-coil-helix-coiled-coil-helix domain containing 2 (CHCHD2), a protein involved in mitochondrial respiration, have been linked to late onset autosomal dominant PD (Funayama *et al*., 2015). Interestingly, two populations, one with high, and one with very low expression levels were detected within the healthy individuals, whereas the patients all had equally high levels. This implies that lower levels of CHCHD2 might be protective for PD, but this speculation eventually needs further analysis among a bigger cohort. Lastly, DNAJC15, a negative regulator of the mitochondrial respiratory chain, was upregulated in patients and is thought to prevent mitochondrial hyperpolarization. Various other heat shock proteins, such as DNAJC6, HSP90, and HSP70, have been linked to LRRK2 and PD before (Köroğlu *et al*., 2013; Wang *et al*., 2008). Overall, different DEGs in patient NESCs could be associated with the major pathways of PD and, as such, might be important contributors to its pathogenesis.

Here, the focus was put on serine racemase (*SRR*) as a genetic modifier of the disease and it was discovered that D-serine, its enzymatic product, was able to rescue the impaired stem cell renewal phenotypes underlying the patient genetic background, which could not be rescued by gene correcting LRRK2-G2019S. From all the highlighted factors, SRR qualified best as genetic modifier for PD, as it was shown to be involved in several neurodegenerative diseases, such as Alzheimer's disease, amyotrophic lateral sclerosis (ALS) and schizophrenia, sharing features with PD (Fujii *et al*., 2006; Morita *et al*., 2007; Sasabe *et al*., 2007). Alzheimer is similar to PD, a severe neurodegenerative disorder with protein aggregates (plaques and tangles) leading to dementia, ALS is characterized by the degeneration of motor neurons and schizophrenia is a severe mental disorder linked to defective glutamate and dopamine neurotransmission. The involvement of SRR in brain diseases is directly linked to its enzymatic product D-serine, which was shown to be a co-neurotransmitter for NMDARs in neurons. As described in chapter A, within NMDARs, glutamate neurotransmission is supported by cofactors such as D-serine and glycine. Consequently, D-serine is involved in motor and cognitive functions, such as learning processes and memory (Durrant and Heresco-levy, 2014; Sasabe *et al*., 2007). Furthermore, SRR has been shown to play an important role in neural development and stem cell maintenance reinforcing its involvement in the observed phenotypes, as will be discussed below.

The role of D-serine in motor circuit dysfunctions in neurons of the PNS have been highlighted for ALS. As already described in chapter A, *in vivo*, a large amount of D-serine is generated by glial cells, and upregulated upon glial activation. In ALS, this upregulation was shown to directly lead to NMDAR over activation, glutamate toxicity and motor neuron cell death (Sasabe *et al*., 2007). There exists, however, a paradoxical role between SRR and D-serine regarding cell death and survival (Thompson *et al*., 2012). SRR has a D-serine producing and elimination function, which indicates that there might exist a complex feedback mechanism between both factors. Thompson and colleagues showed that in an ALS mouse model, D-serine levels were increased and the disruption of SRR led to a longer survival and slower progression. Interestingly, however, administration of D-serine to the ALS mice did not increase, but rather reduced endogenous D-serine levels, leading to the same beneficial effects as SRR deletion (Thompson *et al*., 2012). Besides their ambiguous roles in glutamate excitotoxicity in ALS, SRR and D-serine were shown to have similar paradoxical functions within cellular death and in particular in the apoptotic necrotic shift. Through the association with NMDARs in neurons, D-serine activity is involved in regulating pro and anti-apoptotic cascades within neurons (Canu *et al*., 2014). A decrease in SRR and D-serine promotes cell death upon early phases of apoptosis and an increase induces necrosis in the late phases (Canu *et al*., 2014). Most importantly, however, D-serine administration was shown to counteract cellular death by upregulating pro survival factors in dying rat neurons (Canu *et al*., 2014).

In PD, the only study showing a direct role of SRR and D-serine within the development of PD was established in an MPTP mouse model. In this, the authors showed that both factors were specifically increased in striatal astrocytes and neurons, but not within DNs and most probably led to the observed MPTP hypersensitivity through NMDAR signaling (Lu *et al.*, 2011). However, as the functions of D-serine within neurons are coupled to NMDAR signaling it is worth noticing that NMDARs have an essential function in PD. It is known that NMDAR assembly and signaling through glutamate plays a crucial role in dopaminergic neurotransmission (dopamine synthesis and release), degeneration as well as synaptogenesis (Lu *et al.*, 2011; Thomas and Sigrist, 2012; Gelfin *et al.*, 2011). NMDARs have several important functions within the motor circuit of the basal ganglia. The striatum receives not only dopaminergic input from the *SNpc*, but also glutamatergic signals from the cortex and, as such, lies at the crossroad of dopamine and glutamate signaling (Hallett and Standaert, 2004). On the one hand, DNs of the *SNpc* themselves are regulated by NMDAR signaling, which can increase their firing and dopamine release (Hallett and Standaert, 2004). On the other hand, in PD, hyperactive glutamatergic transmission from the subthalamic nucleus, the major target for deep brain stimulation, to the *Substantia Nigra pars reticularis* could cause and worsens DN degeneration (Johnson *et al.*, 2009) (Figure 1). In addition, although counterintuitive, NMDAR dysregulation is increased by levodopa treatment (Hallett and Standaert, 2004). In animal models of PD, for instance, NMDAR antagonists have antiparkinsonian actions and can prevent levodopa-related motor complications (Hallett and Standaert, 2004). Consequently NMDAR modulation has been in the limelight as an alternative target for PD treatment for several years (Hallett and Standaert, 2004).

Besides the role in motor neuron dysfunctions, D-serine deregulations were shown to play a role in several neuropsychiatric disorders, such as schizophrenia, depression, anhedonia, anxiety, and dementia that are related to the non-motor symptoms of Parkinson's (Durrant and Heresco-levy, 2014). Genetic variants of SRR were linked, for instance, to schizophrenia and D-serine levels were reduced in the cerebrospinal fluid of patients (Durrant and Heresco-levy, 2014; Morita *et al.*, 2007). D-serine deficiency in schizophrenia is thought to underlie NMDAR hypofunction and typically cause severe cognitive impairments, such as psychosis (Canu *et al.*, 2014). In addition, the cognitive impairments in psychiatric diseases are generally linked to adult stem cell deregulations, raising the question of whether SRR and D-serine might also play a role within stem cells (Apple *et al.*, 2016). In consonance with the foregoing, D-serine was shown to regulate proliferation and differentiation of neural stem cells, reinforcing the question of its involvement in neuropsychiatric symptoms (Huang *et al.*, 2012). Contrary to schizophrenia, however, Alzheimer's, which is the most common form of dementia, has increased D-serine levels. D-serine was shown to be upregulated in the brain and cerebrospinal fluid of Alzheimer's patients as well as in experimental mouse models (Madeira *et al.*, 2015). In Alzheimer's,

aberrant activation of glutamate receptors was associated, similarly as in ALS, to synaptic dysfunctions and neurotoxicity (Madeira *et al.*, 2015).

Apart from its function in the adult brain and its involvement in several diseases, D-serine levels were shown to increase during early development, suggesting a role in brain development and synaptic circuit refinements (Van Horn *et al.*, 2013). This observation correlates with the function of D-serine in neuroblast proliferation and it also chemokinetically enhances neuroblast migration (Kim *et al.*, 2005). Moreover, SRR KO mice show lower levels of BDNF, a neurotrophic factor involved in brain and DN development (Balu *et al.*, 2013) (see section 2.1.2). Interestingly, D-serine is also required for the proper development of dendritic arbors (Van Horn *et al.*, 2013). For instance, similar to LRRK2-G2019S mice, neurons from SRR KO mice have less and shorter spines (Figure 17). These defects were not so pronounced when SRR was deleted in neurons of older mice, showing the developmental contribution of SRR to neurogenesis (Balu *et al.*, 2013).

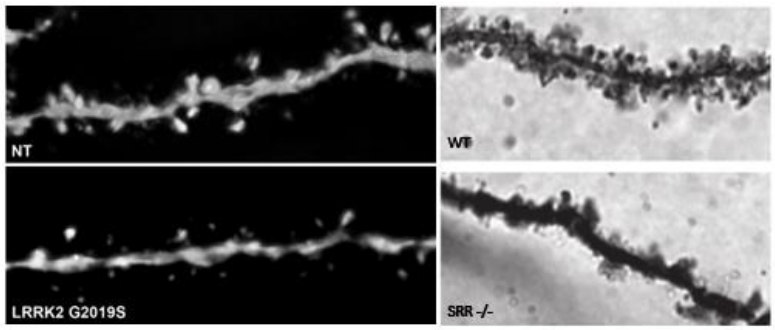

Figure 17. Dendritic arborisation phenotype by LRRK2-G2019S and SRR KO (Balu *et al.*, 2013; Winner *et al.*, 2011a)**.** WT mice compared to SRR KO mice and non-transgenic mice (NT) compared to LRRK2-G2019S transgenic mice.

The similar phenotypes observed by LRRK2-G2019S and SRR KO mice highlight – as expected from what we observed in NESCs and patient blood samples – that LRRK2 and SRR might be partners in crime. In NESCs, LRRK2-G2019S is able to induce similar phenotypes in healthy lines as we observed in the patients. In the patient lines, however, gene-correcting LRRK2-G2019S did not rescue the phenotypes, whereas treatment with D-serine did. In addition, only LRRK2-G2019S carriers showed higher blood serine levels. Thus, there must be an interplay between LRRK2-G2019S and serine metabolism. This hypothesis is reinforced by the knowledge from literature that SRR KO mice show reduced p-4E-BP1 within the synaptoneurosome and 4E-BP1 complexes with eukaryotic translation initiation factor 4E (EIF4E) to interact with LRRK2 (see section 1.2.2) (Balu *et al.*, 2013; Manzoni *et al.*, 2015). 4E-BP1 can be phosphorylated by LRRK2 and pathogenic LRRK2-G2019S increases its phosphorylation and affects DN maintenance by reducing the resistance to oxidative stress and by increasing protein synthesis (Imai *et al.*, 2008). As local protein synthesis plays an important role in synapses, increased kinase activity might alter synaptic structure and function (Imai *et al.*, 2008). The opposite effects of LRRK2-G2019S

and SRR KO on 4E-BP1 phosphorylation suggest a possible compensation mechanism between both proteins. Based on the functions of SRR highlighted above, and its possible involvement in development and LRRK2-G2019S complementation, it best qualified as being the underlying mechanism of the observed phenotypes.

In our PD model we were able to observe a down regulation of SRR within the NESCs and an accumulation of L-serine. As expected, based on the existing literature, a rescue of the cellular phenotypes by D-serine administration was observed. D-serine induced proliferation of neural stem cells and reduced apoptosis in patient cell lines. As D-serine levels per se were not analyzed, the most straightforward idea, as described in paper III, is that SRR downregulation leads to a deficiency of D-serine production. This hypothesis seems to be justified, as SRR converts L-serine to D-serine and we could see an accumulation of L-serine in the cells as well as in the blood stream of patients. Lower levels of D-serine in PD would be in line with the cognitive effects observed in schizophrenia, but not Alzheimer's (Durrant and Heresco-levy, 2014; Madeira *et al.,* 2015). This observation is consistent with the knowledge that schizophrenia is known for its stem cell deregulations. Moreover, similar to schizophrenia, the early occurring non-motor symptoms of PD can include cognitive impairments, such as hallucinations. Conversely, PD-associated dementia, a non–motor symptom shared with Alzheimers, only occurs at the latest stage of the disease, if at all (Chaudhuri and Schapira, 2009). In contrast, however, PD is described, similar to Alzheimer's and ALS, as a disease with hyperactive NMDARs, which would result from an increase and not a decrease of D-serine (Durrant and Heresco-levy, 2014; Hallett and Standaert, 2004; Sasabe et al., 2007). It should be noted that glutamate, the main neurotransmitter of NMDARs, was the second highest metabolite upregulated in NESCs from patients, following serine. Moreover, the only study analyzing D-serine in a PD model, the MPTP mouse model, showed an increase in D-serine and SRR within cells (Lu *et al*., 2011). Therefore, a second less conclusive hypothesis of D-serine expression in NESCs could be that D-serine levels are increased and a similar regulation mechanism as in the ALS mouse model, described above, could be at work. In this case, the downregulation of SRR would be a compensatory effect in patient hNESCs to limit D-serine levels, in order to prolong cellular survival, and the exogenous administration of D-serine would paradoxically further downregulate SRR. To know exactly whether D-serine levels are increased or reduced, and whether exogenous administration reduces or increases D-serine levels within NESCs, further experiments are necessary. As the roles of D-serine in neurons and stem cells are different, it can be concluded that in PD, stem cells most probably have a deficiency in D-serine, as described above, which correlates with their reduced proliferation and increased cellular death. However, the regulation of SRR and D-serine in PD in general and within neurons remains elusive and further experiments are needed to build on the hypotheses described herein. Most importantly, the data confirms that serine

metabolism plays a major role in neurodegenerative diseases, in PD, in neural development and in stem cell regulations.

Overall, our study suggests the usage of D-serine as a treatment strategy for PD. A complementation or compensation mechanism involving LRRK2-G2019S and SRR at the stem cell level reinforces the potential value of D-serine as a complementary treatment for LRRK2-G2019S induced PD. The fact that we were able to observe, a rescue of the phenotypes already at the stem cell level even suggests the use of D-serine as an early preventive strategy. The idea of using D-serine in order to treat PD mainly comes from the positive effects it has on schizophrenia patients, where it significantly improves the symptoms (Durrant and Heresco-levy, 2014). Trial treatments for PD patients using D-serine have been done before and showed promising effects on behavioral and motor symptoms and increased life quality (Gelfin *et al*., 2011). Furthermore, D-serine administration in older adults increased spatial memory, learning, and problem solving (Avellar *et al*., 2016). Apart from D-serine, L-serine administration has been shown to reduce neurofibrillary tangles in a neurotoxic model in drosophila (Cox *et al*., 2016). Moreover, a serine-rich diet (e.g. soybeans) increases the bioavailability of levodopa within the gut, improving its efficiency, which in general decreases over time, and might have beneficial effects on the motor symptom complications occurring under levodopa treatment (Guebila and Thiele, 2016; Nagashima *et al*., 2016). Apart from its usage for treatment and prevention strategies, our data suggests that serine could potentially be used for diagnostics. We observed that serine blood plasma levels were increased in 5 LRRK2-G2019S patients compared to 25 healthy individuals and 25 idiopathic cases. D-serine could eventually be used as very early blood biomarker for LRRK2-G2019S carrier identification. Interestingly, from the five LRRK2-G2019S cases we analyzed, one asymptomatic carrier unexpectedly revealed the highest serine levels, which suggests again that there might be a compensatory mechanism involved. In contrast to what we observed, serine was also increased in 50 idiopathic early-onset untreated PD patients compared to healthy controls (Trezzi *et al*., 2017 unpublished). This discrepancy might be linked to the age of onset of the patients used in that study and to the fact that the blood sampling was performed prior to any treatment. In our study, receipt of treatment and age of onset were not a selection criterium for idiopathic patients. Nevertheless, this observation highlights the importance and necessity of further studying serine in PD.

We identified SRR as a potential genetic modifier within the patient genetic background and showed that serine metabolism is impaired in NESCs and plays a major role in neurodegenerative diseases, as well as in proper neural development. Moreover, SRR and LRRK2 potentially complement or compensate each other and D-serine might represent a valuable diagnostic, prevention, and treatment strategy for PD. Thus, SRR activity, D-serine expression and the potential mechanisms behind the

deregulations in NESCs and DNs with and without LRRK2-G2019S induced PD should be evaluated in future studies.

D - PD AS A NEURODEVELOPMENTAL DISEASE

We discovered several PD-associated phenotypes such as impaired stem cell renewal and neurogenesis and their possible underlying genetic factors including, for instance, LRRK2-G2019S and SRR. In this chapter, the focus will be put on the question of what these deregulations mean for the patients. As described above we used cells reminiscent of the developing neural tube in order to study PD pathogenesis and our model adequately recapitulates this neurodevelopmental stage (see chapter A). As we worked with a developmental model system, first the neurodevelopmental deregulations that we observed within the PD-associated lines should be addressed.

We were able to show that the patient stem cell signature clearly differs from that of the healthy one, and pathway enrichment analysis demonstrated that genes involved in the developmental process in particular are deregulated. From the 865 DEGs between healthy and patient cell lines, listed in paper III, differential disease model networks were generated in order to visualize the interactions between DEGs (see appendix 1.2). These networks appropriately recapitulate the developmental component as they include genes from the homeobox (HOX), SOX, PAX, NOTCH, and OCT family, as well as some major stem cell fate regulator genes of NESCs. The stem cell fate core regulator genes of our healthy NESC model were previously identified using the H3K27ac signature of ChIP-seq data and a computational algorithm (see appendix 1.3). Within the DEGs from healthy individuals and patients, we found three brain-specific OCT genes (POU3F2, POU6F2 POU3F4), where one of them is involved in striatal neuron precursor differentiation and another one represents one of the key regulators of hNESCs (see appendix 1.3) (Shimazaki *et al*., 1999). Two other DEGs, NR2F1 and NR2F2, also represent core regulatory factors of NESCs and are involved in the temporal specification of NSC fate within the CNS (see appendix 1.3) (Naka *et al*., 2008). Additionally, NR2F1 is described as a typical marker for the rosette-like NESC state (Koch *et al*. 2009). Besides the core regulators, SOX3 is differentially expressed and – together with SOX1 and 2 – is required for neural stem cell maintenance and is expressed in the neuroepithelium (Wegner and Stolt, 2005). Further genes differentially expressed and involved in stem cell maintenance, as described in section 2.4.1, are the PAX6 and FGF genes. On the other hand, the DEG SOX11 is transiently expressed in maturing neurons, showing that not only maintenance but also neurodevelopmental genes are affected in patient NESCs (Wegner and Stolt, 2005). We could further identify several differentially expressed HOX genes. HOX genes are an evolutionarily highly conserved family that determines the bilateral anterior-posterior body axis and influences stem cell fates (Seifert *et al*., 2015). It has been shown that in particular HOXB1 and HOXA2, both differentially expressed, are

involved in the formation of the hindbrain and represent important factors in motor neuron development (Jungbluth *et al*., 1999; Studer *et al*., 1996). Moreover DEGs, involved in MHB formation and maintenance, such as PAX2/5 and the NOTCH signaling pathway (NOTCH1 and Hes family BHLH transcription factor 5/3 (HES5/HES3)) must impair neuronal development in the patients (Hirata *et al*. 2001; Louvi & Artavanis-Tsakonas 2006). Other, not so well-known, DEGs involved in neurogenesis are the genes of the ZIC family, which were shown to regulate neurulation and interact with SHH as well as NOTCH signaling (Aruga, 2004). Lastly, different neuronal guiding molecules have been differentially expressed, such as doublecortin (DCX), neuropilins, ephrin receptors and transcription factors NGN1 and 3 but not 2 (NGN2 is needed for DN differentiation, see section 2.1.2). All in all, the genetic signature of patients shows that neurodevelopment must be drastically deregulated in these cells.

Evidence from prior studies have shown the implications of stem cells and genes involved in development for PD (see section 2.3.1 and 2.3.2). Besides the implication of LRRK2-G2019S on developmental genes, as highlighted above, and the substantial LRRK2-G2019S induced stem cell deregulations described in chapter B, we were able to show the involvement of other PD-relevant genes in neurodevelopment. Not only cells carrying the LRRK2-G2019S mutation, but also the cells in which we introduced mutations in α-SYN showed severe cellular phenotypes. Mutations in α-SYN, for instance, impaired basal respiration in isogenic NESC lines. This demonstrates that not only LRRK2-G2019S, but also mutations in *SNCA* cause deregulations that can be recapitulated within stem cells from the developing neural tube, thus emphasizing the importance of PD-associated genes and proteins in neuronal development. Moreover, some of these severe stem cell impairments persist during neuronal differentiation and impair proper neurogenesis. If these *in vitro* observations are extrapolated from our model system to the *in vivo* situation, these deregulations might have drastic consequences for patients.

PD, however, is not a developmental disease, where children are born with deficits, but by definition a variable, slow, progressive, and age-related disorder. So how can a disease with a neurodevelopmental component only manifest in the adult (Gupta and Kulhara, 2010). This is a question schizophrenia studies have already been addressing for several years. The field has come to the conclusion that schizophrenia is a progressive neurodevelopmental disorder where neurodevelopmental deficiencies do not rule out the neurodegenerative aspects of the disease. It is considered “a lifetime disorder of development, plasticity, and ageing with windows of vulnerability at all three stages of life” (Gupta and Kulhara, 2010). For instance, dopamine and glutamate, the two signaling molecules underlying the pathways deregulated in the disease both have neurodevelopmental roles such as cell proliferation, migration, and plasticity, as well as neurodegenerative implications, such as oxidative stress and excitoxicity (Gupta and Kulhara, 2010). This might potentially also be true for LRRK2-G2019S and SRR.

In PD, a progressive neurodevelopmental hypothesis could explain the developmental component we observed (stem cell deregulations and impaired neurogenesis), as well as the existence of severe juvenile cases. The substantial stem cell impairments we observed in our *in vitro* disease model system might not necessarily lead to complete niche depletions *in vivo*, but might instead only slightly impair neurogenesis. Embryonic development is a much more complex process compared to the *in vitro* disease model we used (see chapter A). *In vivo*, the tempo-spatial patterning and three-dimensional environment, as well as the different morphogen gradients and signaling molecules, provide the cells with highly diverse compensatory mechanisms. Furthermore, the cells do not stay within the same state for long. More pronounced protection or compensation opportunities and higher dynamics might result in less dramatic phenotypes *in vivo*. The here described developmental deficiencies are considered as a predisposition or susceptibility for developing PD rather than the trigger of PD itself. With regards to the multiple hit hypothesis, a very early developmental deficiency would only represent the first hit. *In vivo*, even minor neurodevelopmental defects could lead to major complications such as more vulnerable or fewer DNs. Minor deficits during development might lead to a lower compensatory capacity of the entire system. In this case, cumulative hits of genetic or environmental nature, on top of the first developmentally associated hit, could perturb the entire system, which could fall out of balance and lead to what is called Parkinson's disease. The developmental susceptibility for PD might explain why more than one mutation is able to cause the same disease. Furthermore, it could explain the different ages of onsets of the same mutation, which depend on the severity of the hits and the compensatory mechanisms in place.

If the developmental component to PD pathogenesis is justified, very early diagnostic and treatment strategies should be envisioned. The neurodevelopmental deregulations could potentially facilitate the identification and treatment of the disease before irreversible neurodegeneration occurs. Future therapies should strive for very early intervention, prevention and risk management. The use of neurotrophic factors that boost neurodevelopment have been previously used for regenerative and neuroprotective strategies. However, their use was restricted to damage limitations and not promoted as a prevention strategy. Moreover, strategies, such as limiting environmental risk factors and promoting beneficial factors could be adopted. Furthermore, the discovery of early biomarkers for stratification of the disease should be envisioned. Finding a common biomarker that accounts for every form of PD will most likely prove elusive. Therefore, the focus should be placed on personalized therapies based on the individual genetic signatures, and precision medicine should represent the future for PD therapy.

CONCLUSION & OUTLOOK

CONCLUSION & OUTLOOK

E - CONCLUDING REMARKS AND FUTURE PERSPECTIVES

i. GENETIC MODIFIERS IN NSCs PREDISPOSE FOR PD

It can be concluded that patient-specific susceptibility factors within the genetic background of the NESC disease model, together with LRRK2-G2019S, impair development and predispose DNs for PD. Firstly, it has been shown that both NESCs and NSCs represent valid physiological relevant models for neurodegenerative disease modeling. Furthermore, the models were enhanced by the generation and usage of isogenic control lines, which highlighted the genetic contributions to PD. New insights into the disease-causing mechanisms of LRRK2-G2019S were provided. We were able to show that LRRK2-G2019 is sufficient to induce several PD-associated phenotypes in hNESCs, such as an increase in cell death and a decrease in mitosis in healthy NESC lines. Furthermore, we demonstrated that the PD patient genetic background plays an important role and complements LRRK2-G2019S pathogenicity. Gene-correcting LRRK2-G2019S was not sufficient to rescue the phenotypes. We unraveled the potential genetic modifiers underlying the disease phenotypes and identified SRR as a possible origin of the deregulations. D-serine administration reversed the observed phenotypes and validated the model by corrobating the integrity of the results. Our results suggest that D-serine might have the intrinsic potential to be used as a treatment strategy for PD. Moreover, similarly to LRRK2, D-serine plays an important role in development and neural stem cell regulation. The imbalance in the tight regulation of NESC homeostasis by both SRR impairments and LRRK2-G2019S must unavoidably lead to deficiencies in CNS development. In this thesis, various questions were answered, but new ones were also raised. A new hypothesis rose, that due to a complex spatio-temporal developmental procedure, *in vivo* compensatory mechanisms potentially mask the developmental component of PD, but confer an increased vulnerability to DNs. Furthermore the idea that PD is a multisystem and multifactorial disorder where different regions and developmental stages are affected and where different mutations and deregulations are cumulative and together lead to a similar outcome was reinforced. Ultimately, this study highlighted the complexity of PD and potentially produced new trains of thought that may lead to a better understanding of the disease in the future.

ii. CHALLENGES AHEAD

The research of this thesis gives rise to different speculations and opens up a number of research lines that could be explored in future studies. The different *in vitro* model systems could be used in future to study the role of astrocytes in PD, DN development and co-cultures of astrocytes and DNs. To further increase the complexity of the models, 3D organoids should be created. Moreover, the NESC model system should be further pushed into midbrain-specific development. Regarding LRRK2-G2019S, its role should be studied throughout these different cellular models. Additionally, proteomics and ChIP-seq could elucidate whether LRRK2-G2019S insertion and gene-correction does affect other cellular regulator levels, as it seems to have little effect on gene expression. With the discovery of SRR and the incomplete cellular penetrance of LRRK2-G2019S, the question arose as to how these two complement each other. Does SRR interacts directly or indirectly with LRRK2-G2019S, are there SNPs or mutations in the *SRR* gene that could be causative of PD, or is a compensatory mechanism at work? To address these questions, SRR could be studied in an LRRK2 KO cell line. Moreover, SRR KO lines, cololcalization studies, and IPs should be used to further elucidate the function and interaction of SRR and LRRK2. As we did not see any changes in SRR upon insertion or gene-correction of the LRRK2 mutation, the interaction is most probably depending on the healthy protein and might rather be based on an indirect mechanism. Therefore, it might be worth studying 4E-BP1 in our model, as it interacts with SRR and LRRK2. To address the hypothesis of a causative gene, the region in question could be sequenced and checked for potential pathogenic SNPs. An additional question is whether SRR is an LRRK2-G2019S carrier specific genetic modifier. SRR should, for instance, be studied in idiopathic cells. In a next step, the role of SRR in PD should be further elucidated. Serine metabolism, SRR, and D-serine activity should be studied in mature neurons, to see whether the deregulations persist, and to address NMDAR signaling. Moreover, as glial cells represent a major source of D-serine, their interaction could be studied, by co-culturing them with neurons. Additionally, other potential genetic modifiers discovered – apart from SRR – could be further investigated. Finally, the questions of whether PD has a developmental component and whether it can be considered a progressive neurodevelopmental disorder should be further explored, as it could have massive implications for how we perceive, diagnose, and treat the disease. Organoids that better recapitulate embryonic development with different mutations, in particular those causing juvenile PD, could be used for that purpose. For patients, a further layer of complexity inherent to the disease, in the form of a developmental predisposition or a novel genetic susceptibility, might further complicate diagnosis and treatment. Nevertheless, once stratifications and personalized therapies become the state of the art in the medical field, the different genetic and developmental components might facilitate early diagnosis and early

treatment. Every trigger and genetic culprit associated with the disease that can not only be identified, but also potentially targeted before neurodegeneration occurs, brings us one step closer to the prevention and thus the eradication of PD.

REFERENCES

REFERENCES

Abeliovich, A., and Hammond, R. (2007). Midbrain dopamine neuron differentiation: Factors and fates. Dev. Biol. *304*, 447–454.

Abou-Sleiman, P.M., Muqit, M.M., and Wood, N.W. (2006). Expanding insights of mitochondrial dysfunction in Parkinson's disease. Nat Rev Neurosci *7*, 207–219.

Aguila, J.C., Hedlund, E., and Sanchez-Pernaute, R. (2012). Cellular programming and reprogramming: Sculpting cell fate for the production of dopamine neurons for cell therapy. Stem Cells Int. *2*.

Allen, M., Burgess, J.D., Ballard, T., Serie, D., Wang, X., Younkin, C.S., Sun, Z., Kouri, N., Baheti, S., Wang, C., et al. (2016). Gene expression, methylation and neuropathology correlations at progressive supranuclear palsy risk loci. Acta Neuropathol. *132*, 1–15.

Altman, J., and Das, G.D. (1965). Autoradiographic and histologicalevidence of postnatal hippocampal neurogenesis in rats. J. Comp. Neurol. *124*, 319–335.

Apple, D.M., Fonseca, R.S., and Kokovay, E. (2016). The role of adult neurogenesis in psychiatric and cognitive disorders. Brain Res. *1655*, 270–276.

Aruga, J. (2004). The role of Zic genes in neural development. Mol. Cell. Neurosci. *26*, 205–221.

Avellar, M., Scoriels, L., Madeira, C., Vargas-Lopes, C., Nascimento, P. Do, Dantas, C., Manhães, A.C., Leite, H., and Panizzutti, R. (2016). The effect of D-serine administration on cognition and mood in older adults. Oncotarget.

Avior, Y., Sagi, I., and Benvenisty, N. (2016). Pluripotent stem cells in disease modelling and drug discovery. Nat. Rev. Mol. Cell Biol.

Badiola, N., de Oliveira, R.M., Herrera, F., Guardia-Laguarta, C., Gonçalves, S.A., Pera, M., Suárez-Calvet, M., Clarimon, J., Outeiro, T.F., and Lleó, A. (2011). Tau enhances α-synuclein aggregation and toxicity in cellular models of synucleinopathy. PLoS One *6*, 1–9.

Bahnassawy, L., Nicklas, S., Palm, T., Menzl, I., Birzele, F., Gillardon, F., and Schwamborn, J.C. (2013). The parkinson's disease-associated LRRK2 mutation R1441G inhibits neuronal differentiation of neural stem cells. Stem Cells Dev. *22*, 2487–2496.

Balu, D.T., Li, Y., Puhl, M.D., Benneyworth, M.A., Basu, A.C., Takagi, S., Bolshakov, V.Y., and Coyle, J.T. (2013). Multiple risk pathways for schizophrenia converge in serine racemase knockout mice, a mouse model of NMDA receptor hypofunction. Proc. Natl. Acad. Sci. U. S. A. *110*, E2400-9.

Barres, B.A. (2008). The Mystery and Magic of Glia: A Perspective on Their Roles in Health and Disease. Neuron *60*, 430–440.

Bartels, T., Choi, J.G., and Selkoe, D.J. (2011). α-Synuclein occurs physiologically as a helically folded tetramer that resists aggregation. Nature *477*, 107–110.

Beilina, A., Rudenko, I.N., Kaganovich, A., Civiero, L., Chau, H., Kalia, S.K., Kalia, L. V, Lobbestael, E., Chia, R., Ndukwe, K., et al. (2014). Unbiased screen for interactors of leucine-rich repeat kinase 2 supports a common pathway for sporadic and familial Parkinson disease. Proc. Natl. Acad. Sci. U. S. A. *111*, 2626–2631.

Bendor, J.T., Logan, T.P., and Edwards, R.H. (2013). The function of α-synuclein. Neuron *79*, 1044–1066.

Berg, D., Holzmann, C., and Riess, O. (2003). 14-3-3 Proteins in the Nervous System. Nat. Rev. Neurosci. *4*, 752–762.

Berg, D., Schweitzer, K.J., and Leitner, P, E. Al (2005). Type and frequency of mutations in the LRRK2 gene in familial and sporadic Parkinson's disease*. Brain *128*, 3000–3011.

Van Den Berge, S. a., Van Strien, M.E., Korecka, J. a., Dijkstra, A. a., Sluijs, J. a., Kooijman, L., Eggers, R.,

De Filippis, L., Vescovi, A.L., Verhaagen, J., et al. (2011). The proliferative capacity of the subventricular zone is maintained in the parkinsonian brain. Brain *134*, 3249–3263.

Bertoncini, C.W., Fernandez, C.O., Griesinger, C., Jovin, T.M., and Zweckstetter, M. (2005). Familial mutants of α-synuclein with increased neurotoxicity have a destabilized conformation. J. Biol. Chem. *280*, 30649–30652.

Berwick, D.C., and Harvey, K. (2011). LRRK2 signaling pathways: the key to unlocking neurodegeneration? Trends Cell Biol. *21*, 257–265.

Berwick, D.C., and Harvey, K. (2013). LRRK2 : an éminence grise of Wnt-mediated neurogenesis ? Front. Cell. Neurosci. *7*, 1–13.

Betarbet, R., Sherer, T.B., Mackenzie, G., Garcia-osuna, M., Panov, A. V, and Greenamyre, J.T. (2000). Chronic systemic pesticide exposure reproduces features of Parkinson's disease. Nat. Neurosci. *3*, 1301–1306.

Bibel, M., Richter, J., Schrenk, K., Tucker, K.L., Staiger, V., Korte, M., Goetz, M., and Barde, Y.A. (2004). Differentiation of mouse embryonic stem cells into a defined neuronal lineage. Nat Neurosci *7*, 1003–1009.

Biosa, A., Trancikova, A., Civiero, L., Glauser, L., Bubacco, L., Greggio, E., and Moore, D.J. (2013). GTPase activity regulates kinase activity and cellular phenotypes of parkinson's disease-associated LRRK2. Hum. Mol. Genet. *22*, 1140–1156.

Boldrini, M., Underwood, M.D., Hen, R., Rosoklija, G.B., Dwork, A.J., Mann, J.J., and Arango, V. (2009). Antidepressants increase neural progenitor cells in the human hippocampus HHS Public Access. Neuropsychopharmacology *34*, 2376–2389.

Bonifácio, M.J., Palma, P.N., Almeida, L., and Soares-da-Silva, P. (2007). Catechol-*O*-methyltransferase and Its Inhibitors in Parkinson's Disease. CNS Drug Rev. *13*, 352–379.

Bonifati, V., Rizzu, P., van Baren, M.J., Schaap, O., Breedveld, G.J., Krieger, E., Dekker, M.C.J., Squitieri, F., Ibanez, P., Joosse, M., et al. (2003). Mutations in the DJ-1 gene associated with autosomal recessive early-onset parkinsonism. Science *299*, 256–259.

Bonilla, S., Hall, A.C., Pinto, L., Attardo, A., Götz, M., Huttner, W.B., and Arenas, E. (2008). Identification of midbrain floor plate radial glia-like cells as dopaminergic progenitors. Glia *56*, 809–820.

Botta-Orfila, T., Ezquerra, M., Pastor, P., Fernández-Santiago, R., Pont-Sunyer, C., Compta, Y., Lorenzo-Betancor, O., Samaranch, L., Martí, M.J., Valldeoriola, F., et al. (2012). Age at onset in LRRK2-associated PD is modified by *SNCA* variants. J. Mol. Neurosci. *48*, 245–247.

Bourdenx, M., Dovero, S., Engeln, M., Bido, S., Bastide, M.F., Dutheil, N., Vollenweider, I., Baud, L., Piron, C., Grouthier, V., et al. (2015). Lack of additive role of ageing in nigrostriatal neurodegeneration triggered by α-synuclein overexpression. Acta Neuropathol. Commun. *3*, 46.

Boyaval, P., Moineau, S., Romero, D. a, and Horvath, P. (2007). Against Viruses in Prokaryotes. Science (80-.). *315*, 1709–1712.

Braak, H., Del Tredici, K., Rüb, U., De Vos, R. a I., Jansen Steur, E.N.H., and Braak, E. (2003). Staging of brain pathology related to sporadic Parkinson's disease. Neurobiol. Aging *24*, 197–211.

Braak, H., Sastre, M., and Del Tredici, K. (2007). Development of α-synuclein immunoreactive astrocytes in the forebrain parallels stages of intraneuronal pathology in sporadic Parkinson's disease. Acta Neuropathol. *114*, 231–241.

Bramanti, V., Tomassoni, D., Avitabile, M., Amenta, F., and Avola, R. (2010). Biomarkers of glial cell proliferation and differentiation in culture No Title. Front. Biosci. *S2*, 558–570.

Brás, J., Guerreiro, R., and Hardy, J. (2015). SnapShot: Genetics of Parkinson's Disease. Cell *160*, 570–570.e1.

Breitling, R., Armengaud, P., Amtmann, A., and Herzyk, P. (2004). Rank products: A simple, yet powerful, new method to detect differentially regulated genes in replicated microarray experiments. FEBS Lett. *573*, 83–92.

Buckley, K.M., Melikian, H.E., Provoda, C.J., and Waring, M.T. (2000). Regulation of neuronal function by protein trafficking: a role for the endosomal pathway. J. Physiol. *525 Pt 1*, 11–19.

Canu, N., Ciotti, M.T., and Pollegioni, L. (2014). Serine racemase: A key player in apoptosis and necrosis. Front. Synaptic Neurosci. *6*, 1–15.

Carpentier, P.A., and Palmer, T.D. (2009). Immune Influence on Adult Neural Stem Cell Regulation and Function. Neuron *64*, 79–92.

Casarosa, S., Zasso, J., and Conti, L. (2013). Systems for ex-vivo Isolation and Culturing of Neural Stem Cells. Neural Stem Cells - New Perspect. 3–28.

Chai, C., and Lim, K.-L. (2013). Genetic insights into sporadic Parkinson's disease pathogenesis. Curr. Genomics *14*, 486–501.

Chamberlain, S.J., Chen, P., Ng, K.Y., Bourgois-rocha, F., Lemtiri-chlieh, F., Levine, E.S., and Lalande, M. (2010). Induced pluripotent stem cell models of the genomic imprinting disorders Angelman and Prader – Willi syndromes. Pnas *107*, 17668–17673.

Chambers, S.M., Fasano, C. a, Papapetrou, E.P., Tomishima, M., Sadelain, M., and Studer, L. (2009). Highly efficient neural conversion of human ES and iPS cells by dual inhibition of SMAD signaling. Nat. Biotechnol. *27*, 275–280.

Chan, D., Citro, A., Cordy, J.M., Shen, G.C., and Wolozin, B. (2011). Rac1 protein rescues neurite retraction caused by G2019S leucine-rich repeat kinase 2 (LRRK2). J. Biol. Chem. *286*, 16140–16149.

Chandrasekaran, A., Avci, H.X., Leist, M., Kobolák, J., and Dinnyés, A. (2016). Astrocyte Differentiation of Human Pluripotent Stem Cells: New Tools for Neurological Disorder Research. Front. Cell. Neurosci. *10*, 215.

Charlesworth, G., Gandhi, S., Bras, J.M., Barker, R.A., Burn, D.J., Chinnery, P.F., Gentleman, S.M., Guerreiro, R., Hardy, J., Holton, J.L., et al. (2012). Tau acts as an independent genetic risk factor in pathologically proven PD. Neurobiol. Aging *33*, 838.e7-838.e11.

Chartier-Harlin, M.C., Kachergus, J., Roumier, C., Mouroux, V., Douay, X., Lincoln, S., Levecque, C., Larvor, L., Andrieux, J., Hulihan, M., et al. (2004). alpha-Synuclein locus duplication as a cause of familial Parkinson's disease. Lancet *364*, 1167–1169.

Chaudhuri, K.R., and Schapira, A.H. V (2009). Non-motor symptoms of Parkinson's disease: dopaminergic pathophysiology and treatment. Lancet Neurol. *8*, 464–474.

Chen, C.-Y., Weng, Y.-H., Chien, K.-Y., Lin, K.-J., Yeh, T.-H., Cheng, Y.-P., Lu, C.-S., and Wang, H.-L. (2012). (G2019S) LRRK2 activates MKK4-JNK pathway and causes degeneration of SN dopaminergic neurons in a transgenic mouse model of PD. Cell Death Differ. *19*, 1623–1633.

Cheng, H.C., Ulane, C.M., and Burke, R.E. (2010). Clinical progression in Parkinson's disease and the neurobiology of Axons. Ann. Neurol. *67*, 715–725.

Cheon, S.-M., Chan, L., Chan, D.K.Y., and Kim, J.W. (2012). Genetics of Parkinson's Disease - A Clinical Perspective. J. Mov. Disord. *5*, 33–41.

Cho, S.W., Kim, S., Kim, J.M., and Kim, J.-S. (2013). Targeted genome engineering in human cells with the Cas9 RNA-guided endonuclease. Nat. Biotechnol. *31*, 230–232.

Chuang, C.L., Lu, Y.N., Wang, H.C., and Chang, H.Y. (2014). Genetic dissection reveals that Akt is the critical kinase downstream of LRRK2 to phosphorylate and inhibit FOXO1, and promotes neuron survival. Hum. Mol. Genet. *23*, 5649–5658.

Cilia, R., Siri, C., Rusconi, D., Allegra, R., Ghiglietti, A., Sacilotto, G., Zini, M., Zecchinelli, A.L., Asselta, R.,

Duga, S., et al. (2014). LRRK2 mutations in Parkinson's disease: Confirmation of a gender effect in the Italian population. Park. Relat. Disord. *20*, 911–914.

Clark, L.N., Wang, Y., Karlins, E., Saito, L., Mejia-Santana, H., Harris, J., Louis, E.D., Cote, L.J., Andrews, H., Fahn, S., et al. (2006). Frequency of LRRK2 mutations in early- and late-onset Parkinson disease. Neurology *67*, 1786–1791.

Clinton, L.K., Blurton-Jones, M., Myczek, K., Trojanowski, J.Q., and LaFerla, F.M. (2010). Synergistic Interactions between Abeta, tau, and alpha-synuclein: acceleration of neuropathology and cognitive decline. J. Neurosci. *30*, 7281–7289.

Condic, M.L. (2014). Totipotency: What It Is and What It Is Not. Stem Cells Dev. *23*, 796–812.

Cong, L., Ran, F.A., Cox, D., Lin, S., Barretto, R., Hsu, P.D., Wu, X., Jiang, W., and Marraffini, L.A. (2013). Multiplex Genome Engineering Using CRISPR/VCas Systems. Science (80-.). *339*, 819–823.

Conti, L., and Cattaneo, E. (2010). Neural stem cell systems: physiological players or in vitro entities? Nat. Rev. Neurosci. *11*, 176–187.

Conti, L., Pollard, S.M., Gorba, T., Reitano, E., Toselli, M., Biella, G., Sun, Y., Sanzone, S., Ying, Q.L., Cattaneo, E., et al. (2005). Niche-independent symmetrical self-renewal of a mammalian tissue stem cell. PLoS Biol. *3*, 1594–1606.

Cook, D.A., Kannarkat, G.T., Cintron, A.F., Butkovich, L.M., Fraser, K.B., Chang, J., Grigoryan, N., Factor, S.A., West, A.B., Boss, J.M., et al. (2017). LRRK2 levels in immune cells are increased in Parkinson's disease. Npj Park. Dis. *3*, 11.

Cookson, M.R. (2009). alpha-Synuclein and neuronal cell death. Mol Neurodegener *4*, 9.

Cookson, M.R. (2010). The role of leucine-rich repeat kinase 2 (LRRK2) in Parkinson's disease. Nat. Rev. Neurosci. *11*, 791–797.

Cookson, M.R. (2015). LRRK2 Pathways Leading to Neurodegeneration. Curr. Neurol. Neurosci. Rep. *15*.

Cox, P.A., Davis, D.A., Mash, D.C., Metcalf, J.S., and Banack, S.A. (2016). Dietary exposure to an environmental toxin triggers neurofibrillary tangles and amyloid deposits in the brain. Proc. R. Soc. B Biol. Sci. *283*, 1–10.

Cuervo, A.M. (2004). Impaired Degradation of Mutant -Synuclein by Chaperone-Mediated Autophagy. Science (80-.). *305*, 1292–1295.

Cummings, K.A., and Popescu, G.K. (2015). Glycine-dependent activation of NMDA receptors. J. Gen. Physiol. *145*, 513–527.

Curtis, M. a, Eriksson, P.S., and Faull, R.L. (2007a). Progenitor Cells and Adult Neurogenesis in Neurodegenerative Diseases and Injuries of the Basal Ganglia. Clin Exp Pharmacol Physiol *34*, 528–532.

Curtis, M. a, Faull, R.L.M., and Eriksson, P.S. (2007b). The effect of neurodegenerative diseases on the subventricular zone. Nat. Rev. Neurosci. *8*, 712–723.

Daley, G.Q., and Scadden, D.T. (2008). Prospects for Stem Cell-Based Therapy. Cell *132*, 544–548.

Daubner, S.C., Le, T., and Wang, S. (2012). Tyrosine Hydroxylase and Regulation of Dopamine Synthesis. Arch Biochem Biophys *508*, 1–12.

Davis, A.A., Andruska, K.M., Benitez, B.A., Racette, B.A., Perlmutter, J.S., and Cruchaga, C. (2016). Variants in GBA, *SNCA*, and MAPT Influence Parkinson Disease Risk, Age at Onset, and Progression. Neurobiol. Aging *37*, 209.e1-209.e7.

Deleidi, M., and Gasser, T. (2013). The role of inflammation in sporadic and familial Parkinson's disease. Cell. Mol. Life Sci. *70*, 4259–4273.

Deltcheva, E., Chylinski, K., Sharma, C.M., and Gonzales, K. (2011). CRISPR RNA maturation by trans - encoded small RNA and host factor RNase III. Nature *471*, 602–607.

Devine, M.J., Kaganovich, A., Ryten, M., Mamais, A., Trabzuni, D., Manzoni, C., McGoldrick, P., Chan, D., Dillman, A., Zerle, J., et al. (2011). Pathogenic LRRK2 mutations do not alter gene expression in cell model systems or human brain tissue. PLoS One *6*, e22489.

Dick, F.D., De Palma, G., Ahmadi, a, Scott, N.W., Prescott, G.J., Bennett, J., Semple, S., Dick, S., Counsell, C., Mozzoni, P., et al. (2007). Environmental risk factors for Parkinson's disease and parkinsonism: the Geoparkinson study. Occup. Environ. Med. *64*, 666–672.

Dickson, D.W. (2012). Parkinson's Disease and Parkinsonism : Neuropathology. 1–16.

Durrant, A.R., and Heresco-levy, U. (2014). D-Serine in Neuropsychiatric Disorders : New Advances. *2014*.

Van Den Eeden, S.K. (2003). Incidence of Parkinson's Disease: Variation by Age, Gender, and Race/Ethnicity. Am. J. Epidemiol. *157*, 1015–1022.

Elkabetz, Y., Panagiotakos, G., Al Shamy, G., Socci, N.D., Tabar, V., and Studer, L. (2008). Human ES cell-derived neural rosettes reveal a functionally distinct early neural stem cell stage. Genes Dev. *22*, 152–165.

Eriksson, P.S., Perfilieva, E., Björk-Eriksson, T., Alborn, a M., Nordborg, C., Peterson, D. a, and Gage, F.H. (1998). Neurogenesis in the adult human hippocampus. Nat. Med. *4*, 1313–1317.

Ernst, A., Alkass, K., Bernard, S., Salehpour, M., Perl, S., Tisdale, J., Possnert, G., Druid, H., and Frisén, J. (2014). Neurogenesis in the striatum of the adult human brain. Cell *156*, 1072–1083.

Evans, M.J., and Kaufman, M.H. (1981). Establishment in culture of pluripotential cells from mouse embryos. Nature *292*, 154–156.

Falk, A., Koch, P., Kesavan, J., Takashima, Y., Ladewig, J., Alexander, M., Wiskow, O., Tailor, J., Trotter, M., Pollard, S., et al. (2012). Capture of neuroepithelial-like stem cells from pluripotent stem cells provides a versatile system for in vitro production of human neurons. PLoS One *7*, e29597.

Farrer, M.J. (2006). Genetics of Parkinson disease: paradigm shifts and future prospects. Nat. Rev. Genet. *7*, 306–318.

Fedorow, H., Tribl, F., Halliday, G., Gerlach, M., Riederer, P., and Double, K.L. (2005). Neuromelanin in human dopamine neurons: Comparison with peripheral melanins and relevance to Parkinson's disease. Prog. Neurobiol. *75*, 109–124.

Fernández-santiago, R., Carballo-carbajal, I., Castellano, G., Torrent, R., Richaud, Y., Sánchez-danés, A., Vilarrasa-blasi, R., Sánchez-pla, A., Raya, Á., Vila, M., et al. (2015). Aberrant epigenome in iPSC-derived dopaminergic neurons from Parkinson ' s disease patients. 1–18.

Di Fonzo, A., Wu-Chou, Y.H., Lu, C.S., Van Doeselaar, M., Simons, E.J., Rohé, C.F., Chang, H.C., Chen, R.S., Weng, Y.H., Vanacore, N., et al. (2006). A common missense variant in the LRRK2 gene, Gly2385Arg, associated with Parkinson's disease risk in Taiwan. Neurogenetics *7*, 133–138.

Frobel, J., Hemeda, H., Lenz, M., Abagnale, G., Joussen, S., Denecke, B., Šarić, T., Zenke, M., and Wagner, W. (2014). Epigenetic rejuvenation of mesenchymal stromal cells derived from induced pluripotent stem cells. Stem Cell Reports *3*, 414–422.

Fu, M.-H., Li, C.-L., Lin, H.-L., Chen, P.-C., Calkins, M.J., Chang, Y.-F., Cheng, P.-H., and Yang, S.-H. (2015). Stem cell transplantation therapy in Parkinson's disease. Springerplus *4*, 597.

Fu, Y., Foden, J. a, Khayter, C., Maeder, M.L., Reyon, D., Joung, K., and Sander, J.D. (2014a). NIH Public Access. Nat. Biotechnol *31*, 822–826.

Fu, Y., Sander, J.D., Reyon, D., Cascio, V.M., and Joung, J.K. (2014b). Improving CRISPR-Cas nuclease specificity using truncated guide RNAs. Nat. Biotechnol. *32*, 279–284.

Fuchs, J., Nilsson, C., Kachergus, J., Munz, M., Larsson, E.M., Schüle, B., Langston, J.W., Middleton, F.A., Ross, O.A., Hulihan, M., et al. (2007). Phenotypic variation in a large Swedish pedigree due to *SNCA*

duplication and triplication. Neurology *68*, 916–922.

Fujii, K., Maeda, K., Hikida, T., Mustafa, a K., Balkissoon, R., Xia, J., Yamada, T., Ozeki, Y., Kawahara, R., Okawa, M., et al. (2006). Serine racemase binds to PICK1: potential relevance to schizophrenia. Mol. Psychiatry *11*, 150–157.

Funayama, M., Hasegawa, K., Kowa, H., Saito, M., Tsuji, S., and Obata, F. (2002). A new locus for Parkinson's Disease (PARK8) maps to chromosome 12p11.2-q13.1. Ann. Neurol. *51*, 296–301.

Funayama, M., Ohe, K., Amo, T., Furuya, N., Yamaguchi, J., Saiki, S., Li, Y., Ogaki, K., Ando, M., Yoshino, H., et al. (2015). CHCHD2 mutations in autosomal dominant late-onset Parkinson's disease: A genome-wide linkage and sequencing study. Lancet Neurol. *14*, 274–282.

Furness, J.B., Rivera, L.R., Cho, H.J., Bravo, D.M., and Callaghan, B. (2013). The gut as a sensory organ. Nat. Rev. Gastroenterol. Hepatol. *10*, 729–740.

Gage, F.H. (2000). Mammalian Neural Stem Cells. *287*, 1433–1439.

Gaig, C., Martí, M.J., Ezquerra, M., Rey, M.J., Cardozo, A., and Tolosa, E. (2007). G2019S LRRK2 mutation causing Parkinson's disease without Lewy bodies. J. Neurol. Neurosurg. Psychiatry *78*, 626–628.

Gale, E., and Li, M. (2008). Midbrain dopaminergic neuron fate specification: Of mice and embryonic stem cells. Mol. Brain *1*, 8.

Galvez, T., Gilleron, J., Zerial, M., and O'Sullivan, G. a. (2012). SnapShot: Mammalian Rab Proteins in Endocytic Trafficking. Cell *151*, 234–234.e2.

Gamberino, W.C., Berkich, D. a, Lynch, C.J., Xu, B., and LaNoue, K.F. (1997). Role of pyruvate carboxylase in facilitation of synthesis of glutamate and glutamine in cultured astrocytes. J. Neurochem. *69*, 2312–2325.

Garcia-Reitboeck, P., Anichtchik, O., Dalley, J.W., Ninkina, N., Tofaris, G.K., Buchman, V.L., and Spillantini, M.G. (2013). Endogenous alpha-synuclein influences the number of dopaminergic neurons in mouse substantia nigra. Exp. Neurol. *248*, 541–545.

García Ruiz, P.J. (2004). Prehistory of Parkinson's disease. Neurol. 2004 Dec;19(10)735-7.

Gatto, E.M., Parisi, V., Converso, D.P., Poderoso, J.J., Carreras, M.C., Martí-Massó, J.F., and Paisán-Ruiz, C. (2013). The LRRK2 G2019S mutation in a series of Argentinean patients with Parkinson's disease: Clinical and demographic characteristics. Neurosci. Lett. *537*, 1–5.

Gehrke, S., Imai, Y., Sokol, N., and Lu, B. (2010). Pathogenic LRRK2 negatively regulates microRNA-mediated translational repression. Nature *466*, 637–641.

Gelfin, E., Kaufman, Y., Korn-Lubetzki, I., Bloch, B., Kremer, I., Javitt, D.C., and Heresco-Levy, U. (2011). D-serine adjuvant treatment alleviates behavioural and motor symptoms in Parkinson's disease. Int. J. Neuropsychopharmacol. 1–7.

Gilks, W.P., Abou-Sleiman, P.M., Gandhi, S., Jain, S., Singleton, A., Lees, A.J., Shaw, K., Bhatia, K.P., Bonifati, V., Quinn, N.P., et al. (2005). A common LRRK2 mutation in idiopathic Parkinson's disease. Lancet *365*, 415–416.

Glaab, E., and Schneider, R. (2015). Comparative pathway and network analysis of brain transcriptome changes during adult aging and in Parkinson's disease. Neurobiol. Dis. *74*, 1–13.

Goedert, M., Spillantini, M.G., Del Tredici, K., and Braak, H. (2013). 100 years of Lewy pathology. Nat Rev Neurol *9*, 13–24.

Golub, Y., Berg, D., Calne, D.B., Pfeiffer, R.F., Uitti, R.J., Stoessl, a J., Wszolek, Z.K., Farrer, M.J., Mueller, J.C., Gasser, T., et al. (2009). Genetic factors influencing age at onset in LRRK2-linked Parkinson disease. Parkinsonism Relat. Disord. *15*, 539–541.

Gonzalez-cano, L., Menzl, I., Tisserand, J., Nicklas, S., and Jens, C. Parkinson ' s disease associated

mutant LRRK2 mediated inhibition of miRNA activity is antagonized by TRIM32 .

González-Hernández, T. (2010). Vulnerability of mesostriatal dopaminergic neurons in Parkinson's disease. Front. Neuroanat. *4*, 14.

Götz, M., and Huttner, W.B. (2005). The cell biology of neurogenesis. Nat Rev Mol Cell Biol *6*, 777–788.

Le Grand, J.N., Gonzalez-Cano, L., Pavlou, M.A., and Schwamborn, J.C. (2014). Neural stem cells in Parkinson's disease: A role for neurogenesis defects in onset and progression. Cell. Mol. Life Sci. *72*, 773–797.

Greene, J.C., Whitworth, A.J., Kuo, I., Andrews, L.A., Feany, M.B., and Pallanck, L.J. (2003). Mitochondrial pathology and apoptotic muscle degeneration in Drosophila parkin mutants. Proc. Natl. Acad. Sci. U. S. A. *100*, 4078–4083.

Guebila, M. Ben, and Thiele, I. (2016). Model-based dietary optimization for late-stage, levodopa-treated, Parkinson's disease patients. Npj Syst. Biol. Appl. *2*, 16013.

Guerreiro, P.S., Huang, Y., Gysbers, A., Cheng, D., Gai, W.P., Outeiro, T.F., and Halliday, G.M. (2013). LRRK2 interactions with α-synuclein in Parkinson's disease brains and in cell models. J. Mol. Med. (Berl). *91*, 513–522.

Gupta, S., and Kulhara, P. (2010). What is schizophrenia: A neurodevelopmental or neurodegenerative disorder or a combination of both? A critical analysis. Indian J. Psychiatry *52*, 21–27.

Hackett, J.A., and Azim Surani, M. (2014). Regulatory principles of pluripotency: From the ground state up. Cell Stem Cell *15*, 416–430.

Haile, Y., Deng, X., Ortiz-Sandoval, C., Tahbaz, N., Janowicz, A., Lu, J.-Q., Kerr, B.J., Gutowski, N.J., Holley, J.E., Eggleton, P., et al. (2017). Rab32 connects ER stress to mitochondrial defects in multiple sclerosis. J. Neuroinflammation *14*, 19.

Hallett, P.J., and Standaert, D.G. (2004). Rationale for and use of NMDA receptor antagonists in Parkinson's disease. Pharmacol. Ther. *102*, 155–174.

Halliwell, B. (1996). Antioxidants in Human Health and Disease. Annu. Rev. Nutr. *16*, 33–50.

Hargus, G., Ehrlich, M., Araúzo-Bravo, M.J., Hemmer, K., Hallmann, A.L., Reinhardt, P., Kim, K.P., Adachi, K., Santourlidis, S., Ghanjati, F., et al. (2014). Origin-dependent neural cell identities in differentiated human iPSCs in vitro and after transplantation into the mouse brain. Cell Rep. *8*, 1697–1703.

Hasseler, R. (1938). Zur pathologie der paralysis agitans und des postencephalitschen Parkinsonismus. J. Psychol. Neurol. *48,* 387–476.

Healy, D.G., Falchi, M., O'Sullivan, S.S., Bonifati, V., Durr, A., Bressman, S., Brice, A., Aasly, J., Zabetian, C.P., Goldwurm, S., et al. (2008). Phenotype, genotype, and worldwide genetic penetrance of LRRK2-associated Parkinson's disease: a case-control study. Lancet Neurol. *7*, 583–590.

Henneberger, C., Papouin, T., Oliet, S.H.R., and Rusakov, D. a (2010). Long-term potentiation depends on release of D-serine from astrocytes. Nature *463*, 232–236.

Hentati, F., Trinh, J., Thompson, C., Nosova, E., Farrer, M.J., and Aasly, J.O. (2014). LRRK2 parkinsonism in Tunisia and Norway: A comparative analysis of disease penetrance. Neurology *83*, 568–569.

Hiller, K., Hangebrauk, J., Jager, C., Spura, J., Schreiber, K., and Schomburg, D. (2009). MetaboliteDetector: comprehensive analysis tool for targeted and nontargeted GC/MS based metabolome analysis. Anal. Chem. *81*, 3429–3439.

Hillje, A.-L., and Schwamborn, J.C. (2016). Utilization of stem cells to model Parkinson's disease – current state and future challenges. Future Neurol. *11*, 171–186.

Hirata, H., Tomita, K., Bessho, Y., and Kageyama, R. (2001). Hes1 and Hes3 regulate maintenance of the isthmic organizer and development of the mid/hindbrain. EMBO J. *20*, 4454–4466.

Hirsch, E., Graybiel, a M., and Agid, Y. a (1988). Melanized dopaminergic neurons are differentially susceptible to degeneration in Parkinson's disease. Nature *334*, 345–348.

Ho, C.C.-Y., Rideout, H.J., Ribe, E., Troy, C.M., and Dauer, W.T. (2009). The Parkinson disease protein leucine-rich repeat kinase 2 transduces death signals via Fas-associated protein with death domain and caspase-8 in a cellular model of neurodegeneration. J. Neurosci. *29*, 1011–1016.

Hoehn, M.M., and Yahr, M.D. (1967). Parkinsonism : onset , progression , and mortality.

Höglinger, G.U., Rizk, P., Muriel, M.P., Duyckaerts, C., Oertel, W.H., Caille, I., and Hirsch, E.C. (2004). Dopamine depletion impairs precursor cell proliferation in Parkinson disease. Nat. Neurosci. *7*, 726–735.

Höglinger, G.U., Melhem, N.M., Dickson, D.W., Sleiman, P.M. a, Wang, L.-S., Klei, L., Rademakers, R., de Silva, R., Litvan, I., Riley, D.E., et al. (2011). Identification of common variants influencing risk of the tauopathy progressive supranuclear palsy. Nat. Genet. *43*, 699–705.

Van Horn, M.R., Sild, M., and Ruthazer, E.S. (2013). D-serine as a gliotransmitter and its roles in brain development and disease. Front. Cell. Neurosci. *7*, 39.

Horner, P.J., and Gage, F.H. (2000). Regenerating the damaged central nervous system. Nature *407*, 963–970.

Huang, X., Kong, H., Tang, M., Lu, M., Ding, J.-H., and Hu, G. (2012). D-Serine regulates proliferation and neuronal differentiation of neural stem cells from postnatal mouse forebrain. CNS Neurosci. Ther. *18*, 4–13.

Iaccarino, C., Crosio, C., Vitale, C., Sanna, G., Carrí, M.T., and Barone, P. (2007). Apoptotic mechanisms in mutant LRRK2-mediated cell death. Hum. Mol. Genet. *16*, 1319–1326.

Imai, Y., Gehrke, S., Wang, H.-Q., Takahashi, R., Hasegawa, K., Oota, E., and Lu, B. (2008). Phosphorylation of 4E-BP by LRRK2 affects the maintenance of dopaminergic neurons in Drosophila. EMBO J. *27*, 2432–2443.

Ishizawa, T., Mattila, P., Davies, P., Wang, D.S., and Dickson, D.W. (2003). Colocalization of tau and α-synuclein epitopes in Lewy bodies. J. Neuropathol. Exp. Neurol. *62*, 389–397.

Jäger, C., Hiller, K., and Manuel, B. (2016). Metabolic Profiling and Quantification of Neurotransmitters in Mouse Brain by Gas Chromatography-Mass Spectrometry. Curr. Protoc. Mouse Biol. 333–342.

Jaleel, M., Nichols, R.J., Deak, M., Campbell, D.G., Gillardon, F., Knebel, A., and Alessi, D.R. (2007). LRRK2 phosphorylates moesin at threonine-558: characterization of how Parkinson's disease mutants affect kinase activity. Biochem. J. *405*, 307–317.

Jankovic, J., Chen, S., and Le, W.D. (2005). The role of Nurr1 in the development of dopaminergic neurons and Parkinson's disease. Prog. Neurobiol. *77*, 128–138.

Jinek, M., Chylinski, K., Fonfara, I., Hauer, M., Doudna, J.A., and Charpentier, E. (2012). A Programmable Dual-RNA – Guided. *337*, 816–822.

Johnson, K. a, Conn, P.J., and Niswender, C.M. (2009). Glutamate receptors as therapeutic targets for Parkinson's disease. CNS Neurol. Disord. Drug Targets *8*, 475–491.

Jungbluth, S., Bell, E., and Lumsden, A. (1999). Specification of distinct motor neuron identities by the singular activities of individual Hox genes. Development *126*, 2751–2758.

Kalinderi, K., Bostantjopoulou, S., and Fidani, L. (2016). The genetic background of Parkinson's disease: Current progress and future prospects. Acta Neurol. Scand. 314–326.

Kawakami, F., and Ichikawa, T. (2015). The Role of alpha-Synuclein and LRRK2 in Tau Phosphorylation. Parkinsons. Dis. *2015*, 734746.

Keane, P.C., Kurzawa, M., Blain, P.G., and Morris, C.M. (2011). Mitochondrial Dysfunction in Parkinson's

Disease. Parkinsons. Dis. *2011*, 1–18.

Kim, H., and Kim, J.S. (2014). A guide to genome engineering with programmable nucleases. Nat Rev Genet *15*, 321–334.

Kim, K., Doi, A., Wen, B., Ng, K., Zhao, R., Cahan, P., Kim, J., Aryee, M.J., Ji, H., Ehrlich, L.I.R., et al. (2010). Epigenetic memory in induced pluripotent stem cells. Nature *467*, 285–290.

Kim, P.M., Aizawa, H., Kim, P.S., Huang, A.S., Wickramasinghe, S.R., Kashani, A.H., Barrow, R.K., Huganir, R.L., Ghosh, A., and Snyder, S.H. (2005). Serine racemase: activation by glutamate neurotransmission via glutamate receptor interacting protein and mediation of neuronal migration. Proc. Natl. Acad. Sci. U. S. A. *102*, 2105–2110.

Kirik, D., Annett, L.E., Burger, C., Muzyczka, N., Mandel, R.J., and Bjorklund, A. (2003). Nigrostriatal -synucleinopathy induced by viral vector-mediated overexpression of human -synuclein: A new primate model of Parkinson's disease. Proc. Natl. Acad. Sci. *100*, 2884–2889.

Kitada, T., Asakawa, S., Hattori, N., Matsumine, H., Yamamura, Y., Minoshima, S., Yokochi, M., Mizuno, Y., and Shimizu, N. (1998). Mutations in the parkin gene cause autosomal recessive juvenile parkinsonism. Nature *392*, 605–608.

Klein, C., and Schlossmacher, M.G. (2006). The genetics of Parkinson disease: Implications for neurological care. Nat. Clin. Pract. Neurol. *2*, 136–146.

Klein, C., and Westenberger, A. (2012). Genetics of Parkinson's disease. Cold Spring Harb. Perspect. Med. *2*, a008888.

Koch, P., Opitz, T., Steinbeck, J.A., Ladewig, J., and Brüstle, O. (2009). A rosette-type, self-renewing human ES cell-derived neural stem cell with potential for in vitro instruction and synaptic integration. Proc. Natl. Acad. Sci. U. S. A. *106*, 3225–3230.

Köroğlu, Ç., Baysal, L., Cetinkaya, M., Karasoy, H., and Tolun, A. (2013). DNAJC6 is responsible for juvenile parkinsonism with phenotypic variability. Park. Relat. Disord. *19*, 320–324.

Kriegstein, A., and Alvarez-buylla, A. (2011). The Glial Nature of Embryonic and Adult Neural Stem Cells. Annu. Rev. Neurosci. 149–184.

Krüger, R., Kuhn, W., Müller, T., Woitalla, D., Graeber, M., Kösel, S., Przuntek, H., Epplen, J.T., Schöls, L., and Riess, O. (1998). Ala30Pro mutation in the gene encoding alpha-synuclein in Parkinson's disease. Nat. Genet. *18*, 106–108.

Lanciego, J.L., Luquin, N., and Obeso, J.A. (2012). Functional neuroanatomy of the basal ganglia. Cold Spring Harb. Perspect. Med. *2*, 1–20.

Langston, J.W. (2006). The Parkinson's complex: Parkinsonism is just the tip of the Iceberg. Ann. Neurol. *59*, 591–596.

Langston JW, Ballard P, Tetrud JW, I.I. (2010). Chronic Parkinsonism in Humans due to a Product of Meperidine-Analog Synthesis. Adv. Sci. *219*, 979–980.

Latourelle, J.C., Dumitriu, A., Hadzi, T.C., Beach, T.G., and Myers, R.H. (2012). Evaluation of Parkinson Disease Risk Variants as Expression-QTLs. PLoS One *7*.

Lee, H., James, W.S., and Cowley, S.A. (2017). LRRK2 in peripheral and central nervous system innate immunity: its link to Parkinson's disease. Biochem. Soc. Trans. *45*, 131–139.

Lefcort, F., and George, L. (2007). Neural crest cell fate: to be or not to be prespecified. Cell Adh. Migr. *1*, 199–201.

Lendahl, U., Zimmerman, L.B., and McKay, R.D. (1990). CNS stem cells express a new class of intermediate filament protein. Cell *60*, 585–595.

Lesage, S., and Brice, A. (2009). Parkinson's disease: From monogenic forms to genetic susceptibility

factors. Hum. Mol. Genet. *18*, 48–59.

Lesage, S., Dürr, A., Tazir, M., Lohmann, E., Leutenegger, A.-L., Janin, S., Pollak, P., and Brice, A. (2006). *LRRK2* G2019S as a Cause of Parkinson's Disease in North African Arabs. N. Engl. J. Med. *354*, 422–423.

Levine, A.J., and Brivanlou, A.H. (2007). Proposal of a model of mammalian neural induction. Dev. Biol. *308*, 247–256.

Li, H., and Durbin, R. (2009). Fast and accurate short read alignment with Burrows–Wheeler transform. Bioinformatics *25*, 1754–1760.

Li, W., Sun, W., Zhang, Y., Wei, W., Ambasudhan, R., Xia, P., Talantova, M., Lin, T., Kim, J., Wang, X., et al. (2011). Rapid induction and long-term self-renewal of primitive neural precursors from human embryonic stem cells by small molecule inhibitors. Proc. Natl. Acad. Sci. U. S. A. *108*, 8299–8304.

Li, X., Patel, J.C., Wang, J., Avshalumov, M. V, Nicholson, C., Buxbaum, J.D., Elder, G.A., Rice, M.E., and Yue, Z. (2010). Enhanced Striatal Dopamine Transmission and Motor Performance with LRRK2 Overexpression in Mice is Eliminated by familial Parkinson's Disease Mutation G2019S. J. Neurosci. *30*, 1788–1797.

Lichtenberg, M., Mansilla, a, Zecchini, V.R., Fleming, a, and Rubinsztein, D.C. (2011). The Parkinson's disease protein LRRK2 impairs proteasome substrate clearance without affecting proteasome catalytic activity. Cell Death Dis. *2*, e196.

Lin, C.-H., Tsai, P.-I., Wu, R.-M., and Chien, C.-T. (2010). LRRK2 G2019S mutation induces dendrite degeneration through mislocalization and phosphorylation of tau by recruiting autoactivated GSK3ß. J. Neurosci. *30*, 13138–13149.

Lin, L., Doherty, D., Lile, J., Bektesh, S., and Collins, F. (1993). GDNF: a glial cell line-derived neurotrophic factor for midbrain dopaminergic neurons. Science (80-.). *260*, 1130–1132.

Liu, A., and Niswander, L.A. (2005). Bone morphogenetic protein signalling and vertebrate nervous system development. Nat. Rev. Neurosci. *6*, 945–954.

Liu, Z., and Lenardo, M.J. (2012). The role of LRRK2 in inflammatory bowel disease. Dig. Dis. *22*, 1092–1094.

Liu, G., Aliaga, L., and Cai, H. (2012a). α-synuclein, LRRK2 and their interplay in Parkinson's disease. Future Neurol. *7*, 145–153.

Liu, G.-H., Qu, J., Suzuki, K., Nivet, E., Li, M., Montserrat, N., Yi, F., Xu, X., Ruiz, S., Zhang, W., et al. (2012b). Progressive degeneration of human neural stem cells caused by pathogenic LRRK2. Nature *491*, 603–607.

Lobbestael, E., Baekelandt, V., and Taymans, J.-M. (2012). Phosphorylation of LRRK2: from kinase to substrate. Biochem. Soc. Trans. *40*, 1102–1110.

Louveau, A., Smirnov, I., Keyes, T.J., Eccles, J.D., Rouhani, S.J., Peske, J.D., Derecki, N.C., Castle, D., Mandell, J.W., Lee, K.S., et al. (2015). Structural and functional features of central nervous system lymphatic vessels. Nature *523*, 337–341.

Louvi, A., and Artavanis-Tsakonas, S. (2006). Notch signalling in vertebrate neural development. Nat. Rev. Neurosci. *7*, 93–102.

Lu, M., Fan, Y., Tang, M., Qian, X., Ding, J., and Hu, G. (2011). Potentiation of D-Serine involves degeneration of dopaminergic neurons in MPTP/p mouse model of parkinson's disease. CNS Neurosci. Ther. *17*, 796–798.

Lubbe, S.J., Escott-Price, V., Gibbs, J.R., Nalls, M.A., Bras, J., Price, T.R., Nicolas, A., Jansen, I.E., Mok, K.Y., Pittman, A.M., et al. (2016). Additional rare variant analysis in Parkinson's disease cases with and without known pathogenic mutations: Evidence for oligogenic inheritance. Hum. Mol. Genet. *25*, 5483–5489.

Lucassen, P.J., Stumpel, M.W., Wang, Q., and Aronica, E. (2010). Decreased numbers of progenitor cells but no response to antidepressant drugs in the hippocampus of elderly depressed patients. Neuropharmacology *58*, 940–949.

Luk, K.C., Kehm, V., Carroll, J., Zhang, B., Brien, P.O., Trojanowski, J.Q., and Lee, V.M. (2012). in Nontransgenic Mice. Science (80-.). *338*, 949–954.

Lwin, A., Orvisky, E., Goker-Alpan, O., LaMarca, M.E., and Sidransky, E. (2004). Glucocerebrosidase mutations in subjects with parkinsonism. Mol. Genet. Metab. *81*, 70–73.

MacLeod, D., Dowman, J., Hammond, R., Leete, T., Inoue, K., and Abeliovich, A. (2006). The Familial Parkinsonism Gene LRRK2 Regulates Neurite Process Morphology. Neuron *52*, 587–593.

MacLeod, D. a., Rhinn, H., Kuwahara, T., Zolin, A., Di Paolo, G., MacCabe, B.D., Marder, K.S., Honig, L.S., Clark, L.N., Small, S. a., et al. (2013). RAB7L1 Interacts with LRRK2 to Modify Intraneuronal Protein Sorting and Parkinson's Disease Risk. Neuron *77*, 425–439.

Madeira, C., Lourenco, M. V, Vargas-Lopes, C., Suemoto, C.K., Brandão, C.O., Reis, T., Leite, R.E.P., Laks, J., Jacob-Filho, W., Pasqualucci, C.A., et al. (2015). d-serine levels in Alzheimer's disease: implications for novel biomarker development. Transl. Psychiatry *5*, e561.

Mahmoudi, S., and Brunet, A. (2012). Aging and reprogramming: a two-way street. Curr. Opin. Cell Biol. *24*, 744–756.

Manzoni, C., Denny, P., Lovering, R.C., and Lewis, P. a (2015). Computational analysis of the LRRK2 interactome. PeerJ *3*, e778.

Markesbery, W., and Jicha, G. (2009). Lewy body pathology in normal elderly subjects. J. Neuropathol. Exp. Neurol. *68*, 816–822.

Marot, G., Foulley, J.L., Mayer, C.D., and Jaffrézic, F. (2009). Moderated effect size and P-value combinations for microarray meta-analyses. Bioinformatics *25*, 2692–2699.

Marras, C., Alcalay, R.N., Caspell-Garcia, C., Coffey, C., Chan, P., Duda, J.E., Facheris, M.F., Fernández-Santiago, R., Ruíz-Martínez, J., Mestre, T., et al. (2016). Motor and nonmotor heterogeneity of LRRK2-related and idiopathic Parkinson's disease. Mov. Disord. *31*, 1192–1202.

Martin, L.J. (2006). Parkinson's Disease -Synuclein Transgenic Mice Develop Neuronal Mitochondrial Degeneration and Cell Death. J. Neurosci. *26*, 41–50.

Martin, I., Kim, J.W., Lee, B.D., Kang, H.C., Xu, J.C., Jia, H., Stankowski, J., Kim, M.S., Zhong, J., Kumar, M., et al. (2014). Ribosomal protein s15 phosphorylation mediates LRRK2 neurodegeneration in parkinson's disease. Cell *157*, 472–485.

Marxreiter, F., Regensburger, M., and Winkler, J. (2013). Adult neurogenesis in Parkinson's disease. Cell. Mol. Life Sci. *70*, 459–473.

Massano, J., and Bhatia, K.P. (2012). Clinical approach to Parkinson's disease: Features, diagnosis, and principles of management. Cold Spring Harb. Perspect. Med. *2*, 1–15.

Mata, I.F., Wedemeyer, W.J., Farrer, M.J., Taylor, J.P., and Gallo, K. a (2006). LRRK2 in Parkinson's disease: protein domains and functional insights. Trends Neurosci. *29*, 286–293.

McShane, S.G., Molè, M.A., Savery, D., Greene, N.D.E., Tam, P.P.L., and Copp, A.J. (2015). Cellular basis of neuroepithelial bending during mouse spinal neural tube closure. Dev. Biol. *404*, 113–124.

Melrose, H., Lincoln, S., Tyndall, G., Dickson, D., and Farrer, M. (2006). Anatomical localization of leucine-rich repeat kinase 2 in mouse brain. Neuroscience *139*, 791–794.

Melrose, H.L., Dächsel, J.C., Behrouz, B., Lincoln, S.J., Yue, M., Hinkle, K.M., Kent, C.B., Korvatska, E., Taylor, J.P., Witten, L., et al. (2010). Impaired dopaminergic neurotransmission and microtubule-associated protein tau alterations in human LRRK2 transgenic mice. Neurobiol. Dis. *40*, 503–517.

Mena, M.A., and García de Yébenes, J. (2008). Glial Cells as Players in Parkinsonism: The “Good,” the “Bad,” and the “Mysterious” Glia. Neurosci. *14*, 544–560.

Mertens, J., Marchetto, M.C., Bardy, C., and Gage, F.H. (2016). Evaluating cell reprogramming, differentiation and conversion technologies in neuroscience. Nat Rev Neurosci *17*, 424–437.

Miklossy, J., Arai, T., Guo, J.P., Klegeris, a, Yu, S., McGeer, E.G., and McGeer, P.L. (2006). LRRK2 expression in normal and pathologic human brain and in human cell lines. J. Neuropathol. Exp. Neurol. *65*, 953–963.

Milet, C., and Monsoro-Burq, A.H. (2012). Neural crest induction at the neural plate border in vertebrates. Dev. Biol. *366*, 22–33.

Miller, J.D., Ganat, Y.M., Kishinevsky, S., Bowman, R.L., Liu, B., Tu, E.Y., Mandal, P.K., Vera, E., Shim, J.-W., Kriks, S., et al. (2013). Human iPSC-Based Modeling of Late-Onset Disease via Progerin-Induced Aging. Cell Stem Cell *13*, 691–705.

Milosevic, J., Schwarz, S.C., Ogunlade, V., Meyer, A.K., Storch, A., and Schwarz, J. (2009). Emerging role of LRRK2 in human neural progenitor cell cycle progression, survival and differentiation. Mol. Neurodegener. *4*, 25.

Ming, G. li, and Song, H. (2011). Adult Neurogenesis in the Mammalian Brain: Significant Answers and Significant Questions. Neuron *70*, 687–702.

Mirza, B., Hadberg, H., Thomsen, P., and Moos, T. (1999). The absence of reactive astrocytosis is indicative of a unique inflammatory process in Parkinson’s disease. Neuroscience *95*, 425–432.

Mohan, H., Verhoog, M.B., Doreswamy, K.K., Eyal, G., Aardse, R., Lodder, B.N., Goriounova, N.A., Asamoah, B., B. Brakspear, A.B.C., Groot, C., et al. (2015). Dendritic and axonal architecture of individual pyramidal neurons across layers of adult human neocortex. Cereb. Cortex *25*, 4839–4853.

Momcilovic, O., Sivapatham, R., Oron, T.R., Meyer, M., Mooney, S., Rao, M.S., and Zeng, X. (2016). Derivation, characterization, and neural differentiation of integration-free induced pluripotent stem cell lines from Parkinson’s disease patients carrying *SNCA*, LRRK2, PARK2, and GBA mutations. PLoS One *11*, 1–26.

Monzel, A.S., Smits, L.M., Hemmer, K., Hachi, S., Moreno, E.L., van Wuellen, T., Jarazo, J., Walter, J., Brüggemann, I., Boussaad, I., et al. (2017). Derivation of Human Midbrain-Specific Organoids from Neuroepithelial Stem Cells. Stem Cell Reports 1–11.

Morita, Y., Ujike, H., Tanaka, Y., Otani, K., Kishimoto, M., Morio, A., Kotaka, T., Okahisa, Y., Matsushita, M., Morikawa, A., et al. (2007). A Genetic Variant of the Serine Racemase Gene Is Associated with schizophrenia. Biol. Psychiatry *61*, 1200–1203.

Mosmann, T. (1983). Rapid colorimetric assay for cellular growth and survival: Application to proliferation and cytotoxicity assays. J. Immunol. Methods *65*, 55–63.

Muda, K., Bertinetti, D., Gesellchen, F., Hermann, J.S., von Zweydorf, F., Geerlof, a., Jacob, a., Ueffing, M., Gloeckner, C.J., and Herberg, F.W. (2014). Parkinson-related LRRK2 mutation R1441C/G/H impairs PKA phosphorylation of LRRK2 and disrupts its interaction with 14-3-3. Proc. Natl. Acad. Sci. *111*, E34–E43.

Mueller, J.C., Fuchs, J., Hofer, A., Zimprich, A., Lichtner, P., Illig, T., Berg, D., Wüllner, U., Meitinger, T., and Gasser, T. (2005). Multiple regions of α-synuclein are associated with Parkinson’s disease. Ann. Neurol. *57*, 535–541.

Nagashima, Y., Kondo, T., Sakata, M., Koh, J., and Ito, H. (2016). Effects of soybean ingestion on pharmacokinetics of levodopa and motor symptoms of Parkinson’s disease - In relation to the effects of Mucuna pruriens. J. Neurol. Sci. *361*, 229–234.

Naka, H., Nakamura, S., Shimazaki, T., and Okano, H. (2008). Requirement for COUP-TFI and II in the temporal specification of neural stem cells in CNS development. Nat. Neurosci. *11*, 1014–1023.

Nalls, M.A., Saad, M., Noyce, A.J., Keller, M.F., Schrag, A., Bestwick, J.P., Traynor, B.J., Raphael Gibbs, J., Hernandez, D.G., Cookson, M.R., et al. (2014). Genetic comorbidities in parkinson's disease. Hum. Mol. Genet. *23*, 831–841.

Narhi, L., Wood, S.J., Steavenson, S., Jiang, Y., Wu, G.M., Anafi, D., Kaufman, S. a, Martin, F., Sitney, K., Denis, P., et al. (1999). Both familial Parkinson's disease mutations accelerate R-synuclein aggregation, J. Biol. Chem. *274*, 9843–9846.

Nguyen, H.N., Byers, B., Cord, B., Shcheglovitov, A., Byrne, J., Gujar, P., Kee, K., Schüle, B., Dolmetsch, R.E., Langston, W., et al. (2011). LRRK2 mutant iPSC-derived DA neurons demonstrate increased susceptibility to oxidative stress. Cell Stem Cell *8*, 267–280.

Ni, H.M., Williams, J.A., and Ding, W.X. (2015). Mitochondrial dynamics and mitochondrial quality control. Redox Biol. *4*, 6–13.

Nichols, R.J., Dzamko, N., Morrice, N. a, Campbell, D.G., Deak, M., Ordureau, A., Macartney, T., Tong, Y., Shen, J., Prescott, A.R., et al. (2010). 14-3-3 binding to LRRK2 is disrupted by multiple Parkinson's disease-associated mutations and regulates cytoplasmic localization. Biochem. J. *430*, 393–404.

Niciu, M.J., Kelmendi, B., and Sonacora, G. (2013). Overview of Glutermatergic Neurotransmission in Nervous System. Pharmacol Biochem Behav *100*, 656–664.

Nishimasu, H., Ran, F.A., Hsu, P.D., Konermann, S., Shehata, S.I., Dohmae, N., Ishitani, R., Zhang, F., and Nureki, O. (2014). Crystal structure of Cas9 in complex with guide RNA and target DNA. Cell *156*, 935–949.

Noga, M.J., Dane, A., Shi, S., Attali, A., van Aken, H., Suidgeest, E., Tuinstra, T., Muilwijk, B., Coulier, L., Luider, T., et al. (2012). Metabolomics of cerebrospinal fluid reveals changes in the central nervous system metabolism in a rat model of multiple sclerosis. Metabolomics *8*, 253–263.

Ohbayashi, N., Fukuda, M., and Kanaho, Y. (2017). Rab32 subfamily small GTPases: pleiotropic Rabs in endosomal trafficking. J. Biochem. 1–7.

Ohta, E., Kawakami, F., Kubo, M., and Obata, F. (2011). LRRK2 directly phosphorylates Akt1 as a possible physiological substrate: Impairment of the kinase activity by Parkinson's disease-associated mutations. FEBS Lett. *585*, 2165–2170.

Osterberg, V.R., Spinelli, K.J., Weston, L.J., Luk, K.C., Woltjer, R.L., and Unni, V.K. (2015). Progressive Aggregation of Alpha-Synuclein and Selective Degeneration of Lewy Inclusion-Bearing Neurons in a Mouse Model of Parkinsonism. Cell Rep. *10*, 1252–1260.

Ozelius, L.J., Senthil, G., Saunders-Pullman, R., Ohmann, E., Deligtisch, A., Tagliati, M., Hunt, A.L., Klein, C., Henick, B., Hailpern, S.M., et al. (2006). LRRK2 G2019S as a cause of Parkinson's disease in Ashkenazi Jews. N. Engl. J. Med. *354*, 424–425.

Pacelli, C., Giguère, N., Bourque, M.J., Lévesque, M., Slack, R.S., and Trudeau, L.É. (2015). Elevated Mitochondrial Bioenergetics and Axonal Arborization Size Are Key Contributors to the Vulnerability of Dopamine Neurons. Curr. Biol. *25*, 2349–2360.

Paisán-Ruíz, C., Jain, S., Evans, E.W., Gilks, W.P., Simón, J., Van Der Brug, M., De Munain, A.L., Aparicio, S., Gil, A.M., Khan, N., et al. (2004). Cloning of the gene containing mutations that cause PARK8-linked Parkinson's disease. Neuron *44*, 595–600.

Palm, T., Bolognin, S., Meiser, J., Nickels, S., Träger, C., Meilenbrock, R.-L., Brockhaus, J., Schreitmüller, M., Missler, M., and Schwamborn, J.C. (2015). Rapid and robust generation of long-term self-renewing human neural stem cells with the ability to generate mature astroglia. Sci. Rep. *5*, 16321.

Panatier, A., Theodosis, D.T., Mothet, J.P., Touquet, B., Pollegioni, L., Poulain, D.A., and Oliet, S.H.R. (2006). Glia-Derived d-Serine Controls NMDA Receptor Activity and Synaptic Memory. Cell *125*, 775–784.

Pankratz, N., and Foroud, T. (2007). Genetics of Parkinson disease. Genet. Med. *9*, 801–811.

Panopoulos, A.D., Smith, E.N., Arias, A.D., Shepard, P.J., Hishida, Y., Modesto, V., Diffenderfer, K.E., Conner, C., Biggs, W., Sandoval, E., et al. (2017). Aberrant DNA Methylation in Human iPSCs Associates with MYC-Binding Motifs in a Clone-Specific Manner Independent of Genetics. Cell Stem Cell *20*, 505–517.e6.

Parisiadou, L., and Cai, H. (2010). LRRK2 function on actin and microtubule dynamics in Parkinson disease. Commun. Integr. Biol. *3*, 396–400.

Parisiadou, L., Xie, C., Cho, H.J., Lin, X., Gu, X., Lobbestael, E., Baekelandt, V., Taymans, J., and Sun, L. (2010). Phosphorylation of ERM Proteins by LRRK2 Promotes the Rearrangement of Actin Cytoskeleton in Neuronal Morphogenesis. *29*, 13971–13980.

Parisiadou, L., Yu, J., Sgobio, C., Xie, C., Liu, G., Sun, L., Gu, X.-L., Lin, X., Crowley, N. a, Lovinger, D.M., et al. (2014). LRRK2 regulates synaptogenesis and dopamine receptor activation through modulation of PKA activity. Nat. Neurosci. *17*, 367–376.

Paus, M., Kohl, Z., Ben Abdallah, N.M.-B., Galter, D., Gillardon, F., and Winkler, J. (2013). Enhanced dendritogenesis and axogenesis in hippocampal neuroblasts of LRRK2 knockout mice. Brain Res. *1497*, 85–100.

Pissadaki, E.K., and Bolam, J.P. (2013). The energy cost of action potential propagation in dopamine neurons: clues to susceptibility in Parkinson's disease. Front. Comput. Neurosci. *7*, 13.

Plowey, E.D., Cherra, S.J., Liu, Y.J., and Chu, C.T. (2008). Role of autophagy in G2019S-LRRK2-associated neurite shortening in differentiated SH-SY5Y cells. J. Neurochem. *105*, 1048–1056.

Pollanen, M.S., Bergeron, C., and Weyer, L. (1992). Detergent-Insoluble Cortical Lewy Body Fibrils Share Epitopes with Neurofilament and Tau. J. Neurochem. *58*, 1953–1956.

Polymeropoulos, M.H., Lavedan, C., Leroy, E., Ide, S.E., Dehejia, A., Dutra, A., Pike, B., Root, H., Rubenstein, J., Boyer, R., et al. (1997). Mutation in the α-Synuclein Gene Identified in Families with Parkinson's Disease Mutation in the α-Synuclein Gene Identified in Families with Parkinson's Disease. Science (80-.). *276*, 2045–2047.

Power, J.H., Barnes, O.L., and Chegini, F. (2015). Lewy bodies and the mechanisms of neuronal cell death in parkinson's disease and dementia with lewy bodies. Brain Pathol. n/a-n/a.

Pringsheim, T., Jette, N., Frolkis, A., and Steeves, T.D.L. (2014). The prevalence of Parkinson's disease: A systematic review and meta-analysis. Mov. Disord. *29*, 1583–1590.

Ramsden N, Perrin J, Ren Z, Lee BD, Zinn N, Dawson VL, Tam D, Bova M, Lang M, Drewes G, Bantscheff M, Bard F, Dawson TM, H.C. (2011). Chemoproteomics-based design of potent LRRK2-selective lead compounds that attenuate Parkinson's disease-related toxicity in human neurons. ACS Chem. Biol. *6*, 1021–1028.

Ran, F.A., Hsu, P.D., Lin, C.Y., Gootenberg, J.S., Konermann, S., Trevino, A.E., Scott, D.A., Inoue, A., Matoba, S., Zhang, Y., et al. (2013). Double nicking by RNA-guided CRISPR cas9 for enhanced genome editing specificity. Cell *154*, 1380–1389.

Ransohoff, R.M., and Engelhardt, B. (2012). The anatomical and cellular basis of immune surveillance in the central nervous system. Nat. Rev. Immunol. *12*, 623–635.

Rappold, P.M., and Tieu, K. (2010). Astrocytes and Therapeutics for Parkinson's Disease. Neurotherapeutics *7*, 413–423.

Recasens, A., and Dehay, B. (2014). Alpha-synuclein spreading in Parkinson's disease. Front. Neuroanat. *8*, 1–9.

Reeve, A., Simcox, E., and Turnbull, D. (2014). Ageing and Parkinson's disease: Why is advancing age the biggest risk factor? Ageing Res. Rev. *14*, 19–30.

Regensburger, M., Prots, I., and Winner, B. (2014). Adult hippocampal neurogenesis in Parkinson's

disease: impact on neuronal survival and plasticity. Neural Plast *2014*, 454696.

Reinhardt, P., Schmid, B., Burbulla, L.F., Schöndorf, D.C., Wagner, L., Glatza, M., Höing, S., Hargus, G., Heck, S. a, Dhingra, A., et al. (2013a). Genetic correction of a LRRK2 mutation in human iPSCs links parkinsonian neurodegeneration to ERK-dependent changes in gene expression. Cell Stem Cell *12*, 354–367.

Reinhardt, P., Glatza, M., Hemmer, K., Tsytsyura, Y., Thiel, C.S., Höing, S., Moritz, S., Parga, J. a, Wagner, L., Bruder, J.M., et al. (2013b). Derivation and expansion using only small molecules of human neural progenitors for neurodegenerative disease modeling. PLoS One *8*, e59252.

Ren, X., Yang, Z., Xu, J., Sun, J., Mao, D., Hu, Y., Yang, S.J., Qiao, H.H., Wang, X., Hu, Q., et al. (2014). Enhanced specificity and efficiency of the CRISPR/Cas9 system with optimized sgRNA parameters in Drosophila. Cell Rep. *9*, 1151–1162.

Reubinoff, B.E., Pera, M.F., Fong, C.Y., Trounson, A., and Bongso, A. (2000). Embryonic stem cell lines from human blastocysts: somatic differentiation in vitro. Nat. Biotechnol. *18*, 399–404.

Rhinn, M., and Brand, M. (2001). The midbrain – hindbrain boundary organizer. 34–42.

Ritchie, M.E., Phipson, B., Wu, D., Hu, Y., Law, C.W., Shi, W., and Smyth, G.K. (2015). limma powers differential expression analyses for RNA-sequencing and microarray studies. Nucleic Acids Res. *43*, e47–e47.

Robel, S., Berninger, B., and Gotz, M. (2011). The stem cell potential of glia: lessons from reactive gliosis. Nat Rev Neurosci *12*, 88–104.

Roosen, D., and Cookson, M.R. (2016). LRRK2 at the interface of autophagosomes, endosomes and lysosomes. Mol. Neurodegener. *11*, 73.

Roy, N.S., Cleren, C., Singh, S.K., Yang, L., Beal, M.F., and Goldman, S.A. (2006). Functional engraftment of human ES cell–derived dopaminergic neurons enriched by coculture with telomerase-immortalized midbrain astrocytes. Nat. Med. *12*, 1259–1268.

Rusznák, Z., Henskens, W., Schofield, E., Kim, W.S., and Fu, Y. (2016). Adult Neurogenesis and Gliogenesis: Possible Mechanisms for Neurorestoration. Exp. Neurobiol. *25*, 103–112.

Saint-André, V., Federation, A.J., Lin, C.Y., Abraham, B.J., Reddy, J., Lee, T.I., Bradner, J.E., and Young, R.A. (2016). Models of human core transcriptional regulatory circuitries. Genome Res. *26*, 385–396.

Sánchez, S., Jiménez, C., Carrera, A.C., Diaz-Nido, J., Avila, J., and Wandosell, F. (2004). A cAMP-activated pathway, including PKA and PI3K, regulates neuronal differentiation. Neurochem. Int. *44*, 231–242.

Sánchez-Danés, A., Richaud-Patin, Y., Carballo-Carbajal, I., Jiménez-Delgado, S., Caig, C., Mora, S., Di Guglielmo, C., Ezquerra, M., Patel, B., Giralt, A., et al. (2012). Disease-specific phenotypes in dopamine neurons from human iPS-based models of genetic and sporadic Parkinson's disease. EMBO Mol. Med. *4*, 380–395.

Sanders, L.H., Laganière, J., Cooper, O., Mak, S.K., Vu, B.J., Huang, Y.A., Paschon, D.E., Vangipuram, M., Sundararajan, R., Urnov, F.D., et al. (2014). LRRK2 mutations cause mitochondrial DNA damage in iPSC-derived neural cells from Parkinson's disease patients: Reversal by gene correction. Neurobiol. Dis. *62*, 381–386.

Sapranauskas, R., Gasiunas, G., Fremaux, C., Barrangou, R., Horvath, P., and Siksnys, V. (2011). The Streptococcus thermophilus CRISPR/Cas system provides immunity in Escherichia coli. Nucleic Acids Res. *39*, 9275–9282.

Sasabe, J., Chiba, T., Yamada, M., Okamoto, K., Nishimoto, I., Matsuoka, M., and Aiso, S. (2007). D-serine is a key determinant of glutamate toxicity in amyotrophic lateral sclerosis. EMBO J. *26*, 4149–4159.

Saunders-Pullman, R., Barrett, M.J., Stanley, K.M., Luciano, M.S., Shanker, V., Severt, L., Hunt, A., Raymond, D., Ozelius, L.J., and Bressman, S.B. (2010). LRRK2 G2019S mutations are associated with an

increased cancer risk in Parkinson disease. Mov. Disord. *25*, 2536–2541.

Scherman, D., Desnos, C., Darchen, F., Pollak, P., Javoy-Agid, F., and Agid, Y. (1989). Striatal dopamine deficiency in parkinson's disease: Role of aging. Ann. Neurol. *26*, 551–557.

Schlaeger, T.M., Daheron, L., Brickler, T.R., Entwisle, S., Chan, K., Cianci, A., DeVine, A., Ettenger, A., Fitzgerald, K., Godfrey, M., et al. (2015). A comparison of non-integrating reprogramming methods. Nat. Biotechnol. *33*, 58–63.

Schubert, M., Ermini, L., Sarkissian, C. Der, Jónsson, H., Ginolhac, A., Schaefer, R., Martin, M.D., Fernández, R., Kircher, M., McCue, M., et al. (2014). Characterization of ancient and modern genomes by SNP detection and phylogenomic and metagenomic analysis using PALEOMIX. Nat. Protoc. *9*, 1056–1082.

Schulz, C., Paus, M., Frey, K., Schmid, R., Kohl, Z., Mennerich, D., Winkler, J., and Gillardon, F. (2011). Leucine-rich repeat kinase 2 modulates retinoic acid-induced neuronal differentiation of murine embryonic stem cells. PLoS One *6*, e20820.

Schwab, A.J., and Ebert, A.D. (2015). Neurite Aggregation and Calcium Dysfunction in iPSC-Derived Sensory Neurons with Parkinson's Disease-Related LRRK2 G2019S Mutation. Stem Cell Reports *5*, 1039–1052.

Seifert, A., Werheid, D.F., Knapp, S.M., and Tobiasch, E. (2015). Role of Hox genes in stem cell differentiation. World J Stem Cells *7*, 583–595.

Shahzad, K., and Loor, J.J. (2012). Application of Top-Down and Bottom-up Systems Approaches in Ruminant Physiology and Metabolism. Curr. Genomics *13*, 379–394.

Shimazaki, T., Arsenijevic, Y., Ryan, A.K., Rosenfeld, M.G., and Weiss, S. (1999). A role for the POU-III transcription factor Brn-4 in the regulation of striatal neuron precursor differentiation. EMBO J. *18*, 444–456.

Shin, J.-H., Dawson, V.L., and Dawson, T.M. (2009). SnapShot: Pathogenesis of Parkinson's Disease. Cell *139*, 440.e1-440.e2.

Shleper, M. (2005). D-Serine Is the Dominant Endogenous Coagonist for NMDA Receptor Neurotoxicity in Organotypic Hippocampal Slices. J. Neurosci. *25*, 9413–9417.

Sidransky, E., and Lopez, G. (2014). NIH Public Access. *11*, 986–998.

Simón-Sánchez, J., Herranz-Pérez, V., Olucha-Bordonau, F., and Pérez-Tur, J. (2006). LRRK2 is expressed in areas affected by Parkinson's disease in the adult mouse brain. Eur. J. Neurosci. *23*, 659–666.

Simón-Sánchez, J., Schulte, C., Bras, J.M., Sharma, M., Gibbs, J.R., Berg, D., Paisan-Ruiz, C., Lichtner, P., Scholz, S.W., Hernandez, D.G., et al. (2009). Genome-wide association study reveals genetic risk underlying Parkinson's disease. Nat. Genet. *41*, 1308–1312.

Singleton, A.B., Farrer, M.J., and Bonifati, V. (2013). The genetics of Parkinson's disease: progress and therapeutic implications. Mov. Disord. *28*, 14–23.

Smyth, G.K. (2004). Linear Models and Empirical Bayes Methods for Assessing Differential Expression in Microarray Experiments. Stat. Appl. Genet. Mol. Biol. *3*, 1.

Sofroniew, M. V., and Vinters, H. V. (2010). Astrocytes: Biology and pathology. Acta Neuropathol. *119*, 7–35.

Soldner, F., Laganière, J., Cheng, A.W., Hockemeyer, D., Gao, Q., Alagappan, R., Khurana, V., Golbe, L.I., Myers, R.H., Lindquist, S., et al. (2011). Generation of Isogenic Pluripotent Stem Cells Differing Exclusively at Two Early Onset Parkinson Point Mutations. Cell *146*, 318–331.

Song, D.D., Shults, C.W., Sisk, A., Rockenstein, E., and Masliah, E. (2004). Enhanced substantia nigra mitochondrial pathology in human α-synuclein transgenic mice after treatment with MPTP. Exp. Neurol. *186*, 158–172.

Song, H., Stevens, C.C.F., and Gage, F.H.F. (2002). Astroglia induce neurogenesis from adult neural stem cells. Nature *417*, 39–44.

Song, Y.J.C., Halliday, G.M., Holton, J.L., Sullivan, S.O., Mccann, H., Path, B., Lashley, T., Lees, A.J., Ozawa, T., Williams, D.R., et al. (2009). Degeneration in different parkinsonian syndromes relates to astrocyte type and astrocyte protein expression. J. Neuropathol. Exp. Neurol. *68*, 1073–1083.

Sonntag, K.C. (2010). MicroRNAs and deregulated gene expression networks in neurodegeneration. Brain Res. *1338*, 48–57.

Spalding, K.L., Bergmann, O., Alkass, K., Bernard, S., Salehpour, M., Huttner, H.B., Boström, E., Westerlund, I., Vial, C., Buchholz, B. a, et al. (2013). Dynamics of hippocampal neurogenesis in adult humans. Cell *153*, 1219–1227.

Spillantini, M.G., and Goedert, M. (1998). Tau protein pathology in neurodegenerative diseases. Trends Neurosci. *21*, 428–433.

Spillantini, M.G., Schmidt, M.L., Lee, V.M., Trojanowski, J.Q., Jakes, R., and Goedert, M. (1997). Alpha-synuclein in Lewy bodies. Nature *388*, 839–840.

St.-Gelais, F., Jomphe, C., and Trudeau, L.É. (2006). The role of neurotensin in central nervous system pathophysiology: What is the evidence? J. Psychiatry Neurosci. *31*, 229–245.

Steger, M., Tonelli, F., Ito, G., Davies, P., Trost, M., Vetter, M., Wachter, S., Lorentzen, E., Duddy, G., S. Wilson, et al. (2016). Phosphoproteomics reveals that Parkinson's disease kinase LRRK2 regulates a subset of Rab GTPases. Elife *5*.

Studer, M., Lumsden, A., Ariza-McNaughton, L., Bradley, A., and Krumlauf, R. (1996). Altered segmental identity and abnormal migration of motor neurons in mice lacking Hoxb-1. Nature *384*, 630–634.

Su, Y.C., and Qi, X. (2013). Inhibition of excessive mitochondrialfissionreduced aberrant autophagy and neuronal damage caused by LRRK2 G2019S mutation. Hum. Mol. Genet. *22*, 4545–4561.

Sulzer, D. (2007). Multiple hit hypotheses for dopamine neuron loss in Parkinson's disease. Trends Neurosci. *30*, 244–250.

Suzuki, I.K., and Vanderhaeghen, P. (2015). Is this a brain which I see before me? Modeling human neural development with pluripotent stem cells. Development *142*, 3138 LP-3150.

Sweet, E.S., Saunier-Rebori, B., Yue, Z., and Blitzer, R.D. (2015). The Parkinson's Disease-Associated Mutation LRRK2-G2019S Impairs Synaptic Plasticity in Mouse Hippocampus. J. Neurosci. *35*, 11190–11195.

Takahashi, K., and Yamanaka, S. (2006). Induction of Pluripotent Stem Cells from Mouse Embryonic and Adult Fibroblast Cultures by Defined Factors. Cell *126*, 663–676.

Tanaka, M., Kim, Y.M., Lee, G., Junn, E., Iwatsubo, T., and Mouradian, M.M. (2004). Aggresomes Formed by α-Synuclein and Synphilin-1 Are Cytoprotective. J. Biol. Chem. *279*, 4625–4631.

Tang, J., Yoo, A.S., and Crabtree, G.R. (2013). Reprogramming Human Fibroblasts to Neurons by Recapitulating an Essential MicroRNA-Chromatin Switch. Curr. Opin. Genet. Dev. *23*, 591–598.

Tang, W.W.C., Kobayashi, T., Irie, N., Dietmann, S., and Surani, M.A. (2016). Specification and epigenetic programming of the human germ line. Nat. Rev. Genet. *17*, 585–600.

Thakurela, S., Tiwari, N., Schick, S., Garding, A., Ivanek, R., Berninger, B., and Tiwari, V.K. (2016). Mapping gene regulatory circuitry of Pax6 during neurogenesis. Cell Discov. *2*, 15045.

Theveneau, E., and Mayor, R. (2012). Neural crest delamination and migration: From epithelium-to-mesenchyme transition to collective cell migration. Dev. Biol. *366*, 34–54.

Thompson, M., Marecki, J.C., Marinesco, S., Labrie, V., Roder, J.C., Barger, S.W., and Crow, J.P. (2012). Paradoxical roles of serine racemase and d -serine in the G93A mSOD1 mouse model of amyotrophic

lateral sclerosis. J. Neurochem. *120*, 598–610.

Tompkins, M.M., and Hill, W.D. (1997). Contribution of somal Lewy bodies to neuronal death. Brain Res. *775*, 24–29.

Tong, J., Ang, L., Williams, B., Furukawa, Y., Guttman, M., Boileau, I., Hornykiewicz, O., Kish, S.J., Family, C., Health, M., et al. (2015). Low Levels of Astroglial Markers in Parkinson's Disease: Relationship to α-Synuclein Accumulation. Neurobiol Dis. *82*, 243–253.

Tretiakoff (1919). Contribution a L'étude de L'anatomie Pathologique de Locus Niger de Soemmerling. Univ. Paris, Paris.

Trinh, J., and Farrer, M. (2013). Advances in the genetics of Parkinson disease. Nat. Rev. Neurol. *9*, 445–454.

Trinh, J., Gustavsson, E.K., Vilariño-güell, C., Bortnick, S., Latourelle, J., Mckenzie, M.B., Tu, C.S., and Nosova, E. (2016). DNM3 and genetic modifi ers of age of onset in LRRK2 Gly2019Ser parkinsonism : a genome-wide linkage and association study. *4422*, 1–9.

Tropepe, V., Hitoshi, S., Sirard, C., Mak, T.W., Rossant, J., and Van Der Kooy, D. (2001). Direct neural fate specification from embryonic stem cells: A primitive mammalian neural stem cell stage acquired through a default mechanism. Neuron *30*, 65–78.

Valente, E.M., Abou-Sleiman, P.M., Caputo, V., Muqit, M.M.K., Harvey, K., Gispert, S., Ali, Z., Del Turco, D., Bentivoglio, A.R., Healy, D.G., et al. (2004). Hereditary early-onset Parkinson's disease caused by mutations in PINK1. Science *304*, 1158–1160.

Vekrellis, K., Rideout, H.J., and Stefanis, L. (2004). Neurobiology of alpha-synuclein. Mol. Neurobiol. *30*, 1–21.

Verma, M., Steer, E.K., and Chu, C.T. (2014). ERKed by LRRK2: A cell biological perspective on hereditary and sporadic Parkinson's disease. Biochim. Biophys. Acta - Mol. Basis Dis. *1842*, 1273–1281.

Wagner, J., Akerud, P., Castro, D.S., Holm, P.C., Canals, J.M., Snyder, E.Y., Perlmann, T., and Arenas, E. (1999). Induction of a midbrain dopaminergic phenotype in Nurr1-overexpressing neural stem cells by type 1 astrocytes. Nat. Biotechnol. *17*, 653–659.

Wallings, R., Manzoni, C., and Bandopadhyay, R. (2015). Cellular processes associated with LRRK2 function and dysfunction. FEBS J. *282*, 2806–2826.

Wang, L., Xie, C., Greggio, E., Parisiadou, L., Shim, H., Chandran, J., Lin, X., Lai, C., Yang, W., Moore, D.J., et al. (2008). NIH Public Access. *28*, 3384–3391.

Wang, X., Li, K., Xue, B., Wang, Y., Wang, X., and Wang, H. (2009). Ventral mesencephalon astrocytes are more efficient than those of other regions in inducing dopaminergic neurons through higher expression level of TGF-ß3. J. Mol. Neurosci. *37*, 288–300.

Warlich, E., Kuehle, J., Cantz, T., Brugman, M.H., Maetzig, T., Galla, M., Filipczyk, A. a, Halle, S., Klump, H., Schöler, H.R., et al. (2011). Lentiviral Vector Design and Imaging Approaches to Visualize the Early Stages of Cellular Reprogramming. Mol. Ther. *19*, 782–789.

Waschbüsch, D., Michels, H., Strassheim, S., Ossendorf, E., Kessler, D., Gloeckner, C.J., and Barnekow, A. (2014). LRRK2 transport is regulated by its novel interacting partner Rab32. PLoS One *9*.

Wegner, M., and Stolt, C.C. (2005). From stem cells to neurons and glia: A Soxist's view of neural development. Trends Neurosci. *28*, 583–588.

West, A.B., Moore, D.J., Biskup, S., Bugayenko, A., Smith, W.W., Ross, C. a, Dawson, V.L., and Dawson, T.M. (2005). Parkinson's disease-associated mutations in leucine-rich repeat kinase 2 augment kinase activity. Proc. Natl. Acad. Sci. U. S. A. *102*, 16842–16847.

White (2012). Moving Beyond Tyrosine Hydroxylase to Define Dopaminergic Neurons for Use in Cell Replacement Therapies for Parkinson's Disease. CNS Neurol. Disord. - Drug Targets *11*, 340–349.

REFERENCES

William J. Larsen, Lawrence S. Sherman, W.J.L. (2002). Ectoderm: neurulation, neural tube, neural crest. Hum. Embryol. 3rd Ed. 4-1–16.

Winner, B., Melrose, H.L., Zhao, C., Hinkle, K.M., Yue, M., Kent, C., Braithwaite, a T., Ogholikhan, S., Aigner, R., Winkler, J., et al. (2011a). Adult neurogenesis and neurite outgrowth are impaired in LRRK2 G2019S mice. Neurobiol. Dis. *41*, 706–716.

Winner, B., Kohl, Z., and Gage, F.H. (2011b). Neurodegenerative disease and adult neurogenesis. Eur. J. Neurosci. *33*, 1139–1151.

Wirdefeldt, K., Adami, H.-O., Cole, P., Trichopoulos, D., and Mandel, J. (2011). Epidemiology and etiology of Parkinson's disease: a review of the evidence. Eur. J. Epidemiol. *26 Suppl 1*, S1–S58.

Worringer, K. a, Rand, T. a, Hayashi, Y., Sami, S., Takahashi, K., Tanabe, K., Narita, M., Srivastava, D., and Yamanaka, S. (2014). The let-7/LIN-41 Pathway Regulates Reprogramming to Human Induced Pluripotent Stem Cells by Controlling Expression of Prodifferentiation Genes. Cell Stem Cell *14*, 40–52.

Wszolek, Z.K., Pfeiffer, R.F., Tsuboi, Y., Uitti, R.J., McComb, R.D., Stoessl, a J., Strongosky, a J., Zimprich, a, Müller-Myhsok, B., Farrer, M.J., et al. (2004). Autosomal dominant parkinsonism associated with variable synuclein and tau pathology. Neurology *62*, 1619–1622.

WU, Z., and IRIZARRY, R.A. (2005). Stochastic Models Inspired by Hybridization Theory for Short Oligonucleotide Arrays ZHIJIN. J. Comput. Biol. *12*, 882–893.

Xu, J., Kao, S.-Y., Lee, F.J.S., Song, W., Jin, L.-W., and Yankner, B. a (2002). Dopamine-dependent neurotoxicity of alpha-synuclein: a mechanism for selective neurodegeneration in Parkinson disease. Nat. Med. *8*, 600–606.

Xu, J., Du, Y., and Deng, H. (2015). Direct lineage reprogramming: Strategies, mechanisms, and applications. Cell Stem Cell *16*, 119–134.

Yang, F., Liu, Y., Tu, J., Wan, J., Zhang, J., Wu, B., Chen, S., Zhou, J., Mu, Y., and Wang, L. (2014). Activated astrocytes enhance the dopaminergic differentiation of stem cells and promote brain repair through bFGF. Nat. Commun. *5*, 5627.

Yang, L., Esvelt, K.M., Aach, J., Guell, M., Dicarlo, J.E., Norville, J.E., and Church, G.M. (2013). RNA-Guided Human Genome. 823–827.

Yosef Buganim, Dina A. Faddah, R.J. (2013). Mechanisms and models of somatic cell reprogramming. Nat Rev Genet *14*, 427–439.

Zarranz, J.J., Alegre, J., Gómez-Esteban, J.C., Lezcano, E., Ros, R., Ampuero, I., Vidal, L., Hoenicka, J., Rodriguez, O., Atarés, B., et al. (2004). The New Mutation, E46K, of α-Synuclein Causes Parkinson and Lewy Body Dementia. Ann. Neurol. *55*, 164–173.

Zechel, S., Meinhardt, A., Unsicker, K., and von Bohlen und Halbach, O. (2010). Expression of leucine-rich-repeat-kinase 2 (LRRK2) during embryonic development. Int. J. Dev. Neurosci. *28*, 391–399.

Zhang, Y., and Barres, B.A. (2010). Astrocyte heterogeneity: An underappreciated topic in neurobiology. Curr. Opin. Neurobiol. *20*, 588–594.

Zhu, Y., Wang, C., Yu, M., Cui, J., Liu, L., and Xu, Z. (2013). ULK1 and JNK are involved in mitophagy incurred by LRRK2 G2019S expression. Protein Cell *4*, 711–721.

Zickenrott, S., Angarica, V.E., Upadhyaya, B.B., and del Sol, A. (2016). Prediction of disease–gene–drug relationships following a differential network analysis. Cell Death Dis. *7*, e2040.

Zimprich, A., Biskup, S., Leitner, P., Lichtner, P., Farrer, M., Lincoln, S., Kachergus, J., Hulihan, M., Uitti, R.J., Calne, D.B., et al. (2004). Mutations in LRRK2 cause autosomal-dominant parkinsonism with pleomorphic pathology. Neuron *44*, 601–607.

APPENDICES

APPENDICES

1 APPENDIX TO PUBLICATION III

1.1 DEG lists

The following tables contain the complete gene lists of DEGs between isogenic controls. Related to Figure 5.

Table 2. DEGs upon insertion of LRRK2-G2019S into healthy lines.

H vs HG2019S	AveFC.H1	AveFC.H3	FDR
MIRLET7A2	-2.12765	-3.80577	0.024892
JAG1	1.61444	4.530337	0.024892
ELL2	1.576223	3.174687	0.024892
PCDH15	3.646903	1.970603	0.024892
SP5	-1.84635	-2.68489	0.024892
IQGAP2	1.452793	2.33894	0.024892
RBMS3	1.476073	2.39774	0.024892
HHIP	1.69744	2.021037	0.024892
PPP1R3C	1.455573	2.025457	0.024892
SNORA14A	-0.11263	-4.05426	0.024892
TRDC	1.961887	1.80277	0.024892
ADAMTS3	1.61345	1.82938	0.024892
PCDH8	1.518547	2.351807	0.024892
IGFBPL1	1.55329	1.759937	0.024892
LINC00648	1.44344	1.751677	0.024892
CTB-78F1.2	-1.6379	-1.9271	0.024892
NRCAM	1.28581	2.25973	0.024892
DKK1	-1.54261	-2.92498	0.026055
MIR4712	1.269427	2.27374	0.026055
NRG1	1.224407	3.023347	0.026253
FGF14	1.277327	1.96704	0.026253
NEUROD4	1.73478	1.579537	0.026253
SNORA60	-0.46166	-1.71317	0.028023
SESN3	1.500473	1.560207	0.028023
DAAM1	1.854163	1.3595	0.028023
MIR365A	-1.24283	-1.41923	0.028023
ANGPT1	1.877923	1.432453	0.028023
LGR5	1.06756	3.143087	0.028023
PPP4R4	1.217143	1.624687	0.028023
IL6ST	1.26728	1.615713	0.028023
NEUROG3	1.165383	3.154383	0.028023
LOC101929518	-1.40573	-1.49697	0.028023
C8orf88	1.178153	1.791347	0.028023
PLAGL1	2.021153	1.25285	0.028023
LOC105377261	1.066093	2.499887	0.028023
TRDJ1	1.389153	1.52805	0.028023
MIR3178	0.991003	1.941797	0.028023
EPB41L2	1.08877	2.261853	0.028023

CDK6	1.327617	1.382397	0.02867
DGKH	1.245557	1.351703	0.031698
MEIS2	1.227527	1.632057	0.032444
NNAT	2.958077	1.199987	0.033063
CRYBG3	0.994407	2.035077	0.033063
KIZ	1.17234	1.55136	0.033822
ROBO2	1.094283	1.649687	0.038294
LOC101929563	0.909417	1.495657	0.038294
LOC105372990	-1.0866	-1.61408	0.038294
ADAMTS19	0.920323	2.325983	0.040166
CA11	-1.17951	-1.5647	0.040852
ZIC2	-0.82639	-2.9653	0.040852
ANKRD6	1.046333	2.103093	0.040852
DOK5	1.35219	1.22373	0.040852
PLA2G4A	1.026577	1.84043	0.040852
MIR1252	1.67338	1.081493	0.041169
ROCK1P1	-0.74273	-1.87427	0.042253
TEX15	0.892017	2.138273	0.042907
NKX2-2	2.006413	1.105893	0.046776
SPON1	1.97324	1.009317	0.046776
LOC100130976	0.923847	2.737823	0.046776
PCDH18	0.925343	3.249057	0.046776
TCEAL7	0.775097	2.093593	0.046776
SNORD53	-0.91262	-1.28608	0.046776
HSPA12A	1.09858	1.51609	0.046776

Table 3. DEGs upon gene-correction of LRRK2-G2019S in patient lines.

P vs PGC	AveFC.P1.1GC	AveFC.P1GC	AveFC.P2GC	FDR
HIST1H2BB	-8.59383	-8.43885	-3.07169	0.000369
CCDC125	-2.44254	-2.35982	-1.74236	0.000369
HOXB1	-2.51651	-1.83291	-1.24923	0.000369
FIRRE	-1.1481	-1.73847	-2.78205	0.000444
HIST1H4A	-2.23885	-1.92363	-0.78857	0.001742
ZNF667-AS1	-0.6455	-2.65411	-2.11013	0.003283
SHISA6	-0.6733	-1.129	-2.92836	0.003283
ID1	-1.3366	-1.03565	-1.2178	0.003283
PPP1R14C	-0.76545	-1.37554	-1.22022	0.005298
SNORA74A	1.431173	0.323773	0.26444	0.005298
ADAMTS18	-1.28047	-0.55059	-1.76717	0.005529
ROCK1P1	-0.57327	-0.51481	-0.5313	0.007053
AMOT	-0.72134	-1.04419	-0.80004	0.007053
HIST1H3C	-1.45352	-2.42042	-0.2834	0.008423
VTRNA1-3	0.885787	0.47473	2.416507	0.008587
LRRC34	4.027307	1.712277	0.36147	0.008587
ARMCX1	-1.89889	-2.10169	-0.29409	0.008587
SNORD115-5	-0.76568	-0.78546	-0.37647	0.008587
SNORD115-9	-0.76568	-0.78546	-0.37647	0.008587
SNORD115-11	-0.76568	-0.78546	-0.37647	0.008587
ZNF506	-1.36637	-0.17278	-1.61657	0.008587
SNORD115-22	-0.79148	-0.86707	-0.34335	0.009597
SNORD115-44	-0.60509	-0.75825	-0.43198	0.014126
OR5H1	-1.05273	-1.10332	-0.56479	0.014942
VTRNA2-1	-0.12989	-3.00172	-2.71599	0.014942

LINC01198	1.94594	1.202897	0.336427	0.015016
EPHA3	-0.5173	-0.64054	-3.26647	0.015016
ZNF229	0.795707	1.54451	0.589773	0.015655
DDX11L10	-0.27251	-1.00182	-1.03097	0.015655
SNORD115-39	-0.66305	-0.50938	-0.46441	0.016754
PPP1R1A	-0.88846	-0.48776	-1.87592	0.016754
MAB21L2	-0.88967	-0.5265	-2.05959	0.016754
ZNF558	-3.29121	-0.97901	-0.28121	0.017565
CLDN1	-0.63556	-0.3075	-1.86817	0.017766
LOC105373202	-0.9783	-0.12824	-0.71757	0.018533
LOC105375161	-0.35641	-1.50115	-1.28047	0.018533
HES3	-0.49555	-0.3844	-2.02537	0.019641
LOC105378798	0.32778	0.890413	1.572413	0.019641
TSPAN2	0.70358	0.75374	1.39304	0.019641
VPS37B	-0.77986	-0.67749	-1.39104	0.019641
GOLGA8J	-0.8113	-0.45818	-1.55657	0.020697
PPIEL	-0.45282	-1.54506	-0.81444	0.021725
DUX4L25	-0.5062	-0.46668	-0.50935	0.022743
CRABP2	-0.38862	-0.91397	-1.6011	0.025531
SNORD115-45	-1.23889	-0.51278	-0.65937	0.027611
LOC101928307	-0.96081	-0.25317	-2.82308	0.031452
SNORD115-20	-0.62586	-0.50958	-0.36685	0.03147
MIR548AM	-0.4197	-1.24654	-0.78045	0.03147
NAV3	-0.59693	-0.63705	-1.48746	0.03147
TPPP3	-0.7769	-0.02739	-1.26281	0.032329
LOC100507661	-0.72337	-0.48812	-1.25489	0.032329
FAR2P3	-0.53092	-0.02615	-1.04144	0.032329
ADRA2A	-0.34418	-0.23782	-1.65278	0.032329
SNORA11	-0.22216	-0.53881	-0.64794	0.032329
SNORD115-17	-0.4909	-0.67174	-0.38712	0.035359
ZNF429	0.4278	1.519583	0.707207	0.035464
LOC105377261	1.300363	0.00068	0.724503	0.037665
REXO1L1P	-0.41403	-0.03843	-0.41157	0.042344
SNORD115-6	-0.95236	-0.33944	-0.1412	0.042344
SNORD115-42	-0.95236	-0.33944	-0.1412	0.042344
SNORA24	1.01065	0.286267	0.39598	0.042344
CNPY1	1.052797	0.17072	5.873213	0.042788
SCUBE1	-0.86145	-0.08732	-1.02969	0.042879
PAK3	-0.05956	-1.3484	-1.58472	0.043362
CLU	-0.67511	-0.54055	-0.92565	0.043362
SCN3A	-0.81516	-0.62107	-0.91269	0.044062
ZC3HAV1L	-0.75605	-0.3172	-1.57344	0.044995
LINC00470	0.63468	0.442963	2.532447	0.047576
PCDHB13	-0.65717	-0.08142	-1.45305	0.047576

1.2 Disease model networks

The information here below, has not been published in the corresponding manuscript but is relevant for the coherence of the thesis. The disease model networks are based on the DEGs between healthy individuals and patients. The links are based on connections from literature. By targeted perturbation (downregulation) of PAX2 one of the core genes within the network, 50 of the DEGs could be adjusted from the diseased state (b) to the healthy one (a). The procedure of generating the network is shortly described within the material and method part and was performed by Muhammad Ali.

a)

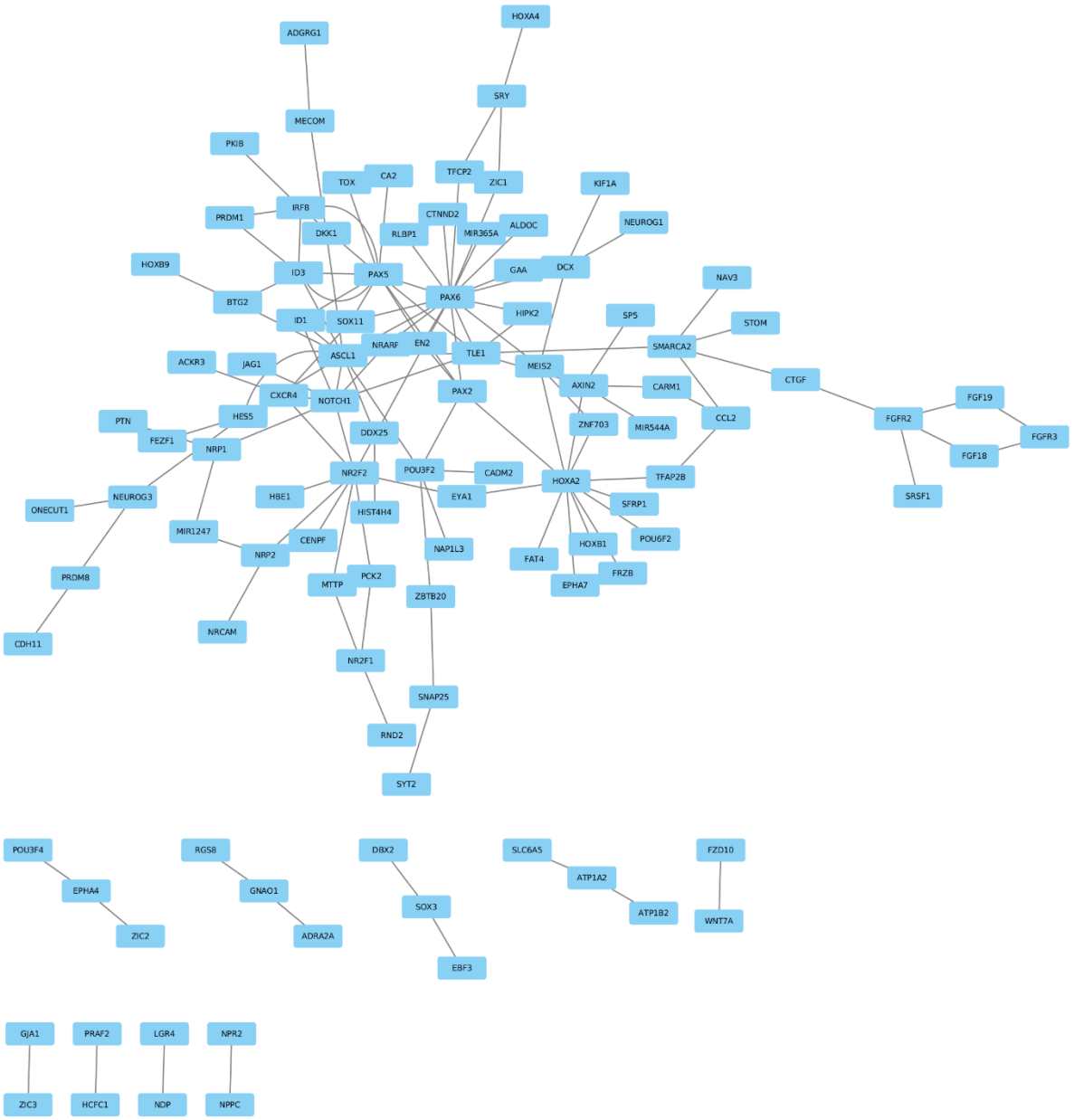

b)

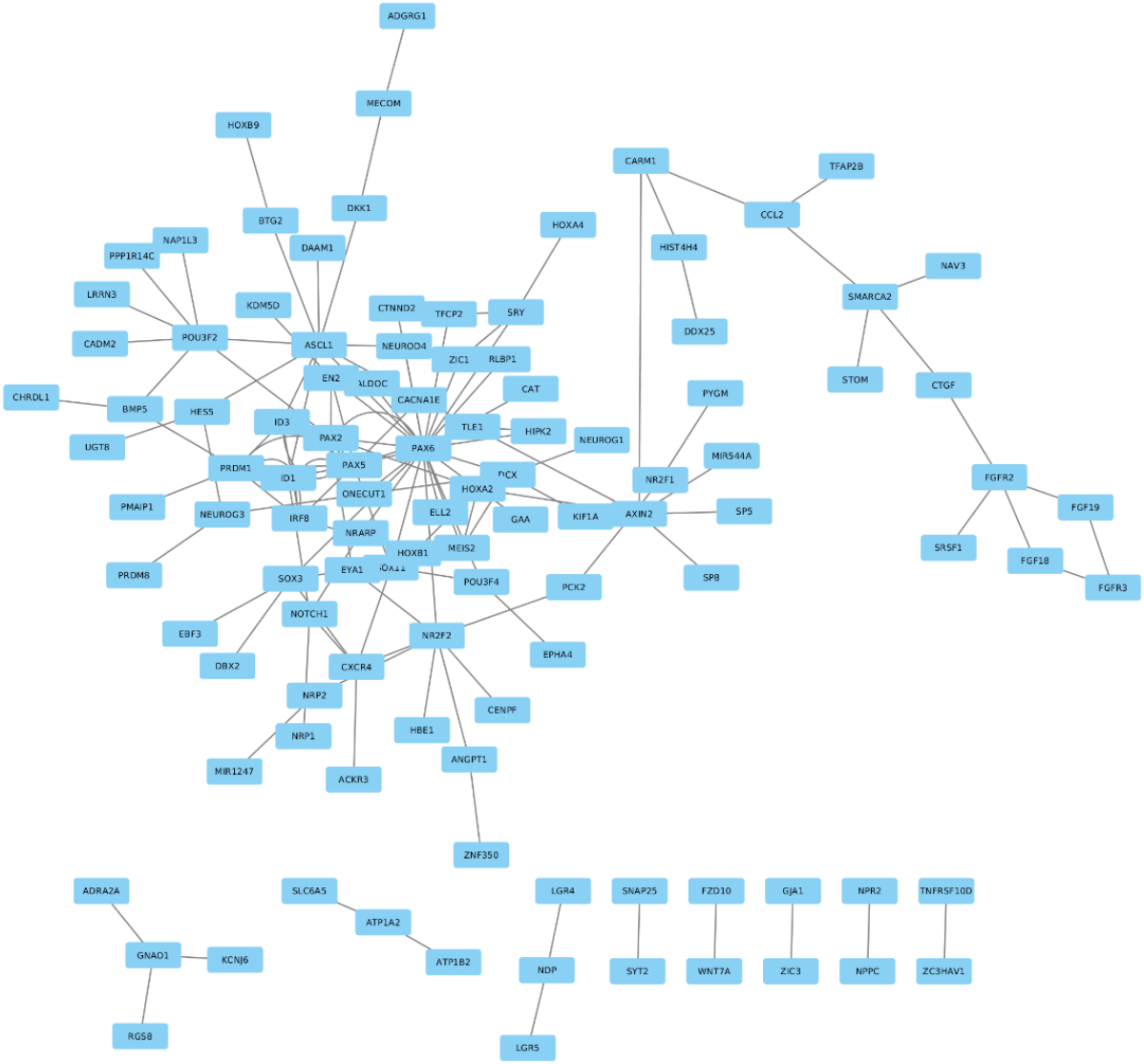

Figure 18. Differentially expressed disease model network of healthy (a) and patient (b) cells. By Muhammed Ali.

1.3 Core regulatory circuit

The information here below, has not been published in the corresponding manuscript but is relevant for the coherence of this work. The core regulatory circuit (CRC) and its extended circuits was created out of the H3K27ac peaks of ChIP-seq data from H1. Each identified transcription factor binds its own super-enhancer (SE) and will also bind into the SE of the other transcription factors that are in the core. The extended circuit is composed of genes that are active (i.e. having H3K27ac signal at their TSS) and that are regulated by at least half of the transcription factors from the CRC. The circuit reveals the core regulators of NESC maintenance. The algorithm to model human core transcriptional regulatory circuits was published by Violaine Saint-André *et al*. (2016) (Saint-André *et al*. 2016). The IP and computational analysis were performed by Déborah Gérard as described in the material and method section.

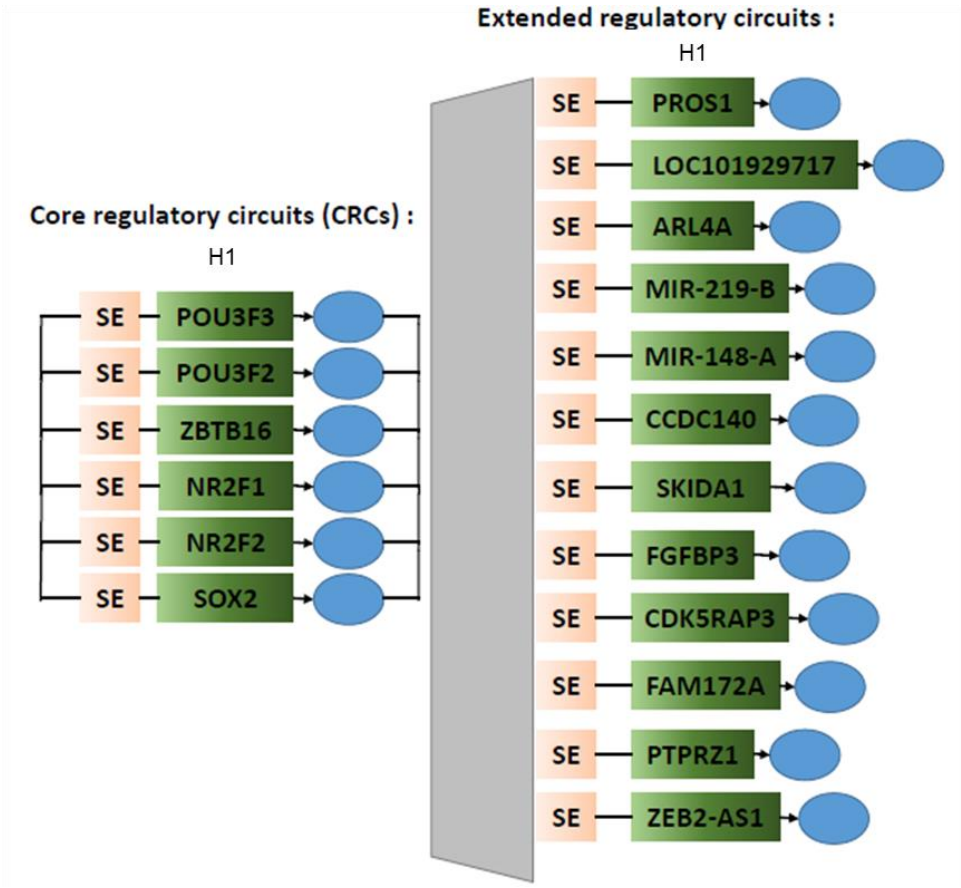

Figure 19. Core regulatory circuit of H1 a healthy cell line. By Deborah Gérard

1.4 DEGs healthy vs patient (e-Bayes method)

The information here below, has not been published in the corresponding manuscript but is relevant for the coherence of the thesis. The heatmap represents the top 50 DEGs between healthy and patient individuals. The data was generated by Aurélin Ginholac using the limma package from Bioconductor and the eBayes method as described in the material and method section. The heatmap was created by Enrico Glaab as described for paper III.

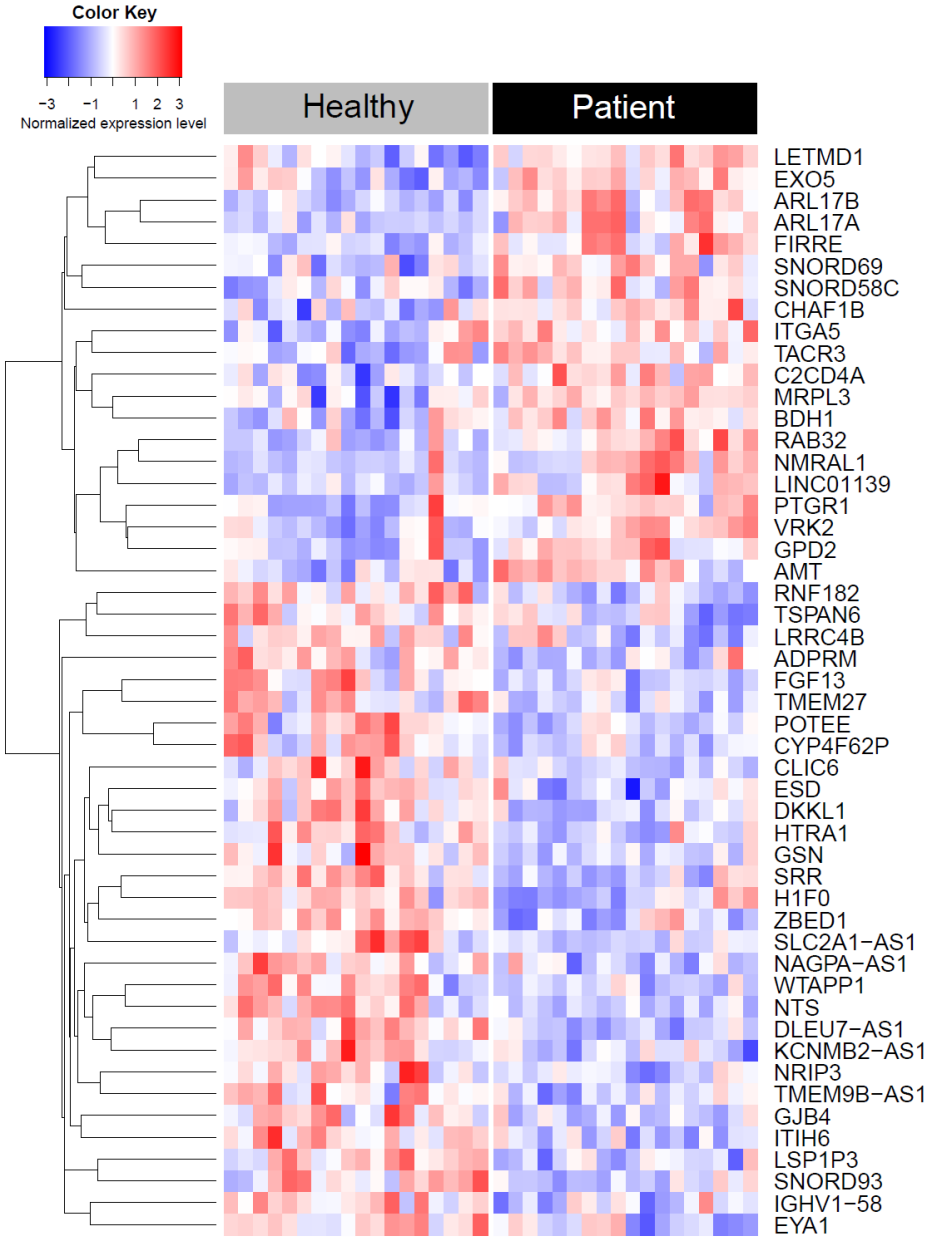

Figure 20. DEGs between healthy and patient cell lines (eBayes). P-values ≤ 0.05. By Aurélien Ginholac and Enrico Glaab.

1.5 Percentage of TH positive neurons

The information here below, has not been published in the corresponding manuscript but is relevant for the coherence of the thesis. TH and TUJ1 positive neurons were stained according to the protocol in paper III and analyzed using OPERA high-throughput imaging and an in house generated matlab script as described in the material and methods part of this thesis. The average number of TH positive generated neurons is around 15%. Note that the individual differences between cell lines are very high.

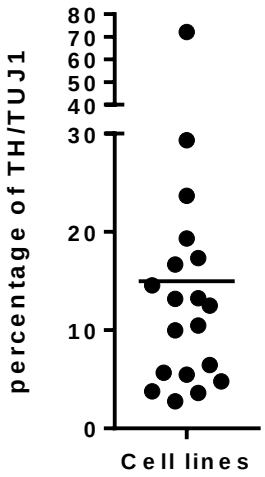

Figure 21. Percentage of TH positive neurons. Quantification of TH positive neurons compared to TUJ1 positive neurons within all 19 cell lines used in paper III. The amount of TH and TUJ1 were assessed at day 14. Each dot represents the average of 4 biological replicates for one cell line. The TH mask was normalized to the TUJ1 mask.

2 CURRICULUM VITAE

Personal details

Name	Nickels Sarah Louise
Address	83, rue d' Anvers L-1130 Luxembourg
Telephone	00352 621243461
Email	sarah.nickels@uni.lu
Birthday	09.12.1988 / Esch-Alzette
Nationality	L

Education

September 2001- July 2008	Lycée de Garçons / Esch-Alzette (L)
September 2008- July 2011	Université Libre de Bruxelles / Brussels (Be)
September 2011- July 2013	MSc University of Luxembourg / Luxembourg (L)
October 2013- today	PhD at the University of Luxembourg / Luxembourg (L)

Degrees

2008: Post-secondary diploma (Première C/Sciences)	Good
2011: Bachelor in Biology	Distinction
2013: Master in Integrated Systems Biology	Good

Work experience

February 2012- July 2012: Student job in the department of Metabolomics at the Luxembourg Centre of Systems Biomedicine (LCSB).

January 2013- July 2013: Master Thesis in the Life Science Research Unit (LSRU); Neuro-inflammation lab at the University of Luxembourg: TNFα modulates astrocyte differentiation.

October 2013- present: PhD in the department of Developmental and Cellular Biology at the LCSB and the Laboratory of Systems Biology, LSRU; University of Luxembourg: Systemic analysis of genome-wide regulation of metabolism in human neuroepithelial stem cells carrying LRRK2-G2019S. Funded by the Doctoral school in systems and molecular biology.

Educational activities

2013- 2014: Teaching practicals in gene regulation and transcriptomics, Master in integrated systems biology, University of Luxemburg.

2014- 2015: Teaching summer school in advanced cell biology, LCSB.

2015- 2016: Teaching practicals and lecture in advanced cell biology, Master in integrated systems biology, University of Luxemburg.

2016- 2017: Teaching practicals in advanced cell biology, Master in integrated systems biology, University of Luxemburg.

Training/ Workshops attended

October 2013- 2017: Doctoral school in systems and molecular biomedicine, University of Luxembourg.

20th March 2014 and 23rd September 2014: AFR-PhD grant application.

October 2014: EMBO workshop, Epigenetic plasticity: Implications in neural (dys) function.

November 2016: Committee member of the organization of Life Sciences PhD days 2016, University of Luxembourg, Doctoral school for systems and molecular biomedicine.

Poster and Oral Presentations

Poster: October 2014: EMBO workshop, Epigenetic plasticity: Implications in neural (dys) function. Systemic analysis of genome-wide regulation of metabolism in human neuroepithelial stem cells carrying LRRK2-G2019S.

Poster: October 2014: 45th Annual conference of the German Genetics Society & 2nd International PD symposium. Systemic analysis of genome-wide regulation of metabolism in human neuroepithelial stem cells carrying LRRK2-G2019S.

Poster: September 2015: Life Sciences PhD days 2015 University of Luxemburg. Systemic analysis of genome-wide regulation of metabolism in human neuroepithelial stem cells carrying LRRK2-G2019S.

Poster: October 2016: 11th Annual Meeting of the GEoPD Consortium & 3rd International Parkinson´s Disease Symposium. The PD patient's genetic background complements LRRK2-G2019S pathogenesis in hNESC.

Poster: November 2016: Life Sciences PhD days 2016. The PD patient's genetic background complements LRRK2-G2019S pathogenesis in hNESC.

Oral Presentation: April 2017: The 13th International Conference on Alzheimer's & Parkinson's Diseases. The PD patient genetic background complements LRRK2-G2019S pathogenicity in human neuroepithelial stem cells.

Publications

Palm, T., Bolognin, S., Meiser, J., **Nickels, S**., Träger, C., Meilenbrock, R.-L., Brockhaus, J., Schreitmüller, M., Missler, M., and Schwamborn, J.C. (2015). Rapid and robust generation of long-term self-renewing human neural stem cells with the ability to generate mature astroglia. Sci. Rep. *5*, 16321.

J. Arias-Fuenzalida*, J. Jarazo*, X. Qing, J. Walter, G.Gomez-Giro, **S. L. Nickels**, H. Zaehres, H. R. Schöler, J. C. Schwamborn. FACS assisted CRISPR-Cas9 genome editing facilitates Parkinson's disease modeling. Under revision in Stem Cell Reports 2017.

J. Walter, P.M.A. Antony*, **S. L. Nickels***, S. K. Poovathingal*, L. Salamanca, S. Magnin, R. Perfeito, F. Noel, X. Qing, J. Jarazo, J. Arias-Fuenzalida, A. Monzel, L. Gonzalez-Cano, S. Bolognin, L. Almeida, A. Skupin, K. Tronstad, J. C. Schwamborn. The genetic form of Parkinson's diseases primes neural stem cells and alters neurodevelopment. In preparation for submission Cell Press.

S. L. Nickels, J. Walter, S. Bolognin, C. Jaeger, X. Qing, J. Tisserand, J. Jarazo, K. Hemmer, A. Harms, P. M. A. Antony, E. Glaab, T. Hankemeier, C. Klein, L. Sinkkonen , T. Sauter, J. C. Schwamborn. The PD patient genetic background complements LRRK2-G2019S pathogenicity in human neuroepithelial stem cells. Submitted Developmental Cell 2017.